



Modelling Fire Behaviour of Composite Materials

PIETRO DI MODICA

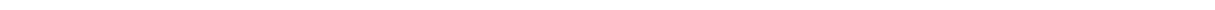
A thesis submitted
in accordance with requirements of
Newcastle University in candidature for the
Degree of Doctor of Philosophy

Supervisors: A. G. Gibson and G. Kotsikos
School of Mechanical and Systems Engineering

October 2016

© Copyright by P. Di Modica, 2016.

All Rights Reserved



Abstract

Despite the outstanding mechanical properties of composites, their structural application has been hindered by their poor structural performance in fire. A gap analysis identified the need to (i) develop a small-scale fire resistance test to be used before full-scale standardised fire tests, (ii) develop a novel method to measure thermal diffusivity, and (iii) develop and validate the thermal-mechanical model of aerospace grade unidirectional carbon fibre epoxy composites exposed to high heat fluxes. In this sense, the “small-scale propane burner fire test” was developed, with repeatable calibration method, to allow for a material development framework at low-cost. Furthermore, the “step-change method” was developed for simple and cost-effective thermal diffusivity measurements. The thermal and mechanical properties of carbon fibre epoxy composites at high temperature have been measured, with both traditional and developed techniques, to be implemented in COMFIRE-50, a 1D finite difference thermo-mechanical modelling software which takes into account heat transfer through conduction, gas mass flow and endothermic decomposition processes. The mechanical models implemented in COMFIRE-50 are the post-fire model and the strength based model, used to predict, respectively, compressive post-fire and survivability times during fire. Thermal model optimisation and validation with long-fire-exposure experiments to high heat flux has been performed with good results. On the other hand, setup issues and limited number of replicates limited the validation of the mechanical fire model, in spite of showing encouraging results under the tested conditions, i.e. no anti-buckling guides, high heat fluxes (between 70 and 180 kW m⁻²), low loading conditions compared to RT failure load, one sided heat flux and short survival times. Further to this validation for carbon fibre epoxy composites at high temperature, a graphic user interface has been developed for COMFIRE-50 (COMFIRE-50-GUI), allowing for user-friendly thermal and mechanical calculation through library and totally custom chosen parameters, supporting the wider use of this free software. Future work should focus on extending the temperature range of the thermal-mechanical property measurements, both in terms of the step-change method and mechanical testing methods.

Acknowledgements

I would like to thank all the people that made this project happen from the moral to the technical side. To Dr. Giuseppe Pitarresi, from Università di Palermo, that put me in contact with the Newcastle University team and in particular NewRail members. Without his connection and support this would not have happened.

I would like to express my gratitude to my supervisors, Prof Geoff Gibson and Dr. George Kotsikos, for the invaluable support, the stimulating conversations, the technical contribution, in the high and in the low times, to push me harder and harder every time so that I could achieve this result. It has been a pleasure to work with them and travel with them to international conferences. Hopefully there will be other future occasion to work together on new stimulating research challenges.

I would like to express my gratitude to all the technicians in the machining workshop of the Stephenson building to help me and support me in all the crazy alternative testing ideas. To Malcolm Black and Mike Foster for their stimulating contribution in performing the mechanical tests, thank you. To Brian Stocker and Stevie Charlton for all the samples manufacturing, thank you. To Ken Madden, the school superintendent, for making things happen, most of the time with a very short notice, thank you. Special thanks go to Billy Craig, the technician of the civil engineering department which helped me in making the fire-under-load testing machine work.

I also want to thank my family, without their moral support this project would not have happened, my most sincere and heartfelt thank you! I cannot repay you enough for being always there in the good times and in the bad times, to push me harder and harder and to make me believe in my capability. A special thank goes to my girlfriend which has supported me during this long journey especially during those several long boring coding working days in front of a screen, and in the last stretch to finish the writing up, thank you!

During my journey I also had the pleasure to meet Dr. Paolo Vollaro, from IMAST srl, and to work with him in fire related topics, in particular I wish to thank him for the company during the travels and for performing the thermal conductivity measurements in the COCET-PON020000293206086 project.

Last but not the least I wish to thank the Fire Resist project (FP7 European funded project grant agreement number 246037) and project partners for the wonderful experience working in an international environment and in particular I wish to thank Dr. Sophie Cozien-Cazuc and Mike Davies, from Cyttec, for the support in the mechanical tests.

Thanks to all of you mentioned and especially the non-mentioned but without whom I would not have been capable of completing this project...and as we use to say in Sicily (Palermo area) to mark the end of an event or a play, *“Agnieddu e sucu e finìu u vattiu”*.

Table of contents

Abstract	i
Acknowledgements	ii
Table of contents	iv
List of figures	viii
List of tables	xvi
 Chapter 1 Literature review	 1
1.1 Introduction	1
1.2 Fire reaction vs fire resistance	2
1.2.1 Fire reaction tests	3
1.2.1.1 Cone calorimetry	3
1.2.1.2 Intermediate-Scale cone Calorimeter	4
1.2.1.3 Single Burning Item Test	5
1.2.1.4 OSU calorimeter	5
1.2.1.5 Smoke density chamber	6
1.2.1.6 LOI	7
1.2.1.7 UL94	8
1.2.1.8 Flame spread	9
1.2.1.9 Other fire reaction tests	10
1.2.2 Fire resistance tests	10
1.2.2.1 Furnace tests	10
1.2.2.2 Aerospace burner tests	12
1.2.2.3 Jet fire	14
1.2.2.4 Other fire tests	16
1.3 Composites in fire	16
1.4 Decomposition: characterisation and reactions	18
1.4.1 Characterisation of decomposition	18
1.4.1.1 TGA	18
1.4.1.2 DSC	19
1.4.1.3 DMA/DMTA	20
1.4.2 Decomposition reactions	20
1.5 Modelling fire response of composites	21
1.5.1 Thermal response of composites at high temperature	21
1.5.1.1 Fire models	23
1.5.1.2 Henderson-Gibson model	26

1.5.1.3	COMFIRE_40.....	29
1.5.1.4	ATD	30
1.5.2	Mechanical response of composites at high temperature.....	31
1.5.2.1	Composites fire-under-compression structural models.....	36
1.5.2.2	Composites fire-under-tension structural models	38
1.5.2.3	Post-fire structural models.....	38
1.6	Project aims	39
Chapter 2	COMFIRE-50	42
2.1	COMFIRE40	42
2.1.1	Introduction.....	42
2.1.2	Governing equation.....	42
2.1.3	Decomposition effects through Arrhenius equation.....	45
2.1.4	Kinetic parameters	46
2.1.5	Thermal boundary conditions	46
2.1.6	Discretisation and numerical scheme adopted.....	49
2.1.7	Thermal properties at high temperatures.....	49
2.1.8	Type of heating source	51
2.1.9	Stability criterion and Fourier Number in Heat Transfer Analysis.....	51
2.2	COMFIRE-50.....	52
2.2.1	Fourier number stability criterion routine check	53
2.2.2	Selectable number of total nodes for the discretisation.....	54
2.2.3	Thermal conductivity and specific heat temperature evolution	54
2.2.3.1	Thermal properties function of temperature using polynomial functions.....	55
2.2.3.2	Thermal properties function of RRC using a modified rule of mixture	55
2.2.3.3	Thermal properties function of virgin and char material properties	57
2.2.4	Constant initial heat convective transfer value.....	58
2.2.5	Optimisation.....	59
2.2.6	Contact resistance	59
2.2.7	Liquid heat sink.....	63
2.2.8	Flashover	64
2.2.9	Mechanical response/model.....	65
2.2.9.1	Two layer model.....	65
2.2.9.2	Average strength model.....	68
2.3	COMFIRE-50-GUI.....	69
2.3.1	Installation.....	69

2.3.2	I/O.....	70
Chapter 3	Experimental Techniques.....	74
3.1	<i>Heat transport property characterisation.....</i>	<i>74</i>
3.1.1	Step-change method	75
3.1.2	Guarded hot plate	82
3.2	<i>Mechanical characterisation.....</i>	<i>83</i>
3.2.1	Mechanical tests at room temperature	83
3.2.2	Mechanical tests at high temperature	85
3.2.3	DMA/DMTA.....	87
3.3	<i>Fire under compressive load (time to failure)</i>	<i>89</i>
3.3.1	Flame calibration	90
3.3.2	Buckling	91
3.3.3	Testing procedure	92
Chapter 4	Material characterisation: thermal, mechanical and fire resistance properties	94
4.1	<i>Materials.....</i>	<i>94</i>
4.2	<i>Thermal characterisation.....</i>	<i>95</i>
4.3	<i>Mechanical characterisation at high temperatures.....</i>	<i>108</i>
4.3.1	Tensile tests.....	108
4.3.2	Compression tests	112
4.3.3	DMA tests	117
4.4	<i>Fire Resistance tests.....</i>	<i>124</i>
4.4.1	Heat flux calibration	125
4.4.2	Fire-under-load Results	126
4.4.3	Long-fire-exposure tests.....	132
Chapter 5	Modelling the fire behaviour of composites.....	138
5.1	<i>Thermal response.....</i>	<i>138</i>
5.1.1	Long-fire-exposure and optimum Arrhenius and heat of decomposition parameters fitting 139	
5.1.2	Thermal modelling of fire-under-load tests	157
5.2	<i>Mechanical response</i>	<i>160</i>
Chapter 6	General discussion and conclusions	164

6.1	<i>Thermal characterisation</i>	165
6.2	<i>Mechanical properties</i>	166
6.3	<i>Fire tests</i>	169
6.4	<i>Modelling</i>	171
6.5	<i>Future recommendations</i>	173
Chapter 7	List of publications	175
Chapter 8	Appendix	177
8.1	<i>Appendix 1: Cytec MTM44-1 Datasheet</i>	177
8.2	<i>Tensile test report summary from Cytec</i>	182
8.3	<i>Hysol EA9394 Lap shear strength extracted from Product data sheet, LOCTITE HYSOL EA9394, Rev. 9/2013.</i>	183
Chapter 9	References	185

List of figures

Figure 1.1: a) FTT cone calorimeter (FTT Ltd, 2014); b) Schematic of a cone Calorimeter.	4
Figure 1.2: Schematic of the SBI test (Mouritz and Gibson, 2006).....	5
Figure 1.3: a) OSU Calorimeter, picture taken from FTT website; b) schematic of OSU calorimeter adiabatic chamber (Babrauskas, 2000).	6
Figure 1.4: view of LOI apparatus. Photograph taken from FTT website.....	7
Figure 1.5: schematic representation of UL94 test. Source: Troitzsch J, "Plastics Flammability Handbook Principles, Regulations, Testing, and Approval", 3rd edition, Hanser 2004	8
Figure 1.6: a) Fire resistance test furnace from FTT website; b) hydrocarbon fire and cellulosic fire curves (Mouritz and Gibson, 2006).....	11
Figure 1.7: Schematic representation of temperature vs time in different fire scenarios: a) typical curve for enclosure fire; b) annotated fire growth diagram illustrating what fire resistance properties assess in a fire scenario.	12
Figure 1.8: a) FAA Finalised insulation burn-through test apparatus with a Park DPL 3400 burner (Marker et al., 2008); b) Calibration of an ISO 2685 gas burner from http://www.ase.uc.edu/~firetest/ftc/iso.html	13
Figure 1.9: CAD model of the “NexGen” Burner.	14
Figure 1.10: Jet fire tests in progress: a) from Hydrocarbon Processing; b) from DNV websites; c) impact of the flame on a full scale steel pipe with fire protection	15
Figure 1.11: Through-thickness reaction processes diagram of a decomposing polymer composite (Mouritz et al., 2009).	23
Figure 2.1: One 1D FD element.....	43
Figure 2.2: Example of thermal properties considered as single point value in respect to temperature but function of the RRC according to the modified rule of mixture in Equation 2.24 to Equation 2.26 using carbon fibre, epoxy resin and air properties at room temperature see Table 2.1.	57
Figure 2.3: Example of thermal properties considered as single point value in respect to temperature but function of the RRC without considering the contribution of the gaseous decomposition products.....	57
Figure 2.4: Copper block	59

Figure 2.5: Thermocouple output from a 30 minute test on 7mm thick composite fire protection. Upper curve is the measured temperature 10 mm in front of the hot face (mean value 868°C). Lower curve: copper block temperature (multiplied by 10); figure reported from Browne et al. (2006).....	60
Figure 2.6: Temperatures for a 7 mm thick Glass -Polyester composite Fibres, $V_f = 30\%$	62
Figure 2.7: Comparison between experimental results and modelled results with COMFIRE-50.....	62
Figure 2.8: Liquid heat sink (HS) calculated temperatures through an epoxy-carbon laminate (66% fibre volume fraction) of 8 mm thickness, exposed to 116 kW m^{-2} heat flux.	63
Figure 2.9: Temperature profile of a 3 mm thickness pure polycarbonate exposed to 75 kW m^{-2} on one side and insulated on the other side.....	64
Figure 2.10: Schematic of the two layer model	66
Figure 2.11: GUI of developed COMFIRE_50_1_6GUI.	70
Figure 3.1: a) UNITHERM® model 2022 equipment for thermal resistance measurement (picture of Paolo Vollaro); b) sample positioning in the UNITHERM® model 2022 machine (picture of Paolo Vollaro); c) measuring principle diagram..	82
Figure 3.2:a) picture of the mounted compression test jig; b) picture showing the inside of the compression test jig; c) schematic of working principle according to BS EN ISO 14126 method 2; d) exploded view of CAD model of the compression test jig.	84
Figure 3.3: Tensile testing jaws enclosed in the furnace, picture taken at Cytec premises, Heanor, UK.	85
Figure 3.4: CAD model of the tensile test furnace adopted at Newcastle University: left side exploded view, assembled view; picture reproduced from (Browne et al., 2006).	86
Figure 3.5: Tensile testing setup: a) annotated picture of the furnace thermally insulated with the sample inside ready to be tensile tested; b) detail of the insulated furnace.....	87
Figure 3.6: on the left schematic of compression tests sample mounting (note the anti-buckling guides); on the right schematic of sample ready for fire exposure under load, picture reproduced from Browne et al. (2006).....	91

Figure 3.7: hydraulic and signal monitoring circuits block diagram of the in house compression testing machine used to perform fire tests.	92
Figure 3.8 compression testing machine used to perform fire tests: a) annotated picture; b) simplified diagram.	93
Figure 4.1: CFRP sample ready for thermal diffusivity measurements: a) through-thickness direction; b) along the fibres.	95
Figure 4.2: a) Step-change experiment setup picture: temperature controlled environment, DAQ-PC system, digital temperature controlled agitated water bath and samples; b) typical step-change temperature curve used for thermal diffusivity calculation.	96
Figure 4.3: Comparison of transverse thermal diffusivity measured using the step-change method with one thickness sample of 10 mm, using c_p according to Equation 4.1, and two different thicknesses of 10 and 8 mm; error bars represent deviation from the average value.	97
Figure 4.4: Approximate and exact density variation in function of ΔT according to Equation 4.2.	100
Figure 4.5: Through-thickness thermal diffusivity measurements comparison using nominal and measured density using step-change technique using just one thickness of 10mm; error bars represent deviation from average values....	102
Figure 4.6: Through-thickness thermal diffusivity measurements comparison using nominal and measured density using step-method technique using 8 and 10mm samples routine; error bars represent deviation from average values.	102
Figure 4.7: Thermal diffusivity and estimated thermal conductivity: a) through-thickness; b) in-plane; error bars represent deviation from average.	103
Figure 4.8: CFRP samples, dimension of Ø50.8mm x 10mm, for thermal conductivity measurements using guarded hot plate method: a) through-thickness direction; b) in-plane direction.	104
Figure 4.9: Comparison between through-thickness thermal conductivity measured by different methods; error bars represent deviation from average for the step-change method and accuracy limits of $\pm 8\%$ for the guarded hot plate.	105

Figure 4.10: Comparison between in-plane thermal conductivity measured by different methods; error bars represent deviation from average for the step-change method and accuracy limits of $\pm 8\%$ for the guarded hot plate.	105
Figure 4.11: Comparison of measured through-thickness thermal diffusivity using step-change method with 1 sample of thickness 10mm and literature values from Zalameda (1999) and Kalogiannakis et al. (2004); error bars for step-change method are as previously mentioned, error bars for literature values are according to source values if available.	106
Figure 4.12: Comparison of measured through-thickness thermal conductivity using step-change method with 1 sample of thickness 10mm and literature values from Rolfes and Hammerschmidt (1995), Pilling et al. (1979), and Kalogiannakis et al. (2004), Fanucci (1987) is not present in the figure but reported a constant estimated value of around $0.74 \text{ [Wm}^{-1}\text{K}^{-1}]$ up to 343.3°C ; error bars for step-change method are as previously mentioned, error bars for literature values are according to source values.	107
Figure 4.13 Comparison of measured in-plane thermal conductivity using step-change method with 1 sample of thickness 10mm and literature values from Pilling et al. (1979); error bars for step-change method are as previously mentioned, error bars for literature values are according to source values.....	107
Figure 4.14: Tensile test results on 2mm thick UD CFRP samples at different temperature from 20°C to 200°C at intervals of 20°C : a) Tensile stresses vs Strains; b) Applied load vs Strains; c) Picture of the tested samples at different temperature showing the pulled-out tabs.	109
Figure 4.15: Tensile properties vs temperature of 2mm thick UD CFRP: a) tensile strength; b) tensile modulus.	110
Figure 4.16: Compression tests results on CFRP samples at different temperature from 20°C to 200°C at intervals of 20°C	113
Figure 4.17: Compression tested samples at high temperature from 20°C to 200°C at intervals of 20°C from left to right : a) Tested samples front view; b) tested samples side view.....	114
Figure 4.18: Magnified pictures of 200°C tested sample showing the classic fibre kinking bands with 60° angle inclination: a) face and side view showing the continues	

compression kink band; b) tested sample side view with highlighted kink bands and inclination angle.....	115
Figure 4.19: Compression strength at high temperature of CFRP samples using data from manufacturer and from experiments.	117
Figure 4.20: CFRP longitudinal storage (elastic) modulus versus temperature, the large modulus drop around T_g is due to the shear component of the deflection eclipsing the bending component.....	119
Figure 4.21: CFRP transverse storage (elastic) modulus versus temperature: sample 7 fluctuations below zero after T_g might be due, vibrations in the surroundings the DMA8000; loss of accuracy because of the high temperature modulus falls out of the optimal range for the used fixture.....	119
Figure 4.22: CFRP moduli simulating DMA conditions; on the left the longitudinal modulus is calculated according to Equation 4.6 and Table 4.7; on the right the transverse modulus is calculated according to Equation 4.8 and Table 4.8.	123
Figure 4.23: Heat flux [kW m^{-2}] vs Flame Temperature [$^{\circ}\text{C}$] showing a very good empirical fit using an exponential function with no-SI units.	125
Figure 4.24: Flame Temperature [$^{\circ}\text{C}$] and Gas Flow [l min^{-1}] vs Heat flux [kW m^{-2}] showing an empirical perfect fit using exponential and linear function respectively using non-SI units.	126
Figure 4.25: CFRP sample for Fire-under-load testing.....	127
Figure 4.26: Fire-under-load tested sample side view.	128
Figure 4.27: Fire-under-load test results for the case of 5%FL and 70kW m^{-2} heat flux.	129
Figure 4.28: Comparison of cold face thermal responses during fire tests under load at a constant compressive load of 5%FL and different heat fluxes adopted in this study.	130
Figure 4.29: Compressive load vs time to failure at different heat fluxes.	131
Figure 4.30: Time to failure vs compressive load at different heat fluxes.....	131
Figure 4.31: Flame temperature and cold face temperature for the long-fire-exposures at both 70 and 180 kW m^{-2} ; the increase in the cold face corresponding to 180 kW m^{-2} is due to the starting of decomposition and burning of the resin used to install the thermocouple.	133

- Figure 4.32: Temperature profile for long time fire exposure with both thermocouple and infrared (IR) camera; the flat constant initial temperature of the IR camera is due to the cold face temperature being lower than the minimum threshold of the chosen IR camera temperature range (125-900 °C) and not corresponding to an actual surface temperature; it can also be noticed that both thermocouple and IR measurements are confirming the short flame penetration for the 180 kW m⁻² and that the IR measurements are constantly 10-20 °C lower compared to thermocouple ones. 134
- Figure 4.33: Long-fire-exposure tests at 70 kW m⁻² IR snapshots at different time instants: top right and bottom left numbers are the average temperature in Area 1, which is considered representative of the cold face temperature; top left corner is the temperature at the cursor which is at the centre of the image; bottom right is a time temperature graph of the average temperature in Area 1; colours are automatically adjusted according to max and min temperature each time. 136
- Figure 4.34: Long-fire-exposure tests at 180 kW m⁻² IR snapshots at different time instants: top right and bottom left numbers are the average temperature in Area 1, which is considered representative of the cold face temperature; top left corner is the temperature at the cursor which is at the centre of the image; bottom right is a time temperature graph of the average temperature in Area 1; colours are automatically adjusted according to max and min temperature each time. 137
- Figure 5.1: Average error for thermocouple measurements function of A , E and Q_p . . 142
- Figure 5.2: Average error for IR camera measurements function of A , E and Q_p 142
- Figure 5.3: Error function for varying E and Q_p and the two values of A corresponding to the minimum error according to Table 5.3. 144
- Figure 5.4: 3D surface and contour plots of average error function in respect to thermocouple measurements for $A=1000$ s⁻¹. 144
- Figure 5.5: 3D surface and contour plots of average error function in respect to IR measurements for $A=500$ s⁻¹. 145
- Figure 5.6: Long-fire-exposure temperature profiles for both 70 and 180 kW m⁻² using thermocouple and IR camera results: the black lines are the 70 kW m⁻² and the

blue lines are 180 kW m ⁻² results; calculated temperatures were produced using the 2 sets of parameters reported in Table 5.3.....	146
Figure 5.7: Temperature error percentage between the measured and calculated temperature using the best fitting Arrhenius and resin decomposition parameters for both thermocouple and IR camera measurements reported in Table 5.3.....	146
Figure 5.8: Average error for thermocouple measurements function of A, E, Q _p and thermal properties function of decomposition state.....	147
Figure 5.9: Average error for IR measurements function of A, E, Q _p and thermal properties function of decomposition state.....	148
Figure 5.10: Error function for varying E and Q _p , A=500 s ⁻¹ and thermal properties function of decomposition state.....	149
Figure 5.11: 3D surface and contour plots of average error function in respect to thermocouple measurements for A=500 s ⁻¹	149
Figure 5.12: 3D surface and contour plots of average error function in respect to IR measurements for A=500 s ⁻¹	150
Figure 5.13: Long-fire-exposure temperature profiles for both 70 and 180 kW m ⁻² using thermocouple and IR camera results: the black lines are the 70 kW m ⁻² and the blue lines are 180 kW m ⁻² results; calculated temperatures were produced using the parameter sets reported in Table 5.4.....	150
Figure 5.14: Temperature error percentage between the measured and calculated temperature using the best fitting Arrhenius and resin decomposition parameters for both thermocouple and IR camera measurements reported in Table 5.4.....	151
Figure 5.15 Average error for thermocouple measurements function of A, E, Q _p and thermal properties function of decomposition state.....	153
Figure 5.16 Average error for IR measurements function of A, E, Q _p and thermal properties function of decomposition state.....	153
Figure 5.17: Error function for varying E and Q _p , A=300 s ⁻¹ and thermal properties function of decomposition state.....	154
Figure 5.18: 3D surface and contour plots of average error function in respect to thermocouple measurements for A=300 s ⁻¹	154

Figure 5.19: 3D surface and contour plots of average error function in respect to IR measurements for $A=300 \text{ s}^{-1}$.	155
Figure 5.20: Long-fire-exposure temperature profiles for both 70 kW m^{-2} and 180 kW m^{-2} using thermocouple and IR camera results: the black lines are the 70 kW m^{-2} and the blue lines are 180 kW m^{-2} results; the calculated temperatures were produced using the parameter sets reported in Table 5.6.	155
Figure 5.21: Temperature error percentage between the measured and calculated temperature using the best fitting Arrhenius and resin decomposition parameter sets reported in Table 5.6.	156
Figure 5.22: Fire-under-load cold face temperature profiles and simulated cold face temperature at different heat fluxes and applied loads for 10mm thick UD CFRP samples.	159
Figure 5.23: Error between simulated and experimental results in % of the measured temperature.	160
Figure 5.24: Experimental time to failure and COMFIRE-50 failure time prediction according to modelling parameters reported in Table 5.7 and Table 5.8; “o” are experimental measurements, “★” are the buckling failure predictions while the compressive failure predictions are not visible because out of x axis range.	162
Figure 5.25: Experimental time to failure, normalised residual compression and normalised buckling strength curves for the different heat fluxes and loads used for the fire-under-load tests; o are experimental measurements, continues line is the normalised compressive strength and the dashed line is the normalised buckling strength.	163
Figure 6.1: Tensile strength and modulus vs temperature for UD CFRP according to Equation 4.3 and Equation 4.4, respectively.	167
Figure 6.2: Ashby plots for engineering materials: a) thermal conductivity vs electrical resistivity; b) thermal conductivity vs thermal diffusivity, (pictures taken form GRANTA booklet at http://www.mie.uth.gr/ekp_yliko/2_materials-charts-2009.pdf).	171

List of tables

Table 1.1: Fire reaction and fire resistance differences.	2
Table 1.2: UL94 classification and meaning.....	9
Table 2.1: Room temperature thermal properties used for prediction of thermal properties function of RRC.	56
Table 2.2: Liquid heat sink physical properties.	63
Table 2.3: Input parameters and description of COMFIRE-50-GUI.	70
Table 3.1: Summary of techniques to measure thermal transport properties.....	75
Table 3.2: Flame temperature and other propane gas circuit parameters calibration table to obtain the required heat fluxes of 70, 116 and 180kW m ⁻²	90
Table 4.1: Through-thickness thermal diffusivity (α), its deviation from average and error [%] using 1 thickness technique (10 mm thick sample) and 2 thicknesses technique (10 and 8 mm thick samples).....	101
Table 4.2: Lap shear strength of Hysol EA9394 at high temperature according to product datasheet.	108
Table 4.3: Tensile strength [MPa] and tensile modulus [GPa] at different temperatures	110
Table 4.4: Values used to fit the tensile strength (tensile modulus) reported in Figure 4.15.	111
Table 4.5: Remaining resin content values corresponding to sample temperature.....	111
Table 4.6: Values used to fit the compression strength represented in Figure 4.19, values of	116
Table 4.7: Values used to plot longitudinal modulus in Figure 4.22	121
Table 4.8: Values used to plot transverse modulus in Figure 4.22	122
Table 4.9: Approximate ignition times [s] for each test condition.	127
Table 5.1: Investigated Arrhenius and resin heat of decomposition parameters.	139
Table 5.2: Constant parameters.....	140
Table 5.3: Optimum and literature (Dodds et al., 2000 and Looyeh et al., 2001) Arrhenius and heat of decomposition values for single point thermal properties model.	143
Table 5.4: Optimum and literature (Dodds et al., 2000 and Looyeh et al., 2001) Arrhenius and heat of decomposition values for thermal properties function of remaining resin content.	148

Table 5.5: Investigated Arrhenius and resin heat of decomposition parameters.	152
Table 5.6: Optimum and literature (Dodds et al., 2000 and Looyeh et al., 2001) Arrhenius and heat of decomposition values for thermal properties function of remaining resin content.	152
Table 5.7: Parameters values used to obtain the results reported in Figure 5.22 and Figure 5.23.	158
Table 5.8: Parameters values used to obtain the results reported in Figure 5.24 and Figure 5.25.	161

Chapter 1 Literature review

1.1 Introduction

Interest in composite materials has risen greatly over the past few decades, being of widespread use nowadays, from day-to-day items to high performance applications. Fibre reinforced plastics are used in applications where a high strength-to-weight ratio, a high stiffness-to-weight ratio and corrosion resistance are critical (Burns et al., 2010; Mouritz et al., 2001; Mouritz and Mathys, 2001; Mouritz, 2003) such as in the transport industry, offshore platforms, pipelines, repairs, race competition, prostheses and individual protection devices. However, in spite of their advantages, one of the recognised drawbacks is fire resistance and how to model it to support design strategies (Cao et al., 2009; Dodds et al., 2000; Fisher, 1993, Mouritz and Gibson, 2006, Lyon, 1996, Mouritz et al., 2006, Mouritz et al., 2009, Sorathia et al., 1996). In the case of fire exposure, fibre reinforced polymer (FRP) materials lose their compressive strength above T_g (Mouritz and Gibson, 2006) and flammable and toxic decomposition products are developed (Mouritz and Gibson, 2006, Mouritz et al., 2006, Mouritz et al., 2009, Sorathia et al., 1996). The phenomenon of flaming drips may also occur, which for applications in mass transport sectors is an important factor to be taken into account, since it affects fire spread and fire control.

Structural applications seem to be the most suitable for composites when a lightweight design is required; however they are not used as structural components where fire hazard is a possibility, the issue being mainly their behaviour in compression rather than in tension, since compression properties are matrix dominated. No FEM model is capable of modelling composites behaviour with good accuracy at temperature above 350°C because they do not take decomposition into account both for the thermal part and for the structural part (Urso Miano, 2011). Structural behaviour of composites in fire is complex and according to Mouritz et al. (2009) the occurring phenomena can be grouped in thermal, chemical, physical, and failure processes, this will be detailed ahead.

In this chapter the difference between fire reaction and fire resistance properties is addressed and a literature review of the associated testing methods along with characterisation of decomposition and modelling procedures is presented. A literature review on modelling fire behaviour of composite materials will then be presented, focusing on the thermo-decomposition models which are initial and the most important part. The outputs of the thermo-decomposition models could then be used as inputs of a mechanical model of different sort such as FEM or other types.

1.2 Fire reaction vs fire resistance

The expressions “fire reaction” and “fire resistance” are often encountered in the literature but sometimes they are misused. Fire reaction properties of a composite material are those properties that upon exposure to a heat source may cause fire start-up and/or harm to people. Instead, fire resistance properties characterise the capability of a material to withstand exposure to fire in terms of keeping structural integrity and/or hindering fire penetration and heat conduction throughout the material. Table 1.1 summarises the main types of fire test grouping them into the two main categories of fire resistance and fire reaction tests.

Fire Reaction	Oxygen index	LOI	Start-up and fire progress	Small-scale, low cost tests
	Combustibility	LOI		
	Time-to-ignition	Cone calorimetry		
	Surface spread of flame	Flame spread		
	Peak heat release	Cone Calorimetry		
	Average heat release	Cone calorimetry		
	Single burning item	SBI	Human survivability	
	Smoke generation	NBS		
	Toxicity index	FTIR		
Fire Resistance	Pool fire		Structural failure or insulation failure	Large-scale, expensive Tests
	Burner tests			
	Furnace tests			
	Jet-fire tests			

Table 1.1: Fire reaction and fire resistance differences.

Table 1.1 also highlights the main difference between the 2 different types of test: fire reaction tests tends to be small-scale and low cost tests compared to fire resistance tests that are rather large scale (if not in full-scale) and expensive tests.

1.2.1 Fire reaction tests

In the following section fire reaction testing techniques and standards are presented. Fire reaction testing methods are characterised by being either small-scale to intermediate-scale benchmark tests. They are presented starting from the most important/relevant one, the cone calorimeter.

1.2.1.1 Cone calorimetry

Based on the oxygen consumption principle, the cone calorimetry technique is capable of measuring time of ignition (t_i), Heat Release Rate (HRR), CO and CO₂ yield, Smoke density (D_s), and several other properties. The Cone Calorimeter, see Figure 1.1 a), is the apparatus used to perform this test which is ruled by ISO 5660-1, 2002, Second Edition and ISO 5660-3, 2012.

It consists of a conical radiant electrical heater rod capable of creating a constant heat flux (0 to 100 kW m⁻²) on a limited surface beneath it. The heated sample will then start to decompose and, when the critical gas concentration will be reached, ignition is triggered by an electrical spark. The gas products are aspirated by a hood, then analysed to measure CO and CO₂ yield. Depending on the equipment connected to it, other decomposition/combustion products can eventually be analysed. The mass loss is monitored by a balance holding the sample in place for all the duration of the test. A laser in the extraction duct is used to measure the smoke production.

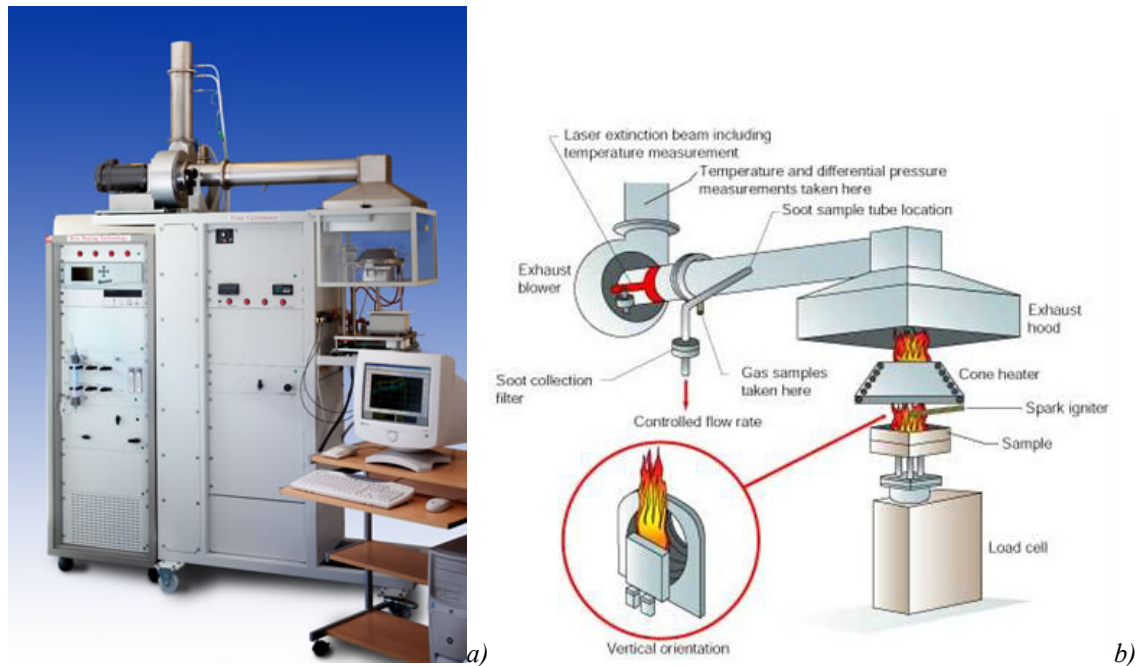


Figure 1.1: a) FTT cone calorimeter (FTT Ltd, 2014); b) Schematic of a cone Calorimeter.

With all these embedded capabilities, the cone calorimeter is considered the most versatile of the bench scale testing equipment for measuring fire reaction properties of combustible materials (Mouritz and Gibson, 2006). Due to the fact the test runs in an atmosphere which is considered representative of a vast majority of the actual fire scenarios, especially those characterised by a well-ventilated room, the cone calorimeter results are mandatory for any material used in transport modes (Mouritz and Gibson, 2006). The outcomes are also very useful in the validation of fire models (Mouritz and Gibson, 2006). However as highlighted by Mouritz and Gibson (2006) the limitation of this method is the fact that the sample maximum size is of 100mm x 100mm and different thicknesses so full or section of structures cannot be tested with this method to assess fire resistance.

1.2.1.2 Intermediate-Scale cone Calorimeter

The intermediate-scale cone calorimeter (ASTM E1623-11, 2011) is an alternative method that overcomes the limitation of the cone calorimeter on being a bench scale test. The cone calorimeter is a very useful tool but it does not give information regarding a full structure of components because of the small size of the sample. The capability of the intermediate-scale cone calorimeter of testing sample as large as 1.0 m x 1.0 m and

different thicknesses permits to test small structures or final components to study the overall assembly fire behaviour.

1.2.1.3 Single Burning Item Test

The Single Burning Item (SBI) test (BS EN 13823:2010+A1:2014), is a procedure where 2 flat specimen are tested against a fire that simulate a fire coming from a waste-paper bin corresponding approximately to 50 kW m^{-2} .

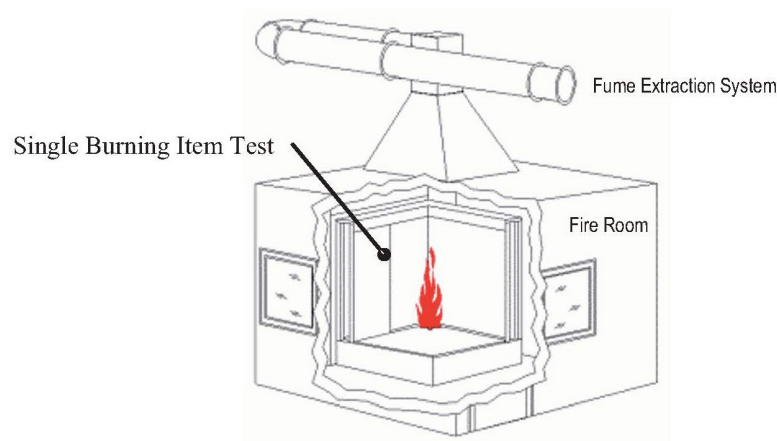


Figure 1.2: Schematic of the SBI test (Mouritz and Gibson, 2006)

Although it is more a fire resistance test, the outputs are very similar to the cone calorimeter, compressive dead-loads can be applied on the panels to measure stiffness loss and time to failure of the wall panels which are fire resistance characteristics. The main limitation of this method is that just flat specimens can be tested, which makes it not suitable for complicated shape components.

1.2.1.4 OSU calorimeter

The Ohio State University calorimeter is a bench scale fire test that measures HRR of combustible materials (ASTM E906 / E906M - 10, 2010). The OSU Calorimeter consists of an adiabatic chamber, see Figure 1.3 b), where the bench-scale sample is placed and exposed to the heat radiated from 4 electrical rods and ignited by a high temperature pilot flame impinging on the sample surface. Figure 1.3 shows a picture of the OSU Calorimeter and a schematic of the adiabatic chamber. The apparatus can perform tests at

heat flux up to 100 kW m^{-2} although tests are usually performed at around 35 kW m^{-2} . Heat release and smoke production can be measured continuously during the test. This apparatus is widely used although its results are prone to greater errors compared to the cone calorimeter (Mouritz and Gibson, 2006).

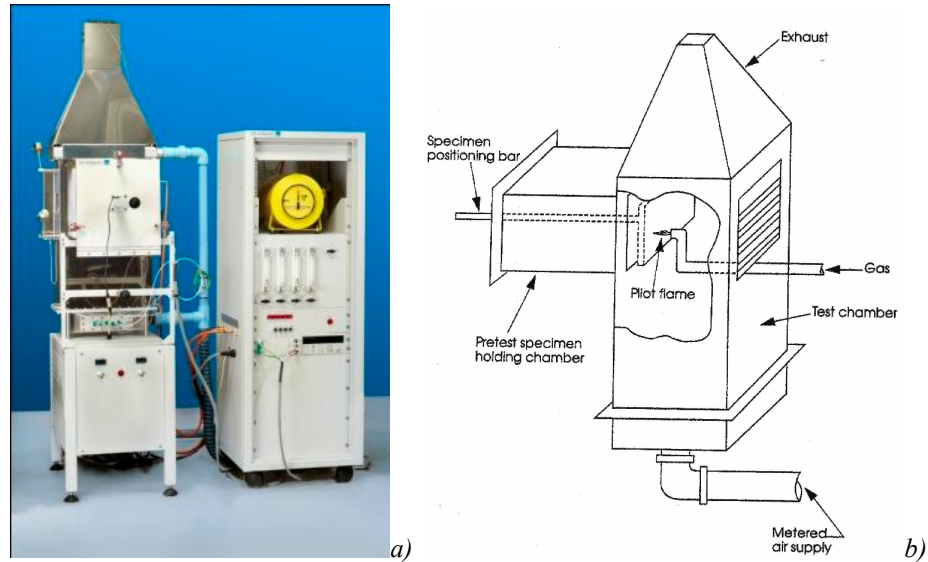


Figure 1.3: a) OSU Calorimeter, picture taken from FTT website; b) schematic of OSU calorimeter adiabatic chamber (Babrauskas, 2000).

Despite the non-perfect results, the OSU is widely used to assess fire performance of composites. The Federal Aviation Agency (FAA), for instance, has made it their reference fire safety standard of aircraft cabin materials at 35 kW m^{-2} heat flux.

1.2.1.5 Smoke density chamber

Smoke is an important factor in fire reaction measurements mainly because, depending on the thickness of the smoke, it limits visibility and so reduces people capability to escape and fire fighters to locate and suppress the fire. Although smoke production can be measured using the cone calorimeter, OSU Calorimeter and radiant panel flame techniques, the most widely used test apparatus for this purpose is the N.B.S. smoke chamber. This consists of a sealed chamber where a bench-scale size specimen in a vertical position is exposed to a radiant incident heat flux up to 50 kW m^{-2} (ASTM E662, 2013; ASTM F814-84B, 1995; BS 6401, 1983; NFPA 258, 2001). The smoke produced

is measured in terms of light transmittance in the chamber using an optical laser and a photo detector, the result is then converted in specific optical density, a dimensionless quantity.

1.2.1.6 LOI

Limiting Oxygen Index (LOI) is a test that assesses the flammability of a combustible material (ASTM D2863-13, 2013; ISO 4589-2, 1999). It represents the minimum amount of oxygen, in terms of volume percentage, necessary to just support candle like sustained flaming of the specimen. Figure 1.4 shows an example of the LOI apparatus which usually consists of a vertical specimen (the red material in the chimney), ignited from the top inside an oxygen-nitrogen controlled atmosphere chamber. The oxygen percentage is regulated in the chamber until a candle like sustained flame is achieved.



Figure 1.4: view of LOI apparatus. Photograph taken from FTT website

Although it is a widespread test, it has several deficiencies. The most relevant one is that it does not correlate to any real full scale fires. Its relevance is also questionable because of the downwards burning which is again not representative of any real fire scenario. It has to be noticed that most of the tests are run at oxygen concentration above the normal oxygen content of air which never happens in any fire hazard. For these reasons this test is not useful, except very rare cases, to predict a real fire performance of a material (it is not a fire reaction property).

1.2.1.7 UL94

UL94 is another flammability test which can be performed in horizontal (ISO 9772) or vertical orientation (ISO 9773). A schematic representation of the test is reported in Figure 1.5. The specimen is held upright by the top while the bottom part of the specimen is exposed to a small flame from a burner for a certain time. The flame is then removed and the time to extinguishment is recorded.

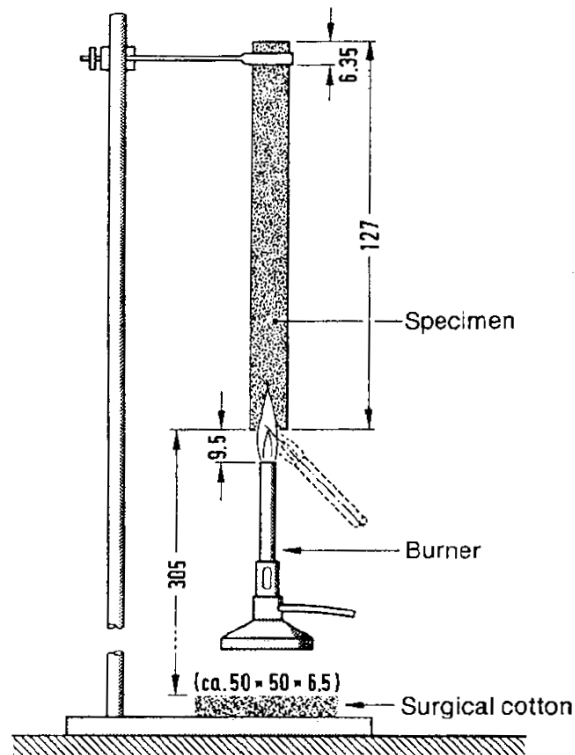


Figure 1.5: schematic representation of UL94 test. Source: Troitzsch J, "Plastics Flammability Handbook Principles, Regulations, Testing, and Approval", 3rd edition, Hanser 2004

Depending on the burning behaviour a material can be classified in a scale from V0 to V2 as summarised in Table 1.2. UL94 classification is mandatory for combustible materials used for cable insulation and electronic components although it cannot be correlated to any full-scale fire scenarios (Mouritz and Gibson, 2006).

Alternatively UL94 tests can be performed in horizontal orientation as well and in that case it measures the flame spread of the material although, as stated previously, it is not correlated to any full-size fires (Mouritz and Gibson, 2006).

Table 1.2: UL94 classification and meaning.

UL94		
Classification	Extinction time	Dripping particles
V0	<10 seconds	Allowed but extinguished
V1	<30 seconds	Allowed but extinguished
V2	<30 seconds	Allowed although on fire

The test does not measure any fire reaction properties because the results are very dependent on the orientation of the specimen and thickness of the specimen. In fact a specimen classified as V1 or V2 could result as self-extinguishing and become even a V0 if tested in vertical position but ignited from the top rather than from the bottom.

1.2.1.8 Flame spread

Flame spread tests usually involve flat rectangular specimens exposed to a gas fired radiant panel and ignited on just one of the borders (ASTM D3675-14, 2014; ASTM E162 - 13 2013). Typical flame spread tests are performed in a vertical direction with the specimen ignited from the top and measuring the downwards flame spread as the time it takes for the flames to travel downwards. The meaningfulness of this test is questionable because the higher risk on a real fire is the upwards flame spread which is far quicker compared to the downwards flame spread (Mouritz and Gibson, 2006). Other fire tests have been developed to create a more realistic fire scenario. One of these is NASA Upward Flame Propagation test (NASA-STD-6001, 1998) while other national standards include the lateral flame spread (ASTM E1321-13, 2013; BS 476-7; BS 476-6) and the fire tunnel (ASTM E84-13a, 2013).

1.2.1.9 Other fire reaction tests

The SBI is performed on samples of 1.5 m x 1.0m and 1.5m x 0.5 m, so still not a full-scale specimen. For this reason other room fire tests have been developed to recreate a real full-scale final product fire test to assess the whole structure of buildings and ship compartments against fire.

Other specialised fire reaction tests and standards exists for very specialised applications such as for electrical cables installation, for material used in transport sectors like seats and in the OilGas industry. Examples are the Glow Wire Flammability Test, Glow Wire Ignitability Test for testing upholstery used in the transport sector.

1.2.2 Fire resistance tests

In the following section fire resistance testing techniques and standards are presented. Fire resistance testing methods are characterised by being large-scale tests. Fire resistance tests are also known to be expensive, the reason is to be found on the large amount of fuel used to perform the tests at heat flux up to 200 kW m^{-2} for exposure times up to hours, on the number of sensors and data collection equipment to assess the fire resistance performances and on the full-scale sample dimensions. Fire resistance tests usually measure burn-through and time to failure of certify materials and structures against fire.

1.2.2.1 Furnace tests

Furnace tests are fire resistance tests where the component to be assessed against specific fire requirements is inserted in a furnace capable of reproducing standardised temperature-time curves associated with certain fire scenarios, examples are the cellulosic curve and the hydrocarbon curve shown in Figure 1.6.

During a test, the sample temperature evolution through time is monitored using embedded thermocouples at different location in the through-thickness dimension. In the meantime the gas flux into the furnace is regulated through a very sophisticated

temperature sensors and electronic valve actuator network to achieve the wanted furnace temperature throughout the test.

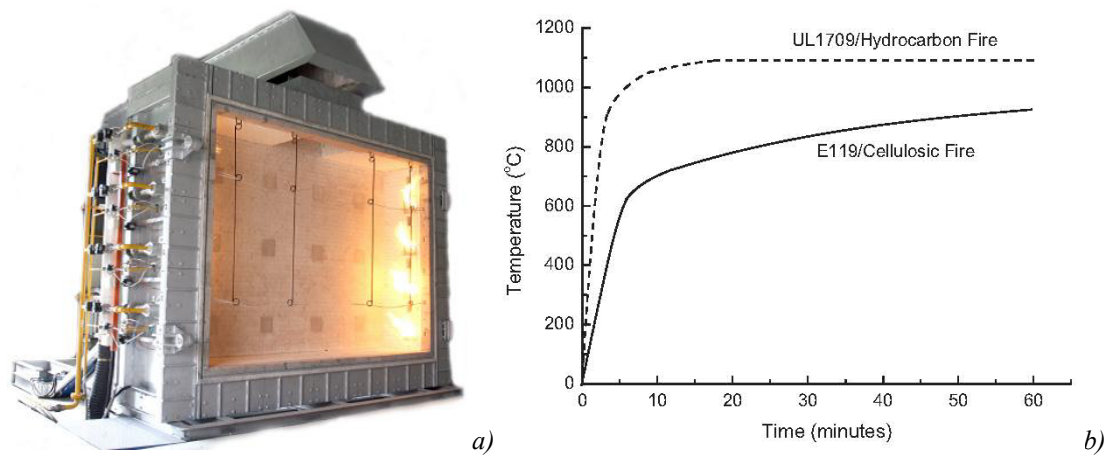


Figure 1.6: a) Fire resistance test furnace from FTT website; b) hydrocarbon fire and cellulosic fire curves (Mouritz and Gibson, 2006).

Plate thermometers are used to monitor the temperature evolution of the furnace. These plate thermometers are claimed to protect the thermocouples from the radiation and convection. The issue with furnaces is that an instantaneous rise of temperature is not possible due to the thermal inertia of the furnace itself. The initial part of the temperature curve can be more or less steep but step-change cannot be achieved.

The furnace temperature is regulated because each fire scenario is characterised by a different fire growth as it can be noticed in Figure 1.7 a) and b). Fire reaction bench scale tests, such as the cone calorimeter, are not capable of reproducing the same fire condition of a compartment fire because of aeration conditions and other factors. This is the reason why once a material is developed using the low cost bench scale tests, then a full scale fire test is necessary and the SBI or the furnace tests are recognised as the fire resistance standard tests.

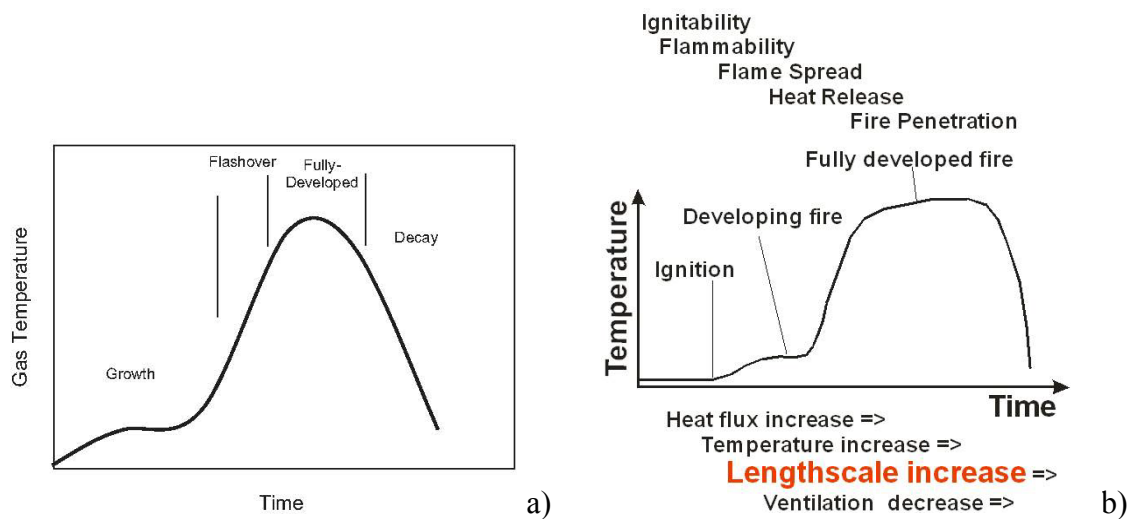


Figure 1.7: Schematic representation of temperature vs time in different fire scenarios: a) typical curve for enclosure fire; b) annotated fire growth diagram illustrating what fire resistance properties assess in a fire scenario.

It can be noticed in Figure 1.7 b) how bench scale tests can just measure fire properties until the very beginning of the fully developed fire, whereas large scale fire tests can measure fire properties until the end of a fire scenario, which occurs when all the combustible material has been consumed and no combustible products are left.

1.2.2.2 Aerospace burner tests

The aerospace industry has the necessity of assessing their products against real fire scenarios that may be generated by an engine failure or other similar accidents that may happen either during airborne or taxiing. For this reason several standards from the Federal Aviation Agency (FAA) have been developed to replicate different fire scenarios from the in-flight fire to the post-crash fire situation.

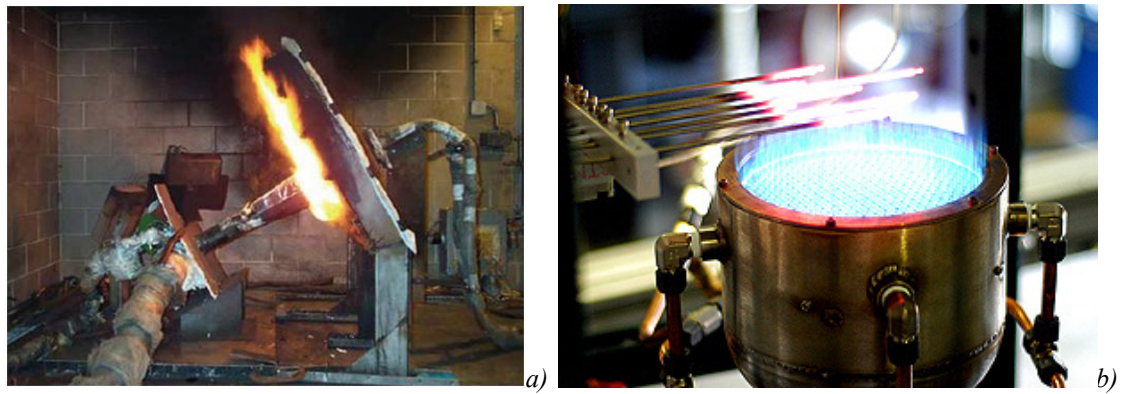


Figure 1.8: a) FAA Finalised insulation burn-through test apparatus with a Park DPL 3400 burner (Marker et al., 2008); b) Calibration of an ISO 2685 gas burner from <http://www.ase.uc.edu/~firetest/ftc/iso.html>.

Figure 1.8 a) shows a kerosene aerospace burner capable of creating a heat flux of up to 185 kW m^{-2} whose test results correlate well with full-scale fire tests on the whole fuselage section fully furnished (La Delfa, 2010). Figure 1.8 b) shows a special aerospace burner that can be used for small to intermediate scale tests (ISO 2685, 1998). This ISO 2685 burner is characterised by having a very complicated design to allow a controlled mixture of air and gas to ignite through several small hoses creating a very stable flame temperature and hence a very stable heat flux. The sample usually stands in front of the burner at a distance between 50 and 75 mm, so that the heat transfer happens almost entirely by radiation since there is no impingement of hot high speed gases on the specimen surface. Fire requirements are different depending on the burner used in fact with the Park burner the heat flux has to be higher than 106 kW m^{-2} instead with the ISO2685 burner the heat flux has to be higher than 116 kW m^{-2} . This highlights that the two tests do not replicate exactly the same conditions, as investigated by Le Neve (2008). Le Neve (2008) showed that although ISO2685 is used by the aerospace industry to show compliance with FAR/CS requirements, tests performed with different burners and standards, such as oil and gas burners according to FAA-AC20-135, 1990 and ISO2685, using the same samples and sample mounting setups would give different results. In particular the study showed that the ISO2685 test is less severe and sample would be classified as passed whereas the Park burner is more demanding and the same sample would be classified as failed. As the Park burner is no longer produced the FAA had to find a substitute for it. The “NexGen” burner, see Figure 1.9, has been designed, manufactured and assessed against the Park burner showing that recreates the same

conditions of the Park burner, with a more stable flame profile (Kao et al., 2012; Ochs et al., 2009).

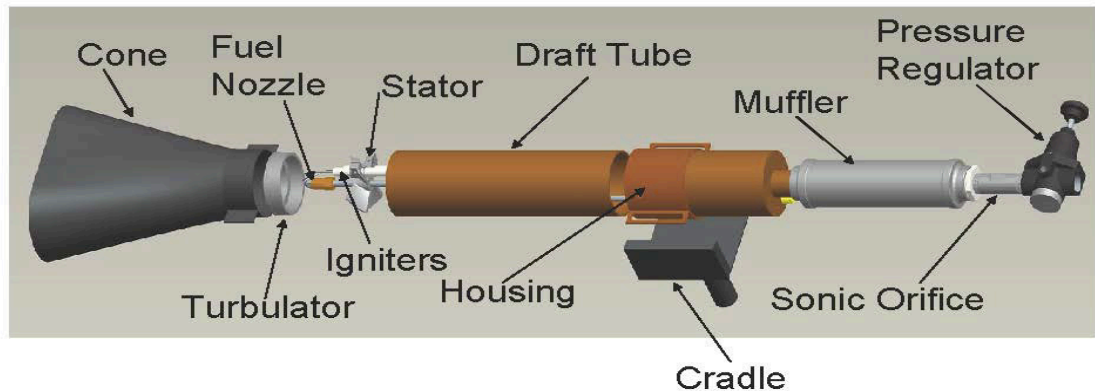


Figure 1.9: CAD model of the "NexGen" Burner.

Anyway the harmonisation of the type of the burner, the fuel, the thermocouples for calibration and the heat flux meter type should be made to avoid discrepancies among laboratories and material fire certification.

1.2.2.3 Jet fire

The Jet fire test is one of the most severe and expensive fire resistance tests and consists of natural gas or propane gas coming out of a small hole on a high-pressure pipe. The sample is placed half way down the flame length where it is exposed to not only a very high heat flux, up to 300 kW m^{-2} , but to high velocity impinging gas flow, up to 50 ms^{-1} , creating an additional ablation effect on the exposed surfaces of the component (Mouritz and Gibson, 2006). This makes the jet fire testing condition the most severe of all the fire tests.



Figure 1.10: Jet fire tests in progress: a) from Hydrocarbon Processing; b) from DNV websites; c) impact of the flame on a full scale steel pipe with fire protection

In Figure 1.10 a) and b) the scale of a jet fire can be appreciated. The pictures have all been taken from far away to allow the whole flame length, few meters, to be captured in one shot. In Figure 1.10 c) can be noticed how the high-speed gases generated during the test are pushing on the flame impinged test specimen causing an ablation effect on the sample surface. This phenomenon may cause material removal if the material is not strong enough (the same way as the wind erosion effect has on rocks but on a much quicker time scale), causing faster loss of fire protection and/or load bearing capacity. The requirements vary according to the industrial sector where the component and/or material is applied, anyway the main sectors are the maritime transportation sector and the Oil and Gas offshore sector. Further information regarding jet fire tests can be found in British Gas plc, 1996; ISO 834-3, First edition, 1999; ISO 834-1, 1999; ISO 22899, 2007; MATHER, 1997.

Jet fire tests can last up to 2 hours and the main output is the fire protection level, in terms of the time needed to achieve a certain temperature on the opposite side of the sample. Rarely load bearing capacity of the structure on fire is assessed while subjecting the test specimen to the real load as if it would be in service.

1.2.2.4 Other fire tests

There are several other types of fire tests, standardised and non-standardised, that try to recreate particular fire scenarios. A huge interest is in the development of small-scale fire scenarios for the development of fire resistant material. Such a trial will be proposed further in the development of this work.

1.3 Composites in fire

As already mentioned, fibre reinforced polymers (FRP) are widely used for their advantageous stiffness to weight ratio, strength to weight ratio and good corrosion resistance (Burns et al., 2010; Mouritz et al., 2001; Mouritz and Mathys, 2001; Mouritz, 2003). The Oil and Gas industry uses composites for piping, pipe repairing and floor gratings because of their light weight and their corrosion resistance especially in the case of offshore platforms (Gibson et al., 2013; Mablesen et al., 2000; Majid et al., 2011; Mistry et al., 1992). Wind turbine blades are made of composites because of their low density. It allows increasing their performances either by increasing their peripheral speed or by increasing their blade length making them more efficient and more productive (Stewart, 2012). Offshore wind farms have sea water corrosion problem as well and this turns into an advantage for composite materials applications. Other transport industries would take advantage of using composites in structural design because it will allow them either to decrease the energy consumption for the same payload or to increase the payload keeping the same energy consumption (Hudson et al., 2010; Mangino et al., 2007).

Mouritz et al. (2001) presented a review of composite structural application in naval ships and submarines stating the advantages and disadvantages of composites against traditional ship building materials. A wider use of composites in engineering structures is mostly affected by their fire performance (Fisher, 1993; Lyon 1996; Mouritz and Gibson, 2006; Mouritz et al., 2006; Mouritz et al., 2009; Sorathia et al., 1996). Fire exposed FRPs start degrading at temperatures around 300-400 °C losing mass to create volatiles that can be ignitable and so representing a fuel source in the fire event (Bai et al., 2008; Mouritz et al., 2006b; Urso Miano, 2011). The gas decomposition products cannot be determined with high accuracy because the composition of the gases depends on the polymer matrix

type, on the reinforcement and on the ventilation conditions (Mouritz and Gibson, 2006). Depending on the nature of the polymer used as matrix, a certain amount of residual char can be produced once decomposition has fully occurred (Mouritz and Gibson, 2006). The amount of char goes from as little as around 5% of the original mass, in the case of vinyl esters and polyesters, to as high as around 50% in the case of phenolics and or aerospace epoxies (Easby et al., 2007; Urso Miano, 2011).

Since composite material tensile properties, such as tensile strength and tensile modulus, are fibre dominated properties, whereas compression properties, such as compression strength and compression modulus, are matrix dominated properties, char formation may significantly enhance residual post-fire compression type properties compared to tension type properties. Comparing results from Mouritz and Mathys (2001) and Mouritz and Mathys (2000) it can be noticed that polyester based composites completely lose their compression strength whereas phenolic based composites, a naturally high charring resin type, retain between 10% and 20% of their compression strength in the same fire conditions and fire exposures. In fact, the high amount of char production of the latter type of composites is what enables them to retain some residual load bearing capacities in compression, as the char still holding the fibres together produces a weak but still present composite effect (Easby et al., 2007; Gibson et al., 2013; Urso Miano, 2011).

As previously mentioned, according to Mouritz et al. (2009) composite structural fire behaviour can be grouped in 4 main processes: thermal, chemical, physical and failure. The thermal processes comprise of heat conduction onto and through the composite, heat generation/absorption from decomposition reaction, convective heat loss from the escaping hot gases/vapour and heat generated by char formation and ignition of flammable gases (Mouritz et al., (2009)). The chemical processes (which are linked to the thermal processes) comprise of viscous softening, melting, decomposition and volatilisation of polymeric material, formation, growth and oxidation of char, char-fibre reactions and carbon fibre oxidation (Mouritz et al., (2009)). The physical processes comprise of thermal expansion/contraction, internal pressure built up due to decomposition gases/vapour, matrix cracking, fibre-matrix debonding, delamination,

surface ablation and melting/fusion of fibres (Mouritz et al., (2009). The failure processes depend a lot on the fire temperature, time of exposure, loading type and magnitude and geometry of the composite structure. It is a very complex problem to take into account all of these phenomena which are highly dependent on the composite type and architecture so they cannot be generalised for any type of composite. The present study will focus on measuring thermal and mechanical properties at high temperature and then use some proven literature decomposition data to model a unidirectional carbon fibre composite sample subjected to fire and load at the same time. In the following section a literature review is presented from decomposition reaction happening in composites and how to characterise it to available fire structural models.

1.4 Decomposition: characterisation and reactions

Here a brief introduction to methods to characterise decomposition and a summary of decomposition reaction on composites and in particular on carbon fibre composites is presented.

1.4.1 Characterisation of decomposition

Composite decomposition can be characterised using various methods. The most common used techniques are TGA (ThermoGravimetric Analysis), DSC (Differential Scanning Calorimetry), DMA (Dynamic Mechanical Analysis), DMTA (Dynamic Mechanical Thermal Analysis), GC-MS (Gas Chromatography-Mass Spectrometry). Each of these techniques gives a different understanding of the thermo-decomposition reactions of a composite.

1.4.1.1 TGA

Thermogravimetric analysis (TGA) is a standardised technique where the sample is heated up at a constant heating rate to measure the mass loss and mass loss rate of the sample as a function of temperature. Residual mass after decomposition can be measured through TGA. Polymers decomposition is heating rate dependent so measurements at different heating rates on the same material are necessary to fully analyse the

decomposition behaviour of a polymer material. The tests can be run in an oxidative environment, such as oxygen or air, if the oxidation reaction is required to happen, or in an inert atmosphere, such as in nitrogen, if the oxidation reaction has not to occur. TGAs run in nitrogen are more realistic of fire conditions since decomposed composites tend to present a certain amount of char, which is a result of an oxygen deprived environment (Mouritz and Gibson, 2006). Polymers decomposing with multiple stages can be analysed through the TGA curve identifying all the different steps. TGA results are usually fitted with the Arrhenius equation that can be used to model the decomposition reaction of a polymer material at different heating rates.

1.4.1.2 DSC

DSC or differential scanning calorimetry is a standardised technique (ASTM E1269-11, 2011; BS EN ISO 11357-1:2009, 2009) to measure specific heat capacity of non-decomposing solid or liquid materials by comparison with a well-known reference material. The sample is usually heated up with a constant heating rate and the heat flow in the sample is measured along with the temperature rise. This technique also allows measuring the glass transition temperature (T_g), the melting point and the percentage of crystallinity of a polymer. Henderson et al. (1982) showed how to use the DSC technique to measure specific heat capacity and heat of decomposition of decomposing materials using a well-known reference material, such as sapphire, and TGA results through Equation 1.1 **Error! Reference source not found..**

$$c_{P,S}(T) = \frac{\left(\frac{dq}{dt}\right)_S}{\left(\frac{dq}{dt}\right)_{STD}} \frac{m_{STD}}{m(T)_S} c_{P,STD}(T) \quad \text{Equation 1.1}$$

Here $c_{P,S}(T)$ and $c_{P,STD}(T)$ are the specific heat of the sample and the standard material at temperature T respectively, $\left(\frac{dq}{dt}\right)_S$ and $\left(\frac{dq}{dt}\right)_{STD}$ are the heat flow in the sample and in

the standard material respectively, $m(T)_S$ and m_{STD} are the mass of the sample at temperature T and the standard material respectively.

1.4.1.3 DMA/DMTA

The DMA or dynamic mechanical analysis (DMTA dynamic mechanical thermal analysis) is a method that applies a sinusoidal force or stress (see Equation 3.17 or Equation 3.18 respectively) to the sample to measure the elastic and damping response of materials (Gabbott, 2008; Menard, 2008) and it is particularly used for polymers. It also allows measuring the T_g of a material. Since the T_g measured with the DSC and the T_g measured with the DMA are based on slightly different phenomena to occur, although both accounting for a transition from a glassy to rubbery behaviour, a difference of up to 25°C is perfectly normal.

1.4.2 Decomposition reactions

The main effect of fire on composites is polymer matrix decomposition until 350-400°C. Above 400-500°C then significant fibre weakening can occur for both glass and carbon fibres (Feih et al., 2007a; Feih et al., 2007c; Feih and Mouritz, 2012). Different polymers show different decomposition reactions which corresponds to the scission of the macromolecule bonds in different location along the polymer chain. One beneficial decomposition reaction is the cross-linking (between 100 °C and 200 °C) which increases the bond network thus giving rigidity and strength to the final polymer. This generally happens during the post-curing process. The different decomposition reactions rule the TGA curve which has a high influence on the post-fire mechanical performances.

If composite fibre reinforcement is made of polymeric fibres, then decomposition reactions will occur in the fibres as well. In the case of non-organic or non-combustible fibres such as glass fibres and carbon fibres other phenomena occur. Glass fibres experience a gradual strength loss once heated up until around 600°C where their residual strength becomes negligible (Feih et al., 2007a; Feih et al., 2007c). Glass fibres are not the objective of this study so their softening mechanisms and failure modes will not be researched further. Carbon fibres exposed to high temperature in an oxidative

environment experience diameter and length reduction due to oxidation reaction and fibrillation phenomenon (Feih and Mouritz, 2012). Indeed Feih and Mouritz (2012) found that their tensile modulus remains almost unchanged in inert environment, whereas in an oxidative environment the oxidation of the outer fibre layer with a highly-oriented layer is responsible for modulus loss with temperature. On the other hand, tensile strength decreases with temperature regardless of the type of environment (Feih and Mouritz, 2012). The same authors attribute the decrease in tensile strength to sub-micron surface flaws already partially present on the carbon fibres rather than an intrinsic temperature softening phenomenon.

1.5 Modelling fire response of composites

Modelling composite fire response is a complex and demanding task. According to Bai et al. (2008) it can be decoupled in two main different fire responses: the thermal response which accounts for the thermal conduction, degradation and chemical-physical phenomena; and the mechanical response which accounts for structural integrity which is highly dependent on temperature and degree of degradation. The thermal response is the basic response which then can be used for mechanical predictions (Bai et al., 2008; Vizzini and Milke, 1991). This is the reason why modelling the thermal response is the main focus of this work, followed by the modelling the mechanical response.

1.5.1 Thermal response of composites at high temperature

Composite fire behaviour is complex as chemical, physical, thermal and mechanical processes happen all at once and their modelling is not easy (Mouritz et al., 2009). Polymer mechanical and thermal properties versus temperature are very important because they rule the heat transport and the mechanical failure of composites at the same time (Mouritz et al., 2009). Although they are intimately correlated, in some models the two responses can be treated as separate problems and then put together to obtain the global response.

Several studies exist on thermal properties of carbon fibre epoxy composites with different stacking sequences, carbon fibre types and epoxy resins (e.g. Berlin et al., 1992; Fanucci, 1987; Pilling et al., 1979; Kalogiannakis et al., 2004; Rolfes and Hammerschmidt, 1995; Zalameda., 1999). Although different types and batches of carbon fibres and epoxy resins may result in slight different thermal transport properties due to the non-determinist manufacturing processes (Grange et al., 2016), these publications represent a useful starting point in measuring and modelling thermal transport properties of carbon fibre epoxy composites.

Composites mechanical properties are constant until near the matrix T_g , at which temperature they start softening and a steep decay of the mechanical response is experienced (Bai et al., 2007; Bai et al., 2008; Berlin et al., 1992; Poropatic and Brayden, 1989; Street et al., 1988). At the pyrolysis temperature the polymer starts decomposing, creating combustible and non-combustible gases and a certain percentage of solid char depending on the matrix type. For long-fire-exposure and in an oxidative environment even the char may totally oxidise. At this point the only material left would be the fibres, if not made of carbon or glass, meaning that the composite effect is lost and the material properties rapidly decay. Carbon fibres will eventually oxidise (Dao et al., 2013; Feih and Mouritz, 2012) and disappear for long time fire exposure in an oxidative environment. Combustible fibres, such as aramid fibres, will decompose and burn away and the material thickness will just be reduced until it will completely become char and/or disappear, depending on fire temperature and time of exposure.

Figure 1.11 represents the various reaction processes and their location in composites exposed to a heat source. If a picture of a hot decomposing polymer composite going from the exposed surface towards the unexposed one could be taken, there would be a layer on the exposed face where the gaseous products ignite, followed by a layer of fibres and char, that sits there because all the decomposition reactions have happened. Beneath this, a decomposing reaction front would travel towards the cold face creating a thicker layer of fibre-char layer and reducing the virgin material thickness and in the other end there would be a virgin material zone (Mouritz et al., 2009).

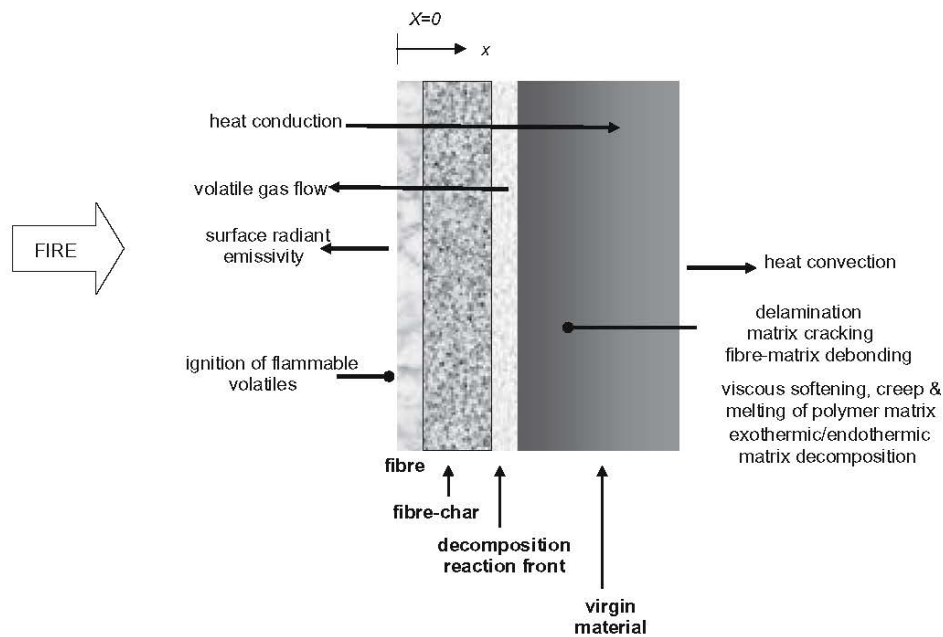


Figure 1.11: Through-thickness reaction processes diagram of a decomposing polymer composite (Mouritz et al., 2009).

1.5.1.1 Fire models

There exist different models of composites in fire, from 1D to 3D, each taking into account different aspects of thermal transport and fire induced damage. Unfortunately not all the occurring phenomena are considered in all the models simultaneously.

One of the first attempts to model transient heat conduction on CFRP (carbon fibre reinforced polymers) exposed to rapid heating was performed by Griffis et al. (1981). After this, many other models have been developed trying to insert different phenomena occurring during fire. The models of Henderson et al. (1985), Tant et al. (1985), Henderson and Doherty (1987), Henderson and Wiecek (1987), Florio et al. (1989) and Gibson et al. (1995) all include heat conduction through virgin and charred material, matrix and fibres decomposition effects and heat transfer due to gas flow through the composite. In particular the studies performed by Henderson and co-workers (Henderson et al., 1985; Henderson and Wiecek, 1987) on glass fibre phenolic composite exposed to radiant electrical heaters showed very good agreement between measured and modelled temperature (Bai et al., 2008).

The models of Sullivan (1990), Sullivan (1993), Sullivan and Salamon (1992a), Sullivan and Salamon (1992b), Dimitrienko (1995) and Dimitrienko (1997) include thermal expansion/contraction and pressure rise effects as well. Pering et al. (1980), McManus and Springer (1992a), McManus and Springer (1992b) models further added ablation effects. Vizzini and Milke (1991) also modelled thermal response of composites but since the heat fluxes used in their work were no higher than $17.6 \pm 0.1 \text{ kW m}^{-2}$, melting, ablation, or ignition of the surface did not occur and the model may not give accurate predictions in real fire scenarios. The model also does not consider pyrolysis explicitly, it included pyrolysis effects because they were indirectly encountered in the thermal properties, the so called effective or apparent thermal properties, using results from Chen et al. (1985).

According to Sikoutris et al. (2012), one of the first studies of composite structures in fire was done by Dodds et al, (2000). Glass reinforced composite panels of different thicknesses were fire tested using a furnace reproducing the standard hydrocarbon fire curve and their thermal profiles were modelled using Gibson et al. (1995) model. Decomposition kinetic parameters of the different matrix type used were measured. The cooling effect of the decomposition reaction was highlighted and, although room temperature single point thermal properties for both resin, char and fibres were used, cold face modelled results were in agreement with measured temperatures for most of the tests. Exception was made when a high delamination phenomena occurred (i.e. in the phenolic composites, locally changing the thermal conduction properties through the panels) effect that the model did not take into account. Finally a design chart against thermal response of composites in fire was produced in order to make fire protection design and testing cheaper.

Bai et al. (2007) and Bai et al. (2008) also modelled fire response of composites applying the Fourier heat transfer, law without taking into consideration ablation and decomposition reactions explicitly. Material degradation was implicitly taken into consideration by adopting apparent thermal properties (Chen et al., 1985; Fanucci, 1987; McManus and Coyne, 1982; Vizzini and Milke., 1991) which were function of the

temperature and the residual mass, degraded using an Arrhenius type law. Bai's et al. (2008) model novelty resides on the fact that the implicit finite differences solution method, rather than the explicit one, was used eliminating instability associated with wrong choice of discretisation parameters. Furthermore their model results had good agreement with the measured temperatures on glass reinforced polyester with both natural and forced convection.

More recent studies have focused on developing sophisticated 3D models of real components using the above mentioned analytical composite fire models. Sikoutris et al. (2012) performed a decoupled CFD-FEM (Computational fluid dynamic–finite element modelling) study of CFRP on fire. The study consisted on characterising the BS ISO 2685 flame temperature pattern with CFD and experimental tests, then the results of the CFD model were used as thermal load on an FEM model using 2 different materials, aluminium and CFRP composite panels. The FEM model took into consideration decomposition effects, in the sense that a progressive damage material model was used based on Arrhenius type decomposition model (Bai et al., 2007; Mouritz and Gibson, 2006b). Although the authors claim that decomposition was taken into consideration by changing the thermal properties according to the progressive damage model, the effect of hot gases abandoning the composite and heat of decomposition were not included since the model just updated the thermal properties according to the damaged status or the decomposition status. Nevertheless it has to be noticed that there is good agreement between experimental and calculated temperatures trends, with the final measured temperature being 100 K lower than the simulated ones. The authors claim that this discrepancy could be reduced if the assumption of a constant sample absorbed heat flux during the whole simulation time would not have been made since, during the tests and CFD simulations, it was observed that as time elapsed the absorbed heat flux decreased.

Grange et al. (2016) performed a fireproof study of an aerospace APU (Auxiliary Power Unit) made of carbon-phenolic composite using 3D CFD approach to investigate possible engineering solution to achieve fireproof certification according to standard BS ISO 2685 and FAA-AC20-135. Their effort was more focused in finding the most suitable flame

turbulence model then accurately modelling composite fire behaviour and the model did not include pyrolysis and flame interaction effects. Compare to Vizzini and Milke (1991), it is not clear if pyrolysis is implicitly included in the thermal conductivity and heat capacity by using the thermal properties at high temperature measured by Engelke et al. (1967) or not, since the authors do not clearly state it in their work nor they define the range of temperature their estimated thermal properties vs temperature function is valid.

1.5.1.2 Henderson-Gibson model

The basis of heat transfer through a decomposing material can be found in earlier studies on wood fire behaviour (e.g. Kung et al., 1972; Murty Kanury et al., 1972; Fredlund, 1993). Henderson et al. (1985) formulated a one dimensional model for the heat transport in phenol-formaldehyde/carbon composite which takes into account for the contribution of the endothermic polymer decomposition and the gas mass transport. Later on these two terms were rearranged and simplifying the expression, the modified Henderson equation is obtained (Henderson et al., 1985; Mouritz and Gibson, 2006b; Urso Miano, 2011) and reported in Equation 1.2 below.

$$\left(\rho C_p(T)\right)_{com} \frac{\partial T}{\partial t} = \frac{\partial}{\partial x} \left(k_{com}(T) \frac{\partial T}{\partial x} \right) + \dot{M}_g c_{pg} \left(\frac{\partial T}{\partial x} \right) - \frac{\partial \rho_{com}}{\partial t} (Q_p - h_{com} - h_g) \quad \text{Equation 1.2}$$

Here ρ is the density of the composite [kg m^{-3}], c_p is the specific heat of the composite [$\text{J kg}^{-1} \text{K}^{-1}$], T is the temperature [K], t is the time [s], x is the through-thickness coordinate [m]; k_{com} is the thermal conductivity [$\text{W m}^{-1} \text{K}^{-1}$]; \dot{M}_g is the volatiles mass flow rate [$\text{kg m}^{-2} \text{s}^{-1}$]; c_{pg} is the specific heat of the volatiles [$\text{J kg}^{-1} \text{K}^{-1}$]; Q_p is the heat of decomposition and it is negative for endothermic reaction [J kg^{-1}]; h_{com} and h_g are the enthalpy of the composite and the volatiles respectively [J kg^{-1}].

The equation describes the heat transport through a composite that, once it starts decomposing, has 3 main terms contributing to the energy balance of the composite:

- Internal energy evolution function of temperature (term on the left hand side);
- Conduction contribution to the change in internal energy which usually results in a positive contribution (first term on the right hand side);
- Convective cooling contribution due to the hot gas products abandoning the material from the cold face towards the hot face (second term on the right hand side);
- Cooling contribution of the endothermic reaction (Mouritz and Gibson, 2006) and the enthalpy change (third term on the right hand side).

It is clear in Equation 1.2 that the thermal transport properties, such as thermal conductivity and specific heat, are treated as function of temperature. A variation of the Henderson equation was proposed by Gibson et al. (1995) by expressing the change in density using a single stage Arrhenius model (Henderson et al., 1985) that can be found in Equation 1.3 below, higher order reactions need a multi-stage Arrhenius model.

$$\frac{\partial \rho}{\partial t} = -A\rho_0 \left[\frac{\rho - \rho_f}{\rho_0} \right]^n \exp(-E/RT) \quad \text{Equation 1.3}$$

Here ρ is the density [kg m^{-3}], ρ_0 is initial value of the density [kg m^{-3}], ρ_f is final value of the density [kg m^{-3}], A is the pre-exponential factor [s^{-1}], n is the reaction order [-], E is the activation energy [J mol^{-1}], T is the temperature [K] and R is the universal gas constant [$\text{J mol}^{-1} \text{K}^{-1}$].

The Arrhenius equation parameters can be found from TGA measurements but their values are not unique since different combination of A , E and n can best fit the TGA results. Methods to estimate kinetic parameters go from simplified graphic methods to very refined genetic algorithms to fit the data. Although they are very different in between each other, all methods have in common the need to measure three different TGA at three different heating rates to make the estimated parameters independent of the heating rate

used during the measurements. The set of kinetic parameters that would fit a TGA set of data is not unique in fact different sets of kinetic parameters may well fit the same set of data. A complete review, comparison and validation of different methods has been presented by Matala et al. (2013) and Matala et al. (2012). Chemically speaking, a reaction order greater than one has no sense but most of the time there are more than one reaction happening at the same time. Reaction orders other than one are used to model several simultaneous reactions with just one set of kinetic parameters (Matala et al., 2013). Once the kinetic parameters are estimated, they are used to model the mass loss, mass loss rate and gas mass flux, quantities used in the second and third term of the left hand side of the modified Henderson equation, Equation 1.2. The mass loss is also used to update the thermal transport properties of the decomposing material.

A composite material exposed to fire is subjected to a fast temperature rise. As stated before, the thermal properties have to be used as temperature dependent and most of the time the thermal transport properties are known for the fibres and the matrix separately. These properties can still be used to estimate the thermal properties of a composite laminate using the mixing rule and the serial/parallel model in the following manner (Lua et al., 2006; Mouritz and Gibson, 2006):

$$\rho_{comp} = \rho_f V_f + \rho_m (1 - V_f) \quad \text{Equation 1.4}$$

$$\frac{1}{k_{\perp, comp}} = \frac{V_f}{k_f} + \frac{(1 - V_f)}{k_m} \quad \text{Equation 1.5}$$

$$C_{p, comp} = \frac{C_{p, f} \rho_f V_f + C_{p, m} \rho_m (1 - V_f)}{\rho_f V_f + \rho_m (1 - V_f)} \quad \text{Equation 1.6}$$

Here V_f is the fibre volume fraction, ρ is the density [kg m^{-3}], k is the thermal conductivity [$\text{W m}^{-1} \text{K}^{-1}$], C_p is the specific heat [$\text{J kg}^{-1} \text{K}^{-1}$] and the subscripts f , m and $comp$ stands for fibres, matrix and composite respectively.

Equation 1.5 is not perfectly correct since the model is neither totally serial nor parallel in the through-thickness direction, but it is accurate enough to have a good estimate of the composite thermal conductivity if measurements are not available (Mouritz and Gibson, 2006).

When decomposition starts, the density changes and so the thermal properties change, not only as function of temperature but as function of the remaining resin content (RRC) and char formed. These phenomena have to be taken into account to make a more accurate temperature prediction. In this work the thermal transport properties are treated as single point value if they have not previously been measured.

The mathematical problem can be solved through the finite element method, using apparent thermal diffusivity (ATD) in 1.5.1.4, which involves solving the exact mathematical problem applied to a simplified structure and/or component; or it can be solved using the finite difference approach which simplifies the mathematical problem without approximating the structure or the component. The latter was the method applied in this work. The model is developed for 1-D although 2-D and 3-D model can be solved as well. The main issues in extending the model in more than 1-D is establishing in which directions the gases are swept away from the material, which is not an easy task, and specifying a 2-D or 3-D geometry in a finite difference model is a very demanding task. Finite element models can solve the geometry issue and adding permeability effects could help in solving the gas mass flow direction issue.

1.5.1.3 COMFIRE_40

COMFIRE_40 is a FORTRAN program that has been developed at the Centre for Composite Materials Engineering (CCME) at Newcastle University in the past years

which predicts the transient thermal response of composite laminates. The model solves the modified Henderson equation using a 1-D finite difference model; it takes into account degradation effects through the Arrhenius equation where the reaction order is assumed to be 1. If a higher reaction order characterises the material degradation behaviour, then the decomposition has to be broken in 2 stages, finding the kinetic parameters independently for each phase and then the four kinetic parameters can be input in the program with the percentage of RRC at which stage 1 finishes and stage 2 starts.

Full description of the analytical problem, boundary conditions, degradation model and thermal properties at high temperature can be found in Urso Miano, (2011).

1.5.1.4 ATD

ATD stands for apparent thermal diffusivity and it is a model that, rather than using all the three thermal transport properties, density, thermal conductivity and specific heat, uses just one thermal property which is the ratio between them, see Equation 1.7, ignoring the gas mass flux term.

$$\alpha(T) = \frac{k(T)}{\rho(T)C_p(T)} \quad \text{Equation 1.7}$$

Adopting these simplifications the heat conduction equation can be simplified as a Laplace equation, see Equation 1.8, where all the decomposition effects in the thermal transport properties are lumped into one property, the apparent thermal diffusivity. This allows the decomposition effects to be simply modelled as a temperature dependent property rather than temperature and temperature rate dependent property.

$$\frac{\partial T}{\partial t} = \alpha(T) \frac{\partial^2 T}{\partial x^2}$$

Equation 1.8

This formulation allows implementation of this model in commercial FEM software such as ANSYS or ABAQUS for instance. Good agreement has been found by Urso Miano, (2011).

1.5.2 Mechanical response of composites at high temperature

One of the main concerns in using polymer composites in structural applications is the low softening temperature of the matrix which may be affected by distortion, weakening and failure of heavily loaded structures to moderate fire's temperatures, i.e. over 150-200 °C. There exist multiple theoretical and experimental studies on structural laminate and sandwich composites in fire, mainly focusing on glass fibre reinforced polymers fire behaviour under compression where the thermal softening of the polymeric matrix dominates the mechanical failure (Anjang et al., 2014; Anjang et al., 2015; Asaro et al., 2009; Boyd et al., 2007a; Boyd et al., 2007b; Easby et al., 2007; Feih et al., 2007a; Feih et al., 2007b; Feih et al., 2007c; Gu and Asaro, 2009; Liu et al., 2006; Lua et al., 2006; Mouritz and Gibson, 2006; Mouritz et al., 2009; Gibson et al., 2004; Gibson et al., 2006). Tensile behaviour of glass fibres composites is instead dependent on both fibres and matrix thermal softening, as reported by Feih et al. (2007c).

On the other hand fewer, studies have been reported on structural integrity of carbon fibre laminate and sandwich materials (Burns et al., 2010; Berlin et al, 1992; Feih and Mouritz, 2012; Griffiths et al., 1986; Johnston et al., 1999; McManus and Springer 1992b; Mouritz, 2003; Nawaz, 2011; Pering et al., 1980; Seggewiss, 2004; Tranchard et al., 2015). The main difference between mechanical performance of glass fibres and carbon fibres during and after fire is the fact that carbon fibres oxidise compared to glass fibres (Feih and Mouritz, 2012).

A comparative study between post-fire structural performance of carbon and glass fibre composites exposed to low-to-medium heat fluxes (up to 60 kW m^{-2}) can be found in Berlin et al. (1992). The authors found that for thermosetting unidirectional laminates, no visible damage means no degradation in flexural mechanical properties whereas for cross-ply and thermoplastic composites mechanical properties may be affected even though damage could not be visually detected. They were also capable of predicting well the time of appearance of visible damage with an empirical formula (based on thickness, minimum heat flux and a material constant) for the laminates they , which could be used to predict the onset of flexural properties degradation for the unidirectional laminate. The authors also concluded that, since damage of both UD carbon and glass epoxy composites occurred at around 300°C , the loss in flexural properties at high temperature is highly dependent on the chemical degradation phenomenon of the polymeric matrix rather than on the fibre reinforcement type.

Furthermore Burns et al. (2010) and Nawaz (2011) studied the fire under compression loading of carbon fibres. The authors found that the structural integrity of carbon fibre composites is highly dependent on matrix softening, upon any other effect, which occur at relatively low intensity fire. These findings match what has already been reported on glass fibres reinforced composites structural behaviour on fire by several authors (Asaro et al., 2009; Boyd et al., 2007a; Boyd et al., 2007b; Easby et al., 2007; Feih et al., 2007a; Feih et al., 2007b; Gu and Asaro, 2009; Johnston et al., 1999; Lua et al., 2006; Mouritz and Gibson, 2006; Mouritz et al., 2009; Gibson et al., 2004; Gibson et al., 2006).

Burns et al. (2010) further investigated carbon fibre laminate fire behaviour under compression at relatively low heat fluxes, 10, 25 and 50 kW m^{-2} corresponding to fire temperature of 270 , 480 and 650°C respectively, well below postcrash fire conditions in the range of 1000 - 1200°C . However it has to be noticed that their study was performed using a non-aerospace grade material. The present work deals with aerospace grade unidirectional carbon fibre laminates which provides an opportunity to add new research insight into fire behaviour of composite materials.

In regards to isothermal tensile properties of carbon fibre composites, these have been measured by Cao et al. (2009), Nakada et al. (2002) and Yoon and Kim (2000). Yoon and Kim (2000) mainly investigated thermal expansion properties of carbon epoxy laminates up to 150°C whereas Cao et al. (2009) and Nakada et al. (2002) works investigated carbon epoxy composites tensile behaviour from room temperature up to 200°C, all temperatures well below any real fire condition. In particular Cao et al. (2009) used a very low T_g epoxy resin based carbon fibre composites and so they found a constant tensile strength loss from room temperature up to 60°C at which temperature the tensile strength remained constant up to 200°C.

While a good amount of work has been performed in investigating carbon fibres behaviour at temperature higher than 1500°C, especially for carbon-carbon composite applications, not much has been done between 400°C and 1100°C (Feih and Mouritz, 2012), which is the temperature range of most fire hazards. Feih and Mouritz (2012) findings on tensile properties of carbon fibres and carbon fibre composites in fire partially confirms findings of previous studies of Fitzer (1998), Sauder et al. (2002) and Sauder et al. (2004) which claim that carbon fibres retain their tensile strength and their tensile stiffness at temperatures up to 2000°C in inert atmospheres or vacuum conditions. Although both Fitzer (1988) and Cao et al. (2009) state that carbon fibre tensile strength remains constant up to 2000°C and their tensile stiffness increases up to 2500°C, no experimental or literature validation is given in their work. At the same time Sauder et al. (2002) and Sauder et al. (2004) both confirmed that carbon fibres tensile stiffness remains fairly constant up to the range 1000-1200°C, depending on the type of fibre precursor, after which it experiences a rapid loss in tensile stiffness up to 2000°C-2400°C. On the other hand carbon fibre tensile strength instead increases with temperature up to 1600°C or higher depending, once again, on the type of fibre precursor.

Feih and Mouritz (2012) investigated the tensile behaviour of carbon fibres and carbon fibre composites from room temperature up to 700°C and found that, in the absence of oxidation phenomena, carbon fibres retain their stiffness up to 700°C, confirming literature evidence of Fitzer (1998), Sauder et al. (2002), Sauder et al. (2004) and Yoon

and Kim (2000). On the other hand their findings on tensile strength do not align with Fitzer (1998), Sauder et al. (2002) and Sauder et al. (2004) since their tensile strength is constant up to around 400°C, temperature at which it decreases until 600°C reaching a stable value corresponding to around 60% of the room temperature value despite of the type of environment (inert or not). They also found that structural performance of carbon fibres composites in fire does not match their findings on carbon fibres tensile properties at high temperature. In fact, the composites exposed to two heat fluxes of 35 kW m⁻² and 50 kW m⁻², representative of two typical fire temperatures of 500°C and 600°C respectively, failed at around 50% and 35% of their room temperature tensile failure load respectively, compared to the 60% capacity retained by the carbon fibres. They attributed the early failure to shear lag effects due to matrix softening which might significantly reduce tensile strength of composites, as shown in Feih et al. (2007c) for glass fibres composites exposed to fire.

There is vast consensus in the literature that structural failure of composite in fire under compression load is dominated by creep effects in the case of low heat flux (up to 20 kW m⁻²) and low loading conditions; whereas for medium to high heat flux fires (above 20 kW m⁻²) failure is generally dominated by matrix decomposition effects (e.g. Bausano et al., 2005; Bausano et al., 2006; Burns et al., 2010; Nawaz, 2011; Feih et al., 2007a; Feih et al., 2007b).

Fire structural models of composites in fire can be divided into two main families, structural models during fire and after fire, usually called post-fire models. Structural models of composites during fire try to take into consideration changes of material properties and eventual structural failure during fire exposure. This means they take into account changes of physical properties and mechanical properties as function of temperature and eventually time. On the other hand, post-fire structural models try to model room temperature residual mechanical failure of composites damaged by fire. In the case of structural models during fire it should be highlighted that composite fire behaviour is different depending on the type of loading. For these models, composite properties at high temperature are modelled differently depending on the type of loading,

tension or compression. This is usually done by performing the so called isothermal mechanical properties measurements, which give the values of mechanical properties at different, constant temperatures.

Composites mechanical properties are also known to be fairly constant up until matrix T_g , at which temperature they experience a steep drop. One of the first models to take into account for this behaviour was developed by Mahieux et al. (2001) and Mahieux and Reifsnider (2002) which describes the general temperature dependent property using a cumulative Weibull distribution function of temperature, see Equation 1.9 below.

$$P(T) = P_R + (P_U - P_R) \exp \left[- \left(\frac{T}{T_0} \right)^m \right] \quad \text{Equation 1.9}$$

Here P is a particular property and the subscript U and R stands for unrelaxed (low temperature) and relaxed (high temperature) respectively, T_0 is the relaxation temperature and m is the Weibull exponent, it has to be noticed that the temperatures in here are in kelvin. This model was then modified by Gibson et al. (2006), which introduced the use of the tanh function, and reported in Equation 1.10 below (a more thorough description is given in section 2.2.9.2).

$$P(T) = \left(\frac{P_U + P_R}{2} - \left(\frac{P_U - P_R}{2} \right) \tanh(k(T - T')) \right) R^n \quad \text{Equation 1.10}$$

where $P(T)$ represents a general composite property function of temperature, P_U and P_R are the unrelaxed and relaxed properties, k is a constant representing the breadth of the relaxation, T' is the transition temperature, R is the remaining resin content and n is an empirical constant.

The model takes into consideration softening due to both viscous and resin decomposition phenomena and it does not take into consideration time dependent failure such as creep, meaning that it is suitable to model medium to high heat fluxes composite fire exposure. Gibson et al. (2006) found good agreement between modelled and experimental results but it should be noticed that the two models are valid for materials experiencing a single stage softening mechanism, i.e. not for phenolic based composites. In the case of multiple stages softening mechanisms Gibson et al. (2006) model can be extended introducing further terms on the right hand side of Equation 1.10.

All composite structural fire models are based on the idea of evaluating the thermo-mechanical properties as function of temperature at different location through the thickness. The differences are in the way that failure is estimated. The following sections will introduce composites in fire-under-load models, both in tension and compression, and post-fire structural models.

1.5.2.1 Composites fire-under-compression structural models

There are several studies on modelling behaviour of composite in fire under compression loading and the most relevant are described below.

Liu et al. (2006) studied and modelled the effect of a restrained vertical composite column subject to a linear temperature distribution through the thickness, i.e. not considering transient thermal transport. They were capable of predicting the complicated out-of-plane movement of the beam, due to both thermal load and neutral axis movements. They discovered that as the equivalent heat flux that would generate a certain linear temperature distribution would go from low to high, the thermal induced deflection of the beam would go from away from the heat source to towards the heat source, while the mechanical induced deflection induced by eccentric loading is always away from the heat source. Summers (2010) extended Liu et al. (2006) model to include various temperature fields, boundary conditions and specimen length.

Bausano et al. (2005) and Bausano et al. (2006) investigated and modelled compressive failure of glass-vinyl ester quasi isotropic composites under sustained heating at different heat fluxes from 5 to 30 kW m⁻². They predicted time to failure using both FEA (finite element analysis) and CLT (classic laminate theory) in their work, focussing in predicting the kinking failure of the 0° laminae, as they observed this phenomenon being the cause of failure of their laminates. Both models predicted the time to failure reasonably well for heat fluxes above 10 kW m⁻² and for compression stresses above 13 MPa since their model did not account for time dependent failure mechanisms, such as creep.

Boyd and co-workers (Boyd et al., 2007a; Boyd et al., 2007b) further added creep effects on the work of Bausano and co-workers (Bausano et al., 2005; Bausano et al., 2006) improving the time to failure prediction at low heat fluxes although the development of delamination affected some tests and for which the model did not account for. Bai and Keller (2011) presented a different approach to model compression failure of composites in fire.

A general model to predict time to failure of composites in fire under compression loading is the so called average strength model. This calculates the average residual strength of the composite according to temperature and remaining resin content (other effects might be included depending on the formulation of the constitutive laws and failure criteria) and compares it to the applied stresses/load so that when the latter reaches or goes over the former, failure is predicted. Several works have been published following this model by Burns et al. (2010), Feih et al. (2007a), Feih et al. (2007b) and Gibson et al. (2012).

In particular Gibson et al. (2012) used a semi empirical relation to describe the stresses in the laminate which was then averaged along the thickness, finding good agreement with both tensile and compression time to failure for different glass based composites exposed to 50kW m⁻² heat flux. Feih et al. (2007a) and Feih et al. (2007b) used the Simpson integration technique to compute an average strength along the thickness of the laminate, to then compare it to the applied stress. They found good agreement with experimental results for high heat fluxes, since the model does not include time dependent

mechanisms. Burns et al. (2010) applied the same model used by Feih et al. (2007a) and Feih et al. (2007b) to carbon fibres composites also reporting good results between calculated and experimental time to failure for heat fluxes above 10kW m^{-2} .

Due to the simplicity of application, the good predictions found in literature and the high heat fluxes used in the experimental characterisation (from 70 to 180 kW m^{-2} , according to literature compression failure is not dependent on time dependent effects such as creep), the average strength method seems the most appropriate method and will be used for modelling carbon fibre composites fire behaviour under compressive load.

1.5.2.2 Composites fire-under-tension structural models

There has been much less research into tensile properties and tensile structural modelling of composites in fire compared to the available literature on compression. Feih et al. (2007a), Feih et al. (2007c), Feih and Mouritz (2012), Gibson et al. (2006) and Gibson et al. (2012), modelled tensile properties of composite laminate in fire under tension loading, finding that composites tensile behaviour in fire is a lot more complicated than the one in compression. Gibson et al. (2006) used the classic laminate theory to predict time to failure of composites in fire and tensile loading. In spite of encouraging results using an averaging method, the model still needs improvement though. Feih et al. (2007a) and Feih et al. (2007c) used a slightly different model for tensile strength which takes into consideration not only the matrix softening but also the glass fibres softening. Despite the high intrinsic scatter of experimental data regarding time to failure, the model predicts reasonably well the life of fibreglass composites in fire except in the case of low heat flux (below 25kW m^{-2}) and low loading. In this conditions time dependence failure is predominant and the model does not include those effects.

1.5.2.3 Post-fire structural models

The most used post-fire structural model is the so called “*two layer model*” first introduced by Mouritz and Mathys (1999) and then validated in several other works (Gibson et al., 2003; Gibson et al., 2004; Mathys et al., 2002; Mouritz and Mathys, 1999; Mouritz and Mathys, 2001). The model is very suitable for estimating residual

compression strength at room temperature of composites exposed to medium to high heat flux because it ignores time dependent effects such as creep, viscoelasticity, viscoplasticity, etc. A more detailed description and implementation in the COMFIRE-50-GUI, developed and used in this study, is given in section 2.2.9.1.

1.6 Project aims

Thanks to their high stiffness-to-weight ratio, high strength-to-weight ratio and corrosion resistance compared to traditional metal materials composites are very suitable alternative when light-weight design is required but their structural fire performance is yet to be fully characterised and thermo-mechanical modelling software such FEM and CFD models lack in fire-mechanical models.

Although Bai et al. (2008) stated that thermal response of composites in fire needs to be understood and predicted, fire reaction behaviour of structural composites has been thoroughly investigated by several authors (e.g. Chen et al, 1985; Dao et al., 2013; Fisher, 1993; Gibson and Hume, 1995; Grenier et al., 1998; Griffis et al, 1981; Griffis et al, 1986; Hsieh, 1997; Le Bras et al., 1998; Lyon, 1996; Mouritz and Gibson, 2006; Mouritz et al., 2006; Perring et al, 1980; Ventriglio, 1982). Progress in modelling fire reaction has also been done by Lyon et al. (2005) and Mouritz and Gibson (2006) in trying to predict heat release rate, mass loss and ignition time in particular. However the state of the art in fire resistance modelling is not as developed as the fire reaction modelling one. There exists CFD software capable of modelling the fire reaction behaviour but not the structural one. On the other hand, FEM packages are capable of accurately modelling composite mechanical behaviour but no fire model exists. This is the reason why a coupling tool has been developed in the Fire Resist project that passes the temperatures calculated with FDS (for what concerns the fire simulation) to the FEM grid of Ansys or Abaqus or similar software to perform the structural calculations. Recent attempts to develop fire models for engineering structures have been performed by Gutkin et al. (2014), McGrattan et al. (2010), Nawaz (2011) and Prasad and Baum (2005). Mouritz et al. (2009) also presents a comprehensive review of fire structural modelling of polymer composites.

Additionally there is extensive literature on carbon fibres and carbon fibres epoxy composites, thermal transport properties, mechanical properties, fire reaction and fire resistance with different carbon fibres types and epoxy matrices types. However, though some studies involve relatively low heat fluxes (corresponding to low temperature fires), no comprehensive study has measured thermal transport properties, mechanical properties at high temperature and have used them to model the fire resistance behaviour, validating it with fire-under-load tests. In fact, the present study aimed to address this gap focusing on unidirectional aerospace grade carbon fibre laminates. There are no studies measuring the structural behaviour of unidirectional aerospace grade carbon fibre laminates in fire under compression load at high heat flux since both Nawaz (2011) and Burns et al. (2010) used cross-ply carbon epoxy composites and heat fluxes of up to 50 kW m^{-2} , generated by a radiant heater rather than an actual fire. In addition Burns et al. (2010) used a non-aerospace matrix with a low T_g of around 65°C which is not representative of an aerospace grade carbon fibre based material.

The present work has focused on:

- Measuring thermal and mechanical properties vs temperature of a unidirectional aerospace grade carbon fibre reinforced polymer (Cytac MTM44-1 UD laminate) by means of innovative techniques;
- Building a thermo-mechanical model in Matlab® which takes into account both resin decomposition and gas mass flow effects, along with thermal properties changes with temperature for the thermal model, and mechanical properties losses due to temperature dependency and resin decomposition.
- Validating the model with high heat flux fire tests under compressive load;
- Developing an innovative, low cost small scale propane burner technique capable of recreating fire conditions similar to standardised aerospace full scale fire tests.

The main aim is to create software tool capable of solving the thermo-mechanical problem for research and/or first material design screening purpose, so that composite fire resistance behaviour could in future be easily modelled and predicted.

To tackle these scientific shortcomings, unidirectional aerospace grade carbon-epoxy have been manufactured by material producer. Since it is reported in literature that knowing thermal transport and mechanical properties is crucial to obtain a good fitting between experimental and modelled results, effort has been made to measure their thermal and mechanical properties at high temperature within restriction of material availability and school health and safety restrictions. COMFIRE-50, a Matlab based software has been created to model thermal and mechanical behaviour of composites in fire and a new innovative, low cost small scale propane burner technique has been developed to perform fire-under-load tests to validate COMFIRE-50 modelling software.

The first of the following chapters contains a detailed description of the COMFIRE-50, a Matlab developed software and where it comes from. Although it is based on the same mathematical model and structure of the previous COMFIRE40, additional functionalities and the GUI have been added to spread the tool for free to the research and industrial community. Chapter 3 contains an explanation of the experimental techniques used to measure thermo-mechanical properties and to perform fire-under-load tests. Most of them are standard techniques with the exception of the fire-under-load tests which uses a innovative, low cost small scale propane burner technique with a repeatable calibration procedure. Chapter 4 contains a description of the material used, the results of the thermal and mechanical characterisation tests and finally the fire resistance test. Chapter 5 reports the modelling results using COMFIRE-50 for both thermal and time to failure prediction. Finally Chapter 6 presents discussion on the results obtained in this work, draws some conclusions and suggests the way forward.

Chapter 2 COMFIRE-50

COMFIRE40 is a piece of software which solves the modified Henderson equation, see Equation 1.3 previously shown, using the finite difference method (FD). For the reasons previously mentioned in section 1.5.1, COMFIRE40 is applied on a 1-D physical problem. The code was originally written in FORTRAN and takes into account conduction, degradation effects and gas mass flow effects. Several types of boundary conditions can be incorporated such as constant heat flux, convection and radiation. In this work the core FORTRAN code has been translated into Matlab® language, creating COMFIRE-50, bugs were fixed and new features and extended cold face boundary options have been inserted. Furthermore a new user friendly graphic user interface (GUI) has been developed during these three years' work and the new program is called COMFIRE-50-GUI.

2.1 COMFIRE40

2.1.1 Introduction

COMFIRE was initially developed in 1994 for predictions of thermal resistance of thick GFRP laminates when exposed (with one of its two faces) to hydrocarbon fire only, based on the 1-D model (Gibson et al., 1995) using finite difference numerical analysis approach. COMFIRE40 can be used to predict thermal responses of composite laminates exposed to different heating sources. Resin systems and fibre reinforcements involved can be of different types. A database of thermal properties for the most common resins and fibres systems is embedded in the program.

2.1.2 Governing equation

Hereafter is presented the development of the mathematical model in the through-thickness direction. A 1D FD element cut from the composite laminate under examination with a unit cross-sectional area and a finite length of Δx is shown in Figure 2.1.

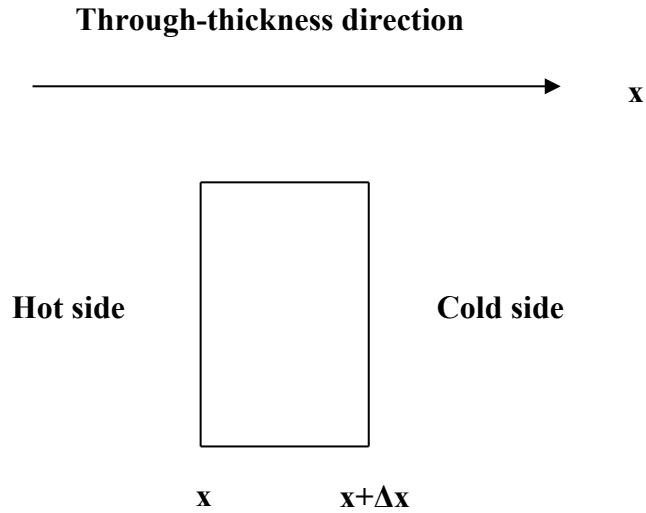


Figure 2.1: One 1D FD element

The rate of change of internal energy in a 1D FD composite element is given by:

$$\frac{\partial}{\partial t}(\rho_{comp} h_{comp})(\Delta x) \quad 2.1$$

where ρ_{comp} is density of the composite material [kg m^{-3}] and h_{comp} is the enthalpy of the material [J kg^{-1}]. The internal energy change of the single element is due to three main different contributions: the conventional heat transfer through conduction, 2.2, gaseous mass flow (from the cold side to the hot side), 2.3, and heat generation or absorption, 2.4 shown and annotated hereafter.

$$\frac{\partial}{\partial x} \left(k_{comp}(T) \frac{\partial T}{\partial x} \right) (\Delta x) \quad 2.2$$

$$\frac{\partial}{\partial x} \left(\dot{M}_g h_g \right) (\Delta x) \quad 2.3$$

$$-Q_p \frac{\partial \rho_{comp}}{\partial t} (\Delta x)$$

where k_{comp} represents thermal conductivity of the composite material [$\text{W m}^{-1} \text{K}^{-1}$], T is the temperature of the body [K], \dot{M}_g is gaseous mass flux, or rate of gaseous mass flow [$\text{kg m}^{-2}\text{s}^{-1}$], h_g is enthalpy of the gases generated during decomposition [J kg^{-1}] and Q_p is heat of decomposition and it is negative for endothermic reaction [J kg^{-1}].

Assuming that there is no gas accumulation in the composite during fire exposure and considering the energy conservation of the element under examination leads to the following non-linear partial differential equation:

$$\frac{\partial}{\partial t}(\rho h)_{comp} = \frac{\partial}{\partial x} \left(k_{comp}(T) \frac{\partial T}{\partial x} \right) + \frac{\partial}{\partial x} \left(\dot{M}_g h_g \right) - Q_p \frac{\partial \rho_{comp}}{\partial t} \quad \text{Equation 2.5}$$

The term on the left hand side of Equation 2.5 can be re-written as shown in Equation 2.6.

$$\rho_{comp} \frac{\partial h_{comp}}{\partial t} + h_{comp} \frac{\partial \rho_{comp}}{\partial t} = (\rho c_p)_{comp} \frac{\partial T}{\partial t} + h_{comp} \frac{\partial \rho_{comp}}{\partial t} \quad \text{Equation 2.6}$$

and the second term on right hand side of Equation 2.5 can be re-written as shown in Equation 2.7.

$$\dot{M}_g \frac{\partial h_g}{\partial x} + h_g \frac{\partial}{\partial x} \left(\dot{M}_g \right) = \dot{M}_g (c_{pg}) \frac{\partial T}{\partial x} + h_g \frac{\partial}{\partial x} \left(\dot{M}_g \right) \quad \text{Equation 2.7}$$

Here, c_{pg} represents specific heat of the generated gases. Through considering mass conservation over the element, this gives:

$$\frac{\partial}{\partial x} \left(\dot{M}_g \right) = - \frac{\partial \rho_{comp}}{\partial t} \quad \text{Equation 2.8}$$

and therefore, the gas mass flux, \dot{M}_g , at any position, x , and at any time, t , may be calculated by integrating Equation 2.8:

$$\dot{M}_g = \int_{coldface}^x - \frac{\partial}{\partial t} (\rho_{comp}) dx \quad \text{Equation 2.9}$$

Substitution of Equation 2.6, Equation 2.7, Equation 2.8 and Equation 2.9 into Equation 2.5 leads to the following governing equation adopted in the program:

$$(\rho C_p)_{com} \frac{\partial T}{\partial t} = \frac{\partial}{\partial x} \left(k_{com} \frac{\partial T}{\partial x} \right) + \dot{M}_g c_{pg} \left(\frac{\partial T}{\partial x} \right) - \frac{\partial \rho_{com}}{\partial t} (Q_p - h_{com} - h_g) \quad \text{Equation 2.10}$$

2.1.3 Decomposition effects through Arrhenius equation

When a composite sample reaches a sufficiently high temperature, chemical reactions begin to occur and its resin component degrades to form gaseous products. An n^{th} order Arrhenius equation was adopted in thermal analysis to simulate the decomposition process of the resin system involved:

$$\frac{\partial m}{\partial t} = -Am_0 \left[\frac{m - m_f}{m_0} \right]^n \exp(-E / RT)$$

Here m is the mass of the resin [kg], m_0 is the initial mass of the resin [kg], m_f is the final mass of the resin at the end of decomposition [kg], A is the pre-exponential factor [sec^{-1}], T is the temperature of the resin [K], n is the order of the chemical reaction, E is the activation energy [J mol^{-1}], R is the gas constant ($8.314 \text{ [J mol}^{-1} \text{ K}^{-1}]$). The governing equation, Equation 2.10, must be solved simultaneously with Equation 2.11 to fully describe the fire behaviour on terms of temperature.

2.1.4 Kinetic parameters

The four kinetic parameters appearing in Equation 2.11, i.e. activation energy, E , pre-exponential factor, A , order of the chemical reaction, n and final mass of the resin at the end of decomposition, m_f , can be derived from thermogravimetric data using either Anderson's single heating rate technique (Anderson et al., 1959) or Friedman's multiple heating rate technique (Friedman, 1964). In the present version, $n = 1$ has been assumed and the other kinetic parameters derived since, as previously mentioned, different sets of kinetic parameters can fit the same TGA data. These kinetic parameters of the resin system derived from processing TGA data, in theory, should be independent from the heating rate. One may have the kinetic parameters of a resin system required for running this program by averaging values derived from relevant TGA data with different heating rates (Matala et al., 2012; Feih et al., 2005).

2.1.5 Thermal boundary conditions

There are two mechanisms of heat transfer at the boundaries, radiation and convection. Depending on the temperature range, one contribution can usually be neglected compared to the other and/or vice versa. The boundary conditions inserted in the program are the same for both the hot face (HF) and the cold face (CF) and involved free radiation and natural convection, see Equation 2.12.

$$q = \sigma(\varepsilon_s \alpha_m T_s^4 - \varepsilon_m T_c^4) + h_{nc}(T_{sc} - T_c) \quad \text{Equation 2.12}$$

Here q is heat flux into the hot face of the sample [W m^{-2}], T_{sc} is the surrounding temperature [K], T_c is the temperature on hot face of the sample [K], T_s is the heating source temperature [K], h_{nc} is the heat transfer coefficient through natural convection [$\text{W m}^{-2} \text{K}^{-1}$], ε_s is the emissivity of the heating source, α_m and ε_m are the absorptivity and the emissivity of the sample HF respectively and σ is the Stefan-Boltzmann constant, equal to 5.67×10^{-12} [$\text{W m}^{-2} \text{K}^{-4}$].

Radiation is the main heat transfer contribution in a fire scenario especially compared to natural convection; the software does not deal with forced convection. Hence in the program there are different boundary options depending if it is dealing with the hot face or with the cold face. Hot face boundary conditions are either just radiation or radiation and natural convection where the convective heat transfer coefficient for a vertical wall of not over 1m high from the ground is described by an empirical formula (Eastop McConkey, 1978; Perry and Green, 2008), see Equation 2.13 below.

$$h_{nc} = 1.31(\theta^{1/3}) \quad \text{for } 10^9 < Gr < 10^{12} \quad \text{Equation 2.13}$$

where θ is the temperature difference between the heating source and the HF of the sample [K], and Gr is the Grashof number. Using Equation 2.13 means that the flow boundary layer of circulating air on the vertical surface due to natural convection is turbulent, resulting in large Grashof number.

For lower range of Grashof number, i.e. for laminar flow on the boundary layer of the sample surface, the following equation may be used for evaluating the heat transfer coefficient (Eastop et al. 1978) (not used in the program), see Equation 2.14 below.

$$h_{nc} = 1.42 \left(\frac{\theta}{l} \right)^{1/4} \quad \text{for } 10^4 < Gr < 10^9$$

Equation 2.14

where l is the characteristic linear dimension in the particular case. For example, l may be taken as the distance between the centre of the exposed hot face and the floor during the test.

The software offers a choice of different hot face conditions such as a constant heat flux, which can be input by the user of the program, typical standard curves such as the SOLAS curve, the Hydrocarbon Curve, a more general ambient measured temperatures data file or the temperature-time evolution of the hot face boundary node.

The cold face can be thermally insulated, can be subjected to natural convection and free radiation, or it can be in thermal contact with a heat sink (user input). The convective heat transfer coefficient for the cold face is estimated using Equation 2.15 below.

$$h = h_{in} + 0.003T + 0.0001T^2$$

Equation 2.15

Where h_{in} is the initial heat transfer coefficient that for natural convection is in between 5 and 10 [W m⁻² K⁻¹] and T [K] is the temperature of the cold face.

Once all the input files have been written and saved in the correct format and file extension, COMFIRE40 reads these files, calculates the thermal response of the model and returns output files as TXT files where all the major information are reported depending on the enabled model option chosen. Typical outputs are the temperature profiles of 7 of the 50 finite difference nodes, their remaining resin content (RRC) and the gas mass flow time evolution.

2.1.6 Discretisation and numerical scheme adopted

In the 1D modelling, the laminate is discretised automatically by the program in the through-thickness direction with 51 nodes, forming uniform 50 one-dimensional FD elements or layers in any case. The non-linear partial differential Equation 2.10 (Gibson et al., 1995) governing the heat transfer process from a heating source to a composite laminate is numerically solved using a straightforward explicit finite difference method.

2.1.7 Thermal properties at high temperatures

It is clear that thermal properties of FRP composites are resin volume fraction-dependent. These properties may vary considerably at high temperatures due to changes in resin volume fraction, and changes in composition of the materials due to chemical reactions. In this program the initial density, thermal conductivity and specific heat of a given virgin composite material are evaluated for a specified fibre volume fraction, V_f , according to the Rule of Mixtures:

$$\rho_{comp} = \rho_f V_f + \rho_m (1 - V_f) \quad \text{Equation 2.16}$$

$$\frac{1}{k_{\perp, comp}} = \frac{V_f}{k_{\perp f}} + \frac{(1 - V_f)}{k_m} \quad \text{Equation 2.17}$$

$$C_{p, comp} = \frac{C_{p, f} \rho_f V_f + C_{p, m} \rho_m (1 - V_f)}{\rho_f V_f + \rho_m (1 - V_f)} \quad \text{Equation 2.18}$$

Optionally, thermal properties can be inserted as function of temperature in a table format and the software will perform a linear interpolation between the values of the table to find the estimated value of the thermal properties for every node. Re-evaluation of density of the composite material is repeated at each node and each time-step during computation to account for changes caused by resin decomposition. The predicted Remaining Resin

Content [%] at a certain time and for a layer at a given depth in the through-thickness direction of the composite is called **RRC** in the analysis.

No density change in E-glass fibres is expected for temperatures up to about 1000 °C. Carbon fibres and aramid fibres may undergo oxidation or decomposition action at high temperatures, resulting in changes in density of the composite material. However such effects are not included in the analysis for the time being since carbon fibres do not decompose in inert environments up to 1000 °C such as the inner part of a decomposing composite (Feih and Mouritz, 2012). Effects of gases or air filled in the voids within the body of the composite material on density change during fire exposure are also ignored.

Although it has been found unsatisfactory to use single point thermal property values, in this program through-thickness thermal conductivity and specific heat at high temperatures, for simplicity, are assumed derived from initial values and independent of temperature.

The inaccuracy in predictions caused by the above simplification assumption can be resolved either by directly inputting measured thermal properties of the composite at high temperatures when running the program, or by adopting a modified Rule of Mixtures in the program for evaluating thermal conductivity and specific heat of composites undergoing decomposition at high temperatures.

It is expected that adopting the initial value of thermal conductivity of virgin composite material at room temperature as those at high temperatures might lead to an over-estimation of the actual thermal conductivity of the porous laminate, resulting in a conservative prediction of thermal responses of the composite material in fires. It is suggested that at least, the following two factors are to be taken into account in formulating a modified Rule of Mixtures:

- The existence of gases or air in the voids generated during decomposition of the composite material;
- Different type of fibre reinforcement in the composite, leading to different ways of contact of one individual fibre with another in the through-thickness direction.

2.1.8 Type of heating source

Five different types of heating source are considered in COMFIRE40 and these include:

- The hydrocarbon (HC) curve, which is automatically defined by the program;
- The SOLAS fire curve, which is automatically defined by the program;
- A constant incident heat flux, which is specified by the value of heat flux and the relevant emissivity of the heating source;
- An experimentally or theoretically defined temperature vs time curve as an input data file describing the thermal environment surrounding the front surface of the composite sample under examination.
- An experimentally or theoretically defined temperature vs time curve as an input data file describing temperatures on the front hot surface of the composite sample.

The final type is associated with no particular heating source. This special type of ‘heating source’ is designed for predictions to be compared with predictions obtained from running commercial FEA or FDA packages in a conventional thermal analysis, where thermal boundary conditions are usually defined as temperatures on boundary surfaces as a function of time. For thermal analysis in most commercial packages, effects of decomposition reactions in materials at high temperatures are usually not included.

2.1.9 Stability criterion and Fourier Number in Heat Transfer Analysis

The suggested value of dimensionless Fourier number in heat transfer analysis when running this program is between 0.02 and 0.05 (if a value greater than 0.5 will be chosen

the model will be unstable (Croft et al., 1977)). These values are found suitable in most of cases with laminate thickness ranged from a few mm to about 25 mm. Reducing the value of the Fourier number may lead to an improvement in accuracy in predictions for a given time-step. However, the accumulative error in predictions may increase when using a larger number of time-steps. It exists a certain number of time-steps where the reduction in the error in each single time-step does not compensate for the additional error of the additional time-step. Compromise seems to be the right decision.

2.2 COMFIRE-50

COMFIRE has been translated in Matlab® and upgraded producing a COMFIRE-50 release with new functionalities:

- A Fourier number stability criterion check has been introduced;
- Number of total nodes for the discretisation can be chosen;
- Thermal conductivity and specific heat can vary with RRC and temperature;
- Constant initial heat transfer value can be input for the cold face boundary condition option (even forced convection could be modelled with the appropriate convective heat transfer);
- Optimisation can be performed at the script level of COMFIRE-50;
- A contact resistance cold face boundary option can be input and has been validated against the experimental data of Browne (2006), using a copper block heat sink as cold face boundary condition;
- A liquid heat sink of known volume and exposed face has been added to the cold face boundary condition option;
- Flashover phenomenon has been included as a HF boundary condition option;
- Mechanical model;
- FDS user guide validation.

2.2.1 Fourier number stability criterion routine check

The Fourier number is a dimensionless number which is a measure of the dimensionless time as previously mentioned. In the case of FDE the value of the Fourier number rules the stability of the FD model. It can be shown that depending on the boundary conditions the Fourier number has to be chosen in a certain range of values otherwise the model will result unstable (Croft et al., 1977) meaning that the transient solution may pass from a positive value of the temperature to a negative value and vice versa. This range depends on the boundary conditions as well and the different ranges are reported in Equation 2.19, Equation 2.20, Equation 2.21 and Equation 2.22.

$$Fo \leq 0.5 \quad \text{for conduction within the thickness} \quad \text{Equation 2.19}$$

$$Fo \leq \frac{1}{2(1 + Bi)} \quad \text{for convective boundary condition} \quad \text{Equation 2.20}$$

$$Fo \leq \frac{1}{2(1 + RT_0^3)} \quad \text{for radiative boundary condition} \quad \text{Equation 2.21}$$

$$Fo \leq \frac{1}{2(1 + Bi + RT_0^3)} \quad \text{for radiative and convective condition} \quad \text{Equation 2.22}$$

where Bi is the dimensionless number related to convection and the product RT_0^3 is the dimensionless number related to radiation. In particular $R = \varepsilon\sigma\Delta x/k$ and T_0 is the temperature of the CF [K]. The Fourier number links together the time increment and the space increment of the problem. Since the choice was made to always have 50 inner FD nodes, the Fourier number establishes the time increment used in the model, see Equation 2.23.

$$Fo = \alpha \Delta t / \Delta x^2$$

Equation 2.23

The software checks that the user input Fourier number is lower than any of the above expression and if it is not, it assigns to it the lowest value among all of them to avoid instability by user mistake.

2.2.2 Selectable number of total nodes for the discretisation

The number of total nodes in which to divide the thickness of the model has been inserted as a user input rather than a program constant. This update comes from the necessity to model very thin samples in a reasonable computational time. Using 51 nodes to model a very thin laminate will generate very little space increments, Δx , which turns into a very small time increment, see Equation 2.23, producing too many time-steps and increasing the computational time in an exponential manner. This phenomenon is highlighted in the particular case where the material properties are not taken as single points but as function of temperature and all the nodes material properties matrices have to be updated at every time-step. It is good practice not to do a spatial discretisation with space increments smaller than 0.2 mm. For thicknesses above 10 mm, 51 nodes can easily be used to reach a solution in a reasonable computational time. If the space increment is too small then the time increment will be too small generating a round-off error which makes the simulation non-realistic.

2.2.3 Thermal conductivity and specific heat temperature evolution

Thermal conductivity and specific heat change with respect to temperature and decomposition state of the composite. For this reason the following three options have been introduced in COMFIRE-50:

- Thermal properties function of temperature using polynomial functions;
- Thermal properties function of RRC using a modified rule of mixture;
- Thermal properties function of virgin and char material properties.

2.2.3.1 Thermal properties function of temperature using polynomial functions

Thermal conductivity and specific heat capacity can now be function of temperature as polynomial functions, rather than table format. Polynomial functions are very useful to fit experimental data and now thermal properties function of temperatures can now be used in COMFIRE-50 as input to obtain better results.

2.2.3.2 Thermal properties function of RRC using a modified rule of mixture

Density, thermal conductivity and specific heat capacity can now be updated during calculation according to RRC using a modified rule of mixture which takes into account the thermal properties of the decomposition gas products in the calculation as well, see Equation 2.24 to Equation 2.26 below. Similar thermal properties functions have been used in works by Bai et al. (2007), Bai et al. (2008), Mouritz and Gibson (2006b) and Sikoutris et al. (2012).

$$\rho = V_f \rho_f + V_m \rho_m + V_g \rho_g \quad \text{Equation 2.24}$$

$$k_{\perp} = \frac{k_f k_m k_g}{V_f k_m k_g + k_f V_m k_g + k_f k_m V_g} \quad \text{Equation 2.25}$$

$$c_p = \frac{V_f \rho_f c_{p,f} + V_m \rho_m c_{p,m} + V_g \rho_g c_{p,g}}{V_f \rho_f + V_m \rho_m + V_g \rho_g} \quad \text{Equation 2.26}$$

Here V is the volume fraction [%] of fibre, matrix and decomposition gas products for the subscripts f , m and g respectively; k is the thermal conductivity [$\text{W m}^{-1} \text{K}^{-1}$] of fibre, matrix and decomposition gas products for the subscripts f , m and g respectively; ρ is the density [kg m^{-3}] of fibre, matrix and decomposition gas products for the subscripts f , m and g respectively; c_p is the specific heat capacity [$\text{J kg}^{-1} \text{K}^{-1}$] of fibre, matrix and decomposition gas products for the subscripts f , m and g respectively. Thermal properties of fibre, matrix and gas decomposition products can be function of temperature as well.

Figure 2.2 shows an example of variation of thermal properties in function of RRC when the thermal properties of carbon fibres, epoxy resin and gas decomposition products have been considered single value properties according to Table 2.1. Hot air properties can be found in Gupta et al. (1991).

Table 2.1: Room temperature thermal properties used for prediction of thermal properties function of RRC.

	ρ [kg m ⁻³]	c_p [J kg ⁻¹ K ⁻¹]	k [W m ⁻¹ K ⁻¹]
Carbon fibres	1750	660	0.32
Epoxy matrix	1300	1850	0.35
gas	1.2	2386	0.02

The contribution of the gaseous products in the evaluation of the density and the specific heat capacity according to Equation 2.24 and Equation 2.26 is negligible and therefore in the program the density will only change according to RRC to simplify the calculation (as also done by Bai et al. (2008)). Thermal conductivity instead is highly dependent on considering the gases in the calculation or not therefore thermal conductivity has to be calculated according to Equation 2.25 (as also done by Bai et al. (2008)).

The values of the thermal properties in function of RRC in the two cases of taking into account the contribution of the gaseous products or not, are reported in Figure 2.2 and Figure 2.3 respectively. In the program density variation is calculated according to Arrhenius equation, since the influence of the gaseous products is negligible whereas thermal conductivity and specific heat capacity variations are calculated according to Equation 2.25 and Equation 2.26 since they are calculated out of the results of Arrhenius equation.

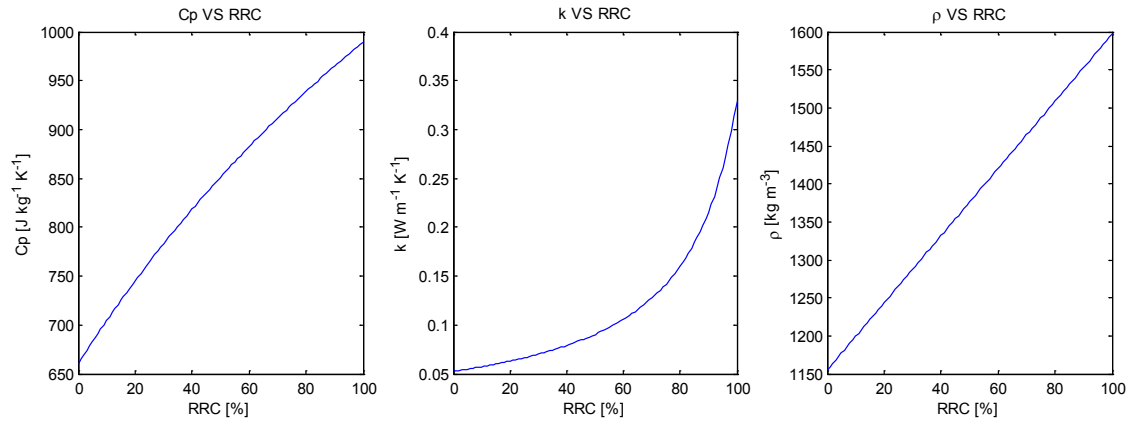


Figure 2.2: Example of thermal properties considered as single point value in respect to temperature but function of the RRC according to the modified rule of mixture in Equation 2.24 to Equation 2.26 using carbon fibre, epoxy resin and air properties at room temperature see Table 2.1.

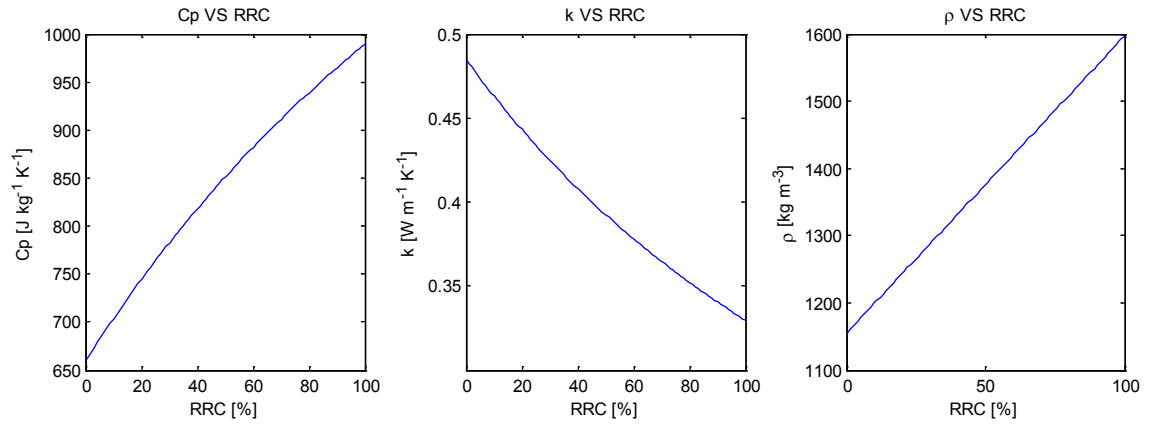


Figure 2.3: Example of thermal properties considered as single point value in respect to temperature but function of the RRC without considering the contribution of the gaseous decomposition products.

2.2.3.3 Thermal properties function of virgin and char material properties

Thermal conductivity and specific heat capacity can now be updated during calculation using the rule of mixtures applied to the material considered as homogeneous and composed just of virgin and char thermal properties, eventually function of temperature (Mouritz and Gibson, 2006);

$$k_{\perp} = \frac{k_v k_c}{V_v k_c + k_v (1 - V_v)} \quad \text{Equation 2.27}$$

$$c_p = c_{p,v} V_v + c_{p,c} (1 - V_v) \quad \text{Equation 2.28}$$

Here V_v is the volume fraction [%] of virgin material in the decomposing composite, k is the thermal conductivity [$\text{W m}^{-1} \text{K}^{-1}$] of virgin and char for the subscripts v and c respectively; c_p is the specific heat capacity [$\text{J kg}^{-1} \text{K}^{-1}$] of virgin and char for the subscripts v and c respectively.

$$V_v = \frac{m - m_f}{m_0 - m_f} \quad \text{Equation 2.29}$$

where m is the mass of the decomposing composite [kg], m_f is the final decomposed mass [kg], m_0 is the initial mass of the composite [kg].

Virgin and char thermal properties can also be function of temperature rather than just of the decomposition status, making predictions more accurate.

2.2.4 Constant initial heat convective transfer value

A constant initial convective heat transfer value can now be selected as an option on the cold face, to simulate the case where the cold face is in contact with a fluid and the convective boundary condition is known. The program will keep the cold face convective heat transfer as a constant value all the way during the calculation. This means that, as far as the convective heat transfer is known and constant, any fluid in contact with the cold face, whether in laminar or turbulent regime, can be modelled in any orientation so that forced convection can be taken into account as well.

2.2.5 Optimisation

If COMFIRE-50 is used at a Matlab® script level then it can be used for optimisation purposes. The variables that can be changed for the optimisation are the convective heat transfer and the decomposition constants used to model the resin decomposition with the Arrhenius equation. The results of every calculation can be compared with experimental data available and the best fit can be detected. Depending on the parameters to optimise, whether temperature profiles or TGA, then the ad hoc script needs to be written to get the best fit.

2.2.6 Contact resistance

COMFIRE-50 is capable of matching the experimental data of Browne et al. (2006) about the calibration of a propane burner heat flux through a copper block. It is assumed that during the calibration procedure the energy losses are negligible due to the surrounding insulation, see Figure 2.4.

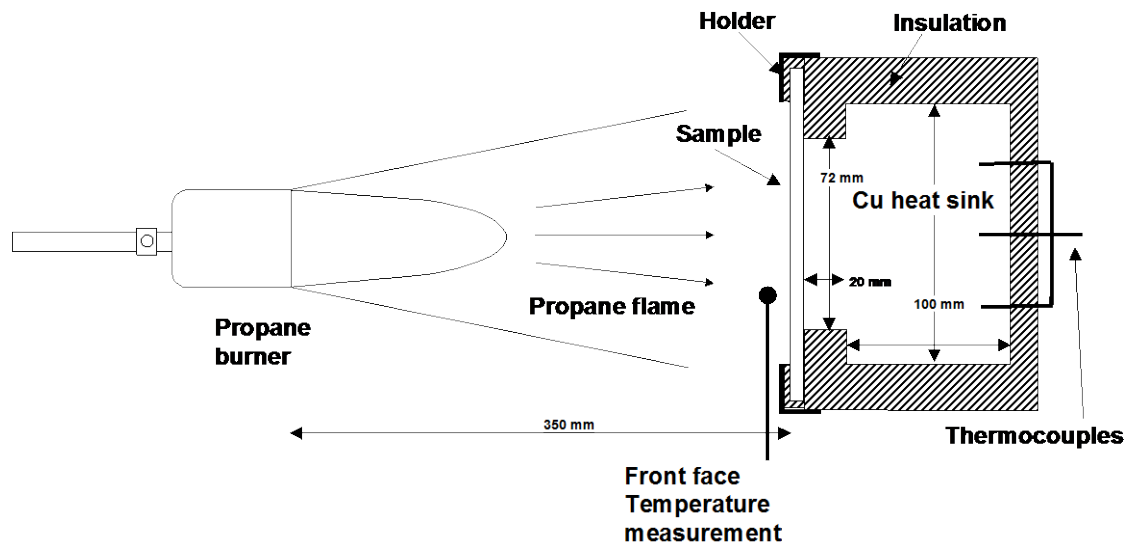


Figure 2.4: Copper block

The increase in temperature of the copper block during Δt time interval is calculated according to the Equation 2.30 below.

$$T' = \frac{Q_{CF} A \Delta t}{C_p V \rho} + T$$

Equation 2.30

where T' is the actual calculated temperature of the copper block after Δt [K], Q_{CF} is the heat flux from the cold face sample into the copper block [W m^{-2}], A is the contact area of the copper block [m^2], Δt [s] is the time-step used in the simulation, C_p is the specific heat of copper [$\text{W kg}^{-1} \text{K}^{-1}$], V is the volume of the copper block [m^3], ρ is the density of copper [kg m^{-3}] and T is the temperature of the copper block at the previous time-step [K].

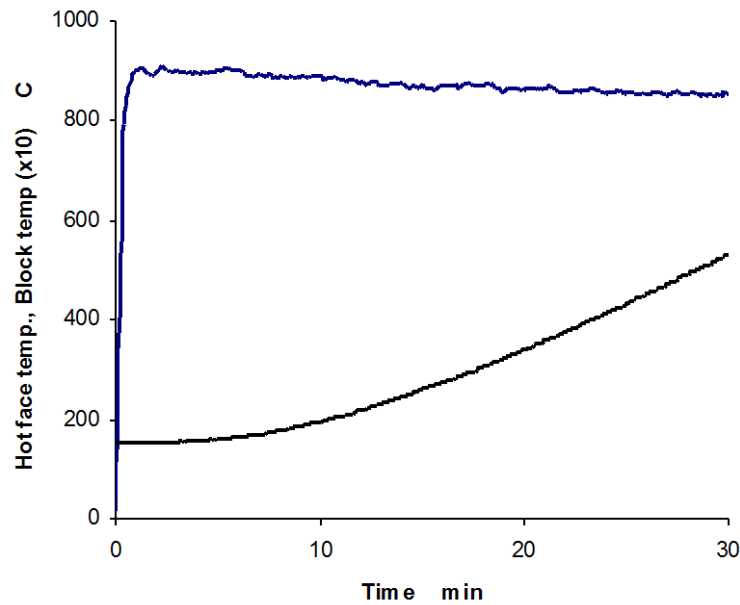


Figure 2.5: Thermocouple output from a 30 minute test on 7mm thick composite fire protection. Upper curve is the measured temperature 10 mm in front of the hot face (mean value 868°C). Lower curve: copper block temperature (multiplied by 10); figure reported from Browne et al. (2006).

The heat flux exchanged between the cold face of the sample and the exposed face of the copper block is calculated in the end of each time-step through the thermal gradient in the CF. The temperatures of the exposed face of the sample are reported in Figure 2.5. As input temperatures of the exposed face of the sample, the hydrocarbon curve has been used due to lack of experimental data. The hydrocarbon curve has a mean temperature of

1100 °C so it has been multiplied by a factor equal to 868/1100, to adjust for the highest temperature of the input file. In a first run the final temperature of the model was around 25 °C higher than the experimental data. This may be explained by the fact that the thermal contact between the cold face of the sample and the copper block surface was not a perfect thermal contact but a contact resistance affected the heat transfer. In a second model, a contact resistance has been inserted in between the two surfaces. The contact resistance is applied according to Equation 2.31.

$$\Delta T_{cont} = R_{cont} Q_{CF} \quad \text{Equation 2.31}$$

Thus the temperature previously calculated through Equation 2.30 can be recalculated as follows:

$$T' = T - \Delta T_{cont} \quad \text{Equation 2.32}$$

The value that allows matching the experimental results with the simulated results is a contact resistance of 0.0003 [m² K/W] (Cengel, 2003). This value is in the range of estimated contact resistances found in the literature (Croft et al., 1977 and Cengel, 2003).

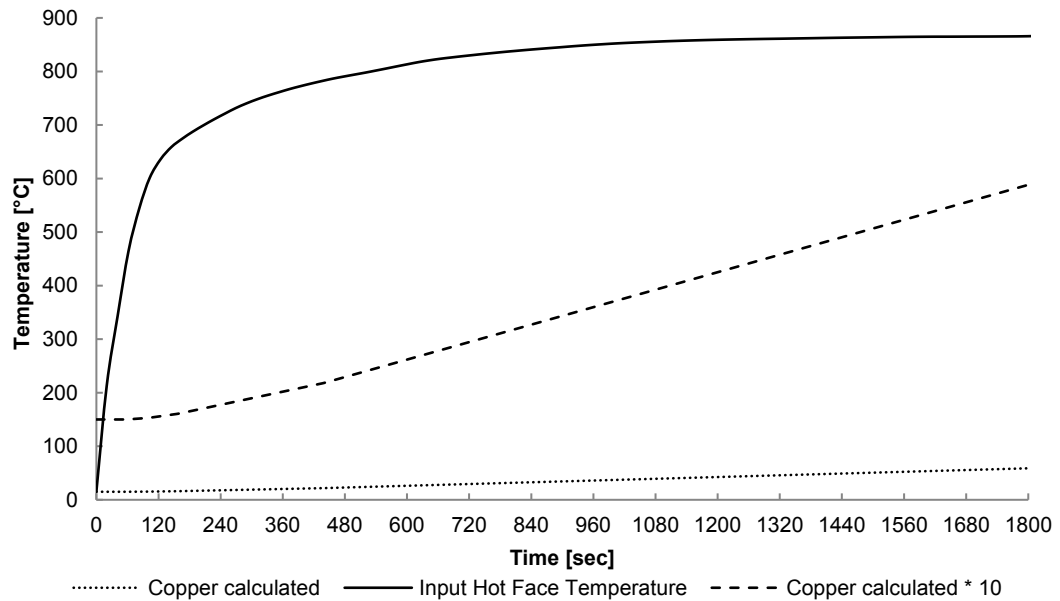


Figure 2.6: Temperatures for a 7 mm thick Glass -Polyester composite Fibres, $V_f= 30\%$.

The calculated temperatures of the model, with the contact resistance option enabled, are reported on Figure 2.6. The differences between the model and the measured temperatures cannot be evaluated point by point in quantity because of the lack of experimental data. Independently the difference between the final calculated temperature and the experimental final temperature is of around 4 °C higher than the evaluated experimental final temperature, which is around 54 °C, which is within experimental error.

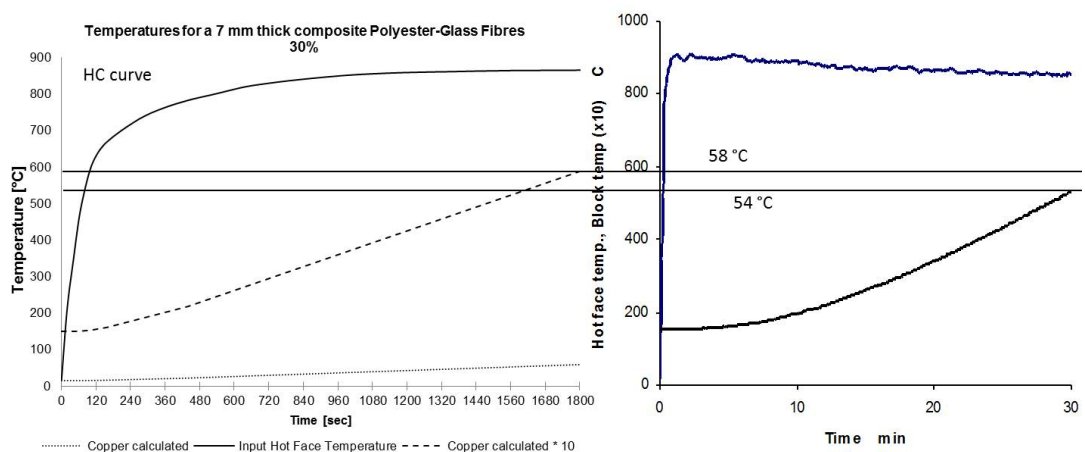


Figure 2.7: Comparison between experimental results and modelled results with COMFIRE-50.

2.2.7 Liquid heat sink

Sometimes it is important to know the temperature rise of a liquid which is in contact with the CF of a composite exposed to fire. An example would be the case of an aircraft post-crash fire scenario, where the flames are impinging on the wing box which contains the fuel. This is the reason why this option has been implemented. If the liquid heat sink boundary condition is selected, an input file has to be provided by the user with the following input parameters: exposed area [m^2], volume of the liquid [m^3], density of the liquid [kg m^{-3}], c_p of the liquid [$\text{J kg}^{-1} \text{K}^{-1}$].

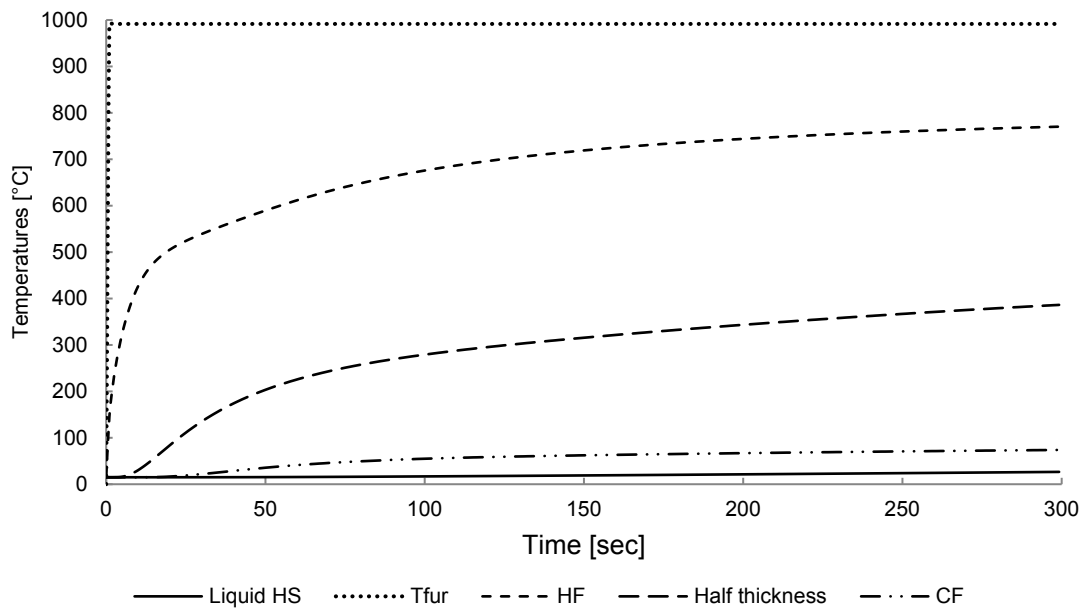


Figure 2.8: Liquid heat sink (HS) calculated temperatures through an epoxy-carbon laminate (66% fibre volume fraction) of 8 mm thickness, exposed to 116 kW m^{-2} heat flux.

Table 2.2: Liquid heat sink physical properties.

Parameter name	Value
Exposed area [m^2]	0.05
Liquid volume [m^3]	0.005
Liquid density [kg m^{-3}]	1000
c_p of the liquid [$\text{J kg}^{-1} \text{K}^{-1}$]	4200

A calculated temperature profile is shown in Figure 2.8. The heat sink was made of water with the characteristic reported in Table 2.2.

The numerical model adopted is the same as reported previously in Equation 2.30. Where the physical properties used are the one of the liquid and not the one of the copper. Although convective currents inside the liquid heat sink were not modelled, the modelled temperatures agree with the experimental curves.

2.2.8 Flashover

Flashover is an important phenomenon that occurs when, once the specimen has started decomposing and releasing flammable gases, the concentration of decomposition products in air has reached a critical value enough to be ignited. The flames due to ignition of those gases create an added heat flux towards the hot face. The temperature rise is steeper than not considering ignition feedback in the simulation.

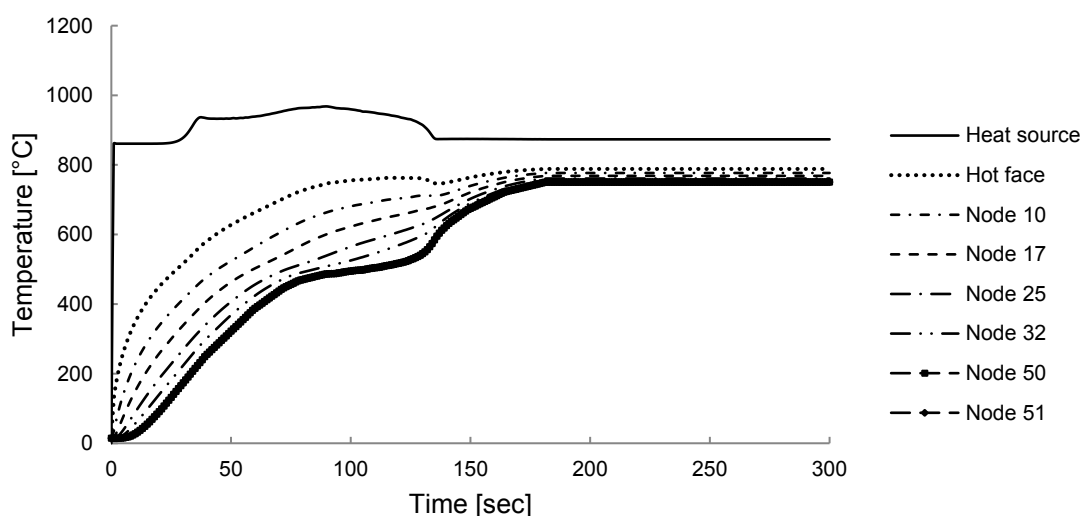


Figure 2.9: Temperature profile of a 3 mm thickness pure polycarbonate exposed to 75 kW m^{-2} on one side and insulated on the other side.

Once the gases are released out of the HF they ignite and they give a heat flux as feedback that is calculated according to Equation 2.33.

$$H_{ign} = \dot{m}_g H_{comb}$$

Equation 2.33

where m_g is the gaseous mass flow [$\text{kg s}^{-1} \text{m}^{-2}$] towards the hot face, H_{comb} is the heat of combustion [kJ kg^{-1}] and H_{ign} is the heat flux back to the HF [kW m^{-2}]. Figure 2.9 shows simulation results using data from the FDS user guide about pure polycarbonate with boundary conditions cone calorimetry testing condition. The ignition clearly affects the heat conduction through the sample as can be seen on Figure 2.9. The thermo-decomposition behaviour is affected by the temperatures and therefore ignition effects have to be taken into account to obtain accurate thermo-decomposition modelled results to be used in further thermo-mechanical modelling.

2.2.9 Mechanical response/model

Mechanical prediction has been added to COMFIRE-50 to predict compression failure of UD laminates loaded in the fibre direction. After the thermal model has finished the thermal prediction for every node and time-step, then a mechanical prediction is performed and the time to failure is calculated. The implemented mechanical models are two: the two layer model, for post-fire mechanical prediction, and the average strength model for mechanical prediction during fire (Mouritz and Gibson, 2006). There are several more sophisticated models that consider effects such as the effects of the stacking sequence of the laminate (Laminate Theory Model) and or to include creep, fire induced damage, viscoelastic and viscoplastic effects but they are out of the scope of this work.

2.2.9.1 Two layer model

The two layer model, see Figure 2.10, only applies for post-fire mechanical properties and not during fire, and assumes a char forming front advancing in the material from the fire exposed face towards the unexposed face (Gibson et al., 2003; Gibson et al., 2004; Mathys et al., 2002; Mouritz and Mathys, 1999; Mouritz and Mathys, 2001). It is usually assumed that once a node of material reaches 400°C or the polymer matrix mass loss reaches 20% then full decomposition occurs dropping the char mechanical properties to 0 or to a very low value, while the remaining part of the material is assumed to preserve

the virgin room temperature mechanical properties, since thermal softening is assumed to be fully recovered to the pre-fire state.

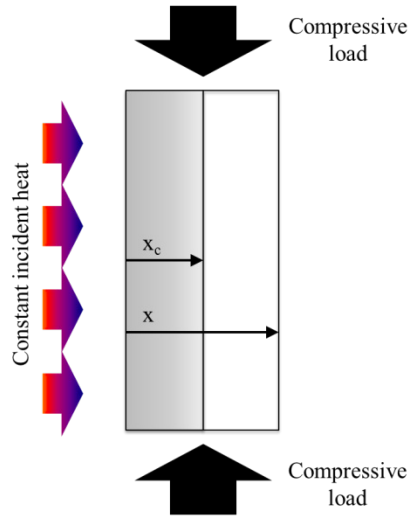


Figure 2.10: Schematic of the two layer model

The two layer model is represented in Equation 2.34 which is basically a rule of mixture applied to a material which changes the char content according to the fire exposure time. The final char thickness is function of the temperature reached in the nodes and the decomposition status in terms of RRC, according to the Arrhenius equation, and the time of exposure.

$$\sigma_{c(comp)}(T, RRC) = \sigma_{c(0)} \left(\frac{x - x_c(T, RRC)}{x} \right) + \frac{x_c}{x} \sigma_{c(char)} \quad \text{Equation 2.34}$$

where $\sigma_{c(comp)}$, $\sigma_{c(0)}$ and $\sigma_{c(char)}$ are the compressive strength of composite, virgin and char respectively [MPa], x and x_c are the thickness of the original composite and of the char portion respectively [mm].

This model is particularly suitable for post-fire compressive residual strength since it ignores the change of mechanical properties as function of temperature and as function

of time such as creep, viscoelasticity, viscoplasticity etc. Depending on the heat flux of the heating source the sample could be exposed for a very long time developing delamination or other fire damage induced phenomena and this model does not consider these factors for the mechanical prediction. Buckling failure is taken into account using Equation 2.35 and Equation 2.36 below.

$$E_{c(comp)}(T, RRC) = E_{c(0)} \left(\frac{x - x_c(T, RRC)}{x} \right) + \frac{x_c}{x} E_{c(char)} \quad \text{Equation 2.35}$$

$$P_{comp, Buckling} = \frac{C\pi^2 E_{c(comp)} b (x - x_c)^3}{12(KL)^2} \quad \text{Equation 2.36}$$

where $P_{comp, Buckling}$ is the buckling load [N], C is the end boundary condition constant, $E_{c(comp)}$, $E_{c(0)}$ and $E_{c(char)}$ are the compressive moduli of composite, virgin material and char respectively [MPa], x and x_c are the thicknesses of the original composite and of the char respectively [mm], b is the width [mm] and the product KL is the unsupported length [mm].

The time to failure by buckling is calculated by calculating the residual compressive modulus according to Equation 2.35 and comparing the corresponding stresses caused by the Eulerian buckling load, see Equation 2.36, to the increased applied stresses due to the virgin material thickness loss according to Equation 2.37.

$$\sigma'_{app} = \frac{\sigma_{app} x}{(x - x_c)} \quad \text{Equation 2.37}$$

where σ'_{app} is the revised applied stress [MPa] considering the loss of virgin material thickness during fire exposure, σ_{app} is the original constant applied stress [MPa].

2.2.9.2 Average strength model

The average strength model instead considers the laminate and its elastic characteristics as function of temperature and remaining resin content (RRC) and for this reason only applies for mechanical properties during fire and not post-fire. The model uses the mechanical properties in function of temperature using Gibson et al. (2006) model reported in the equation below.

$$P(T) = 0.5(P_U + P_R - (P_U - P_R)\tanh(k(T - T')))R^n \quad \text{Equation 2.38}$$

Here $P(T)$ represents a general composite property function of temperature and R remaining resin content, P_U and P_R are the unrelaxed and relaxed properties, k is constant representing the breath of the relaxation (the smaller, the wider), T' is the transition temperature (temperature corresponding to 50% reduction in property), R is the remaining resin content and n is an empirical constant.

Using Equation 2.38 the compressive strength of every node can be calculated in function of the temperature and the RRC in that node and then averaged along the whole thickness. The average residual compressive strength can be calculated through a trapezoidal numerical integration or using Simpson rule (Feih et al., 2007a; Feih et al., 2007b; Gibson et al., 2011). The trapezoidal integral was chosen for this program thanks to its simple implementation compared to the Simpson rule. The applied stresses are then compared to the average residual strength vs time of the composite and when the latter falls below the applied stresses, then the composite is supposed to fail. This model takes into account effects of mechanical properties in function of temperature but no other effects, such as time dependent softening and/or fire induced damage effects are considered.

Buckling failure is taken into account by averaging residual compressive modulus, calculated according to Equation 2.38, along the thickness and comparing the corresponding stresses caused by the Eulerian buckling load, see Equation 2.36, to the increased applied stresses due to the virgin thickness loss according to Equation 2.37.

2.3 COMFIRE-50-GUI

The program has then been integrated with a graphic user interface (GUI) to be more user friendly, then it has been compiled, creating an executable file that can be installed and run in any computer (either 32bit or 64bit) even though Matlab® and/or Matlab® license file are not installed.

2.3.1 *Installation*

It is not necessary to have Matlab® installed. In the case Matlab® is not installed, the Matlab Compiler Runtime (MCR) of the correct version (7.17 in this case)¹ has to be installed to run UICOMFIRE_50.exe. The MCR has not been included in the installation package because it would be too big to share by email or upload on the BAL.PM tool. The MCR may be of different versions in future developments but the correct information can be read on the readme.txt file that is created opening UICOMFIRE_50_1_6_pkg.exe of further upgrades.

The MCR can be downloaded from the following link to the Matlab official website (http://www.mathworks.co.uk/supportfiles/MCR_Runtime/R2012a/MCR_R2012a_installer.exe). There is no license to be bought, it is free and totally legal to be downloaded and used, for any additional information consult the website (http://www.mathworks.co.uk/products/compiler/mcr/index.html?s_cid=BB). Once it is downloaded, install the MCR following the installation wizard. Do not change the installation folder of the MCR and if asked to create the folder, just chose yes. Once the MCR is installed, the UICOMFIRE.exe file can be executed and a GUI like the one reported on Figure 2.11 will appear.

¹ The executable has been compiled in 32 bit to allow all machines to run it; this means that whatever the machine architecture is, the installed MCR has to be the 32 bit version.

2.3.2 I/O

As can be seen in Figure 2.11 the left part of the graphic user interface is entirely dedicated to the input parameters, while the right part is dedicated to the starting button, the exporting button and the visualization of the results of the simulation.

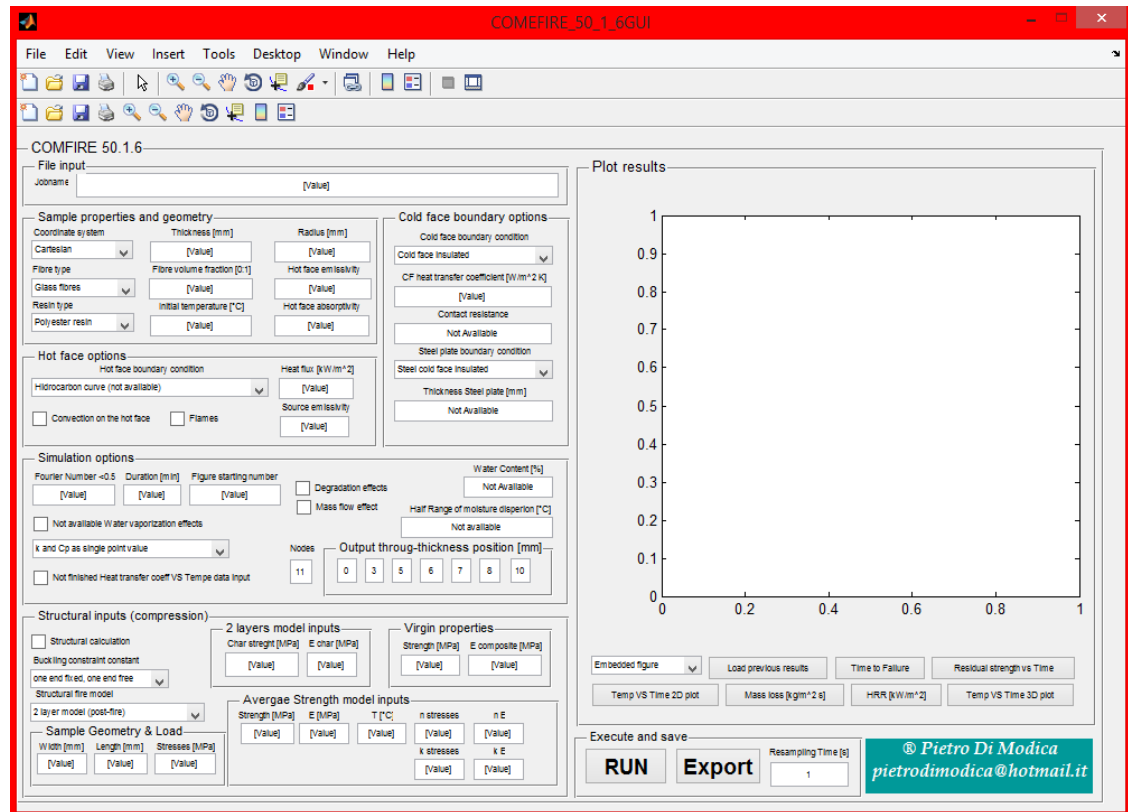


Figure 2.11: GUI of developed COMFIRE_50_1_6GUI.

The GUI needs to be filled in with the information of the case to be investigated. Details of the field are reported and explained in the table below:

Table 2.3: Input parameters and description of COMFIRE-50-GUI.

Field name	Information required	Suggestion
Jobname	Any string of characters used as the name of the file: “ Jobname <i>Results</i> <i>for sample_thickness_of_Thickness mm.mat</i> ”. The program will save a result file of the simulation in the same folder where it has been launched	
Coordinate system	Choose between “Cartesian” for flat geometry or “Cylindrical” for cylindrical symmetry	

Thickness [mm]	Thickness of the model in mm	
Radius [mm]	Outer radius of the model in mm	
Fibre type	Choose among a range of fibres whose properties are already embedded in a library or chose "Other" and a pup up window will appear and ask to insert all the physical properties required for the calculation.	
Fibre volume fraction [0:1]	Insert the fibre volume fraction of your material from 0 (0% so just resin) to 1 (100% of fibres).	
Hot face emissivity	Emissivity of the hot face from 0 to 1, typically around 0.8	
Resin type	Choose among a range of resin whose properties are already embedded in a library or chose "Other" and a pup up window will appear and ask to insert all the physical properties required for the calculation.	
Initial temperature [°C]	Insert the initial temperature of the model in °C.	
Hot face absorptivity	Absorptivity of the hot face from 0 to 1, typically around 0.8	
Hot face boundary condition	Choose among the boundary condition nearer to your case of study.	
Heat flux [kW m⁻²]	If the chosen boundary condition is of constant heat flux then enter the value of the heat flux.	
Source emissivity	Emissivity of the heating source from 0 to 1, typically around 0.8.	
Convection on the hot face	Tick if natural convection on the hot face has to be taken into account.	
Flames	Tick if flame feedback due to ignition of the hot gases on the hot face has to be taken into account.	
Cold face boundary condition	Choose among the boundary condition nearer to your case of study.	
Contact resistance [Km² W⁻¹]	If the model is in contact with the copper block a contact resistance may be inserted in the calculation.	
Steel plate boundary condition	If the "attached to a steel plate" boundary condition has been chosen then chose the cold face boundary condition on the steel plate.	
CF heat transfer coefficient	Insert the starting value of the cold face convection heat transfer coefficient.	
Thickness steel plate [mm]	Insert the thickness of the steel plate.	
Fourier number	Insert the Fourier number for the calculation.	Suggested values between 0.02 and 0.05, anyway no more than 0.5.
Duration [min]	Insert the duration of the simulation in minutes.	
Figure starting number		
Degradation effects	Tick if the degradation effects have to be taken into account in the calculation.	

Mass flow effects	Tick if the mass flow term has to be taken into account in the calculation.
Water vaporization	Tick if water vaporization effect has to be taken into account.
Water content [%]	Insert the percentage of water.
Half range of moisture dispersion [°C]	Typically 50
K and Cp vs Temperature	Tick if files containing thermal transport properties vs temperature are available.
Heat transfer coefficient vs Temperature	Tick if a file containing a table with heat transfer coefficient values vs temperature is available.
Nodes	Chose the nodes you want to display and save in the results file from 2 to 51.
Structural calculation	Tick if compressive structural calculation has to be performed
Buckling constraint constant	Chose the constraint type wanted
Structural fire model	Chose which structural fire model has to be used: 2 layer model or average strength model
Width [mm]	Insert sample width in mm
Length [mm]	Insert the sample length [mm] (mainly for buckling calculation)
Stresses [MPa]	Insert applied stresses [MPa]
Char strength [MPa]	Insert the strength of char [MPa]
E char [MPa]	Insert the char modulus [MPa]
Virgin properties Strength [MPa]	Insert the virgin unrelaxed composite strength [MPa]
Virgin properties E composite [MPa]	Insert the virgin unrelaxed composite modulus [MPa]
Average strength model Strength [MPa]	Insert the relaxed strength according to Gibson model [MPa], it can implement 3 transitions, insert up to 3 different values, each separated by a comma
Average strength model E [MPa]	Insert the relaxed modulus according to Gibson model [MPa], it can implement 3 transitions, insert up to 3 different values, each separated by a comma
Average strength model T [°C]	Insert the transition temperature, it can implement 3 transitions, insert up to 3 different values, each separated by a comma
Average strength model k stresses	Insert the stresses transition broadness parameter
Average strength model n stresses	Insert the stresses remaining resin content power parameter
Average strength model k E	Insert the modulus transition broadness parameter

Average strength model	Insert the modulus remaining resin content power
n E	parameter

The results file can be exported in various formats for further use: Matlab file “.mat”, Spreadsheet file “.xls”, Text file “.txt” and Comma Separated Values “.csv”. If results are exported in EXCEL, TXT or CSV format then the exported results will be saved as one point for every second. This is necessary since excel does not support spreadsheets longer than 1048575 rows, which is a number easily achieved with the typical Fo used.

Plots can also be generated in the GUI by pressing the button at the bottom of the plotting area. It can be chosen if the plot has to be generated in the GUI window or in a separate window through the popup menu below the figure.

Chapter 3 Experimental Techniques

To model fire behaviour of composites thermal and mechanical properties at high temperatures is essential. Accurate measurements of thermal properties at high temperatures are very important to accurately predict the thermal and mechanical response of a material/component exposed to high temperature environments. Furthermore, measurements of mechanical properties at high temperatures are as important to predict mechanical behaviour during fire. This chapter presents the methods employed in this study to measure thermal and mechanical properties at high temperature needed for modelling composites fire behaviour and the fire-under-load testing method used to validate model predictions.

3.1 Heat transport property characterisation

Heat transport properties are very important for understanding the behaviour of composites in fire. Composites are less conductive compared to metals but unfortunately composite materials degrade and lose strength at much lower temperatures than metals. Heat transport properties are thermal conduction, specific heat, density and thermal diffusivity. Although thermal diffusivity is the ratio of the previous three properties, its measurement as function of temperature is very important because it is the heat transport property used for thermal calculations in FEM codes such as ANSYS®.

Thermal diffusivity can be measured using different methods. One method is the TPS or Hot-Disk method which allows thermal diffusivity, thermal conductivity and specific heat capacity measurements in 2 principal directions using one test only provided that the sample has a cylindrical symmetry in the fibres orientation. Another method is the step-change method which measures thermal diffusivity in just one direction. A new and very expensive method to measure thermal diffusivity is the laser flash method which uses a laser to create the heat wave propagating in the material. None of the established, standardised methods to measure thermal transport properties was available and therefore the step-change method was used to measure thermal diffusivity. A summary of techniques to measure thermal transport properties is reported in Table 3.1

Table 3.1: Summary of techniques to measure thermal transport properties.

Methods	α	k	c_p
TPS/Hot Disk	✓	✓	✓
DSC			✓
Guarded hot plate		✓	
Laser flash	✓		✓
Step-change	✓		

Other ways of measuring the thermal diffusivity would be to measure thermal conductivity at different temperatures and in all the different principal directions, specific heat and density at the same temperatures of the thermal conductivity and then calculating the ratio of these three properties. The issue is that even considering the density as constant it requires a lot of effort to measure the other 2 properties separately. For the purpose of comparing the results from the step-change method, the guarded hot plate method was used to measure thermal conductivity and DSC was used to measure specific heat.

3.1.1 Step-change method

The step-change method developed in Newcastle University is based on the solution of the Laplace's equation, in the case of 1-dimensional heat flow in the laminate z-direction (through-thickness direction), Equation 3.1.

$$\dot{T} = \frac{1}{\rho(T)c_p(T)} k_z \frac{\partial^2 T}{\partial z^2} = \alpha_z \frac{\partial^2 T}{\partial z^2} \quad \text{Equation 3.1}$$

Where ρ is the density [kg m^{-3}], c_p is the specific heat [$\text{J kg}^{-1} \text{K}^{-1}$], k_z is the thermal conductivity in the generic z-direction [$\text{W m}^{-1} \text{K}^{-1}$], α_z is the thermal diffusivity in the generic z-direction.

The solution of a step-change experiment can be easily expressed in terms of the dimensionless centre line temperature, given by:

$$\theta(t) = \frac{T_{\infty} - T(t)}{T_{\infty} - T_0} \quad \text{Equation 3.2}$$

Where $T(t)$ is the centreline temperature at time t , T_0 is the initial uniform temperature in the slab and T_{∞} is the temperature suddenly imposed at the slab surface. θ , therefore, varies from 1, at the start of the test, to 0, at long times, regardless of whether the slab is heated or cooled. The principal factor determining the variation of temperature with time is the Fourier number, which is given by:

$$Fo = \frac{\alpha t}{b^2} \quad \text{Equation 3.3}$$

Here b is the slab half-thickness [m] (the distance from the surface to the centreline), t [s] is the time and α is the thermal diffusivity [$\text{m}^2 \text{s}^{-1}$] in the through-thickness direction. The Fourier number can be regarded as a dimensionless measure of time. In the well-known solution of Equation 3.1, for the case of the centreline temperature of an infinite plate, the centreline temperature of the slab is given by the Fourier series:

$$\theta = \frac{T_{\infty} - T}{T_{\infty} - T_0} = \frac{4}{\pi} \exp\left(-\frac{\pi^2 Fo}{4}\right) - \frac{4}{3\pi} \exp\left(-\frac{9\pi^2 Fo}{4}\right) + \frac{4}{5\pi} \exp\left(-\frac{25\pi^2 Fo}{4}\right) - \frac{4}{7\pi} \exp\left(-\frac{49\pi^2 Fo}{4}\right) \dots \quad \text{Equation 3.4}$$

For values of Fo exceeding ~ 0.2 this series can be truncated to the first term without significant loss of accuracy, so:

$$\theta = \frac{4}{\pi} \exp\left(-\frac{\pi^2 Fo}{4}\right)$$

Equation 3.5

This solution is restricted to the situation where the surface temperature is brought instantaneously to T_∞ . In practice it is seldom possible to change the surface temperature quickly enough to determine this boundary condition exactly. When the temperature change is accomplished through contact with a fluid, the rate of heat flow into or out of the solid is influenced by the coefficient for convective heat transfer at the surface. The relative importance of the resistance to surface heat transfer and the resistance to heat flow through the solid are described by the Biot number, which is given by:

$$Bi = \frac{hb}{k} = \frac{hb}{\rho C_p \alpha}$$

Equation 3.6

where h is the surface convective heat transfer coefficient [$\text{W m}^{-2} \text{K}^{-1}$] and k is the thermal conductivity of the material at the surface [$\text{W m}^{-1} \text{K}^{-1}$]. Bi can be regarded as the *resistance to internal heat flow*, divided by the *resistance to external heat flow*. A large value of Bi , exceeding about 100, would be required for Equation 3.5 to apply with sufficient accuracy to enable the thermal diffusivity to be calculated from such a step-change experiment. A small value of Bi , less than about 0.1, would correspond to the case where surface heat transfer was the main limiting effect. In this case the main temperature change would be through the film of fluid at the surface, with very little temperature variation across the solid. Although efforts were made in the present work to maximise the surface heat transfer coefficient the situation of $Bi > 100$ is difficult to achieve, so it was necessary to allow for the effect of surface resistance to heat flow. Heisler (1947) provided an analytical modification to Equation 3.1 that allows for this. In the case where $Fo > 0.2$, Equation 3.5 for the centreline temperature with Heisler (1947) modification becomes:

$$\theta = C \exp(-\zeta^2 Fo)$$

Equation 3.7

where ζ and C are functions of Bi . ζ relates to the roots of the following equation:

$$Bi = \zeta \tan \zeta$$

Equation 3.8

and

$$C = \frac{4 \sin \zeta}{2\zeta + \sin 2\zeta}$$

Equation 3.9

Equation 3.7 implies a linear relationship between $\log(1-\theta)$ and the Fourier number. It forms the basis of the well-known Heisler plots (Heisler, 1947) which were widely used for heat transfer calculations, and which still appear in many heat transfer books. Equation 3.8 poses the minor difficulty of having Bi as a function of ζ , rather than the reverse. The actual values of Bi encountered in the present study were in the range, 0.3-80.

For $-3 < \ln(Bi) < 3$, which correspond to $0.05 < Bi < 20$, Liukov (1968) proposed the following expression as an approximation of the first root of Equation 3.8:

$$\zeta = \frac{\frac{\pi}{2}}{\sqrt{1 + \left(\frac{2.24}{Bi^{1.02}}\right)}}$$

Equation 3.10

Although the equation is stable even for very small Bi , it gives acceptable values of ζ for $Bi \leq 100$. Below that the error in the estimate of ζ is greater than 1%. It is unknown the error introduced in the calculation of the Fourier coefficients, Equation 3.9.

Yovanovich (1996) showed that the expression reported below is capable of calculating with great accuracy the value of ζ for very large or very small Bi regardless of the values of the parameter n . In the intermediate range a suitable value of the parameter n has to be estimated to obtain an accurate relationship between ζ and Bi .

$$\zeta = \frac{\frac{\pi}{2}}{\left(1 + \left(\frac{\frac{\pi}{2}}{\sqrt{Bi}}\right)^n\right)^{\frac{1}{n}}}$$

Equation 3.11

In particular, in the range of $0.5 < Bi < 5$, ζ can be accurately described, with an error of less than 0.4%, by the following expression:

$$\zeta = \frac{\frac{\pi}{2}}{\left(1 + \left(\frac{\frac{\pi}{2}}{\sqrt{Bi}}\right)^{2.139}\right)^{\frac{1}{2.139}}}$$

Equation 3.12

Re-arranging Equation 3.7 gives the following direct relationship, which can be used to determine α from a step-change experiment.

$$\alpha = -\frac{b^2}{\zeta^2 t} \ln\left(\frac{\theta}{C}\right)$$

Equation 3.13

From each set of experimental measurements, three time values were calculated, corresponding to θ values of 0.4, 0.3 and 0.2. Equation 3.13 was used to find three values of α for each set of measurements, from which the mean value of α was taken. This relationship applies for heat flow in any of the three principal laminate directions, as long as one-dimensional heat flow conditions are achieved.

The calculation process involves an iterative step, since, from Equation 3.5, the thermal diffusivity or conductivity of the material must be known in order to calculate the Biot number. The iterative procedure is the following:

1. Estimate a value of ζ ;
2. Calculate Bi and C using Equation 3.8 and Equation 3.9 respectively;
3. Calculate the three thermal diffusivities corresponding to the times of the 40%, 30% and 20% of the dimensionless temperature curve using Equation 3.13;
4. Calculate the average of the three thermal diffusivities;
5. Calculate the thermal conductivity, if the density and specific heat are known, Equation 3.6;
6. Calculate Bi , Equation 3.6;
7. Calculate ζ , Equation 3.12;
8. If the initially estimated ζ is the same of the calculated one then the iteration is finished, otherwise restart from point 1 with a different value;

It has to be highlighted that known or estimated values of density and specific heat are required for this calculation at point 5. Considering the density as constant does not reflect on large errors, typically below 1%, see paragraph 4.2. Knowing specific heat versus temperature is very important to have good estimates of the thermal diffusivity.

Another parameter that has to be known or measured for this technique to be used is the convective heat transfer coefficient at the point 6.

A flat slab of a material with a high conductivity, such as an aluminium slab, can be used to measure the convective heat transfer coefficient provided that the step-change is small enough to consider Newton's law of cooling applicable. The slab can be considered as a lumped parameter system. In this case the solution of the dimensionless temperature can be written in the following exponential form:

$$\theta = 1 - \exp\left(-\frac{h}{b\rho c_p}\right) \quad \text{Equation 3.14}$$

By rearranging Equation 3.14 it can be shown that a linear relation exist between $\ln(1-\theta)$ and $-\frac{h}{b\rho c_p}$, with a simple linear regression the value of the convective heat transfer coefficient can be calculated.

To avoid measuring or estimate the density and specific heat, another procedure could be applied. The use of 2 samples of the same material but of two different thicknesses would allow finding the thermal diffusivity ignoring the heat capacity (ρc_p) of the material. The steps are the following:

1. Guess/estimate Bi for the thinner (thicker) sample;
2. Calculate ζ and C through Equation 3.12 and Equation 3.9 respectively;
3. Calculate the three thermal diffusivities, Equation 3.13, corresponding to the times of the 40% 30% and 20% of the dimensionless temperature curve;
4. Calculate the averages of the three thermal diffusivities;
5. Scale up Bi for the thicker (thinner) sample using Equation 3.6;
6. Calculate ζ , C and α as in points 2 to 4 for the thicker (thinner) sample;

7. Compare the thermal diffusivities found for the 2 different thicknesses and if necessary restart from point 1 with a different value of Bi ;

The convergence of the thermal diffusivities is found using Newton-Raphson method. The drawback of this technique is that the starting time (step time application) of the transient response has to be as accurately as possible recorded with the same accuracy for both experiments regarding the 2 different thicknesses. If an error is introduced, the procedure will not converge with a good accuracy on the correct thermal diffusivity value or may not converge at all.

3.1.2 Guarded hot plate

The guarded hot plate is an experimental method used to measure the thermal resistance of a material in a disk shape. The sample has to be cylindrical of a diameter of 50.8mm (corresponding to exactly 2 inches) with a thickness that can be adjusted to obtain the optimal range of thermal resistance to be measured.

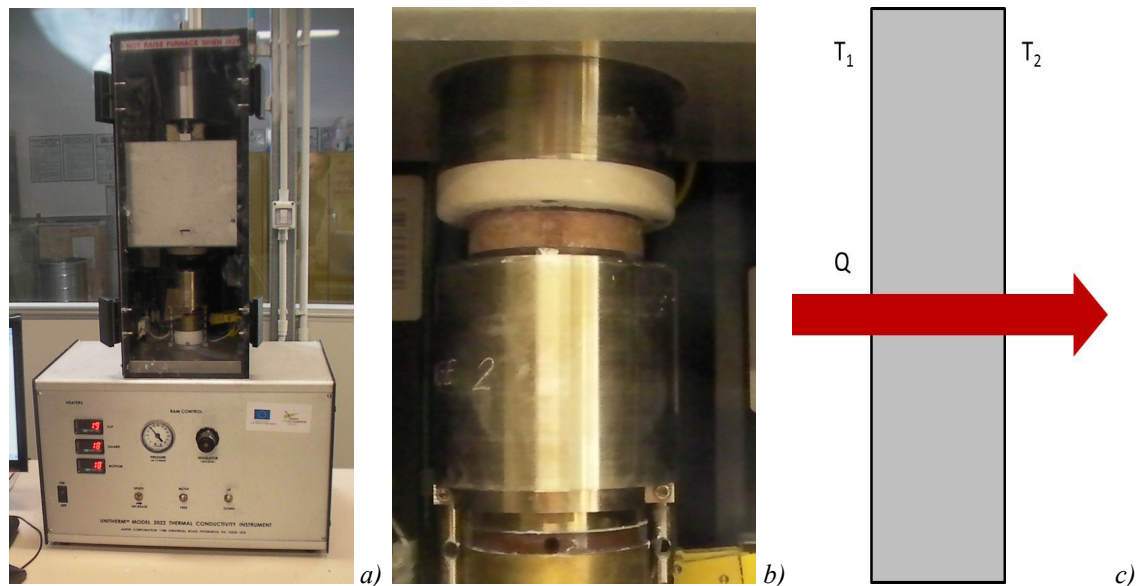


Figure 3.1: a) UNITHERM® model 2022 equipment for thermal resistance measurement (picture of Paolo Vollaro); b) sample positioning in the UNITHERM® model 2022 machine (picture of Paolo Vollaro); c) measuring principle diagram.

In this case, the UNITHERM® model 2022 (UNITHERM, 2006) was used to measure the thermal conductivity of the samples. The measuring principle is very similar to the one to measure electrical resistance. The sample is insulated on the sides and a temperature difference is applied to circular faces of the sample. Once the sample has reached the thermal equilibrium then the heat flow is measured with a heat flow meter and the thermal resistance is measured from that, see Equation 3.15. Thermal conductivity can be calculated from the thermal resistance, see Equation 3.16.

$$R = \frac{\Delta T}{Q}$$

Equation 3.15

$$k = \frac{d}{R}$$

Equation 3.16

Where R is the thermal resistance [$\text{W m}^{-2} \text{K}^{-1}$], ΔT is the temperature difference [K], Q is the heat flux measured through the sample [W m^{-2}], d is the thickness of the sample [m] and k is the thermal conductivity [$\text{W m}^{-1} \text{K}^{-1}$].

3.2 Mechanical characterisation

To model composite mechanical response to fire, mechanical characterisation needs to be performed at room temperature and high temperature as well. This characterisation represents the starting point in feeding the model in order to obtain an accurate response.

3.2.1 Mechanical tests at room temperature

The mechanical tests performed include tensile and compressive tests. The tensile tests have been performed according to BS EN ISO 527-5, 1997 using 2 mm/min crosshead speed. Trials were carried out at Newcastle University but due to the thickness and fibre orientation of the samples (2 mm) an adhesive with a very high lap-shear strength was necessary. Tests were then carried out by Cytec at their premises in Heanor

(Nottinghamshire, UK) because high lap-shear strength adhesive and adequate cutting tools were necessary to prepare the samples in order to successfully perform the tests.

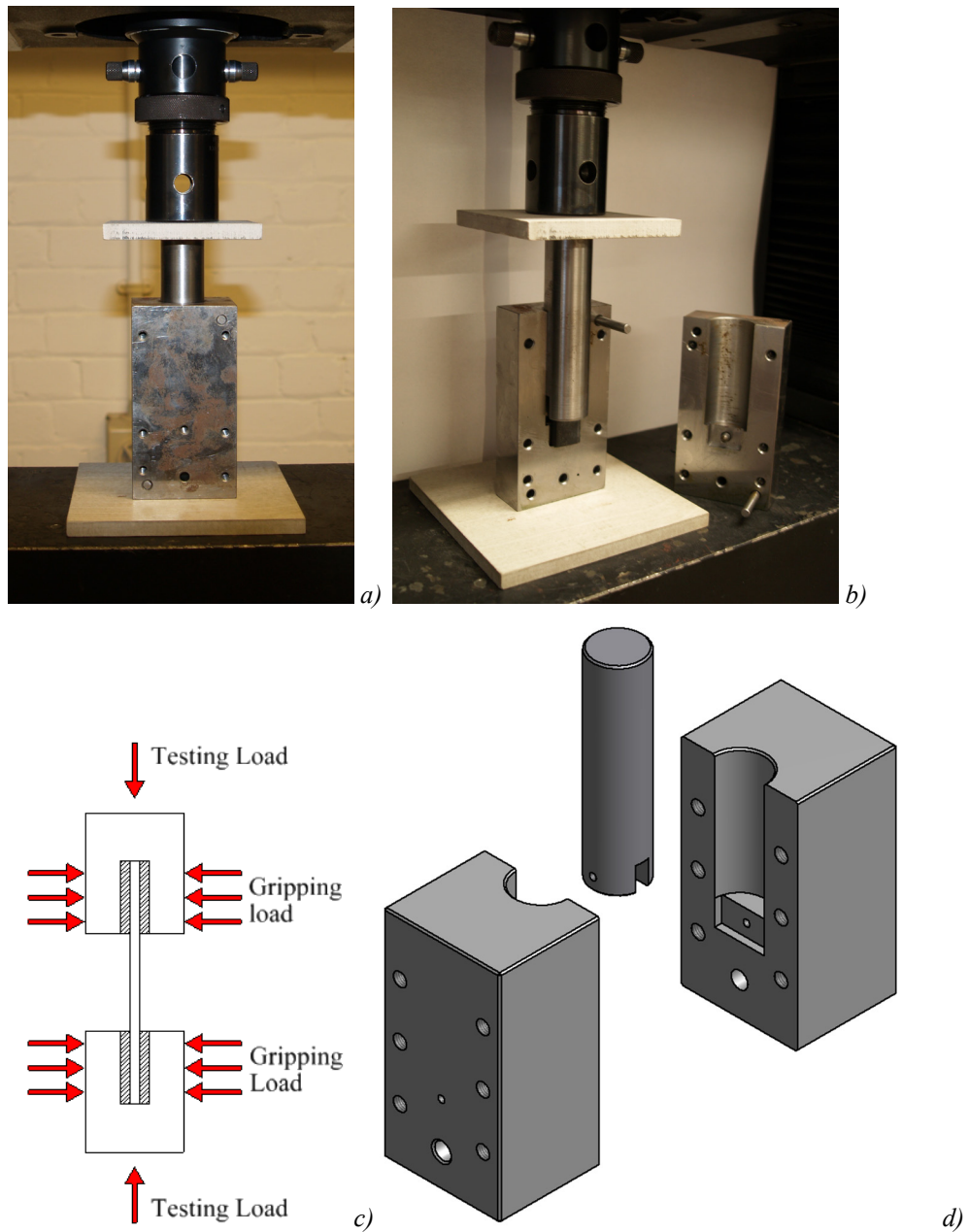


Figure 3.2: a) picture of the mounted compression test jig; b) picture showing the inside of the compression test jig; c) schematic of working principle according to BS EN ISO 14126 method 2; d) exploded view of CAD model of the compression test jig.

Due to short material availability just 10 samples of nominally 15 mm X 2 mm X 200 mm could be tested (one sample for each temperature). Compression strength tests were

performed at Newcastle University on small coupon size samples, nominally 40 mm X 25 mm X 2 mm, trying to replicate the condition described in BS EN ISO 14126 method 2, BS EN ISO 14126, 1999, see Figure 3.2 a) to d), using a crosshead speed of 2 mm/min. Also in this case due to shortage of material available no more than one sample could be tested. A grub screw was used to tighten the steel plates to the sample in order to apply enough load on the surface to avoid crushing of the edges during the tests as shown in Figure 3.2 c) and d). The Mechanical testing machine used was a hydraulic INSTRON model 8801 fitted with 100kN load cell, particular compression platens where not needed due to the perfect alignment of the piston-cylinder mechanism.

3.2.2 Mechanical tests at high temperature

The standardised method would require a furnace that would heat up not only the sample to be tested but the jaws as well, see Figure 3.3.



Figure 3.3: Tensile testing jaws enclosed in the furnace, picture taken at Cytec premises, Heanor, UK.

This means that the adhesive used to apply the tabs would also be at the same temperature of the furnace, which may cause pull out of the tabs since usually the lap shear strength of the adhesive used decays faster than the resin used for the composite manufacturing.

At Newcastle University an ad hoc solution to promote the localised heating up in the sample length has been designed, see Figure 3.4. It is made of 2 steel half jackets that surround the samples. The two half jackets are heated up by two cartridge heaters which inserted in a tight hole and powered up by a PID temperature controller which keeps the jackets temperature stable during the test. This solution allows heating up the sample length without heating up the tabs area and the jaws so that the adhesive keeps the same characteristics.

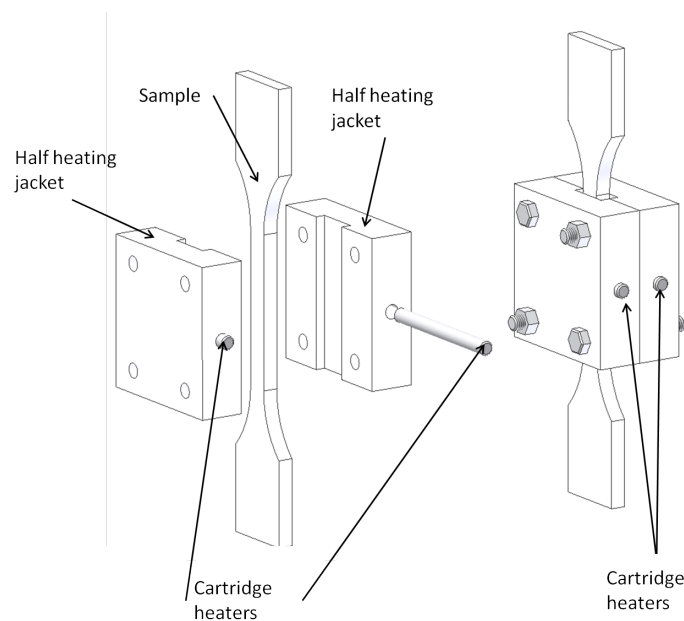


Figure 3.4: CAD model of the tensile test furnace adopted at Newcastle University: left side exploded view, assembled view; picture reproduced from (Browne et al., 2006).

Annotated pictures of the full testing setup are reported in Figure 3.5 a) where the furnace has also been insulated by wrapping it with Fiberfrax® and vacuum bagging film hold together with masking tape. The insulation allows for a more stable temperature profile, minimising the losses and protecting the mechanical testing machine and fixtures. Since the samples were rectangular, the furnace internal chamber allowed to slide in and out the samples to be tested. A thermocouple type K was attached to each sample to monitor the sample temperature and once the reading reached the furnace temperature the sample was left heating up for at least 15 mins before applying the tensile load. Tests have been performed from room temperature (around 20 °C) to 200 °C in steps of 20 °C. The insulation has proven to be very effective and in fact the masking tape adhesive did not

show any sign of degradation even at 200°C. Unfortunately the issue observed during the tests at room temperature was recurrent at high temperature as well; the tabs were pulled out during the tests so Cytec also performed the tensile tests at high temperature with the standardised method described above.

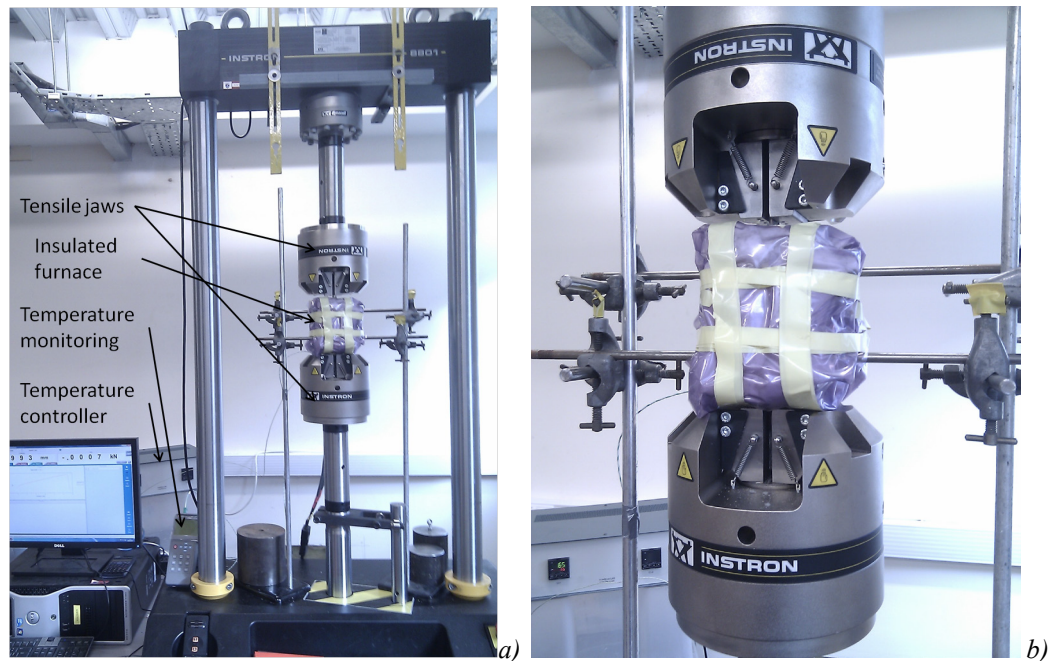


Figure 3.5: Tensile testing setup: a) annotated picture of the furnace thermally insulated with the sample inside ready to be tensile tested; b) detail of the insulated furnace.

Compression tests were performed using the same compression jig described before and reported in Figure 3.2 a) to d) where a cartridge heater and a PID temperature controller were used to bring the jig at the desired temperature to perform the tests. Measurements were taken at the same temperature chosen for the tensile tests at high temperature and the sample was left at the desired temperature for at least 15 minutes before applying the compression load.

3.2.3 DMA/DMTA

DMA was used to mechanically characterise the composite at various temperature. The machine, a PerkinElmer DMA8000, applies a sinusoidal stress or strain, see Equation 3.17 and Equation 3.18 respectively, and register the elastic and dumping response.

$$\sigma = \sigma_0 \sin(\omega t + \delta) \quad \text{Equation 3.17}$$

$$\varepsilon = \varepsilon_0 \sin(\omega t) \quad \text{Equation 3.18}$$

where t is the time [s], ω is the pulsation [rad/s] of the applied force and δ is the phase angle [rad] between stress and strain.

Polymers are materials with time dependent properties. Composites behaviour was investigated and since composites are partially made of polymer and partially made of elastic fibres (no aramid fibres were used) the behaviour will tend more to the elastic than to the plastic model, at least until a certain temperature. The storage modulus, see Equation 3.19, measures the stored energy which represents the elastic portion of the behaviour, whereas the loss modulus, Equation 3.20, measures the energy dissipated as heat and represents the viscous portion of the behaviour.

$$E' = \frac{\sigma_0}{\varepsilon_0} \cos(\delta) \quad \text{Equation 3.19}$$

$$E'' = \frac{\sigma_0}{\varepsilon_0} \sin(\delta) \quad \text{Equation 3.20}$$

The modulus of a viscoelastic material can be expressed using a complex notation as:

$$E = E' + iE'' \quad \text{Equation 3.21}$$

The Young modulus could be estimated from it calculating the modulus of the complex modulus. The output of the DMA are the stored modulus and the $tg(\delta)$. From these two measurements, all the necessary properties can be evaluated using the equations above. T_g of polymers can also be estimated through DMA measurements performing a so called “temperature scan”. The T_g is the temperature at which maximum of the $tg(\delta)$ curve occurs. The characterisation of the storage and the loss moduli at different temperature is the starting point to model the mechanical behaviour of a composite structure subjected to mechanical and thermal loads at the same time.

3.3 Fire under compressive load (time to failure)

Fire resistance properties characterise the capability of a material to withstand exposure to fire in terms of keeping structural integrity and/or hindering fire penetration and heat conduction throughout the material (fire barrier). Fire penetration/propagation is measured by the time it takes to reach a certain temperature on the non-exposed face of a component. Structural integrity on fire is usually measured by the time it takes for a component/sample to fail under a certain load. The test usually called fire-under-load test and the corresponding characteristic is called time to failure. The time to failure is the time the component can withstand the applied load under a fire before failure occurs.

The load could be of any kind but, since the lower mechanical characteristic is the compression strength, tests are usually performed under compression for whatever plies stack sequence used. In this work the focus was on fire-under-load test and measurement of time to failure at different heat fluxes and loads. The typical heat flux used in the aerospace standards is 116 kW m^{-2} . For other industries this may be different. In the present work tests were performed using 3 different heat fluxes 70, 116 and 180 kW m^{-2} . The applied load is a constant compressive load or stress that is reported as a percentage of the room temperature compressive failure load or strength of the material. The room temperature failure load is usually reported in the graphs as the load corresponding to the 0 time to failure.

3.3.1 Flame calibration

The heat flux calibration of the flame was performed following the principles suggested in ISO2685, 1998. The sample is substituted by a ceramic board and a type N thermocouple is positioned around 1cm far away from it. The gas is allowed to flow out of a Bullfinch and the pressure adjusted to obtain the temperature corresponding to the desired heat flux, according to the Stephan-Boltzmann relation, Equation 3.22. Once the temperature of the thermocouple is stable at the desired temperature the signal from the thermocouple is registered for at least 3 minutes. The recording is then analysed to be sure that the average temperature or heat flux falls in the allowed range for the test to be run.

$$\dot{q} = \varepsilon \sigma T^4 \quad \text{Equation 3.22}$$

where \dot{q} [W m^{-2}] is the heat flux radiated by the flames, ε is the emissivity of the flames typically between 0.7 and 0.9, σ is the Stephan-Boltzmann constant [$\text{W m}^{-2} \text{T}^{-4}$], and T is the temperature of the flames [K].

For the purpose of this study an average flame emissivity of 0.8 has been used. The final combinations of pressure-heat flux are reported in Table 3.2 below.

Table 3.2: Flame temperature and other propane gas circuit parameters calibration table to obtain the required heat fluxes of 70, 116 and 180kW m⁻²

Parameters		Values	
Heat flux [kW m^{-2}]	70	116	180
Flame temperature [$^{\circ}\text{C}$]	840	1000	1140
Cylinder regulator Pressure [bar]	Not legible due to the scale of the gage	≈ 0.2	≈ 0.8
Pressure gage [bar]	≈ 0.1 (0.08)	≈ 0.175 (3 lb in ⁻²)	≈ 0.6 (9 lb in ⁻²)
Gas flow [l min^{-1}]	Just below 6	≈ 9	≈ 13.5

The distance used between the Bullfinch burner and the sample surface was set at 320mm and never changed. Some adjustments were required in the height of the burner to compensate for the buoyancy effect of the flames.

3.3.2 Buckling

It has been considered whether to use anti-buckling guides, as reported by Browne et al. (2006) and in Figure 3.6, or not. Due to the dimensions of the test specimens, the compressive modulus of the material, see appendix 8.1, and the maximum loading capacity of the rig (300 kN), the buckling failure load would always be higher than either compressive strength at room temperature or the maximum loading capacity of the rig. For this reason tests were performed without anti-buckling guides.

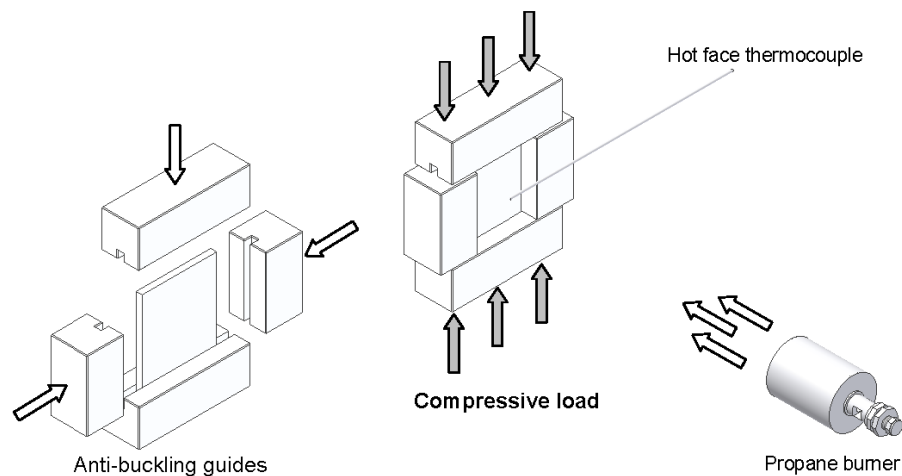


Figure 3.6: on the left schematic of compression tests sample mounting (note the anti-buckling guides); on the right schematic of sample ready for fire exposure under load, picture reproduced from Browne et al. (2006).

It is anyway recommended that compressive tests should always be performed using some anti-buckling guides, when available, following the same principle found in ASTM7137, 2012, which regulates the test to measure compression after impact (CAI) strength.

3.3.3 Testing procedure

Once the sample has been positioned between the two plates, see Figure 3.8 a), and the compression load is applied, the burner is lit and the test starts. Flame temperature, cold face temperature and load were recorded using an IOTech DAQ Shuttle 55 connected to a laptop. The three channels were monitored using the pDaqView software available for the DAQ device. The software allowed to monitor different sensors/transducers at the same time so the thermocouples were monitored using an internal subroutine whereas the load was measured by an ad hoc circuit and subroutine. Figure 3.7 shows a block diagram representing hydraulic and signal monitoring circuits of the in house compression testing machine used to perform fire tests.

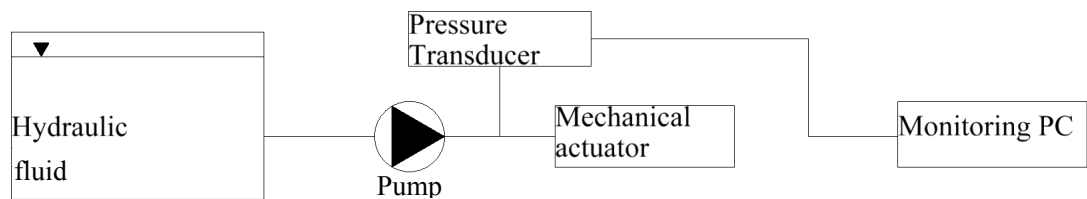
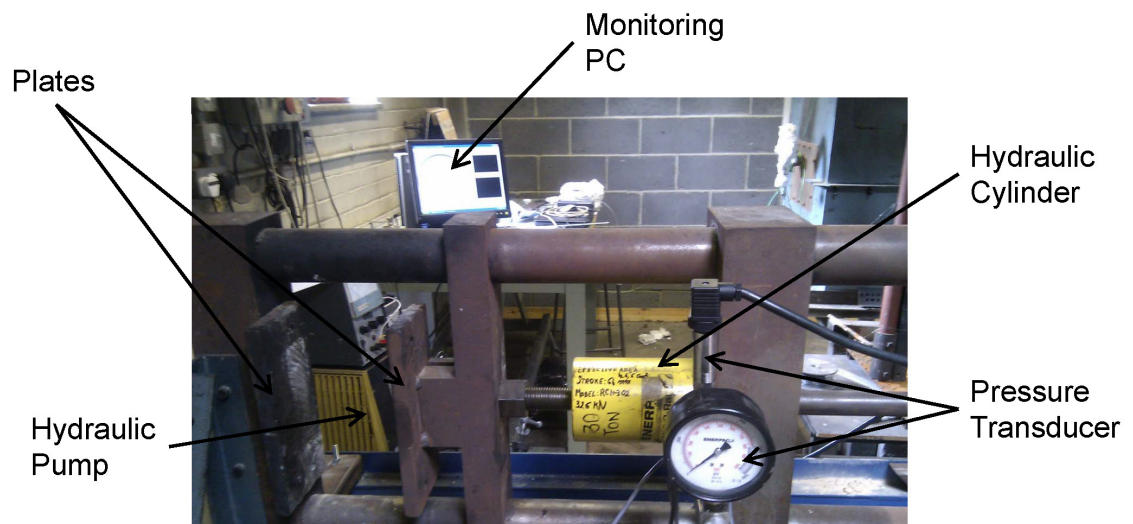


Figure 3.7: hydraulic and signal monitoring circuits block diagram of the in house compression testing machine used to perform fire tests.



a)

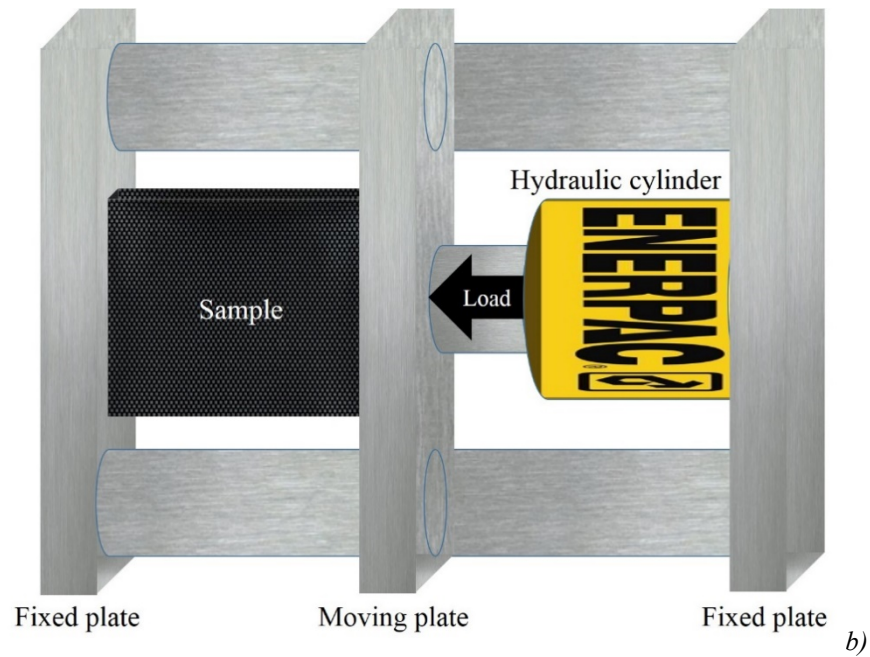


Figure 3.8 compression testing machine used to perform fire tests: a) annotated picture; b) simplified diagram.

The compression testing machine for fire testing is shown in Figure 3.8 a) and b) above. The hydraulic pump generates a constant hydraulic pressure at the inlet of the hollow hydraulic cylinder which then turns into a constant compressive load applied to the crosshead plate. In this way the sample sitting in between the 2 plates is subjected to a constant load, function of the constant pressure at the inlet of the hydraulic cylinder and the effective area according to Equation 3.23 below.

$$F = pA_{eff}$$

Equation 3.23

Where F is the applied load on the sample [N], p is the pressure at the cylinder inlet [N mm⁻²] and A_{eff} is the effective area of the cylinder, specified in the cylinder data sheet, [mm⁻²].

Chapter 4 **Material characterisation: thermal, mechanical and fire resistance properties**

In this chapter material characterisation is described. Thermal and mechanical properties have been measured at room temperature and at high temperature. Fire resistance has been measured in terms of time to failure as discussed previously in section 3.3.

4.1 Materials

Materials used for the thermal transport properties measurements and for the fire resistance characterisation are reported below:

- MTM44-1FR® 145gsm 12K HTS5631 UD (based on Tenax® –E HTS 5631 a family of PAN based high strength carbon fibre) laminates were supplied by Cytec®, laminates were cured according to manufacture datasheet (see paragraph 8.1) as unidirectional flat laminates, with approximate fibre volume fraction of 58.76%, and then used to make samples with the following nominal measurements of 100 mm x 100 mm x 10 mm for thermal diffusivity measurements and fire-under-load tests, 100 mm x 100 mm x 8 mm for thermal diffusivity measurements, 200 mm x 15 mm x 2 mm for tensile tests, 40 mm x 25 mm x 2 mm for compression tests, 50 mm x 5 mm x 2 mm for DMA tests and Ø50.8 mm x 10 mm for thermal conductivity tests;
- CEMTHERM® board, a rigid non-flammable ceramic material with a very low conductivity used for insulation purpose;
- Thermocouples Type-K for temperature measurements;
- Heat transfer compound to improve thermal contact between the thermocouple tip and the sample unexposed surface;
- Araldite®2015 for longitudinal CFRP sample manufacturing, thermocouple and insulation installation.

4.2 Thermal characterisation

Thermal characterisation was performed on a unidirectional carbon-epoxy system, MTM44-1FR® supplied by Cytec®. The orthotropy of the material required measurements in the two principal directions, longitudinal and transverse direction. The samples manufactured by Cytec were in the shape of a flat slab of 100 mm x 100 mm x 10 mm, see Figure 4.1 a). To measure the properties in the longitudinal direction, the slab was cut across the fibres to obtain long stripes in the transverse direction. Each stripe was then rotated of 90° around their length and reassembled stacking every stripe in a way to obtain a sample which had the fibres coming out of the exposed surface, see Figure 4.1 b). The samples were instrumented with a thermocouple type K measuring the centre line temperature and insulated all around with 10 mm thick CEMTHERM® board, see Figure 4.1. To promote the thermal contact between the thermocouple and the specimen a heat transfer compound was used.

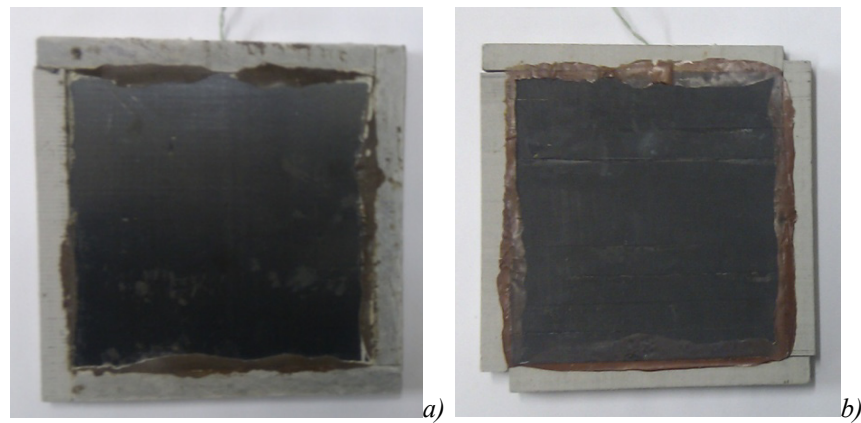


Figure 4.1: CFRP sample ready for thermal diffusivity measurements: a) through-thickness direction; b) along the fibres.

To apply the step-change the samples were left 12 hours or more inside a temperature controlled chamber at a certain temperature (T_0) to reach thermal equilibrium, then very quickly transferred to a temperature controlled agitated water bath at a new temperature (T_∞). The recirculation of the water ensured the highest possible convective heat transfer coefficient to apply the step-change method, see section 3.1.1. For temperatures higher than 100 °C, a fluidised sand bath was used instead of the water bath.

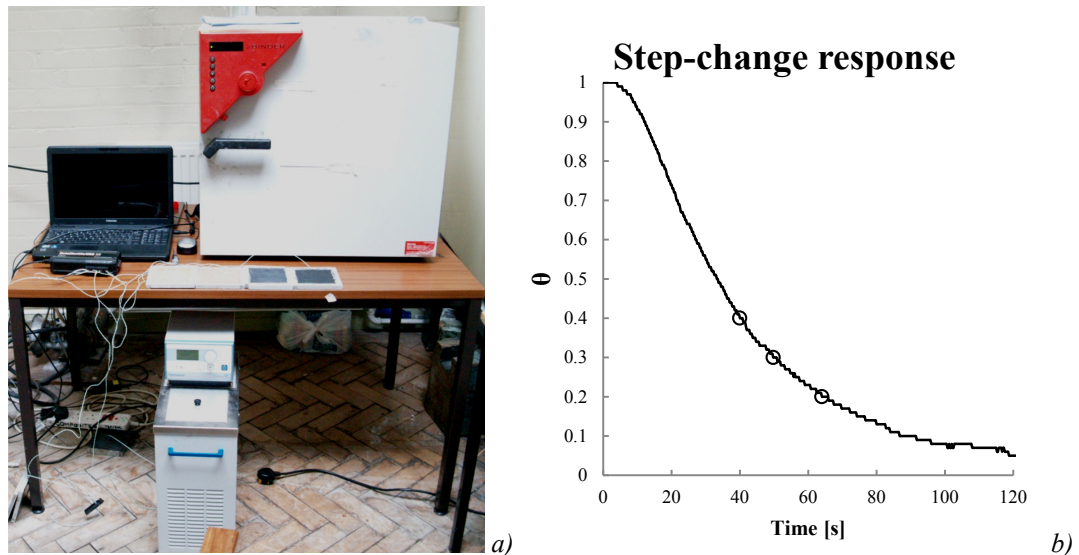


Figure 4.2: a) Step-change experiment setup picture: temperature controlled environment, DAQ-PC system, digital temperature controlled agitated water bath and samples; b) typical step-change temperature curve used for thermal diffusivity calculation.

The measured property was quoted at the average of the temperatures used for the step-change. The step needed to be small enough to consider the thermal diffusivity, as well as the other thermal properties, and constant during the experiment, but large enough to be sensed by the thermocouple. Acceptable step amplitudes were found in practice to be between 10 °C and 20 °C. To record the transient thermal response an IOTech DAQ Shuttle 55 was used. During each experiment the sample centreline temperature and the water bath temperature were recorded at a sampling frequency of 4 Hz. Three replicates were performed for each specimen at each temperature step. From each transient response the thermal diffusivity was measured according to section 3.1.1 (either with one thickness sample routine or with two different sample thicknesses routine) and then the average of the three thermal diffusivities was taken as the thermal diffusivity of the material at the average of the temperature step. Thermal conductivity was estimated using Equation 1.7 where the density has been considered as constant and found to be equal to 1498 kg m⁻³ using specific gravity bottle (manufacturer nominal density is 1520 kg m⁻³). The specific heat, as function of temperature, has been calculated using Equation 4.1 as result of DSC measurements performed by SP in the Fire Resist project (Sjöström, 2013). Similar curves with similar values have been reported for similar material in the same range of temperatures of this study by Kalogiannakis et al. (2004).

$$c_p = 3.10 * T + 885.65$$

Equation 4.1

where c_p is the specific heat [$\text{J kg}^{-1} \text{K}^{-1}$] and T is the temperature [$^{\circ}\text{C}$].

A comparison between the transverse thermal diffusivity results obtained using just one sample, of 10 mm thickness, and two samples of different thickness, 10 and 8 mm thick, is reported in Figure 4.3 below. It shows that the two methods are comparable and results agree with each other and with results found in literature by Fanucci, (1987), Kalogiannakis et al. (2004), Mouritz et al. (2006), Pilling et al. (1979) and Rolfes and Hammerschmidt (1995), on similar materials in the same range of temperatures used in this study. For this reason the other measurements have been performed using just one thickness sample technique, the above mentioned constant density and SP measured c_p , reported in Equation 4.1.

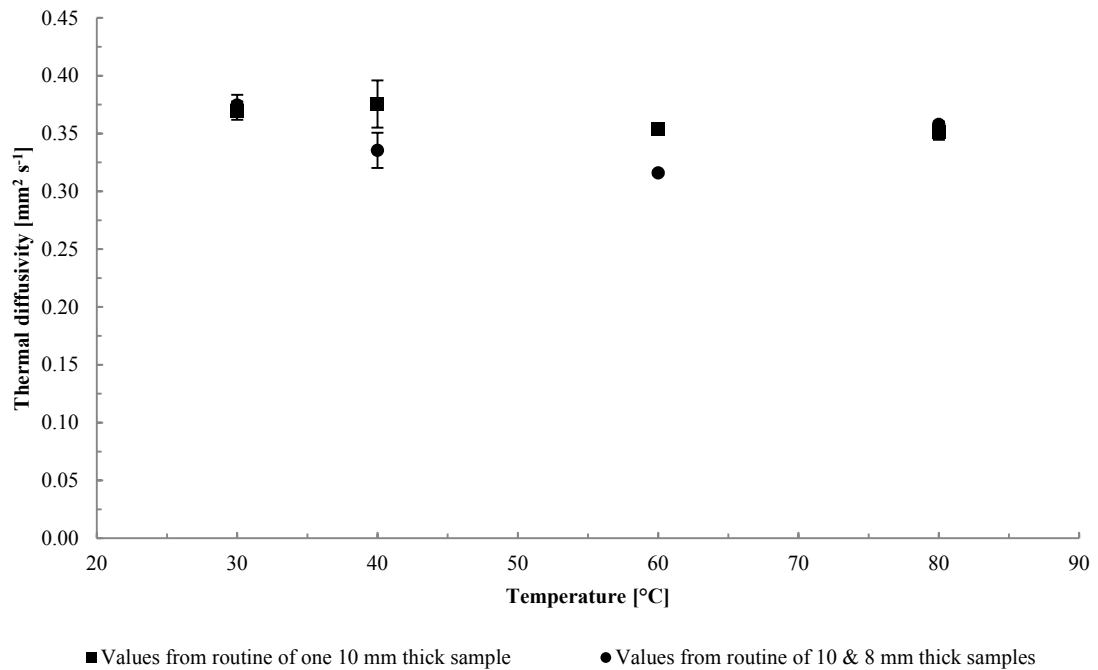


Figure 4.3: Comparison of transverse thermal diffusivity measured using the step-change method with one thickness sample of 10 mm, using c_p according to Equation 4.1, and two different thicknesses of 10 and 8 mm; error bars represent deviation from the average value.

Although measurements above 100°C were performed, their results are not reported due to large errors introduced by the fluidised sand bath. These errors are most likely due to the fact that the fluidised sand bath heat transfer coefficient is not high enough for the mathematical solution to be valid. In addition to that, it has been observed during measurements of the heat transfer coefficient using an aluminium slab, that if the sample is not properly shaken during the test while immersed in the fluidised sand bath, a sand boundary layer may be formed. This phenomenon changes the heat transfer from convection to conduction and invalidates the analysis of the test results.

Additional sources of measurements errors might include:

- the thermocouple delay response time;
- the thermocouple non-perfectly centred in the middle plane;
- the transition time from the high temperature environment to the water bath;
- the recording of starting time of the step temperature and;
- the density and c_p values function of temperature.

The error regarding the delay response time has been minimised by using thermocouples with a very small tip (no more than 0.3 mm probe diameter) to minimise the delay in the response time and at the same time allowing a very tight fitting to the drilled hole which was filled with thermal conductive paste to improve thermal contact. This may have caused the starting time to be recorded with a small delay typically between 0.1 and 0.5s.

If the thermocouple is not perfectly placed at half the thickness, an error is introduced in the evaluation of the thermal diffusivity starting from Equation 3.4 which is valid just for the centre line temperature. In this case an additional term would be needed in the solution which makes the calculation a bit more complicated, adding a periodic term to the solution, which is function of the coordinate of the measuring point and the convective heat transfer coefficient. The error regarding the non-perfectly centred thermocouple was

minimised by paying particular attention to drilling the hole as centred as possible to the middle plane of the sample.

The error regarding the transition time between the high temperature environment and the water bath was minimised by minimising the distance between the two environments and by moving the sample as fast as possible between the two environments. A very short initial transient response in air may be caused by this error. However, thanks to the very low convective heat transfer in air and to the very short time the sample was subjected to this undesired transitory, the associated error is considered as negligible.

The starting time was recorded by taking note of the scan number when the sample touched the water, which might have caused a maximum of 1 s delay in recording the actual transient starting time.

Regarding the error caused by considering the density constant, it can be easily shown to be negligible following the Equation 4.2 below.

$$\begin{aligned} \left\{ \begin{array}{l} \rho_0 = m_0/V_0 \\ V_0 = abc \end{array} \right. &\Rightarrow \left\{ \begin{array}{l} \rho_f = m_0/V_f \\ V_f = a(1 + \beta_{11}\Delta T)b(1 + \beta_{22}\Delta T)c(1 + \beta_{33}\Delta T) \end{array} \right. \Rightarrow \\ &\Rightarrow \left\{ \begin{array}{l} \rho_f = m_0/V_f \\ V_f \approx V_0(1 + \beta_{11}\Delta T)(1 + 2\beta_{22}\Delta T) \end{array} \right. \Rightarrow \left\{ \begin{array}{l} \rho_f = m_0/V_f \\ V_f \approx V_0[1 + (\beta_{11} + 2\beta_{22})\Delta T] \end{array} \right. \end{aligned} \quad \text{Equation 4.2}$$

where ρ_0 and ρ_f are the initial and final densities respectively [kg m^{-3}], m_0 is the initial mass [kg], V_0 and V_f are the initial and final volumes respectively [m^3], a , b and c are the dimension of the generic slab respectively [m], ΔT is the temperature increase [K], and β_{11} , β_{22} and β_{33} are the linear longitudinal and transverse expansion coefficients respectively [K^{-1}].

Assuming that decomposition reactions do not occur in the range of temperatures of this study, the density decreases linearly with temperature (see Figure 4.4) with a factor of, in first approximation, twice the transverse linear thermal expansion coefficient which, for high strength carbon fibre reinforced polymers with a volume fraction of around 60%, is in the range of 25 to $30 \times 10^{-6} \text{ [K}^{-1}]$ since the longitudinal linear thermal expansion coefficient is negligible and between -0.25 and $-0.3 \times 10^{-6} \text{ K}^{-1}$ (Bowles and Tompkins, 1989; Karadeniz and Kumlutas, 2007; Rogers et al., 1977; Yates et al., 1978a; Yates et al., 1978b). Considering the linear thermal expansion coefficients as constant at the highest values, it can be observed that the assumption of constant density in the range of temperature used in this study corresponds to an overestimation of the density of less than 0.6%, this proves it is negligible for the purpose of this study. Since c_p values as function of temperature have been used in this work, there are no associated correlated errors affecting this work and for this reason its influence will not be considered further.

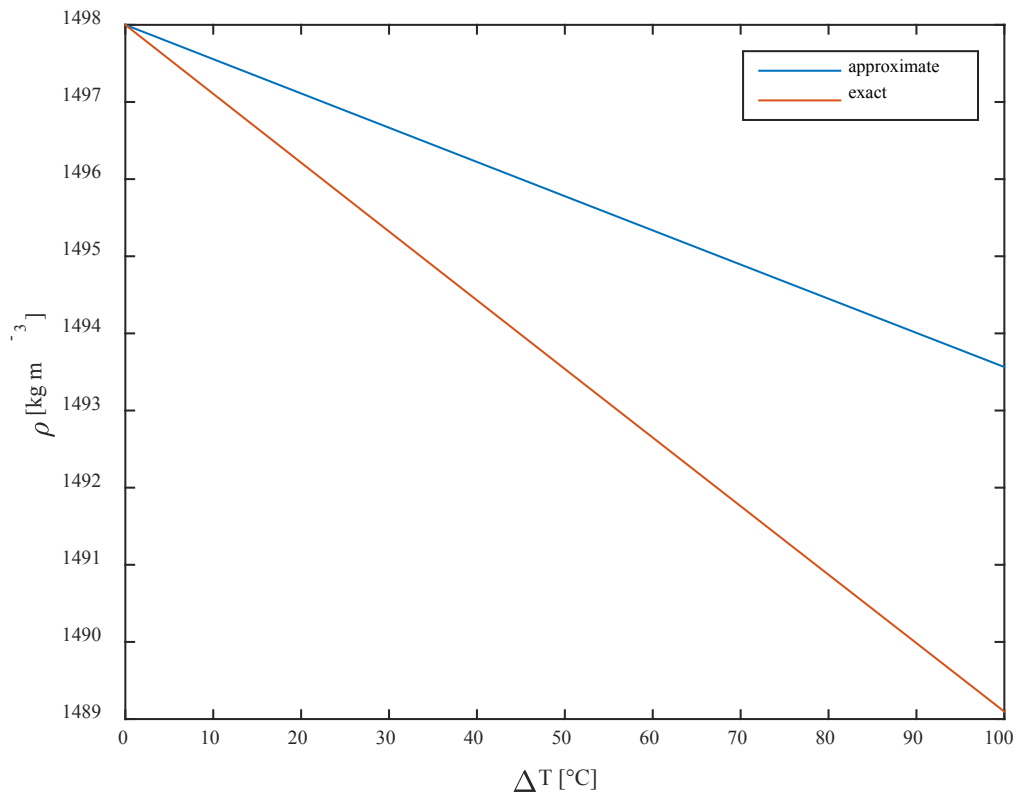


Figure 4.4: Approximate and exact density variation in function of ΔT according to Equation 4.2.

The overall error among the transverse thermal diffusivity measurements at each temperature is anyway within $\pm 5\%$ of the measured values as it is shown in Table 4.1 below and it is considered satisfactory enough for the purpose of this work.

Table 4.1: Through-thickness thermal diffusivity (α), its deviation from average and error [%] using 1 thickness technique (10 mm thick sample) and 2 thicknesses technique (10 and 8 mm thick samples).

Temperature [C]	1 sample			2 samples		
	α [mm ² s ⁻¹]	Deviation [mm ² s ⁻¹]	Error [%]	α [mm ² s ⁻¹]	Deviation [mm ² s ⁻¹]	Error [%]
30	0.370	± 0.008	± 2.15	0.375	± 0.009	± 2.36
40	0.376	± 0.020	± 5.44	0.347	± 0.011	± 3.08
60	0.354	± 0.003	± 0.85	0.316	± 0.002	± 0.55
80	0.351	± 0.007	± 1.91	0.358	± 0.002	± 0.70

Furthermore, the error in using the manufacturer declared density of 1520 kg m⁻³ rather than the measured value of 1498.88 kg m⁻³ was investigated (see Figure 4.5 and Figure 4.6) and the overall error is within $\pm 3.5\%$ for both the through-thickness and in plane thermal diffusivity, $\pm 2\%$ for the through-thickness thermal conductivity and $\pm 5\%$ for the in plane thermal conductivity. The actual error in the measured thermal diffusivity introduced by using nominal density, rather than the measured one, on the routine using just one sample of 10mm thickness, would be equal or inferior to 0.003-0.004 mm² s⁻¹ (lower or equal to 1% of the actual measurements). This proves that accurate measured values of density of the tested sample are not critical to measure thermal diffusivity using the step-change technique as long as a good estimate or manufacturer nominal density value is available.

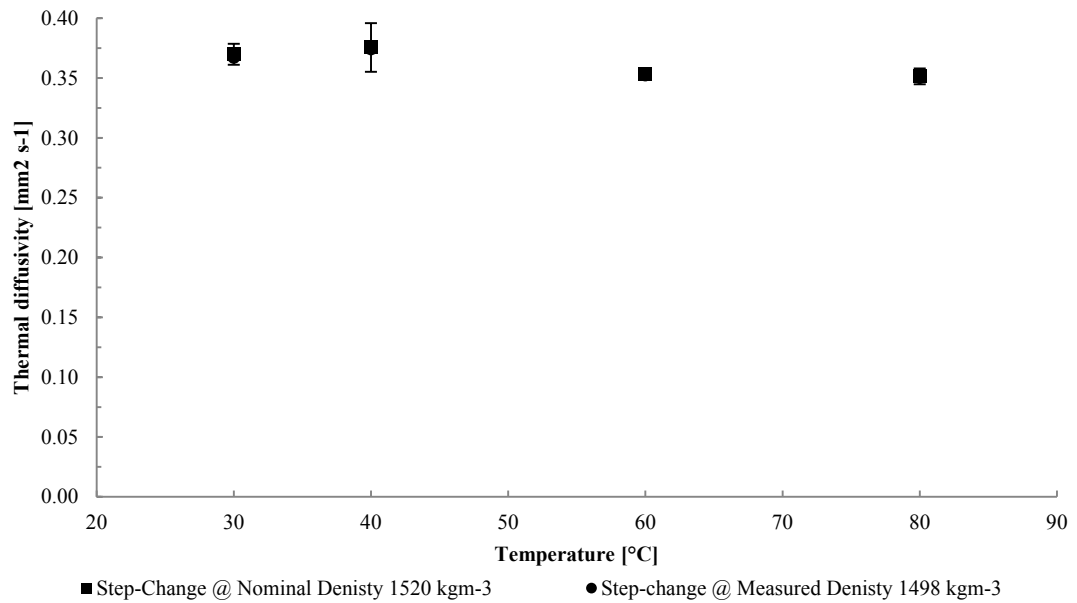


Figure 4.5: Through-thickness thermal diffusivity measurements comparison using nominal and measured density using step-change technique using just one thickness of 10mm; error bars represent deviation from average values.

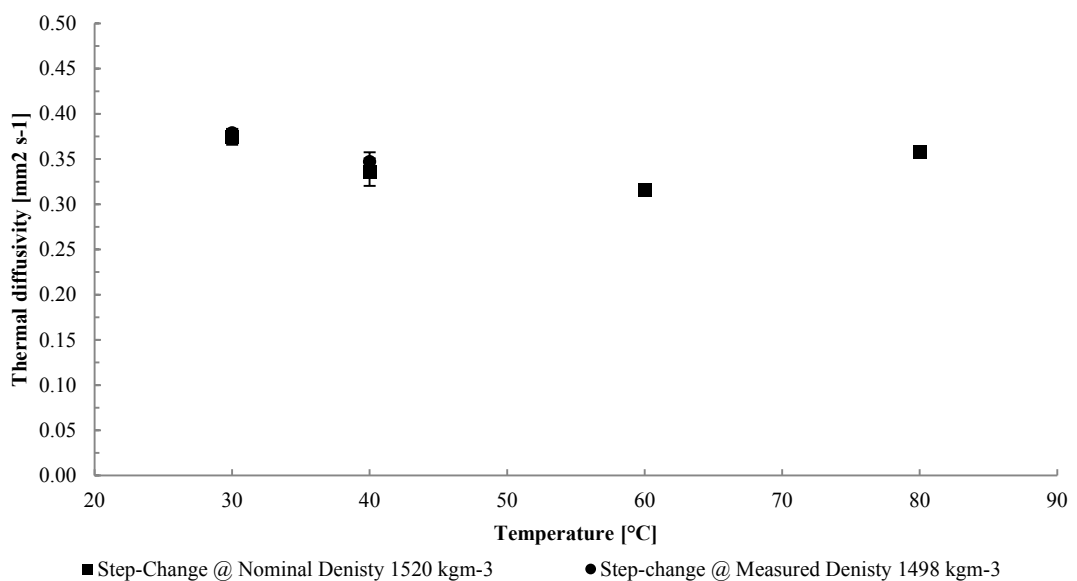


Figure 4.6: Through-thickness thermal diffusivity measurements comparison using nominal and measured density using step-method technique using 8 and 10mm samples routine; error bars represent deviation from average values.

Thermal diffusivity in the two principal directions and the estimated thermal conductivity using Equation 4.1 are reported in the Figure 4.7 a) and b). Room temperature and high temperature values are in agreement with values found in the literature for similar

materials by Mouritz et al. (2006) (room temperature in-plane thermal conductivity between 8 and 12 W m⁻² K⁻¹ depending on fibre content), Kalogiannakis et al. (2004), Zalameda (1999), Rolfes and Hammerschmidt (1995), Fanucci (1987) and Pilling (1979).

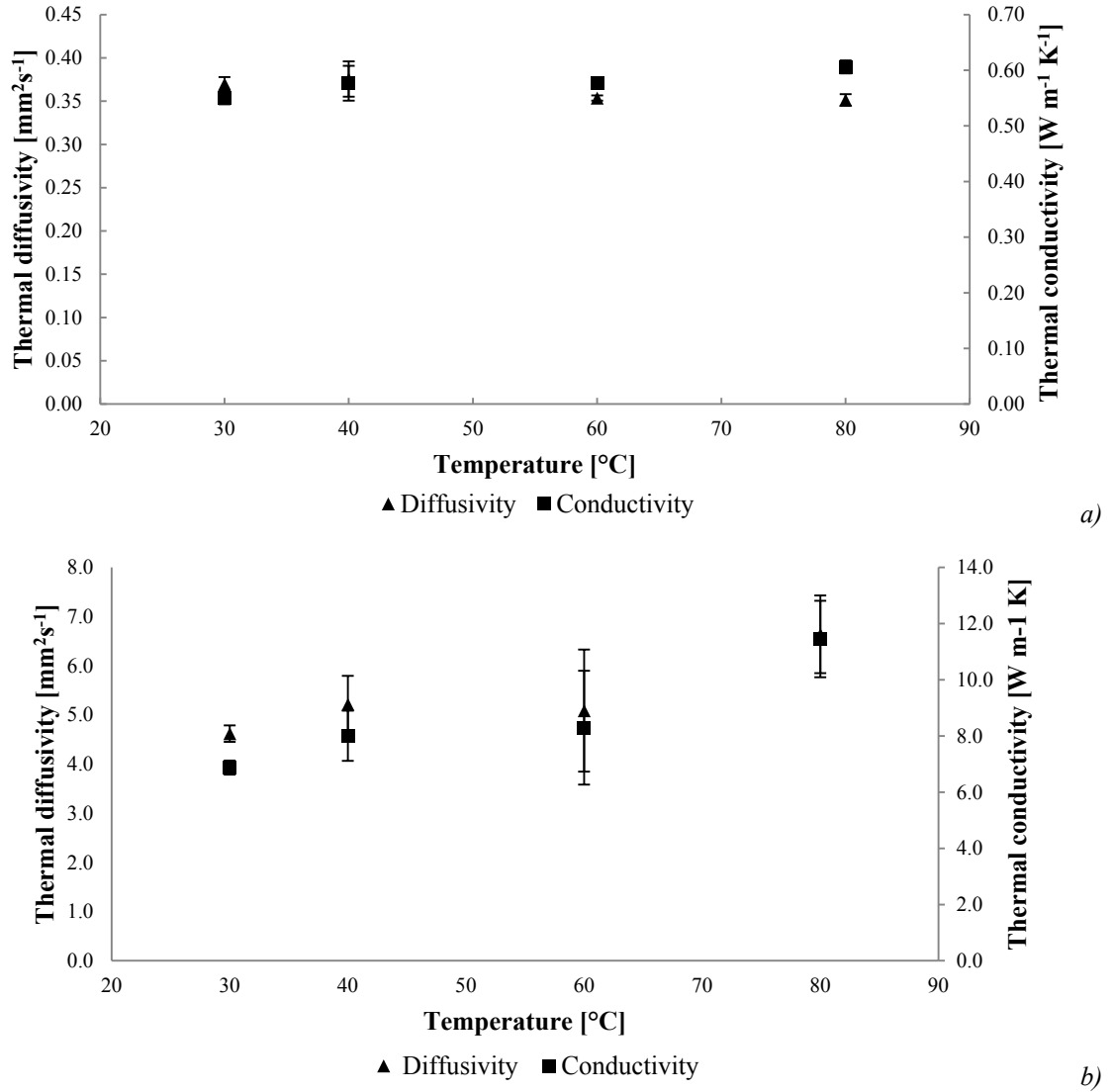


Figure 4.7: Thermal diffusivity and estimated thermal conductivity: a) through-thickness; b) in-plane; error bars represent deviation from average.

It can be noticed that the through-thickness thermal conductivity increases with temperature as found by Yamane et al. (1996) and Kalogiannakis et al. (2004), whereas the through-thickness thermal diffusivity decreases at increasing temperature as reported by Kalogiannkis et al. (2004) for a similar material in the same temperature range. The decrease in thermal diffusivity shows that the higher is the temperature of the CFRP, the

more insulating the material becomes to heat conduction in the through-thickness direction as reported by Fanucci (1987). Comparison between measured and literature values of in-plane and through-thickness thermal diffusivity and thermal conductivity is presented later on, see Figure 4.11, Figure 4.12 and Figure 4.13.

To compare the results obtained with the step-change method, thermal conductivity was measured using the guarded hot plate method. Samples were cut in the required shape, see Figure 4.8, at Newcastle University and sent to IMAST in Naples where Dr. Paolo Vollaro performed the measurements in the COCET-PON020000293206086 project.

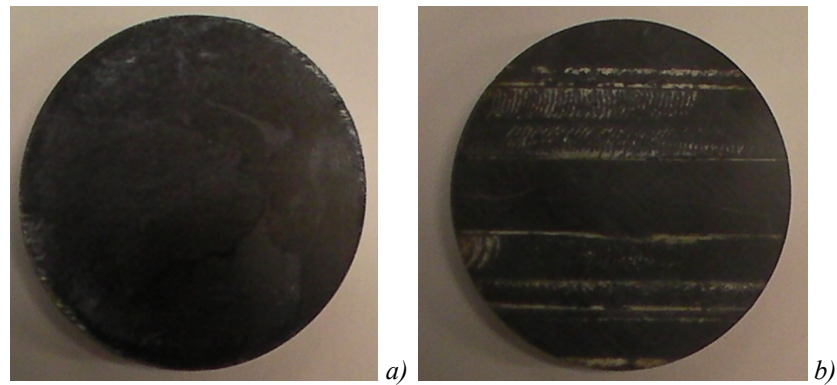


Figure 4.8: CFRP samples, dimension of $\varnothing 50.8\text{mm} \times 10\text{mm}$, for thermal conductivity measurements using guarded hot plate method: a) through-thickness direction; b) in-plane direction.

Due to the different measuring principles the temperatures at which the properties were measured with the two different methods are slightly different to each other but close enough to qualitatively compare the measurements. Results are reported in Figure 4.9 and Figure 4.10 and it can be noticed that the measurements with different principles agree with each other until 100°C . Measurements above 100°C , as previously mentioned, are affected by the same issue of low heat transfer coefficient and sand boundary layer formation described previously using the fluidised sand bath and for this reason they are not reported in the graphs. It has been assumed that the density is constant in the range of temperature of the measurement performed, however, as it has been mentioned before, this has no sensitive influence on the final results.

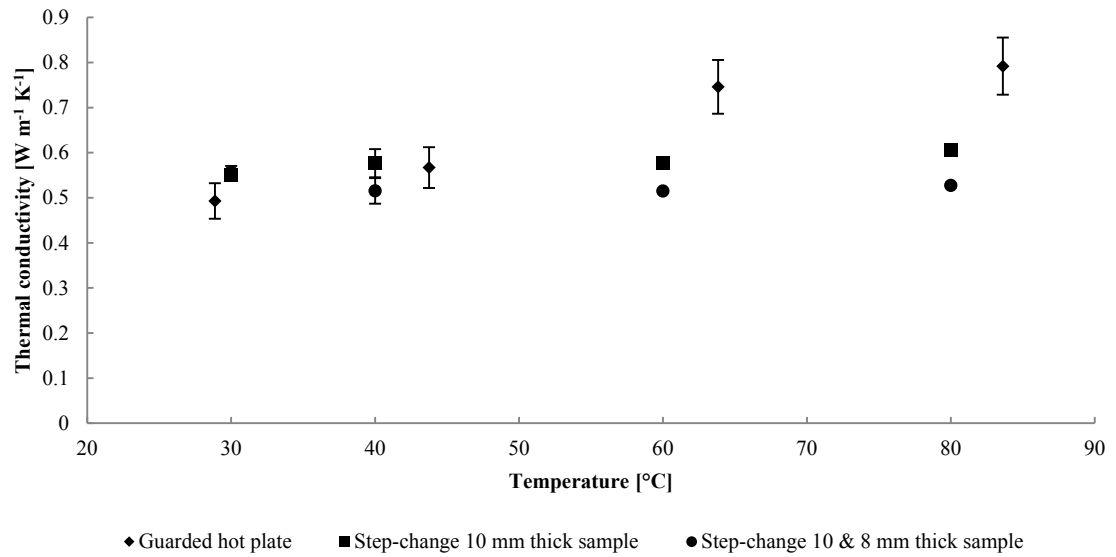


Figure 4.9: Comparison between through-thickness thermal conductivity measured by different methods; error bars represent deviation from average for the step-change method and accuracy limits of $\pm 8\%$ for the guarded hot plate.

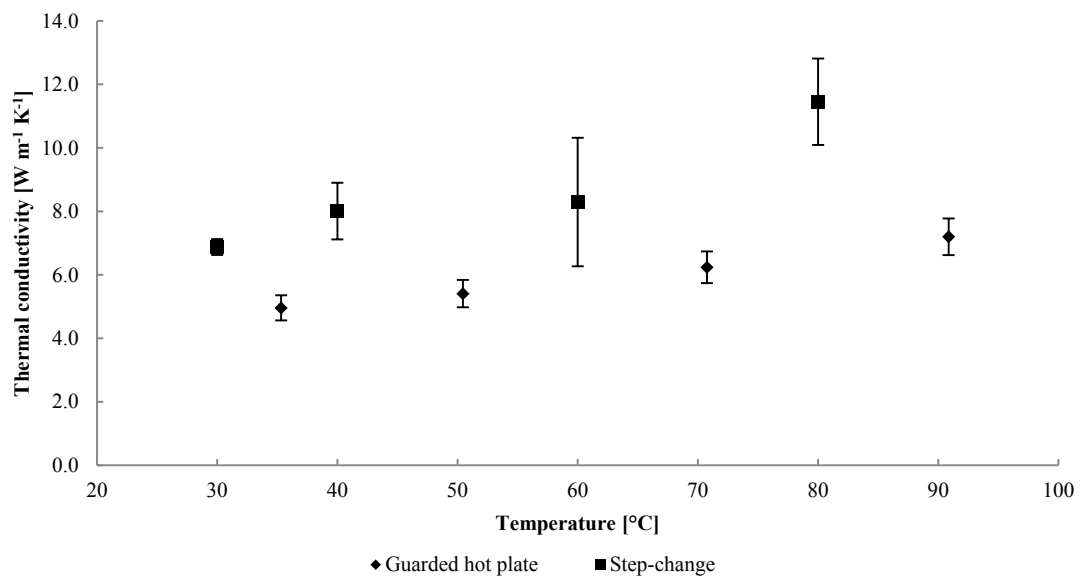


Figure 4.10: Comparison between in-plane thermal conductivity measured by different methods; error bars represent deviation from average for the step-change method and accuracy limits of $\pm 8\%$ for the guarded hot plate.

Furthermore it has no influence on the routine using two samples of different thicknesses since it is intrinsically eliminated by the mathematical analysis see section 3.1.1. It might, however, have added an additional error in estimating the thermal conductivity from the

thermal diffusivity which may explain the small differences among the measurements performed with the two different methods.

Furthermore, Rolfes and Hammerschmidt (1995) also found small discrepancies measuring the thermal conductivity of similar CFRPs using the guarded hot plate and transient hot strip method. Their discrepancies were similar to the one found in this study with the transient method consistently measuring slightly higher values than the steady-state technique. The thermal property values found in this study are comparable with literature values found by Mouritz and Gibson (2006), Kalogiannakis et al. (2004) (linear equation below T_g), Zalameda (1999), Rolfes and Hammerschmidt (1995), Fanucci (1987), and Pilling et al. (1979) as it can be seen in Figure 4.11, Figure 4.12 and Figure 4.13.

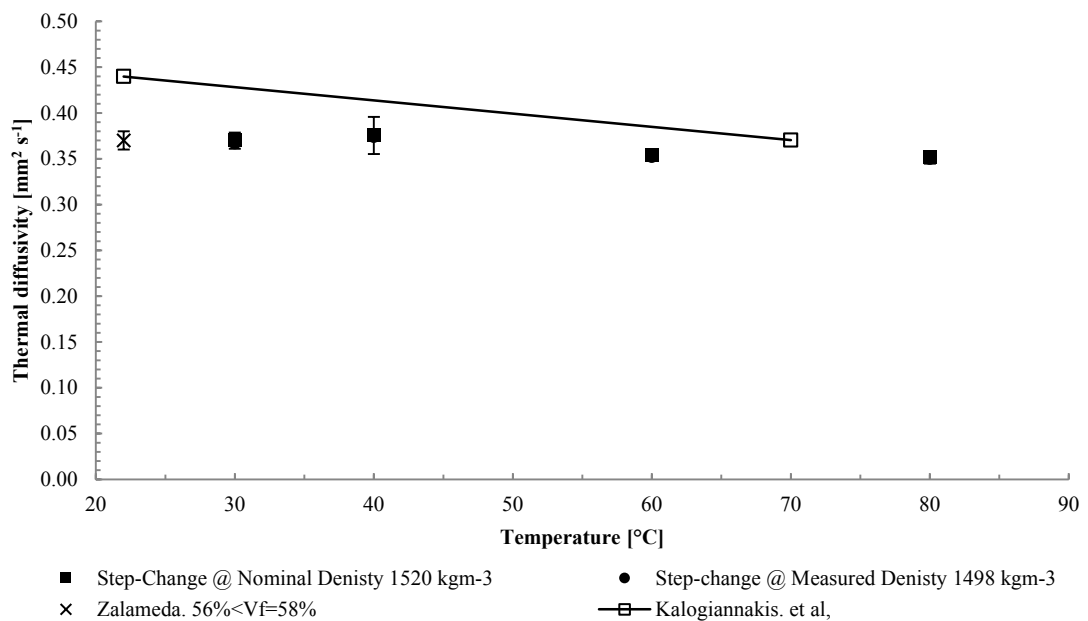


Figure 4.11: Comparison of measured through-thickness thermal diffusivity using step-change method with 1 sample of thickness 10mm and literature values from Zalameda (1999) and Kalogiannakis et al. (2004); error bars for stet-change method are as previously mentioned, error bars for literature values are according to source values if available.

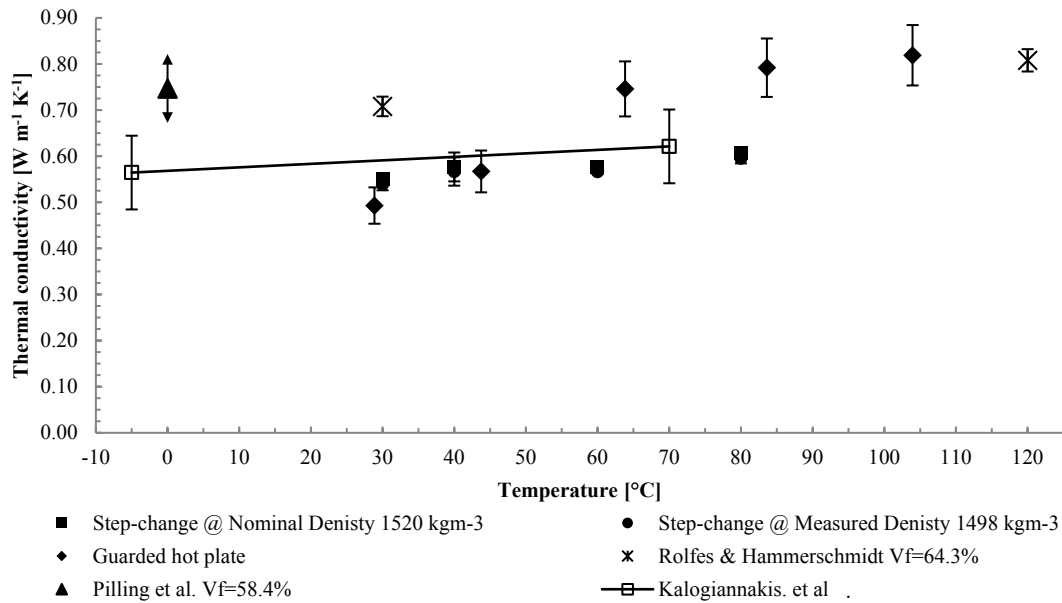


Figure 4.12: Comparison of measured through-thickness thermal conductivity using step-change method with 1 sample of thickness 10mm and literature values from Rolfes and Hammerschmidt (1995), Pilling et al. (1979), and Kalogiannakis et al. (2004), Fanucci (1987) is not present in the figure but reported a constant estimated value of around $0.74 [Wm^{-1}K^{-1}]$ up to $343.3^{\circ}C$; error bars for step-change method are as previously mentioned, error bars for literature values are according to source values.

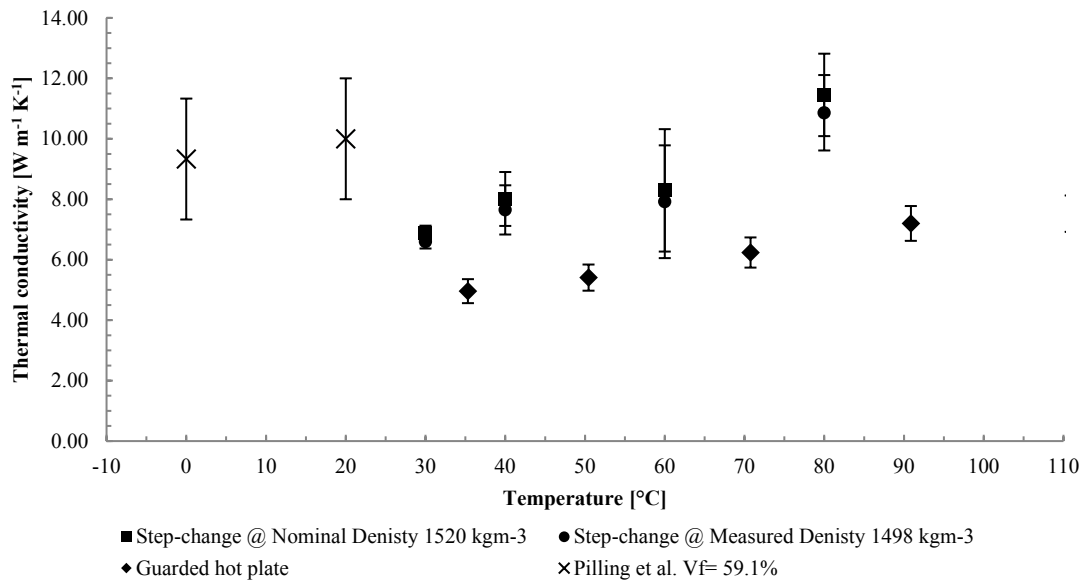


Figure 4.13 Comparison of measured in-plane thermal conductivity using step-change method with 1 sample of thickness 10mm and literature values from Pilling et al. (1979); error bars for step-change method are as previously mentioned, error bars for literature values are according to source values.

4.3 Mechanical characterisation at high temperatures

Although unmodified epoxies decompose at temperature above 350-400 °C, carbon fibres start to loose strength at around 500-550°C. Mechanical characterisation of the composite samples was performed from room temperature until just 200 °C due to project restrictions, health and safety issues and limited material availability. Three different tests were performed on the CFRP UD specimens available: tensile, compression and DMA tests.

4.3.1 Tensile tests

Tensile tests, mentioned before, were attempted at Newcastle University but due to the high strength of the UD CFRP laminate, the samples had to be sent back to Cytec for testing using an adhesive with higher lap-shear strength, in particular Cytec used the Hysol EA9394 with a dry T_g of 78 °C. Table 4.2 reports the Hysol EA9394 lap shear strength at different temperatures, see appendix 8.3.

Table 4.2: Lap shear strength of Hysol EA9394 at high temperature according to product datasheet.

T [°C]	25	82	93	121	149	177	204
σ_{LSS} [MPa]	28.9	20.7	20.0	15.8	11	8.3	4.1

Tensile test results are reported in Figure 4.14 a) and b) and Table 4.3. It can be noticed that the tensile strength does not decay until 160 °C where the first noticeable tensile strength drop occurs. Although the adhesive T_g is well below the temperature range of this study, thanks to its good lap shear strength retention at high temperatures, the adhesive kept working until 160 °C for the purpose of measuring tensile strength and until 180°C for the purpose of measuring the tensile modulus. In fact at 180 °C and 200 °C the failure occurred by tabs pull out invalidating the test results for 180 °C tensile strength and 200 °C tensile strength and tensile modulus. The 180 °C tensile modulus is considered correct since the modulus was calculated from 0.1% up to 0.3% strains measured with the extensometer, as reported in appendix 8.2, and tabs pull out phenomenon did not occur

yet. However it is likely that the tensile strength measured at 180 °C is the first stage relaxed property value of a 2 stage transition Gibson model (Gibson et al., 2006) since the T_g of the resin is exactly 180 °C and carbon fibres do not loose their strength up to 400 °C and above 550 °C their tensile strength reduces to 60% of the room temperature one (Feih and Mouritz, 2012).

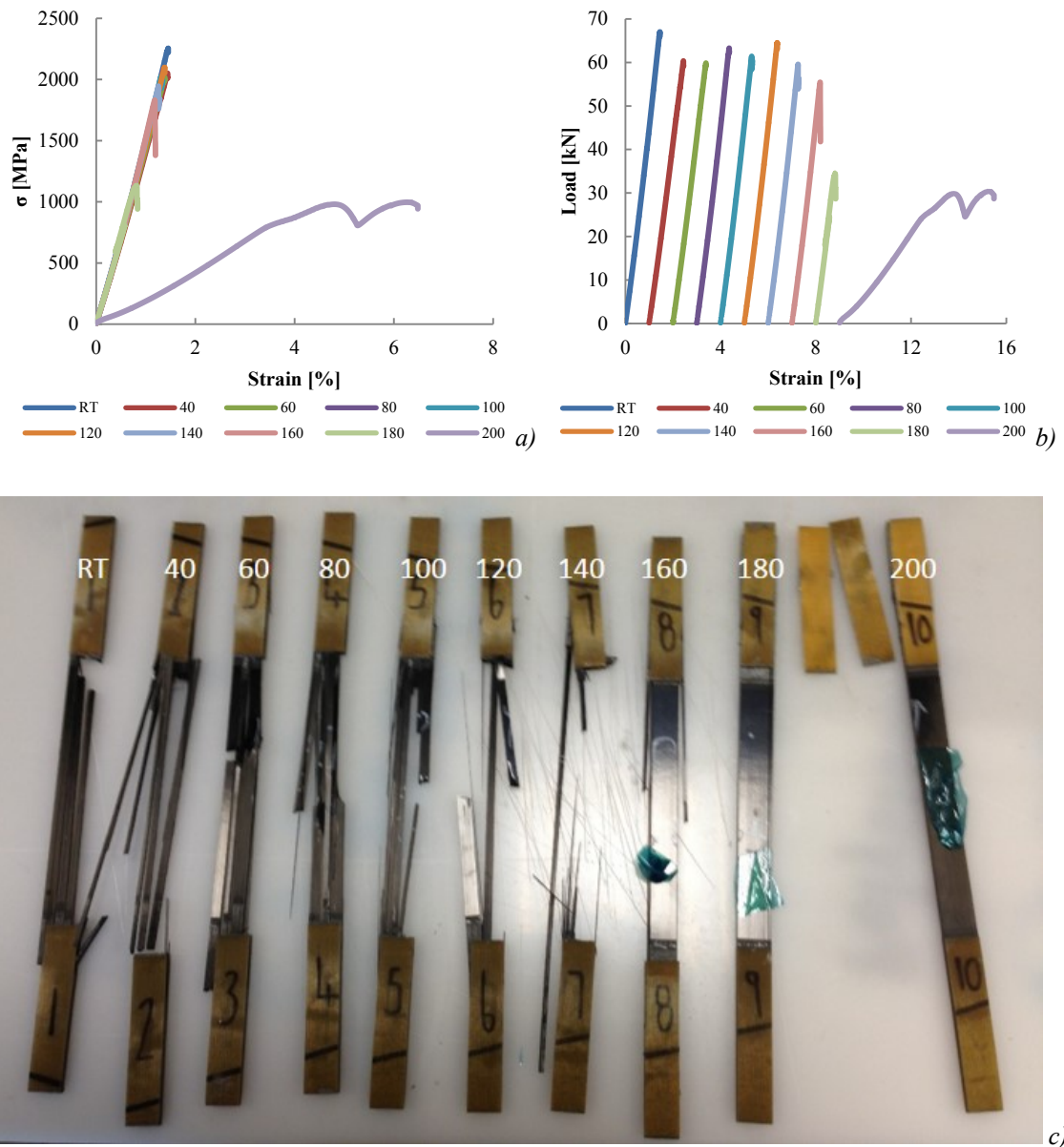


Figure 4.14: Tensile test results on 2mm thick UD CFRP samples at different temperature from 20°C to 200°C at intervals of 20°C: a) Tensile stresses vs Strains; b) Applied load vs Strains; c) Picture of the tested samples at different temperature showing the pulled-out tabs.

In fact, the tensile strength as function of temperature reported in Figure 4.15 shows that both tensile strength and tensile modulus are constant until 160 °C, as reported by Cao et al. (2009), Feih et al. (2007), Feih and Mouritz (2012) and Yoon and Kim (2000), for tensile strength and tensile modulus respectively of CFRP. Above this temperature nothing can be established since the test results are not valid in this study due to tabs pull out failure. However it is very likely that the change in tensile strength would not be noticeable until around 500°C which is the softening temperature of carbon fibres, as reported by Feih and Mouritz (2012).

Table 4.3: Tensile strength [MPa] and tensile modulus [GPa] at different temperatures

T [°C]	RT	40	60	80	100	120	140	160	180	200
σ_U [MPa]	2254.80	2051.01	2015.19	2090.49	2025.72	2098.78	1945.82	1830,57	-	-
E [GPa]	140.99	132.32	134.46	138.21	140.28	136.72	138.25	139.34	136.92	-

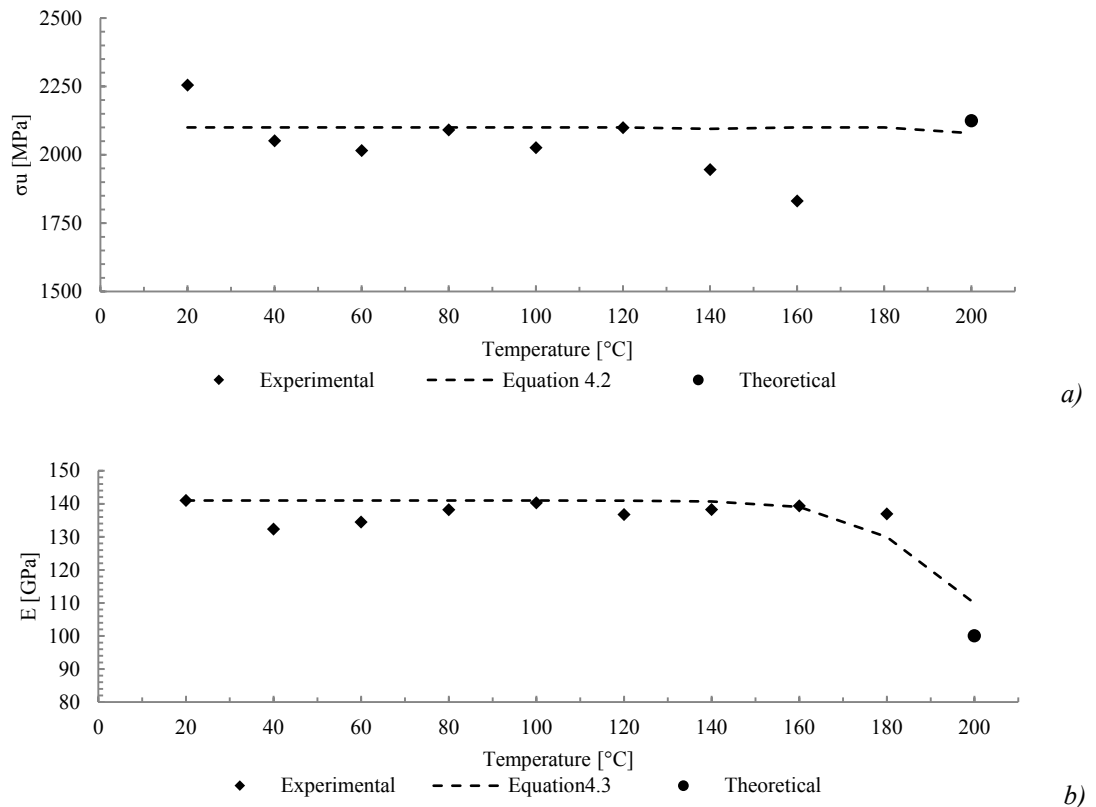


Figure 4.15: Tensile properties vs temperature of 2mm thick UD CFRP: a) tensile strength; b) tensile modulus.

The dashed line in Figure 4.15 a) and b) represent the Gibson model predictions, reported in Equation 2.38, for tensile strength and tensile modulus respectively. Equation 2.38 is modified as reported in Equation 4.3 and Equation 4.4 to describe the tensile strength and the tensile modulus respectively, the parameters values used for the fitting in Figure 4.15 are reported in Table 4.4.

$$\sigma(T) = 0.5(\sigma_U + \sigma_{2R} - (\sigma_U - \sigma_{1R})\tanh(k(T - T'_1)) - (\sigma_{1R} - \sigma_{2R})\tanh(k(T - T'_2)))R^n \quad \text{Equation 4.3}$$

$$E(T) = 0.5(E_U + E_R - (E_U - E_R)\tanh(k(T - T'))R^n \quad \text{Equation 4.4}$$

Table 4.4: Values used to fit the tensile strength (tensile modulus) reported in Figure 4.15.

Parameters	$\sigma_U (E_U)$ [MPa]	$\sigma_{1R} (E_R)$ [MPa]	σ_{2R} [MPa]	k	T' [°C]	R	n
Values	2100 (141)	2100 (100)	1274	0.05 (0.05)	190 (190)	1 (1)	0.5 (0.5)

The remaining resin content values, R, are reported in Table 4.5. All the results, with the exception of the 160 °C tensile strength, are within 10% of the modelled curve. This error might be due to the fact that the adhesive used to attach the tabs may have started to soften enough to alter the tensile strength causing a larger error in this measurement.

Table 4.5: Remaining resin content values corresponding to sample temperature.

T [°C]	RT	40	60	80	100	120	140	160	180	200
R	1	1	1	1	1	1	1	1	1	0.98

Figure 4.15 a) and b) also reports a theoretical value which is the value of tensile strength and tensile modulus respectively, calculated according the rule of mixture formula, see

Equation 4.6, using the room temperature values for the fibres but putting the tensile strength and the tensile modulus of the resin to the worst case scenario of non-contribution to load bearing capacity, which is 0. It can be noticed that, since tensile properties are fibre dominated properties, if there is no fibre softening then the tensile properties of the fibre result almost unchanged. In fact, it has been shown by Feih et al. (2007) that glass fibre softening influences mechanical strength of glass fibre reinforced polymers. However, as found by several authors (Cao et al., 2009; Fitzer, 1988; Feih and Mouritz, 2012; Sauder et al., 2002 and Sauder et al., 2004), carbon fibres do not soften in inert atmosphere up to 700 °C or eventually higher temperatures. In oxidising environment they start softening at about 500-550 °C because of the loss of the outer layer which is made by a highly oriented carbon structure (Feih and Mouritz, 2012). The authors observed tensile strength loss regardless of the atmosphere used to heat the carbon fibres, the tensile strength (considering the fibre diameter loss) decreased between 400 °C and 600 °C, reaching a steady state value of around 60% of the original strength beyond 600 °C. The temperatures of these tests were well below the softening point of carbon fibres and just above the T_g point of the resin and in fact the results are in line with the expected behaviour considering literature findings.

4.3.2 Compression tests

Compression tests were carried out using the in-house jig shown in Figure 4.2 and described in chapter 3.2.2. Compressive stresses vs crosshead displacement and pictures of the tested samples are reported in Figure 4.16 and Figure 4.17, respectively.

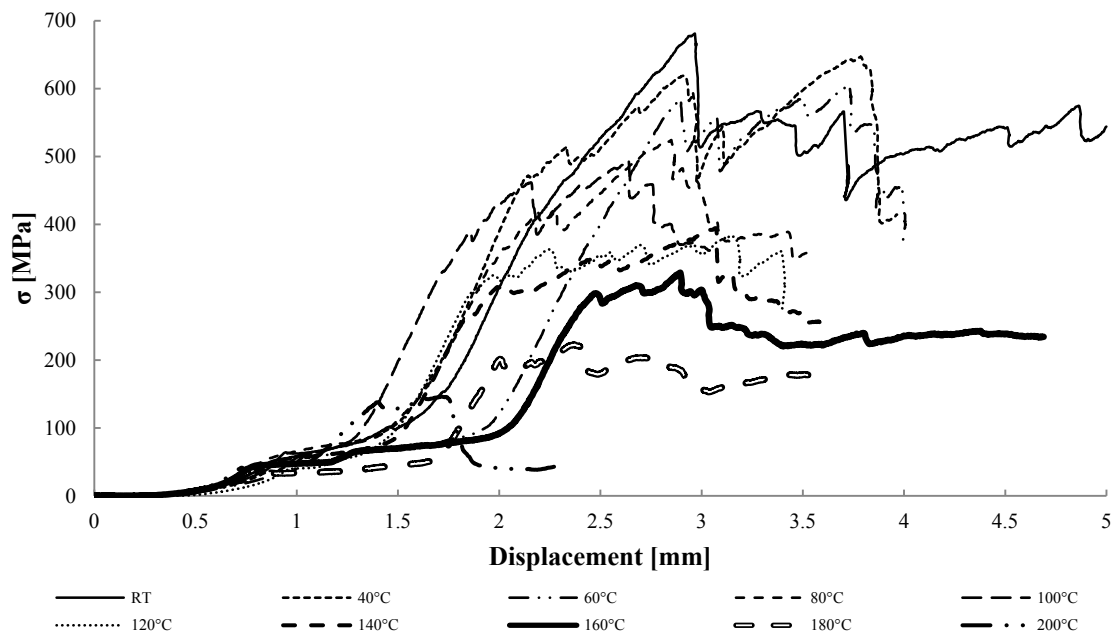


Figure 4.16: Compression tests results on CFRP samples at different temperature from 20°C to 200°C at intervals of 20°C.

Figure 4.16 reports the compression tests as function of the crosshead displacement. Due to the testing setup, it was not possible to measure sample strains and consequently the modulus at high temperatures. All the tests curves are characterised by an initial plateau which can be explained by the fact that the steel plates may not have developed enough gripping force on the sample surfaces to keep the sample in place. This means that once the load started to be applied to the top cylinder of the jig, the sample started to slip between the steel plates until the edges rested on the top and bottom surfaces of the jig, corresponding to method 2 of BS ISO 14126:1999. After this initial plateau another plateau can be observed which may be explained by the fact that, although effort was made to avoid crushing of the edges, the edges started to crash, increasing the area of the applied load until the load could rise again until failure. Effort was made to obtain samples according to standard tolerances on the edges to avoid edge crushing but unfortunately this phenomenon happened since the machining tools available are not adequate to cut carbon fibres samples in the required precision.

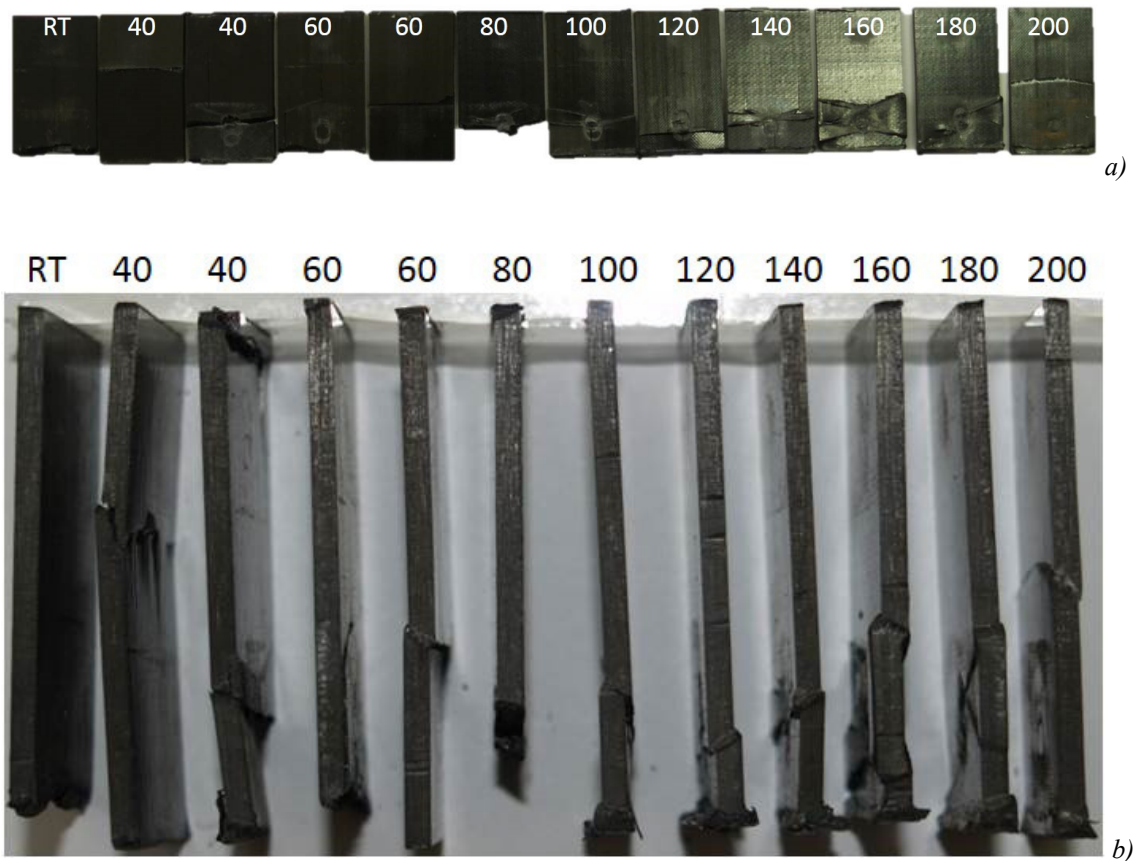


Figure 4.17: Compression tested samples at high temperature from 20°C to 200°C at intervals of 20°C from left to right : a) Tested samples front view; b) tested samples side view.

Pictures of the tested samples are reported in Figure 4.17 a) and b) where the previously discussed edge crushing phenomenon can be observed. It can also be noticed that, with the exception of the last specimen on the right hand side of the pictures in Figure 4.17, all the other specimens did not break in the correct area, i.e. away from gripping area, and in the correct way according to standards. A few tests were replicated trying to apply a higher grip with the grub screw but this instead caused a little imprinting on the steel plates and on the samples causing premature failure of some specimens. The fifth sample from the left presents an almost acceptable failure but it is exactly at the edge of the gripping steel plates so the test was repeated but the result was not good anyway. As expected, above 100 °C, failure surface was characterised by kink bands inclined between 45° and 60° compared to the mid-plane but they were localised in the gripping area which is not good to be considered as valid test results.

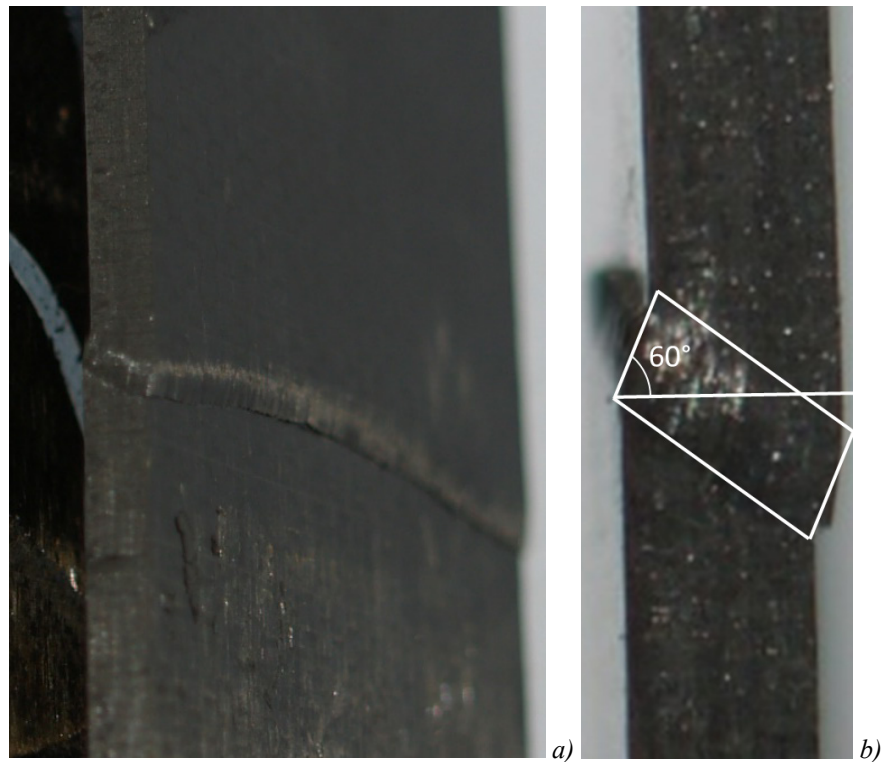


Figure 4.18: Magnified pictures of 200°C tested sample showing the classic fibre kinking bands with 60° angle inclination: a) face and side view showing the continuous compression kink band; b) tested sample side view with highlighted kink bands and inclination angle.

The only sample that failed correctly was the sample tested at 200 °C as can be seen in the sample magnified pictures reported in Figure 4.18. This can be considered as the compression strength of the material at 200 °C. The MTM44-1 datasheet compression strength at room temperature is reported as 1330 MPa which is roughly double of what has been found in these tests. Although sample dimensions were chosen to avoid buckling failure, the slenderness of the samples might have introduced buckling during the tests, hence reducing the room temperature failure load.

Nawaz (2011) found that room temperature compressive strength of CFRP is dependent on sample dimensions and in particular the length and slenderness of the tested samples play an important role. According to the author, the more slender the sample the more the compressive failure mode passes from pure compression to shear of the plies and buckling, influencing the results of the tests. Hancox (1975) and Piggott and Harris (1980) studied the dependency of compressive strength on slenderness using carbon fibre epoxy

and polyester based composites respectively. Nawaz (2011) findings align with Hancox (1975) and Piggott and Harris (1980) findings.

Since the actual test results are not good until high temperature 200 °C, compressive strength data were kindly available from the manufacturer at 20 and 90 °C and reported in Figure 4.19. It can be noticed how the compressive strength at temperature lower than 100 °C is not constant as the tensile strength but it decreases linearly with increasing temperature. Yoon and Kim (2000) found similar trends for CFRP longitudinal and transverse moduli. This phenomenon is dependent on the fact that, as discussed in the literature review, composite compressive properties are matrix dominated properties and matrix properties are highly dependent on temperature. This means that composites compressive properties are more temperature dependent compared to tensile properties which, on the other hand, are fibre dominate. According to Yoon and Kim (2000), this temperature dependency could be described by a linear equation such as:

$$\sigma_U(T) = \sigma_{U,0} + m(T - T_0) \quad \text{Equation 4.5}$$

Here $\sigma_U(T)$ and $\sigma_{U,0}$ are the unrelaxed compressive strength function of temperature and the unrelaxed compressive strength at T_0 [MPa], m is the slope of the unrelaxed compressive strength function of temperature [MPa °C⁻¹], T_0 is the reference temperature (20°C) and T is the temperature [°C].

Table 4.6: Values used to fit the compression strength represented in Figure 4.19, values of .

Parameters	σ_{U0} [MPa]	m	σ_R [MPa]	k	T [°C]	R	n
Values	1330	-3.2	140	0.08	160	1	0.5

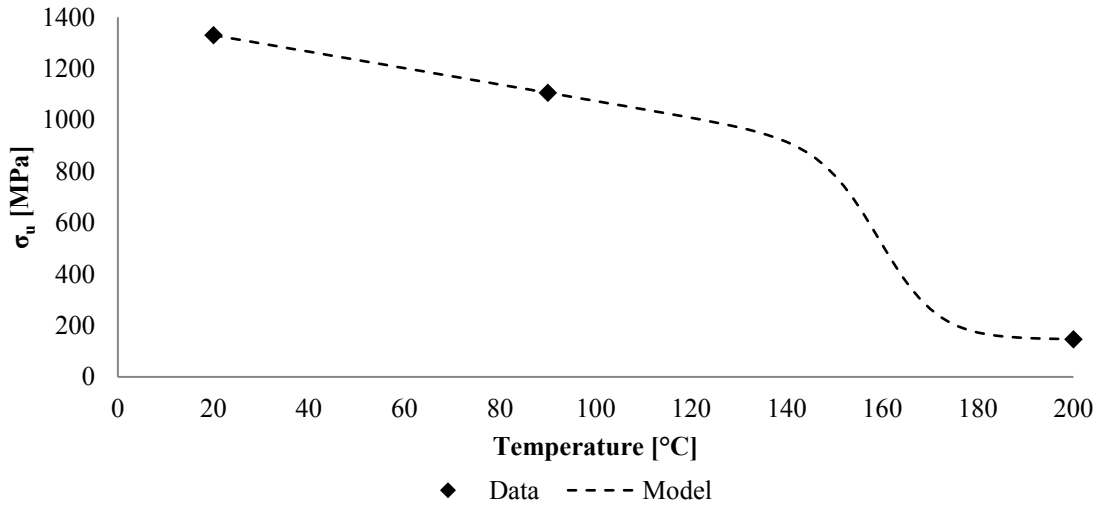


Figure 4.19: Compression strength at high temperature of CFRP samples using data form manufacturer and from experiments.

If Equation 4.3 is used to fit these data with a single transition where the unrelaxed compressive strength is function of temperature according to Equation 4.5, using the values in Table 4.6, then a very good estimate of the compressive strength at high temperature can be performed, as it can be seen in Figure 4.19. To rigorously validate the model, more data are needed both at lower and higher temperature than 200 °C. Nevertheless, although there is no study on compressive strength of unidirectional aerospace grade CFRP, the results align with findings on other materials by Burns et al. (2010), Feih et al. (2007a), Feih et al. (2007b) and Nawaz (2011) in the sense that, since compressive properties are matrix dominated properties, a gradual, small decrease in compressive strength occurs from room temperature up to near transition temperature because of resin behaviour with increasing temperature. The steep loss of compressive failure occurs between transition temperature and resin T_g . The transition temperature, the temperature corresponding to 50% compressive strength loss, has been reported between 0.7 to 0.9 of T_g for different type of composites (Burns et al., 2010; Feih et al., 2007b; Nawaz et al., 2011) and the findings of this work align with literature reported data.

4.3.3 DMA tests

DMA tests, using a three point bending fixture, were carried out on samples to measure mechanical properties as function of temperature in 2 principal directions only, along the

fibres and across the fibres, since the CFRP samples have a unidirectional reinforcement. For each principal direction three samples were investigated at 3 different frequencies, 0.1, 1 and 10 Hz to highlight any differences in frequencies. No substantial differences were noticeable so just the results for 1 Hz are reported in Figure 4.20 and Figure 4.21 for longitudinal and transverse storage moduli respectfully.

The transverse modulus of Sample 7 above 210 °C has some negative values which is physically wrong and impossible because it would mean that to an applied load in a positive direction, it corresponds a displacement in the opposite direction (creation of energy). This might have been caused because of several reasons which are going to be discussed. The machine software has a broken sample detector routine (it stops the test if a very small or null modulus is detected) which was disabled otherwise the test would have stopped at around T_g , before having measured this phenomenon. The vibrational pattern suggests that vibrations might have affected the measurements at high temperature since the sample stiffness is very small. In fact the DMA8000 is not placed on a vibration free lab bench and there is other equipment around which other lab users may use. Building works were necessary on the lab roof and the associated vibrations might also have affected the results at temperature above T_g since the stiffness is very small. The fixture used is optimal for stiff samples, nominally with storage modulus between 10^{-1} and 10^2 GPa as stated by PerkinElmer user guide. At temperature above T_g the sample stiffness falls below the optimal range lower limit. All these phenomena might have affected the results in the way it is reported in Figure 4.21.

Since transverse properties are matrix dominated properties it is expected that the transverse modulus is highly affected by resin behaviour compared to the longitudinal one, in fact, the results reported here are in line with what reported by Li et al. (2000) and Zhou et al. (2007) for modulus vs temperature up to 200 °C of epoxy adhesive and neat resin respectively and Yoon and Kim (2000) for CFRP moduli up to 140 °C.

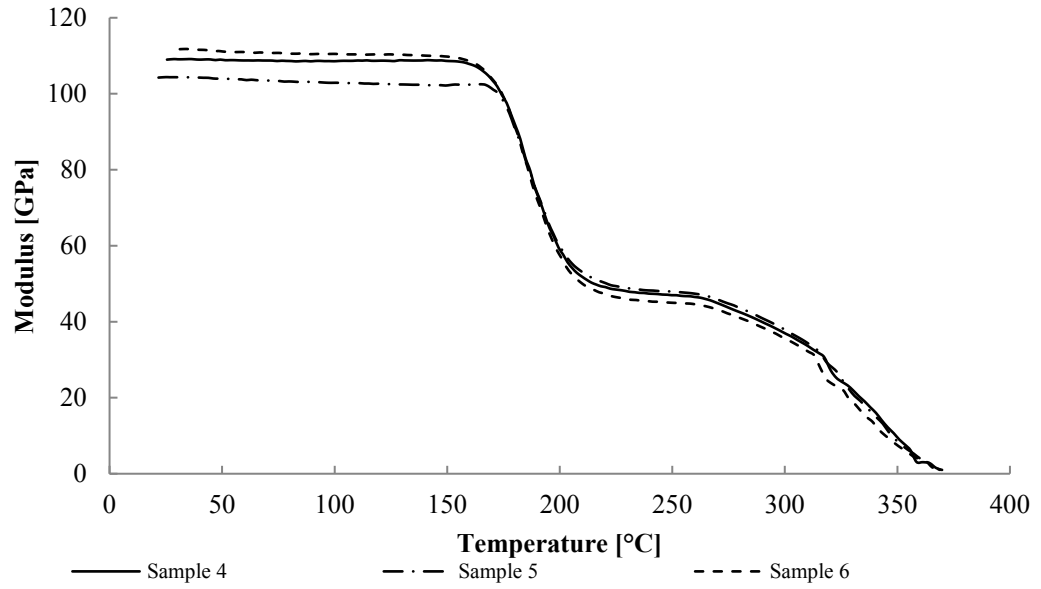


Figure 4.20: CFRP longitudinal storage (elastic) modulus versus temperature, the large modulus drop around T_g is due to the shear component of the deflection eclipsing the bending component.

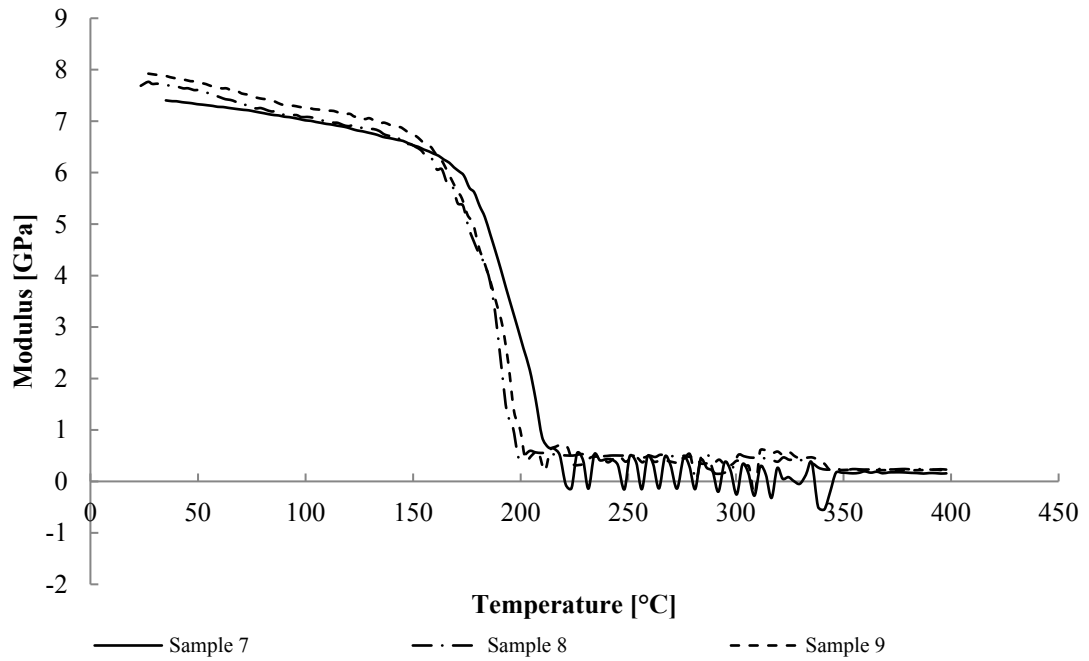


Figure 4.21: CFRP transverse storage (elastic) modulus versus temperature: sample 7 fluctuations below zero after T_g might be due, vibrations in the surroundings the DMA8000; loss of accuracy because of the high temperature modulus falls out of the optimal range for the used fixture.

The small differences in between the storage moduli of the samples might be due to small misalignment of the fibres within the sample shape and/or within the fixture used for

testing. From both figures, the T_g can be extrapolated and corresponds to around 180 °C, confirmed by the material datasheet. Figure 4.20 shows the results for longitudinal direction and it can be noticed that before the T_g a glassy plateau can be observed. Once the T_g is reached, the longitudinal storage modulus decays until another plateau between 230 °C and 260 °C, usually called the rubbery plateau. After that, another transition occurs which is usually associated with thermoplastic polymers rather than thermosets. The material datasheet of the MTM44-1 reports the composite as a toughened epoxy. Epoxy resins are usually toughened for aerospace applications in different ways. Toughening can be achieved for instance by adding thermoplastic or elastomer additives or chemically modifying the network structure to achieve a higher ductility. It is not mentioned in the datasheet of MTM44-1 how the toughening is achieved so the behaviour after the rubbery plateau which is half way between thermosets and thermoplastics cannot be certainly attributed to thermoplastic or elastomer additives.

The glassy plateau of the transverse modulus is not exactly a plateau but constantly decays until the T_g . This is due to the fact that transverse properties of unidirectional composites are matrix dominated properties which are highly temperature dependent properties. After T_g the same phenomena are not present in Figure 4.21 compared to Figure 4.20 because the transverse modulus, as all matrix dominated properties, decays drastically after the T_g . The machine is not capable to follow the small modulus values reached after T_g with the same loading configuration to measure the properties in the transverse direction before T_g occurs.

It also has to be noticed that the first longitudinal modulus drop is quite large and anticipated considering that just the resin loses flexural rigidity while carbon is stable until very high temperatures. If the CFRP modulus is calculated using the rule of mixtures previously introduced, Equation 4.6, and the matrix modulus temperature dependency is described by Equation 4.7, it should be noticed that the modulus should not drop considerably since it is a fibre dominated property.

$$E_{comp,L} = V_f E_{f,L} + (1 - V_f) E_{m,L} \quad \text{Equation 4.6}$$

$$E_m(T) = 0.5(E_{m,U} + E_{m,R} - (E_{m,U} + E_{m,R}) \tanh(k(T - T'))) R^n \quad \text{Equation 4.7}$$

Here $E_{comp,L}$, $E_{f,L}$ and $E_{m,L}$ are the longitudinal modulus of composite, fibres and matrix respectively [MPa], V_f is the fibres volume fraction [-], $E_{m,U}$ and $E_{m,R}$ are the unrelaxed and relaxed moduli of the matrix [MPa].

If the values in Table 4.7 are input into Equation 4.7 which then is input into Equation 4.6, the longitudinal modulus of the CFRP can be estimated. Figure 4.22 shows the longitudinal modulus vs temperature according to Equation 4.6 and Equation 4.7. It can be noticed how the composite should experience a very small drop in modulus compared to what was measured.

Table 4.7: Values used to plot longitudinal modulus in Figure 4.22

Parameters	V_f	$E_{m,U}$ [MPa]	$E_{m,R}$ [MPa]	E_f [GPa]	k	T' [°C]	R	n
Values	0.6	3100	0	238	0.1	180	According to Arrhenius	0.5

As it has been observed in Figure 4.21 the transverse modulus has a steady drop until nearby T_g after which the modulus drops to zero. This may be due to the fact that the transverse modulus is a matrix dominated property and according to the rule of mixtures its value at room temperature can be expressed by Equation 4.8 (Mouritz and Gibson, 2006). We can also observe that, as found by Yoon and Kim (2000), the transverse modulus drop before T_g looks linear so if Equation 4.9 is used to describe the unrelaxed resin transverse modulus and input it in Equation 4.7 then it can be input in Equation 4.8

to describe the composite transverse modulus function of temperature and degradation status.

$$E_{comp,T} = \left(\frac{V_f}{E_{f,T}} + \frac{(1-V_f)}{E_{m,T}} \right)^{-1} \quad \text{Equation 4.8}$$

$$E_{m,T,U}(T) = E_{m,U,0} + m(T - T_0) \quad \text{Equation 4.9}$$

Here $E_{comp,T}$, $E_{f,T}$, $E_{m,T}$, $E_{m,T,U}$ and $E_{m,U,0}$ are the composite transverse modulus, fibre transverse modulus, matrix transverse modulus, the unrelaxed matrix transverse modulus and the unrelaxed initial matrix transverse modulus (for $T=T_0$) respectively [MPa], m is the slope of the modulus function of temperature [MPa °C⁻¹], T_0 and T are the initial (20°C) and final temperature [°C]

Table 4.8: Values used to plot transverse modulus in Figure 4.22

Parameters	V_f	$E_{m,U,0}$ [MPa]	$E_{m,T,R}$ [MPa]	$E_{m,T}$ [GPa]	m [MPa °C ⁻¹]	k	T' [°C]	R	n
Values	0.6	4500	0	10	-10	0.08	180	According to Arrhenius	0.5

The composite longitudinal and transverse moduli as function of temperature and decomposition stage are shown in Figure 4.22.

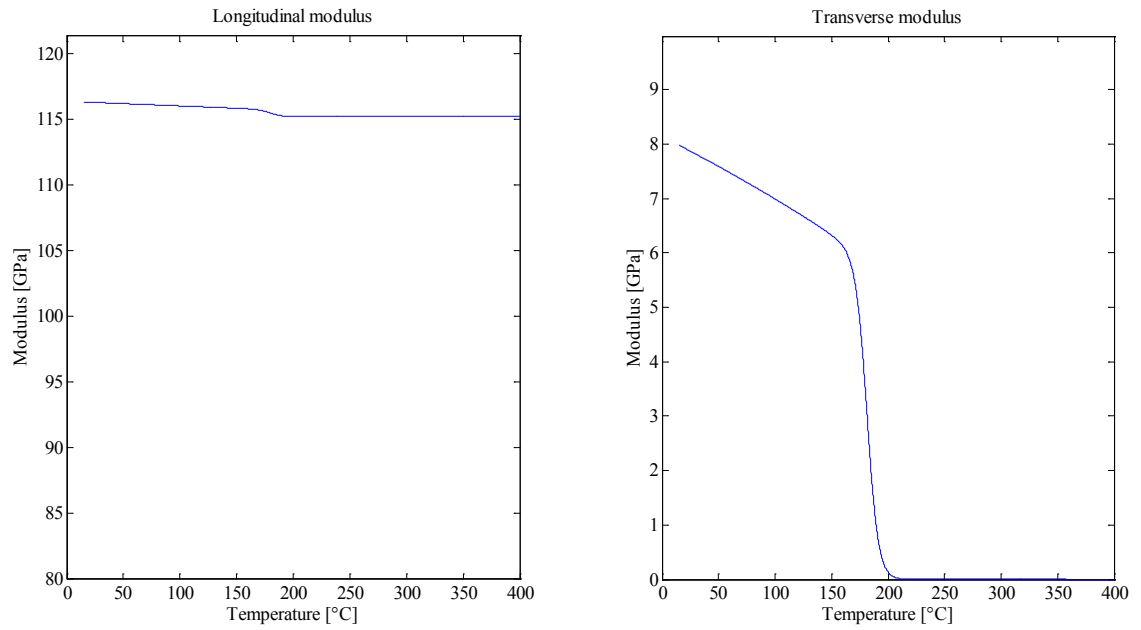


Figure 4.22: CFRP moduli simulating DMA conditions; on the left the longitudinal modulus is calculated according to Equation 4.6 and Table 4.7; on the right the transverse modulus is calculated according to Equation 4.8 and Table 4.8.

The large drop of the experimental results may be due to the shear deformation contribution which cannot be isolated using a three point bending fixture. The deflection of a beam subject to three point bending is function of two different contributions: the bending and the shear deflection. The total deflection equation function of the two terms can be found in Mouritz and Gibson (2006) and is reported in Equation 4.10.

$$\delta = \frac{FL^3}{4EBt^3} \left(1 + \frac{6}{5} \frac{E}{G} \left(\frac{t}{L} \right)^2 \right) \quad \text{Equation 4.10}$$

Here δ is the total deflection [m], F is the centre load [N], L is length of the span between the two supports [m], E is the flexural modulus [Pa], B is the width of the section [m], t is the height of the section [m] and G is the shear modulus [Pa]. If E and G would be expressed in [MPa] and all the other geometric parameters on the right hand side would be expressed in [mm], then the deflection would results in [mm] as well.

Mouritz and Gibson (2006) reported that, for unidirectional carbon fibre composites, the ratio E/G at room temperature is of the order of 60, so for beams with L/t of the order of 10 the shear component of the deflection may be as high as 72% of the total deflection. The ratio E/G changes greatly after T_g since the shear modulus is more resin dependent than the axial modulus, which might cause the shear deflection term to eclipse the bending deflection term. Compensation has to be made when measuring elastic properties at high temperature using flexural arrangements or different fixtures should be used such as the four point bending fixture for instance.

4.4 Fire Resistance tests

Fire resistance tests were performed on nominally 100 mm X 100 mm X 10 mm flat unidirectional samples with the load applied in the longitudinal direction, i.e. along the fibres. Although the RT failure stress measured in section 4.3.2 is not the real value of the material property, it has been chosen as the RT failure condition for this work because the fire tests setup is very similar to the setup used to measure compression strength at high temperatures since edge crushing may occur. This does not invalidate the fire test and/or the modelling results because it just influences the compression time to failure prediction and not the buckling failure time which is what rules the mechanical behaviour at such very low applied loads as it will be shown later in this work.

The usual procedure would be to choose loads of 60%, 40% and 20% of the RT failure load but since the RT strength was found to be 1330 MPa, even the 20% would be too high for the capacity of the loading frame which is 300 kN. For this reason the three different loads have been chosen as 15%, 10% and 5% of the room temperature failure load corresponding to around 200 kN, 120 kN and 80 kN respectively. Three different heat fluxes were used, 70 kW m⁻², 116 kW m⁻² and 180 kW m⁻² as described previously in section 3.3. Due to thickness, dimensions and the RT elastic modulus (140 GPa), of the samples, the Eulerian buckling load (Asaro et al., 2009), see Equation 4.11, is around 1150 kN, higher than the highest applied load so the use of anti-buckling fixture was not necessary to perform the tests. It was chosen not to use anti-buckling fixture also because the sample was too thick to fit in the fixture.

$$F = \frac{\pi^2 EI}{(KL)^2}$$

Equation 4.11

Where F is the buckling load [N], E is the elastic modulus [MPa], I is the area moment of inertia [mm⁴], K is column effective length factor [-], taken as 1 since the edges were free to rotate, and L is the length of the sample [mm].

4.4.1 Heat flux calibration

The flame heat flux calibration procedure has been presented in section 3.3.1. If the heat flux [kW m⁻²] is plotted against the flame temperature [°C] a perfect empirical exponential fitting function can be found using non-SI units, see Figure 4.23. It is important to highlight that although a perfect fit has been found, it should be verified doing other calibration procedures at different heat fluxes and see how the empirical formula performs in terms of predictions.

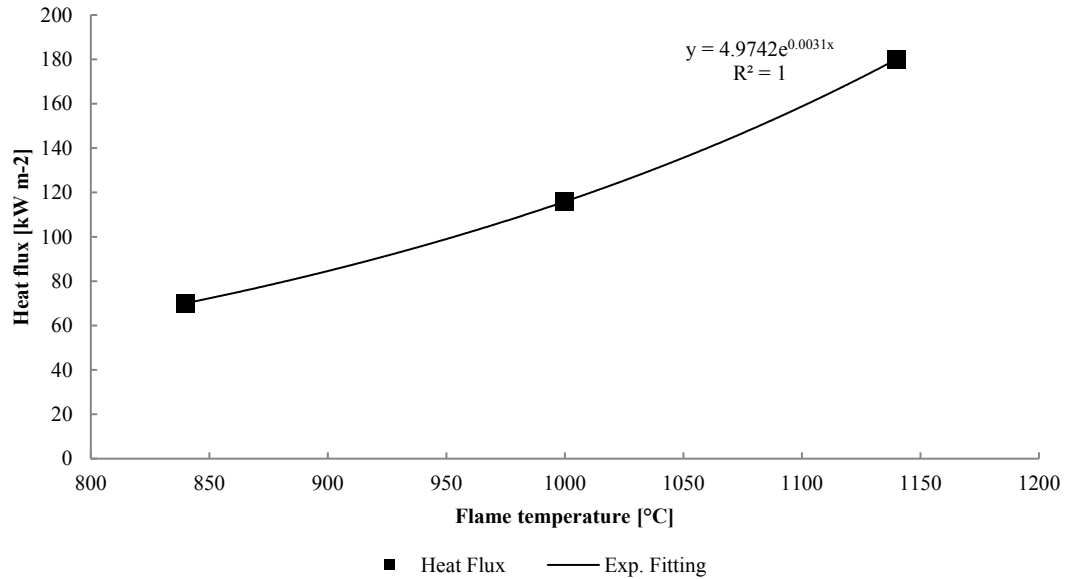


Figure 4.23: Heat flux [kW m⁻²] vs Flame Temperature [°C] showing a very good empirical fit using an exponential function with no-SI units.

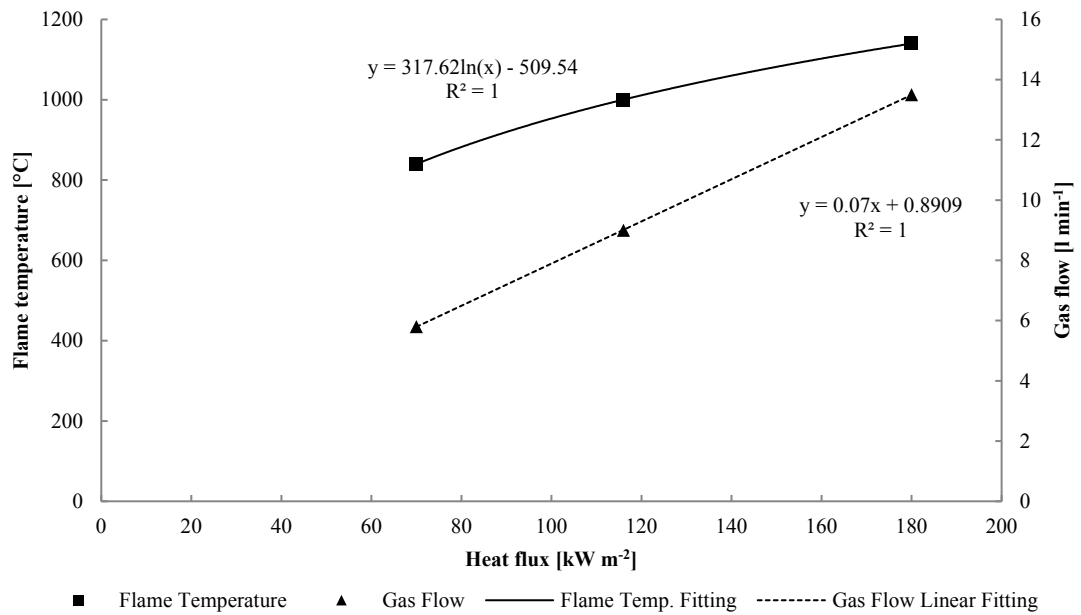


Figure 4.24: Flame Temperature [°C] and Gas Flow [l min⁻¹] vs Heat flux [kW m⁻²] showing an empirical perfect fit using exponential and linear function respectively using non-SI units.

It can also be noticed in Figure 4.24 that the inverse relationship is obviously a logarithmic function which has a perfect fit with the experimental data as well. In addition to that, if the gas flow is plotted against the heat flux generated, a linear equation can be found linking the gas flow and the heat flux. The relations reported in Figure 4.24 are more useful compared to the one in Figure 4.23 because all the time a fire test has to be performed then the flames have to be calibrated. These relations allow estimating the gas flow needed to achieve the required heat flux before even running a calibration routine. These results are valid for the distance between burner and samples used in this work, which is 320 mm. If a different distance is used then a new calibration and/or calibration chart should be produced.

4.4.2 Fire-under-load Results

The samples, previously instrumented with a thermocouple on the cold face to register the temperature profile, see Figure 4.25, were inserted in the middle of the two plates, see Figure 3.8, paying particular attention in reaching a good alignment between fibres orientation and loading direction. Once the correct load is achieved then the propane burner was lightened up and the test would start.

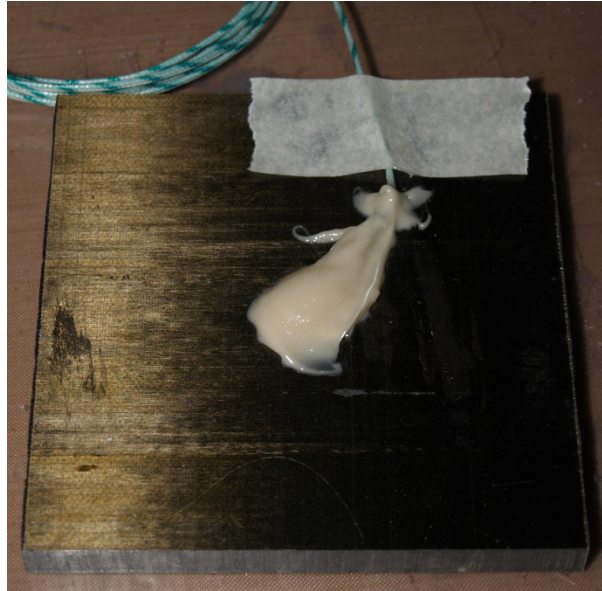


Figure 4.25: CFRP sample for Fire-under-load testing.

It was not possible to mark or record with accuracy the ignition time of the samples due to the setup of the fire tests; however effort was made to note approximate values with an error of $\pm 4-5$ [s], see Table 4.9. It can be noticed that the ignition time consistently decreases with increasing heat flux. The differences within the same heat flux can be explained by the thermal influence of the testing rig, see section 5.1 and 5.2 for a thorough explanation. Insulation could not be used because it would have inserted misalignment between the sample loading direction and the sample longitudinal axis.

Table 4.9: Approximate ignition times [s] for each test condition.

Load [%FL]	Heat flux [kW m^{-2}]		
	70	116	180
15	45	17	Non detectable
10	35	24	15
5	30	24	15

Samples suffered catastrophic failure. Pictures of the fire-under-load tested sample after failure are reported in Figure 4.26 where it can be noticed that all the samples tested present the characteristic fibre kinking as failure mode. Just in 2 cases fibre kinking is

followed by delamination which could be attributed to the fact that, once the sample starts decomposing and losing strength, local micro-buckling may occur which leads to local bending of the sample and then delamination. Just in one case, the 116 kW m⁻² at 15% failure load, the sample crushed most likely due to delamination, hence loss of strength and catastrophic failure as if the sample would shatter on itself. It can also be noticed that when the tested sample is not shattered, a typical fibre kinking band can be observed with a rotation angle very similar to 60° as reported by Mouritz and Gibson (2006).










<div>Load</div> <div>HF</div>	15%	10%	5%
70			
116			
180			

Figure 4.26: Fire-under-load tested sample side view.

Figure 4.27 reports fire-under-load test results for a compressive load of 5% of the failure load (FL) and 70 kW m^{-2} incident heat flux. It has to be highlighted that the initial ramp up of the flame temperature is not due to a real flame measurement but to the response time of the thermocouple which, to withstand such high temperatures, has to be a sheathed type thermocouple which introduces a time delay in the readings. Due to the procedure reported in section 3.3.1 the sample surface was instantaneously exposed to the final flame temperature, which, after the initial delayed response, is constantly at the required temperature depending on the desired heat flux.

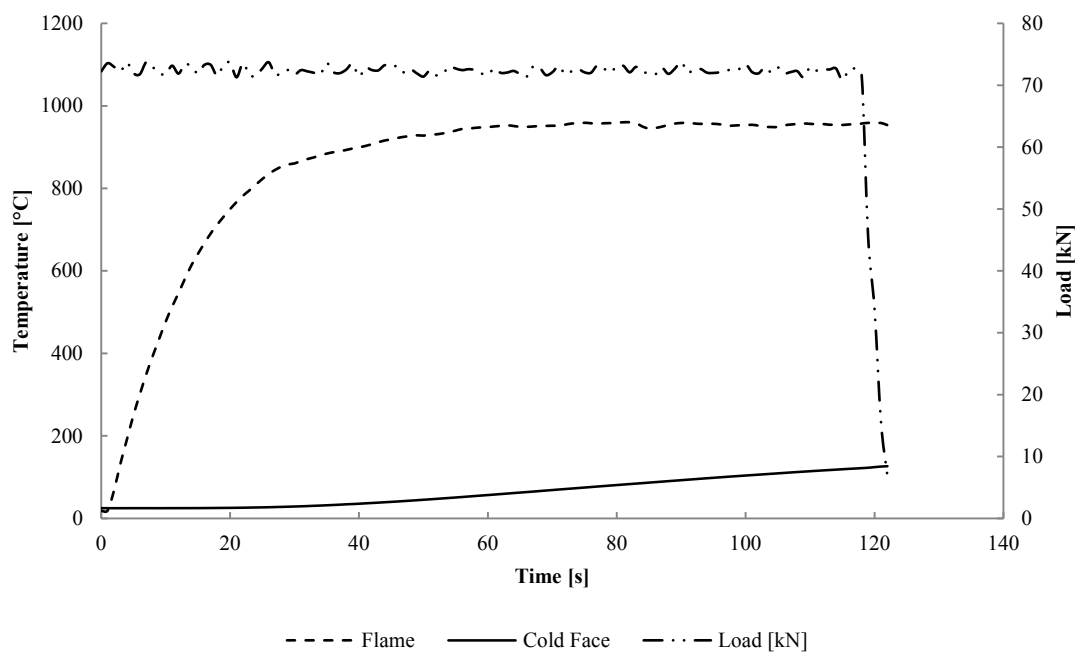


Figure 4.27: Fire-under-load test results for the case of 5%FL and 70 kW m^{-2} heat flux.

A thermal lag can also be noticed in the thermal response of the material in Figure 4.27. This characteristic could be used to measure an apparent thermal diffusivity at high temperatures Gibson et al. (2015).

A comparison between the thermal profiles of the CFRP material at the different heat fluxes applying a constant load of 5% FL is reported in Figure 4.28. The sample exposed to the 70 kW m^{-2} calibrated flames, as expected, has a slower cold face temperature rise compared to the responses to the other two heat fluxes. The thermal profiles registered

during the tests at 116 and 180 kW m⁻² are similar, which could be due to the thermal influence of the testing rig (see section 5.1 and 5.2 for a thorough explanation).

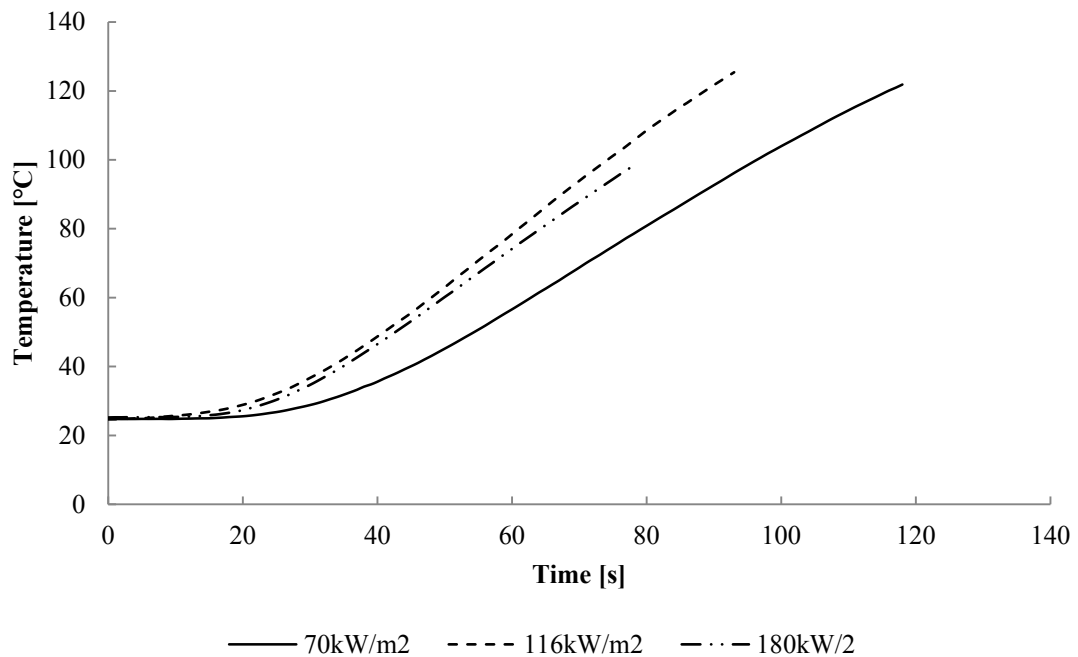


Figure 4.28: Comparison of cold face thermal responses during fire tests under load at a constant compressive load of 5%FL and different heat fluxes adopted in this study.

It can also be noticed that compressive failure at 70 kW m⁻² and 116 kW m⁻² occurs at the same cold face temperature. It has been reported in literature that structural collapse of composite in fire usually occurs when a certain temperature on the non-exposed face has occurred (Gutkin et al., 2014). This can find an explanation on the fact that if the unexposed faces of two samples of the same material have reached similar temperatures; it means that the two composites have reached a similar decomposition state in the through-thickness direction which, according to Gibson model reported in Equation 2.38, also means that they have a similar residual strength left. When this temperature reaches the critical point where the residual strength equals the applied stresses, failure occurs. The fact that for the 180 kW m⁻² test the failure occurs at a lower temperature might be explained by the thermal influence of the testing rig which may modify the actual through-thickness temperature distribution and so the actual decomposition state despite having the same cold face temperature.

This is reflected in the results of time to failure. In fact, at different heat fluxes, the time necessary to reach a certain temperature is different, being shorter at higher incident heat fluxes. Time to failure results of the fire tests under load are reported in Figure 4.29, where the time to reach failure, and to reach 120 °C on the cold face, is longer in the case of 70 kW m⁻² and shorter in the case of 116 kW m⁻².

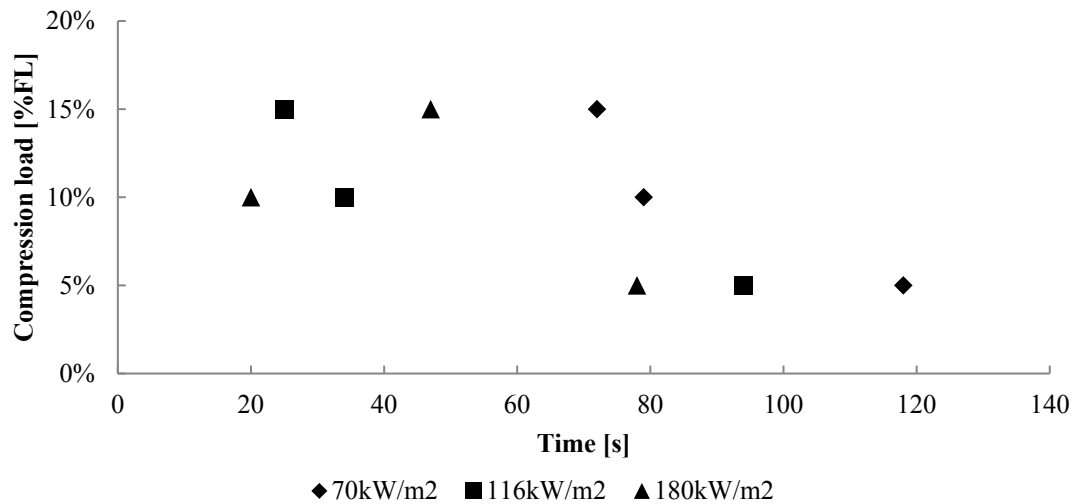


Figure 4.29: Compressive load vs time to failure at different heat fluxes.

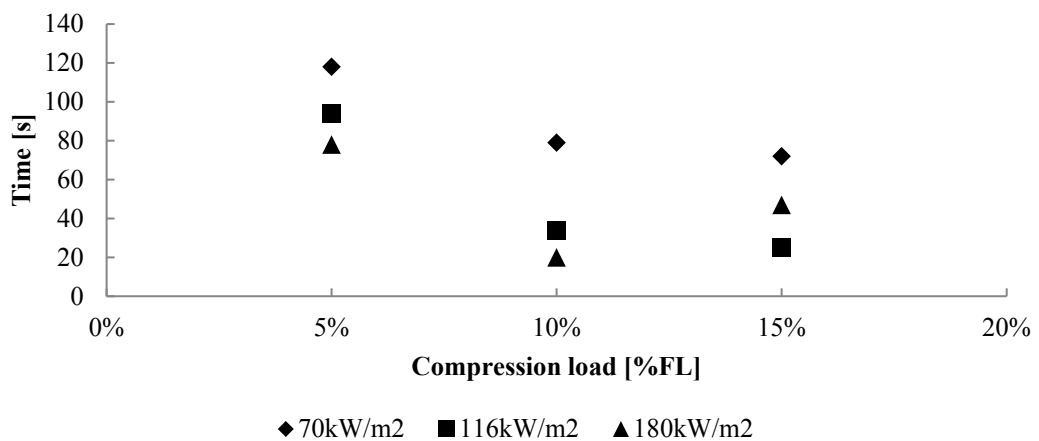


Figure 4.30: Time to failure vs compressive load at different heat fluxes.

Time to failure reported in Figure 4.29 are single experiment data, repetition could not be possible due to scarcity of material and multitude of tests required during the Fire Resist project. Large scatter of experimental data has been reported in fire tests by Bausano et al. (2005), Bausano et al. (2006), Feih et al. (2007a) and Nawaz (2011) and so these results

unfortunately are inconclusive to establish a general behaviour and to fit the data with some particular curve to be claimed as model for time to failure under compressive load of UD CFRP. Further studies with more replicate, using thermocouple and infrared camera and insulated compression after impact fixture (ASTM D7137) should be performed, using eventually different thicknesses as well. It has to be noticed that apart from the 10%FL at 180 kW m^{-2} , all the other results are in the correct trend in the sense that at the same stress condition, a higher heat flux corresponds a smaller time to failure as reported in many scientific works that have been reviewed in Chapter 1. Although it is believed that the results at 10%FL and 180 kW m^{-2} is affected by a heating effect of the jig surrounding the sample, it might actually be part of the large scatter encountered in fire tests under load as reported by Bausano et al. (2005), Bausano et al. (2006), Feih et al. (2007a) and Nawaz (2011) or both effects eventually but due to limited test data available, nothing can be concluded and further tests are needed.

4.4.3 Long-fire-exposure tests

Long-fire-exposure tests were performed to monitor the thermal profiles for long time since the fire-under-load lasted for a very short time. The purpose was to validate COMFIRE-50 for long exposure as well as short exposure times since it has been reported in literature that the model is accurate for short times but for long times fails to fit with experimental data. Figure 4.31 shows the results for long exposures at nominal heat fluxes of 70 and 180 kW m^{-2} for both heat source and the cold face temperatures. Due to a substituted gas cylinder regulator the temperature corresponding to 180 kW m^{-2} could not be achieved this time but 188 kW m^{-2} was achieved. Since this is within the standard limits this was kept as a nominal 180 kW m^{-2} but for the simulation purpose 188 kW m^{-2} is used to validate the model.

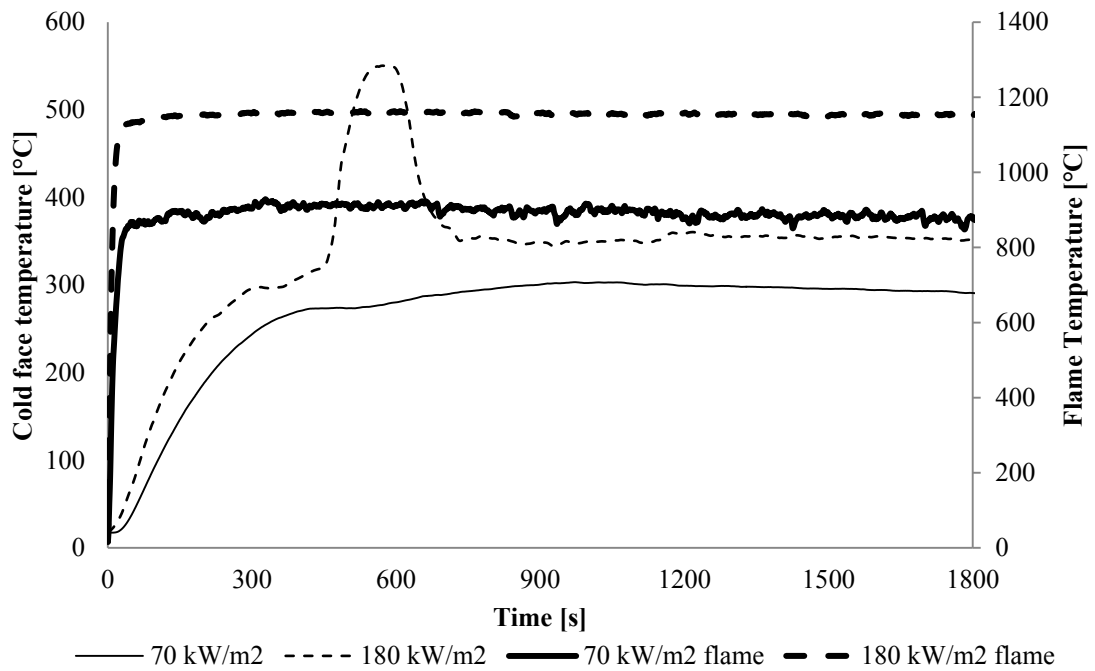


Figure 4.31: Flame temperature and cold face temperature for the long-fire-exposures at both 70 and 180 kW m⁻²; the increase in the cold face corresponding to 180 kW m⁻² is due to the starting of decomposition and burning of the resin used to install the thermocouple.

It can be noticed that there is a peak in the cold face temperature corresponding to the 180kW m⁻² heat flux which does not corresponds to a corresponding peak in the flame temperature of the heat source. This was due to a brief flame penetration between the sample edges and the insulation. There was no more material left to repeat the test but the effects lasted anyway for a very short time and both transient response before flame penetration and steady state response after flame penetration can be considered correct and usable for validating the model in the respective time frames.

For these tests additional equipment, an infrared (IR), camera was available and cold face temperature were monitored using the infrared camera as well as using the thermocouple, to highlight any differences between the two measurements, see Figure 4.32.

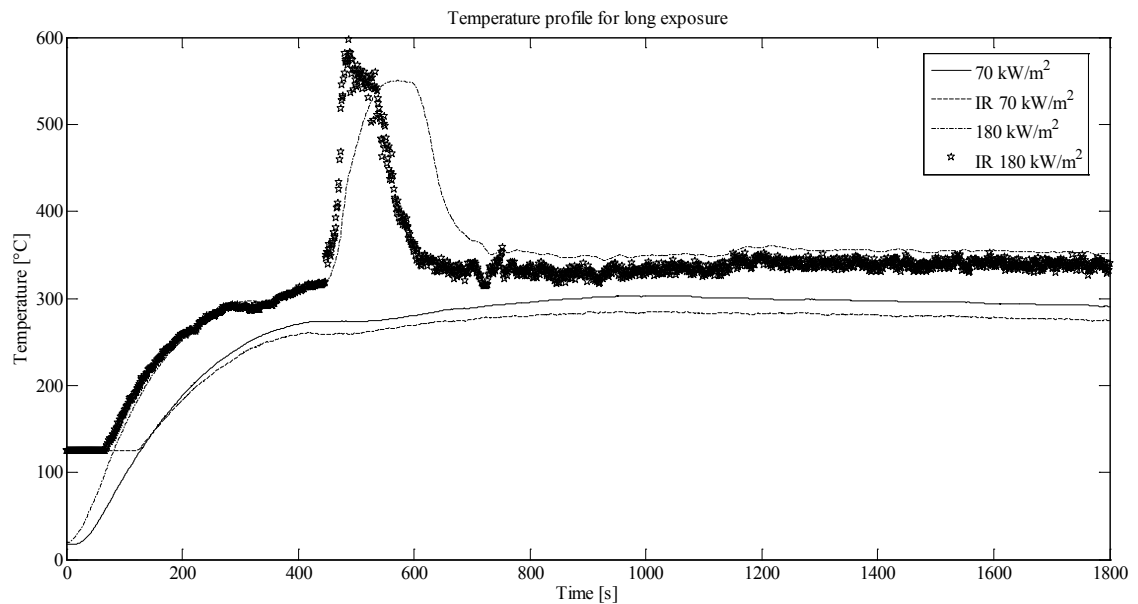


Figure 4.32: Temperature profile for long time fire exposure with both thermocouple and infrared (IR) camera; the flat constant initial temperature of the IR camera is due to the cold face temperature being lower than the minimum threshold of the chosen IR camera temperature range (125-900 °C) and not corresponding to an actual surface temperature; it can also be noticed that both thermocouple and IR measurements are confirming the short flame penetration for the 180 kW m⁻² and that the IR measurements are constantly 10-20 °C lower compared to thermocouple ones.

The IR camera used was an Optris PI 160 (from www.optris.com/thermal-imager-pi160) with a temperature range from -20 to 900 °C. Unfortunately the measurements modes are three, -2 to 100 °C, 0 to 250 °C and 150 to 900 °C. This means that one range does not cover the whole range of cold face temperature of these experiments so the range of 150-900 °C was chosen to correctly monitor most of the tests and this is the reason why the IR camera measurements start at 150 constant for a certain time.

Figure 4.32 confirms the short side flame penetration with both thermocouple and IR measurements, despite this the most important phenomenon to be noticed is that IR measurements are constantly between 10-20 °C lower, compared to the thermocouple measurements. Since the accuracy of the type K class 1 thermocouple used, in the range of temperature of this study, is within ± 1.5 °C, this discrepancy is most likely due to the small insulation effect of the resin keeping in place the measuring thermocouple. This effect is clear in the IR camera snapshots, see Figure 4.33 and Figure 4.34, where it is

evident that the resin surrounding the thermocouple (the small colder blob like shaped area on the left side of Area 1) is colder than the rest of the surface of the sample, and this might have locally risen the temperature actually sensed by the thermocouple. Also in Figure 4.34 the side flame penetration effect that occurred for the 180 kW m^{-2} test can be noticed from the fourth to the sixth snapshot counting from top left to bottom right.

As a result of these findings, not to affect fire tests results, it is advisable to use non-contact measurements techniques or finding a way to just have the thermocouple sensing tip in contact with the cold face. The best way to use contact measurements sensors such as thermocouples or Fibre Bragg Grating sensors would be to place the sensor during the manufacturing process in the middle of the fibres. Although it is not an easy task because of the problems arising on sealing the vacuum bag for the curing process, it is the best way to avoid this local hot spots due to sensor installation. Another option for high temperature measurements of up to $300 \text{ }^{\circ}\text{C}$ would be to use a “*cement on polyimide thin film thermocouple – aerospace grade*” (e.g. from www.TCDirect.co.uk) which, being characterised by having a very small amount of resin for its installation, would reduce the local hot spot effects and improve the temperature measurement accuracy.

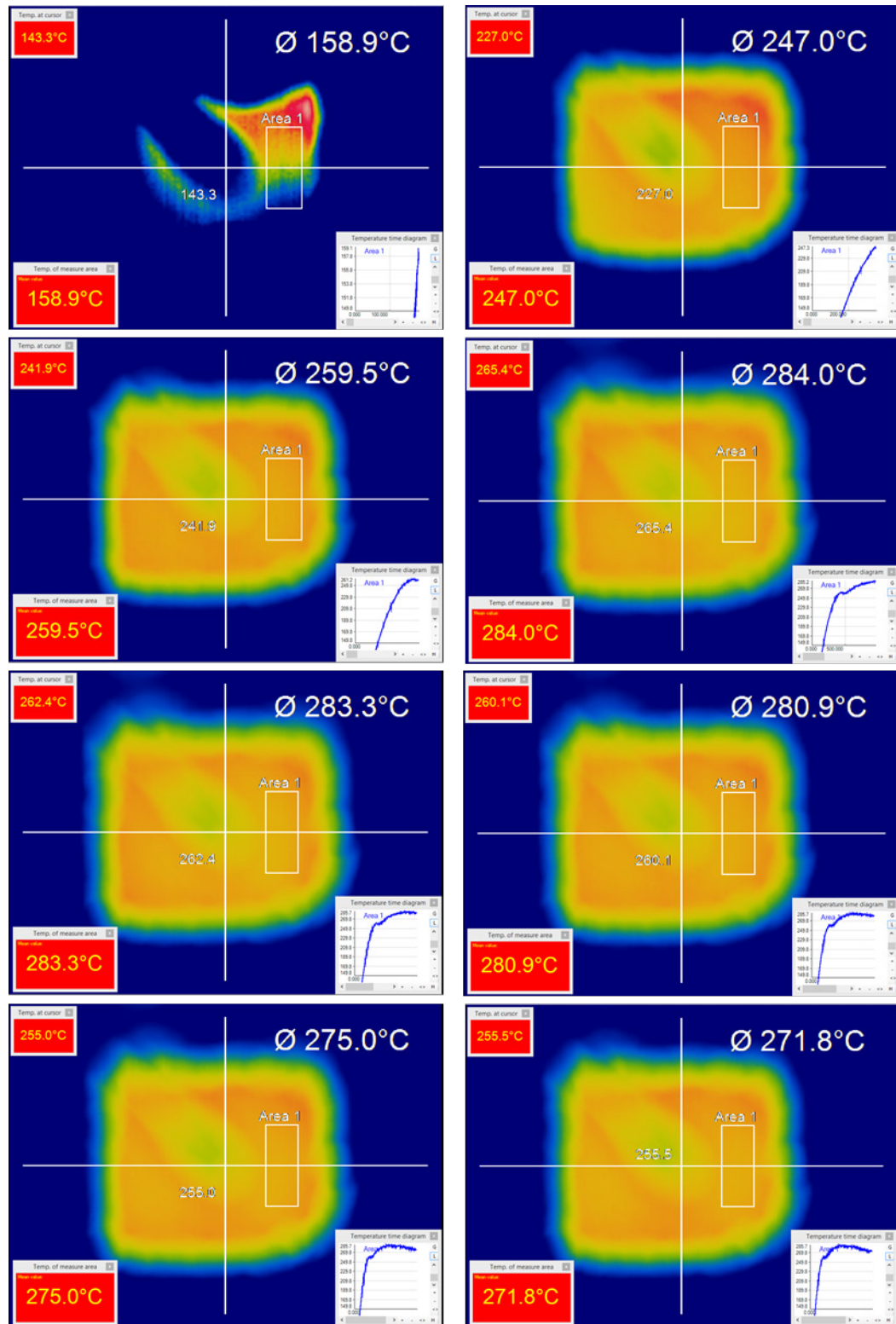


Figure 4.33: Long-fire-exposure tests at 70 kW m^{-2} IR snapshots at different time instants: top right and bottom left numbers are the average temperature in Area 1, which is considered representative of the cold face temperature; top left corner is the temperature at the cursor which is at the centre of the image; bottom right is a time temperature graph of the average temperature in Area 1; colours are automatically adjusted according to max and min temperature each time.

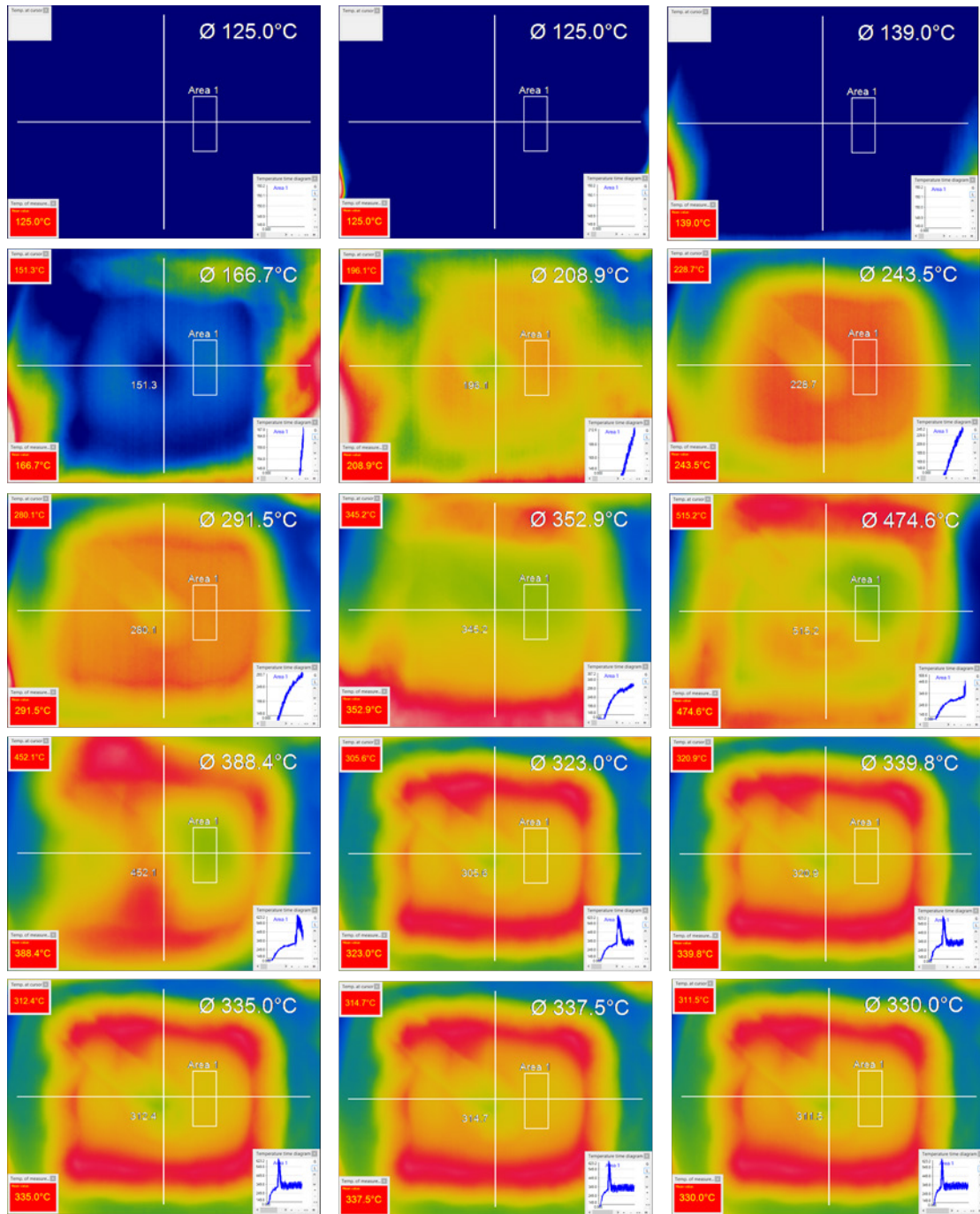


Figure 4.34: Long-fire-exposure tests at 180 kW m^{-2} IR snapshots at different time instants: top right and bottom left numbers are the average temperature in Area 1, which is considered representative of the cold face temperature; top left corner is the temperature at the cursor which is at the centre of the image; bottom right is a time temperature graph of the average temperature in Area 1; colours are automatically adjusted according to max and min temperature each time.

Chapter 5 **Modelling the fire behaviour of composites**

Modelling the fire behaviour of composites is a demanding task, especially when mechanical prediction is involved as well. To model the total fire behaviour, thermal modelling has to be performed as accurately as possible, followed by a mechanical model function not only of temperature but of the status of the decomposing composites, and depending on the material behaviour, of other parameters. What happens to the composite exposed to fire is a rise in temperature, followed by the onset of decomposition and mechanical damage. The typical mechanical damage depends on fabric and laminate layup used for composite manufacturing as well as fire intensity (Berlin, 1992; Burns et al., 2010; Mouritz and Gibson 2006; Nawaz, 2011). However it is usually characterised by resin weakening and the consequent loss of strength due to temperature dependent mechanical properties followed by delamination. If fire intensity and load are low then time dependent failure such as creep may be relevant for mechanical failure as explained in the literature review. Due to these mechanical damages, a realistic structural model should not only be updating according to mechanical and thermal properties as function of temperature and degree of decomposition, but take into consideration changes in geometry as well, e.g. delamination and out of plain thermally induced deformation (Liu et al., 2006; Nawaz, 2011; Summers, 2010; Summers et al., 2012). The COMFIRE-50 model does not take into account changes in geometry or out of plane deformation as this is out of the scope of this work. The two mechanical failure models considered (the two-layer model and the average strength model, Burns et al. (2010)) give surprising good prediction although ignoring fire induced damages and model geometry modifications. The modelling results have been performed with COMFIRE-50. The mechanical models used have been discussed previously in section 2.2.9.

5.1 Thermal response

This section describes the thermal model results. COMFIRE-50 has been used to fit the cold face temperature profiles of the fire-under-load and the long-fire-exposure tests previously described in section 4.4.2 and 4.4.3 respectively. The long-fire-exposure tests are used to find the best combination of Arrhenius parameters and heat of decomposition value that best fits the experimental results. First, an investigation with single point

thermal properties is performed, and then thermal properties function of remaining resin content will be investigated as well. The measured thermal property values in this work are not used because the range used, due to health and safety school regulations, is too narrow compared to the real temperature experienced by the composite exposed to fire.

5.1.1 Long-fire-exposure and optimum Arrhenius and heat of decomposition parameters fitting

The effect of the Arrhenius equation and heat of decomposition parameters, in fitting the experimental data, were investigated. Initially, the Arrhenius equation parameters and the heat of decomposition were investigated using single point thermal property values and they varied according to Table 5.1, while the other parameters were kept constant and are reported in Table 5.2.

Table 5.1: Investigated Arrhenius and resin heat of decomposition parameters.

Parameter	Units	Initial value	Final value	Increment
Epoxy Arrhenius pre-exponential factor (A)	$[s^{-1}]$	0	5000	500
Epoxy resin activation energy (E)	$J\ mol^{-1}$	0	10^5	10^4
Epoxy resin heat of decomposition (Q_p)	$J\ kg^{-1}$	-11723000	0	10^6

The modelled problem corresponds to an infinite composite slab, subject to two different one sided heat fluxes, 70 and 188 kW/m^2 , with single point room temperature thermal property values. The difference between the composite measured density and the modelled density according to the rule of mixture and single matrix and fibre densities and percentage is very small, 1498 and 1564 $kg\ m^{-3}$ for measured and modelled respectively. Although according to Ramroth et al. (2006), material density has a sensitive impact on the modelled results, and a higher density than the real one will lead to lower predicted temperatures, the choice of using the modelled density is dictated by the fact that the model degrades just the polymeric matrix mass and not the fibres (although polymeric or carbon fibres degrade as well depending on conditions as explained in Chapter 1). For this reason COMFIRE-50 needs to have resin mass and fibre mass as

separate entries for degradation calculation purpose. In this case the assumption of fibres not degrading is validated by the fact that carbon fibres experienced almost no mass loss in nitrogen atmosphere for temperature up to 1000 °C and a limited mass loss of lower than 20% up to 800 °C in air to (Feih and Mouritz, 2012). Since just the exposed face is going to be exposed to a somehow oxidising atmosphere, while the rest of the composite is in an oxygen deprived environment not experiencing any oxidation, the hypothesis of not degrading fibres is verified and justified in this work and in works of Burns et al. (2010) and Nawaz (2011).

Table 5.2: Constant parameters.

Parameter	Units	Value
Epoxy resin density (ρ_m)	kg m ⁻³	1300
Epoxy resin Specific Heat ($C_{p,m}$)	J kg ⁻¹ K ⁻¹	1850
Epoxy Resin Thermal conductivity ($k_{\perp m}$)	W m ⁻¹ K ⁻¹	0.35
Final epoxy resin residue	%	2
Gas Specific Heat (C_{pg})	J kg ⁻¹ K ⁻¹	2386.5
Resin Heat of combustion (H_g)	J kg ⁻¹	22.11
Carbon Fibre density (ρ_f)	kg m ⁻³	1750
Carbon fibre specific heat ($C_{p,f}$)	J kg ⁻¹ K ⁻¹	660
Carbon fibre bulk thermal conductivity ($k_{\perp f}$)	W m ⁻¹ K ⁻¹	0.32
Thickness	mm	10
Fibre volume fraction (V_f)	%	58.76
Constant Heat flux	kW m ⁻²	70; 188
Thermal properties option (k and c_p)	-	Treated as single point value
Simulation duration	min	30
Fourier number	-	0.1
Room starting temperature	°C	Depending on experimental value
Flames heat flux feedback	-	Included
Mass flow effects	-	Included
Decomposition effects	-	Included
Heat source emissivity	-	0.8
Hot face absorptivity	-	0.8

Hot face emissivity	-	0.8
Hot face boundary condition	-	Convection + radiation
Cold face boundary condition	-	Free convection + radiation
Number of nodes	-	11

The search for the best fit with the experimental measurements was performed calculating the results for each heat flux and combination of A , E and Q_p parameter values. Then thermocouple and IR camera results were separately compared to the corresponding heat flux modelled results and the error calculated according to Equation 5.1. Both experimental and calculated signal sampling frequencies were 1 Hz so for each A , E and Q_p combination, the whole comparison was performed using 2 x 1801 points for thermocouple measurements and IR camera measurements respectively.

$$Er = \frac{\sum_{k=1}^N \left(\frac{T_{sim,k}}{T_{meas,k}} - 1 \right)^2}{N} \quad \text{Equation 5.1}$$

Here Er is the dimensionless error, N is the number of points (in this case 2 x 1801) and $T_{meas,k}$ and $T_{sim,k}$ are the k^{th} simulated and measured temperature respectively.

Since the error function is a function of 3 independent variable, it cannot be represented as whole in a 3 dimensional graph although results can be wrapped and represented in a 2D plot where the horizontal axis represents the iteration number (embedding A , E and Q_p values) and the vertical axis is the corresponding average error, see Figure 5.1 and Figure 5.2.

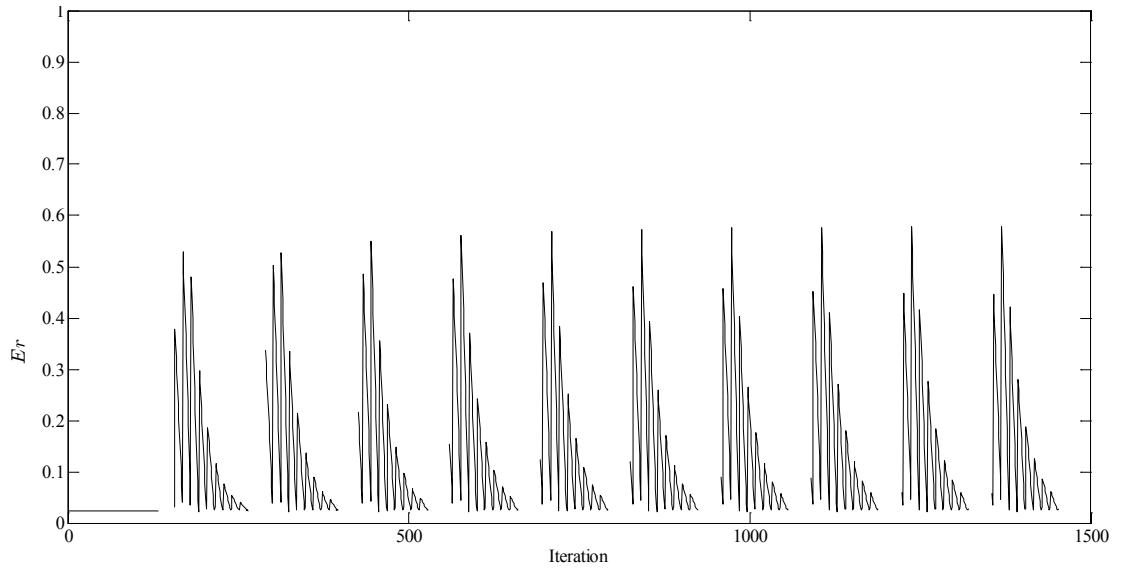


Figure 5.1: Average error for thermocouple measurements function of A , E and Q_p .

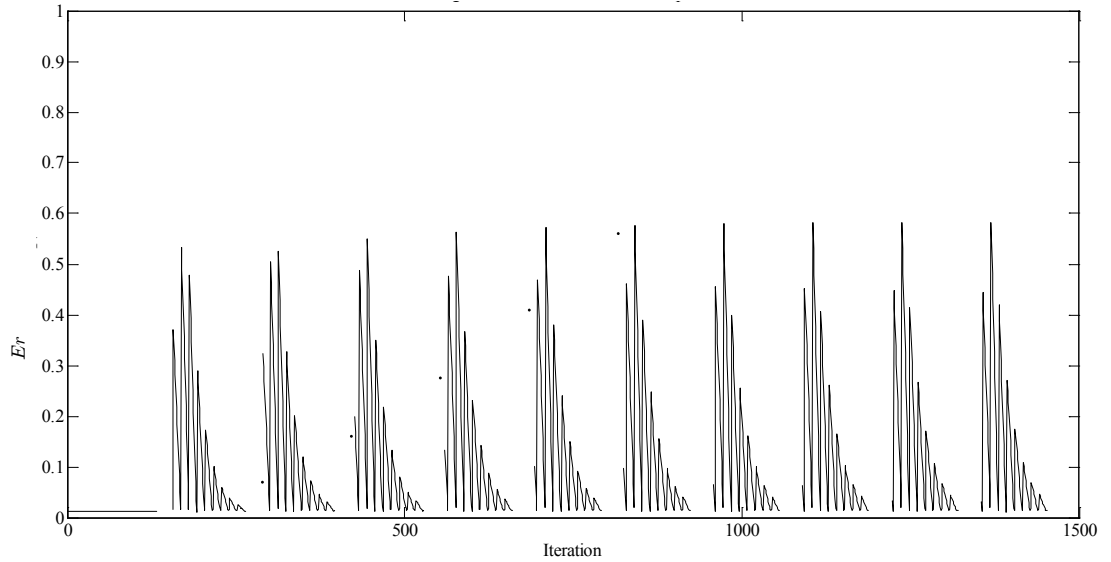


Figure 5.2: Average error for IR camera measurements function of A , E and Q_p .

It can be noticed that except for $A=0$, corresponding to the first 132 iterations, for each value of A , the error function has the same trend, with quite regular peaks and valleys. The initial constant value of the error function is independent of the values of E and Q_p because $A=0$ means that there is no change in mass and/or decomposition, removing any effect that varying E and Q_p would have on the error function. The minimum error for thermocouple was found to be 0.021 while for the IR camera was 0.011, and they were found for A , E and Q_p values reported in Table 5.3. Despite the error calculated here is affected by the short period that some flames passed on the cold face, the overall error is

remarkably low. The corresponding error considering just the 70 kW m^{-2} results for the thermocouple and IR measurements are 0.017 and 0.008 respectively.

Table 5.3: Optimum and literature (Dodds et al., 2000 and Looyeh et al., 2001) Arrhenius and heat of decomposition values for single point thermal properties model.

Parameter	Units	Thermocouple	IR camera	literature
Epoxy Arrhenius pre-exponential factor (A)	s^{-1}	1000	500	500
Epoxy resin activation energy (E)	J mol^{-1}	$4 \cdot 10^4$	$4 \cdot 10^4$	$6.05 \cdot 10^4$
Epoxy resin heat of decomposition (Q_p)	J kg^{-1}	$-7.23 \cdot 10^5$	$-7.23 \cdot 10^5$	$-2.3446 \cdot 10^6$

It is worth noticing that both set of optimum Arrhenius parameters are aligned with values reported in the literature by Dodds et al. (2000). The optimum heat of decomposition differs instead from literature value reported by Looyeh et al. (2001) by one order of magnitude. The difference between the optimum value of heat of decomposition found and the literature one, might be explained by the fact that this value corresponds to the energy used by the matrix in the decomposition process and, since it is endothermic, it corresponds to a subtraction of energy which might implicitly correct the wrong assumption of single point resin thermal properties. Figure 5.3 represents the error function just for the 2 different A optimum values according to Table 5.3 and it can be highlighted that what influences the most the error is the value of E , rather than the one of Q_p . In fact, choosing the wrong value of E (namely each tooth of the saw tooth curve represents the error as function of Q_p , keeping A and E constant) may make the error become too high if a compensating value of Q_p is not chosen. On the other hand, choosing the correct value of E keeps the error more contained and the correct choice of Q_p may just further lower the error which is already low. These findings are confirmed by the work of Ramroth et al. (2006) about sensitivity analysis on the same mathematical model used here, but solved with the finite element method. In fact, Ramroth et al. (2006) found that, while the values of E , c_{pg} , k_v , k_{char} , ρ_v and ρ_{char} play an important role in the model prediction and their values should be evaluated accurately, the values of A and c_p have relative importance and $c_{p, char}$, n and Q_p are the least important.

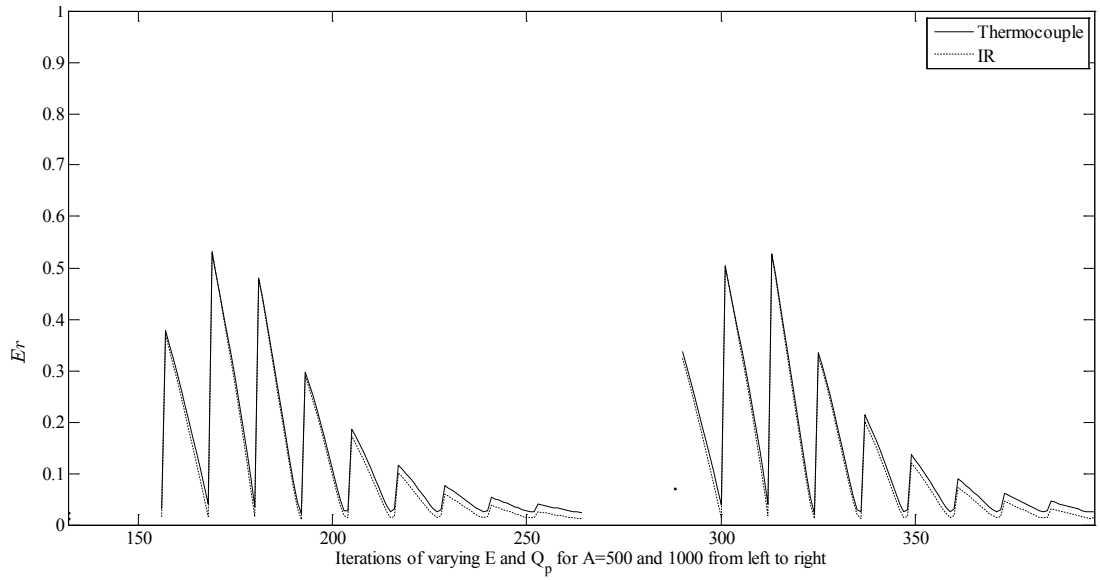


Figure 5.3: Error function for varying E and Q_p and the two values of A corresponding to the minimum error according to Table 5.3.

A 3D surface plot and a contour plot of the error as function of each optimal A value and changing E and Q_p for both thermocouple and IR camera measurements are reported in Figure 5.4 and Figure 5.5 respectively. It is noticeable that it exists a region, i.e. a range of combinations of E and Q_p that tends to minimise the error, no matter their actual value.

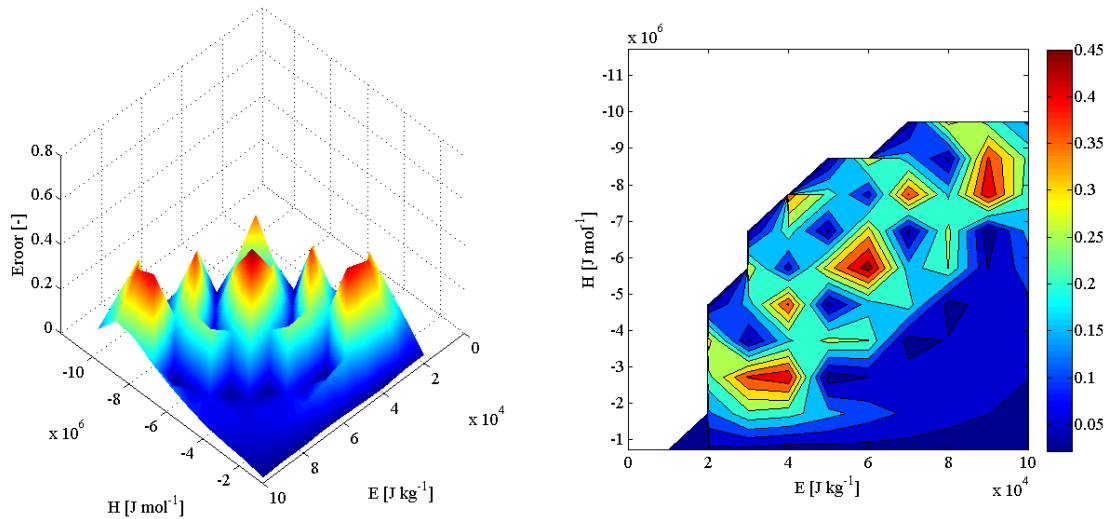


Figure 5.4: 3D surface and contour plots of average error function in respect to thermocouple measurements for $A=1000 \text{ s}^{-1}$.

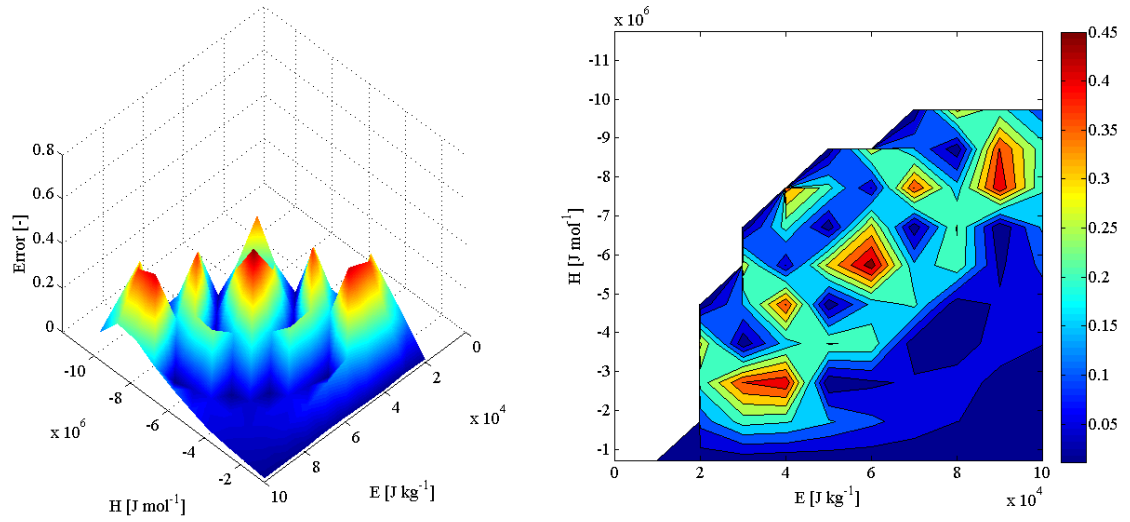


Figure 5.5: 3D surface and contour plots of average error function in respect to IR measurements for $A=500 \text{ s}^{-1}$.

Although it has been stated before that the sets of Arrhenius parameters that fit a TGA curve can be several and made of different values, these and Ramroth et al. (2006) findings reveal that an accurate evaluation of E should be made otherwise the models may not predict the temperature vs time behaviour as accurately, if a compensating value of Q_p is not chosen. The experimental temperature measurements and the best calculated temperature profiles are reported in Figure 5.6 and the corresponding error percentages, according to Equation 5.2, are reported in Figure 5.7.

$$Er_{\%} = \frac{T_{sim}}{T_{meas}} - 1$$

Equation 5.2

Here T_{sim} and T_{meas} are the simulated and measured temperature respectively. A positive error means that the calculated temperatures are over estimated while a negative error means that they are underestimated

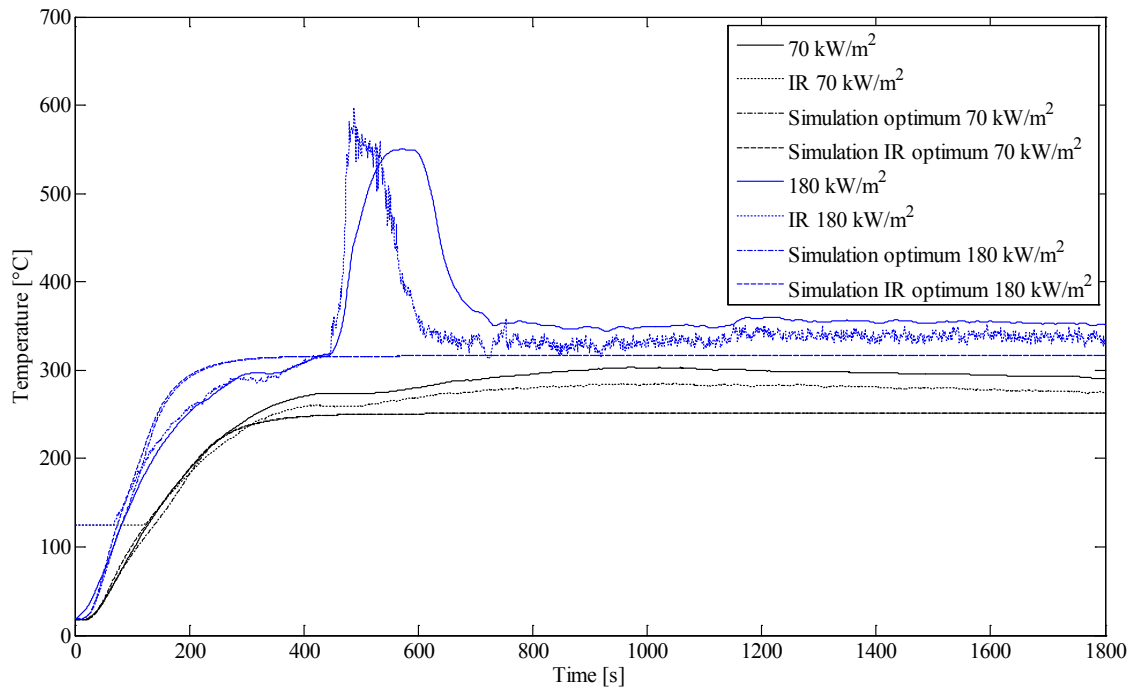


Figure 5.6: Long-fire-exposure temperature profiles for both 70 and 180 kW m⁻² using thermocouple and IR camera results: the black lines are the 70 kW m⁻² and the blue lines are 180 kW m⁻² results; calculated temperatures were produced using the 2 sets of parameters reported in Table 5.3.

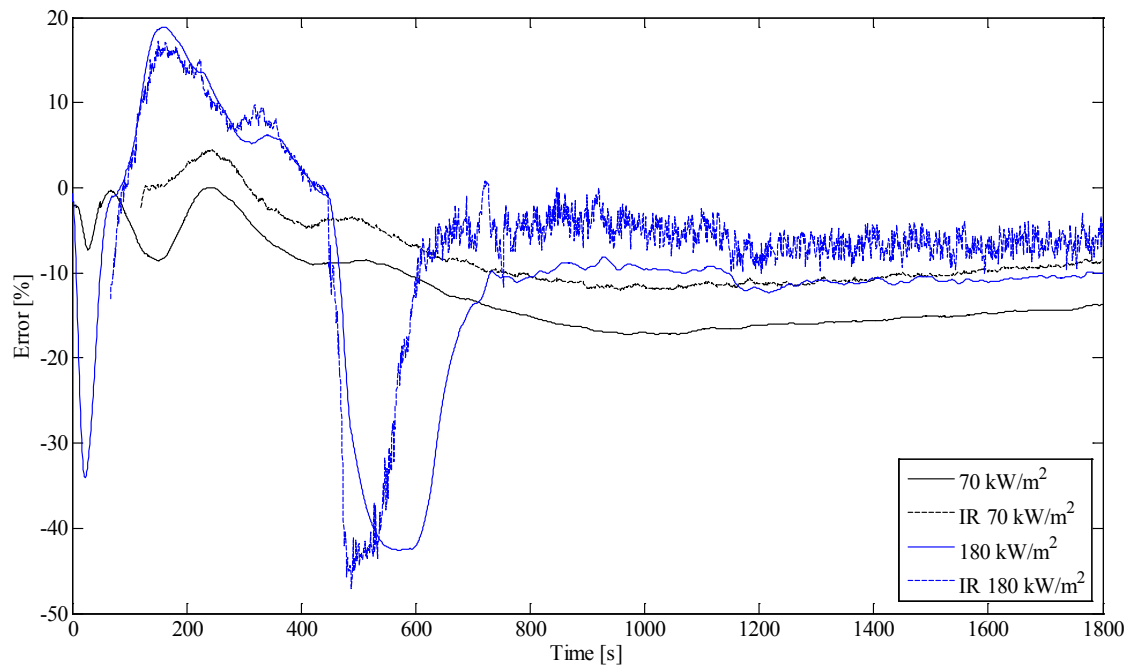


Figure 5.7: Temperature error percentage between the measured and calculated temperature using the best fitting Arrhenius and resin decomposition parameters for both thermocouple and IR camera measurements reported in Table 5.3.

Since Ramroth et al. (2006) found that the model is very sensitive to correct values of thermal properties, another optimisation by varying, A , E and Q_p along with thermal conductivity, specific heat capacity and density according to remaining resin content was performed. The values of A , E and Q_p were varied according to Table 5.1, while the thermal properties were function of the decomposition state according to Equation 2.24, Equation 2.25 and Equation 2.26 but not function of temperature, since the range of temperature used during their evaluation in section 4.2 is limited compared to a real fire scenario. Error results along the whole wide spectrum of Arrhenius and heat of decomposition parameters are reported in Figure 5.8 and Figure 5.9.

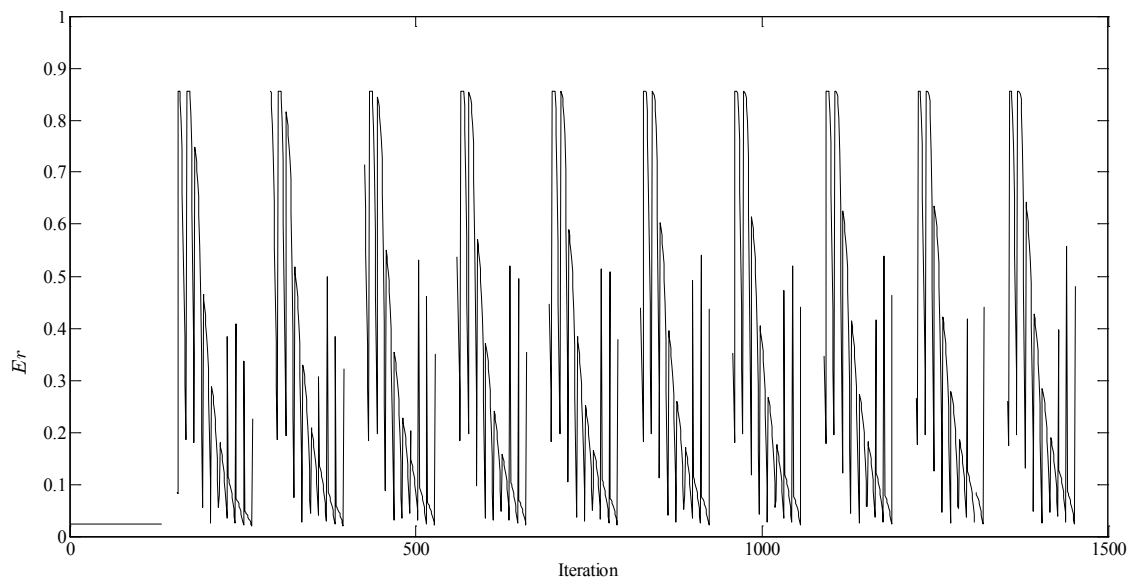


Figure 5.8: Average error for thermocouple measurements function of A , E , Q_p and thermal properties function of decomposition state.

It can be noticed that the shape of the saw tooth curve has slightly changed but the overall trend remains the same. In this case the optimum set of parameters has been found for the same values for both thermocouple and IR camera measurements and reported in Table 5.4. In this case, the optimum values to minimise the error are closer to literature values compared to the ones found when considering the thermal properties as constant room temperature single point values.

Table 5.4: Optimum and literature (Dodds et al., 2000 and Looyeh et al., 2001) Arrhenius and heat of decomposition values for thermal properties function of remaining resin content.

Parameter	Units	Thermocouple	IR camera	Literature
Epoxy Arrhenius pre-exponential factor (A)	s^{-1}	500	500	500
Epoxy resin activation energy (E)	$J\ mol^{-1}$	10^5	10^5	6.05×10^4
Epoxy resin heat of decomposition (Q_p)	$J\ kg^{-1}$	-1.723×10^6	-1.723×10^6	-2.3446×10^6

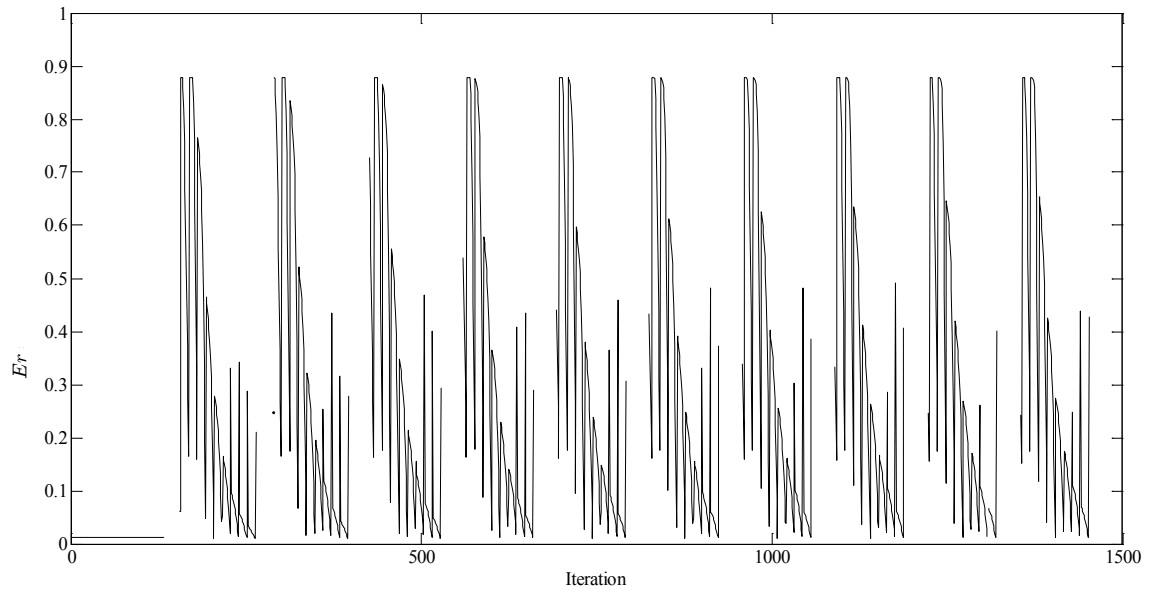


Figure 5.9: Average error for IR measurements function of A , E , Q_p and thermal properties function of decomposition state.

The case of constant optimum value for $A=500\ s^{-1}$ is reported in Figure 5.10 and the minimum error values are 0.019 and 0.010 for thermocouple and IR camera measurements respectively. Discarding the values of the $188\ kW\ m^{-2}$ which are affected by the short flame on the cold face as well, the error values for the $70\ kW\ m^{-2}$ are 0.011 and 0.005 respectively for thermocouple and IR camera measurements. Just varying the thermal properties according to remaining resin content, reduces the overall minimum error by a small amount but finds the same Arrhenius parameters and heat of decomposition which is correct since dealing with the same material. The influence on changing thermal properties as function of remaining resin content on improving the error is even greater if just the $70\ kW\ m^{-2}$ results are considered, in fact the improvement is between one third to half of the error of the single point thermal properties model.

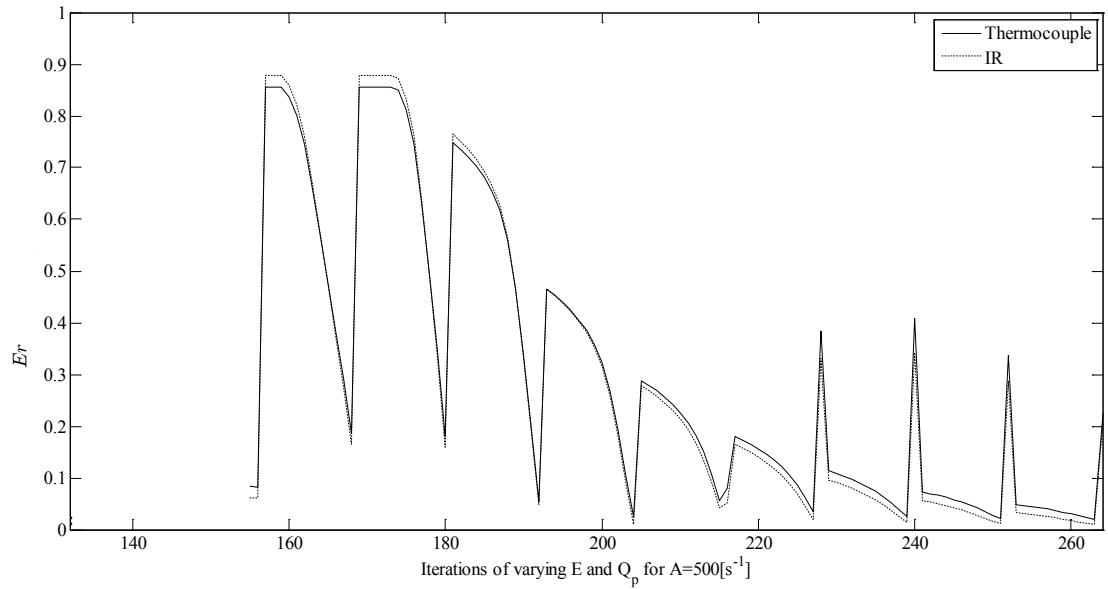


Figure 5.10: Error function for varying E and Q_p , $A = 500 \text{ s}^{-1}$ and thermal properties function of decomposition state.

Figure 5.11 and Figure 5.12 represent the error function as a 3D surface graph and a contour plot for both thermocouple and IR camera measurements separately, they both show similar patterns to each other.

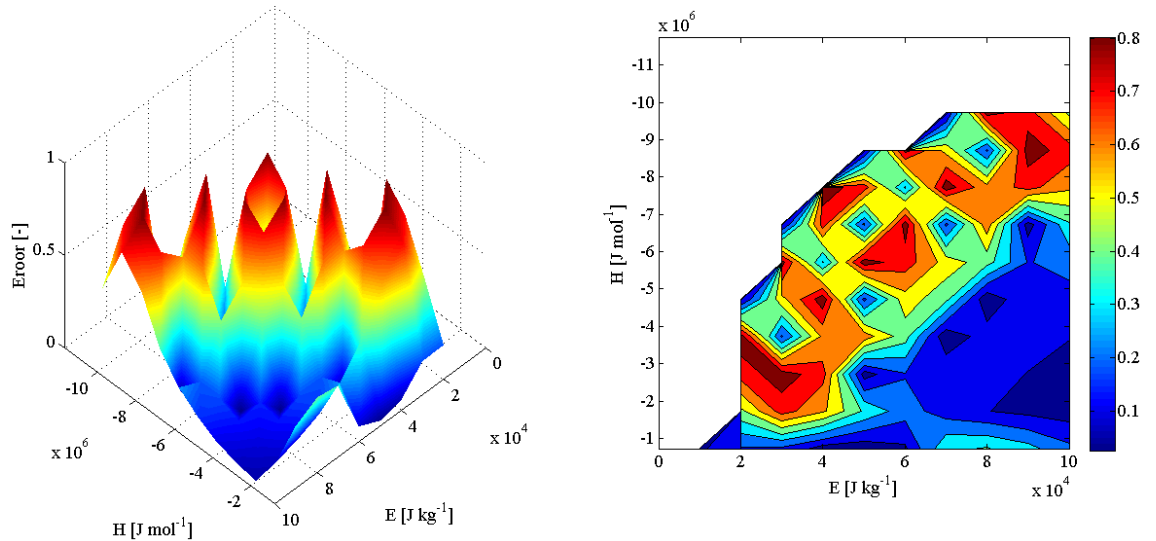


Figure 5.11: 3D surface and contour plots of average error function in respect to thermocouple measurements for $A = 500 \text{ s}^{-1}$.

They are both characterised, as previously found for single point thermal properties model, by an area where different combinations of E and Q_p tend to minimise the error

between calculated and measured temperature, with the error of the IR camera measurements being always lower compared to the thermocouple one.

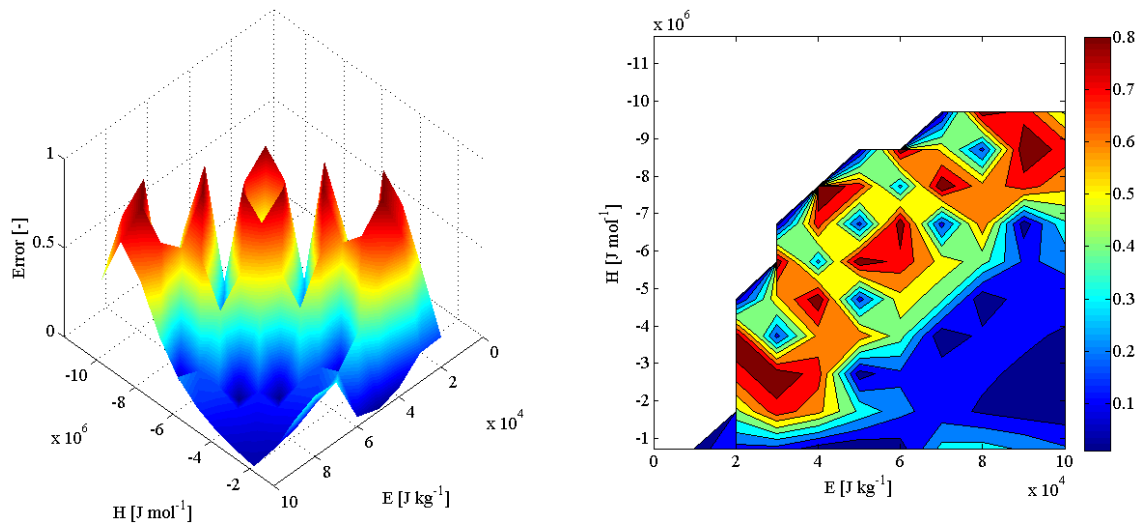


Figure 5.12: 3D surface and contour plots of average error function in respect to IR measurements for $A=500 \text{ s}^{-1}$.

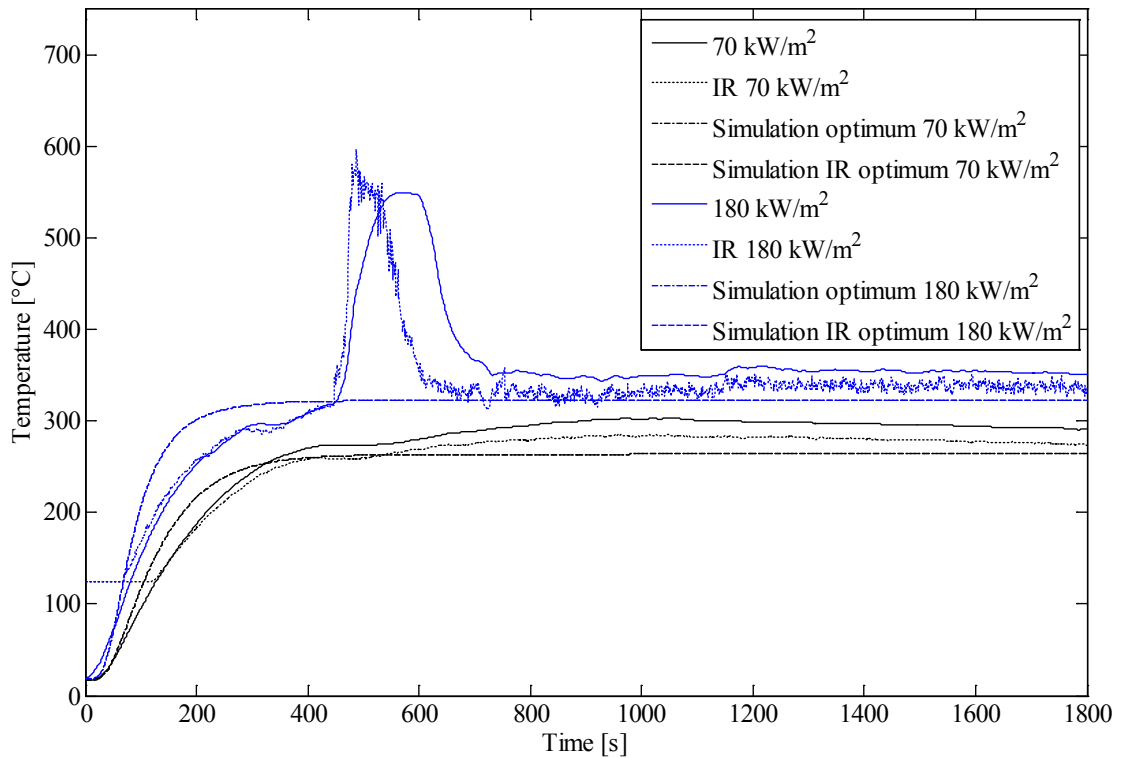


Figure 5.13: Long-fire-exposure temperature profiles for both 70 kW m^{-2} and 180 kW m^{-2} using thermocouple and IR camera results: the black lines are the 70 kW m^{-2} and the blue lines are 180 kW m^{-2} results; calculated temperatures were produced using the parameter sets reported in Table 5.4.

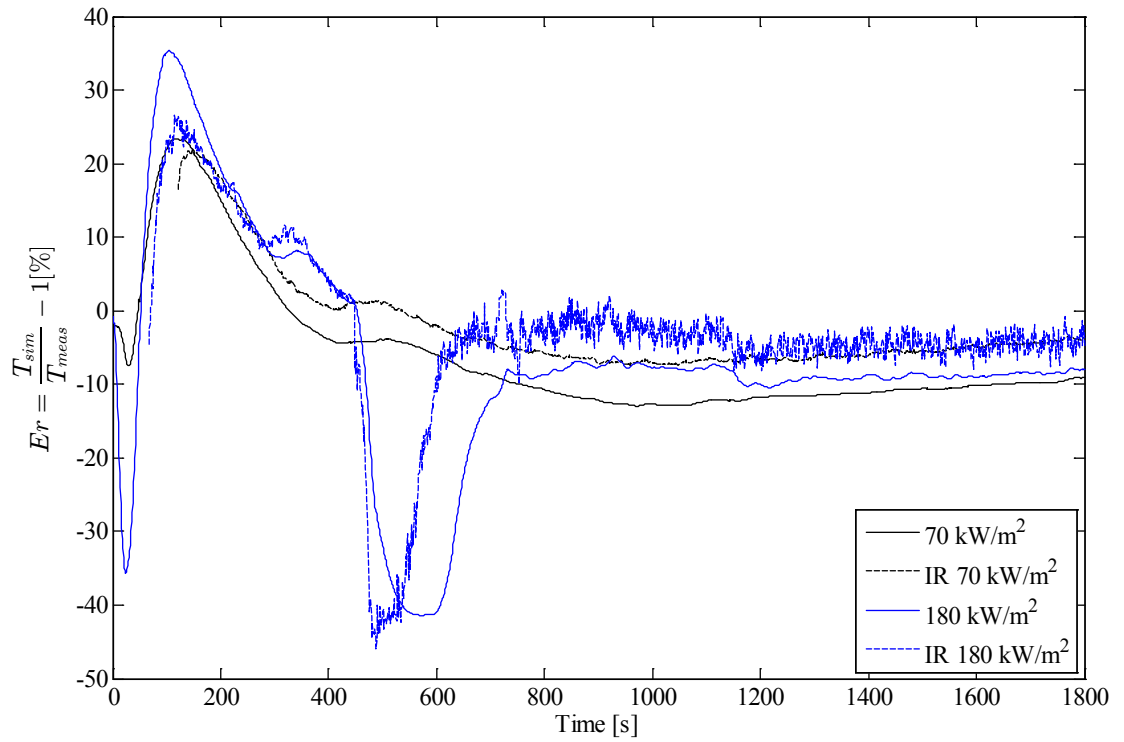


Figure 5.14: Temperature error percentage between the measured and calculated temperature using the best fitting Arrhenius and resin decomposition parameters for both thermocouple and IR camera measurements reported in Table 5.4.

Measured and optimum calculated temperature are reported in Figure 5.13. Figure 5.14 reports the error in percentage of the measured temperature according to Equation 5.2. Although objectively the overall error function value of the predicted temperatures with thermal properties function of remaining resin content is lower compared to the one with single point thermal properties, the single point thermal properties prediction is closer to the experimental measurements because of the smaller percentage error range of the latter comparing Figure 5.7 and Figure 5.14. This is further confirmed by especially comparing the transient response of the 70 kW m⁻² results between Figure 5.6 and Figure 5.13. The better results of the prediction with thermal properties function of remaining resin content lays on the fact that it better predicts the steady state response. In fact, it has a greater influence on the error value since is longer than the transient response which accounts for 1/6, or less, of the total number of sample used for this comparison. In fact the steady state response (between 300 and 1800 seconds, excluding the short flame penetration effects) is characterised by an error within $\pm 10\%$ for the calculated temperature with thermal properties function of remaining resin content, and -20% to 10% for the single point thermal properties predictions. On the other hand, comparing the transient part of

the response, the error is between $\pm 30\%$ for the calculated temperatures with thermal properties as function of remaining resin content and between -30% to 20% for the single point one. This might be due to the fact that the model with the optimum parameters found for thermal properties changing with remaining resin content, better predicts the final thermal properties than the one with single point values. On the other hand the thermal properties evolution with remaining resin content during the transient state are not yet well captured, in fact the single point thermal properties model better captures this behaviour, almost perfectly for the 70 kW m^{-2} tests.

Another optimum search was performed, using narrower range of variation of A , E and Q_p around the optimum values already identified, see Table 5.5, and changing thermal properties according to remaining resin content, while the other parameters were kept constant according to Table 5.2.

Table 5.5: Investigated Arrhenius and resin heat of decomposition parameters.

Parameter	Units	Initial value	Final value	Increment
Epoxy Arrhenius pre-exponential factor (A)	s^{-1}	300	700	100
Epoxy resin activation energy (E)	J mol^{-1}	10^4	10^5	10^4
Epoxy resin heat of decomposition (Q_p)	J kg^{-1}	-2.5×10^6	-1.5×10^6	10^5

This further optimisation led to the results reported in Figure 5.15 to Figure 5.21. The sets of optimum parameters realising the minimum error are reported in Table 5.6.

Table 5.6: Optimum and literature (Dodds et al., 2000 and Looyeh et al., 2001) Arrhenius and heat of decomposition values for thermal properties function of remaining resin content.

Parameter	Units	Thermocouple	IR camera	literature
Epoxy Arrhenius pre-exponential factor (A)	s^{-1}	300	300	500
Epoxy resin activation energy (E)	J mol^{-1}	10^5	10^5	6.05×10^4
Epoxy resin heat of decomposition (Q_p)	J kg^{-1}	-1.5×10^6	-1.7×10^6	-2.3446×10^6

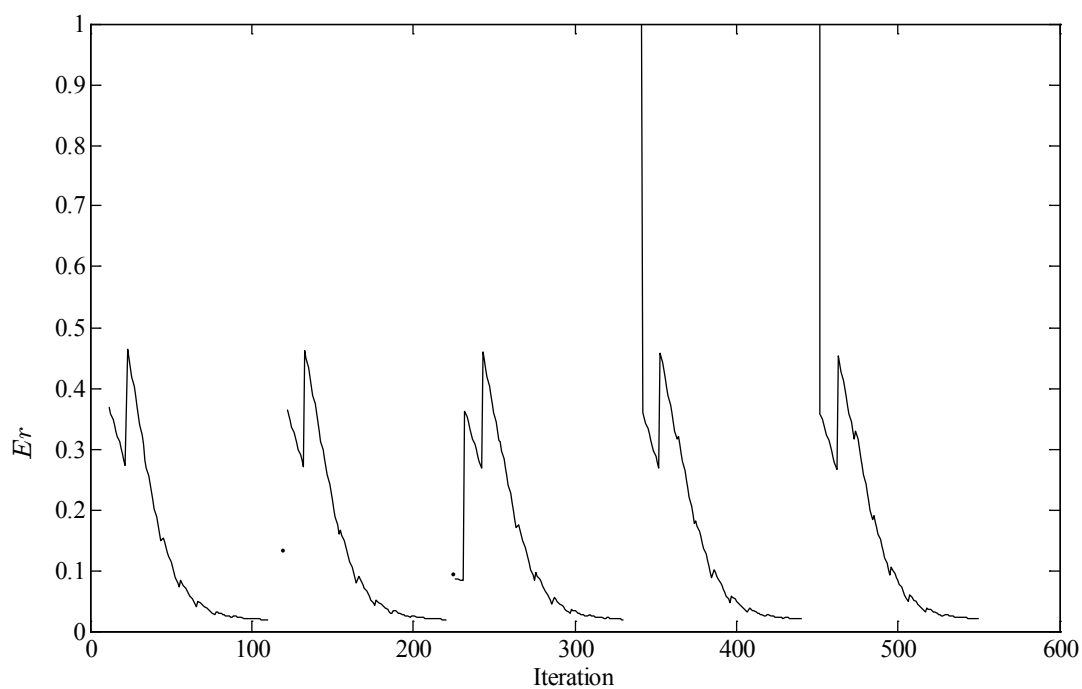


Figure 5.15 Average error for thermocouple measurements function of A , E , Q_p and thermal properties function of decomposition state.

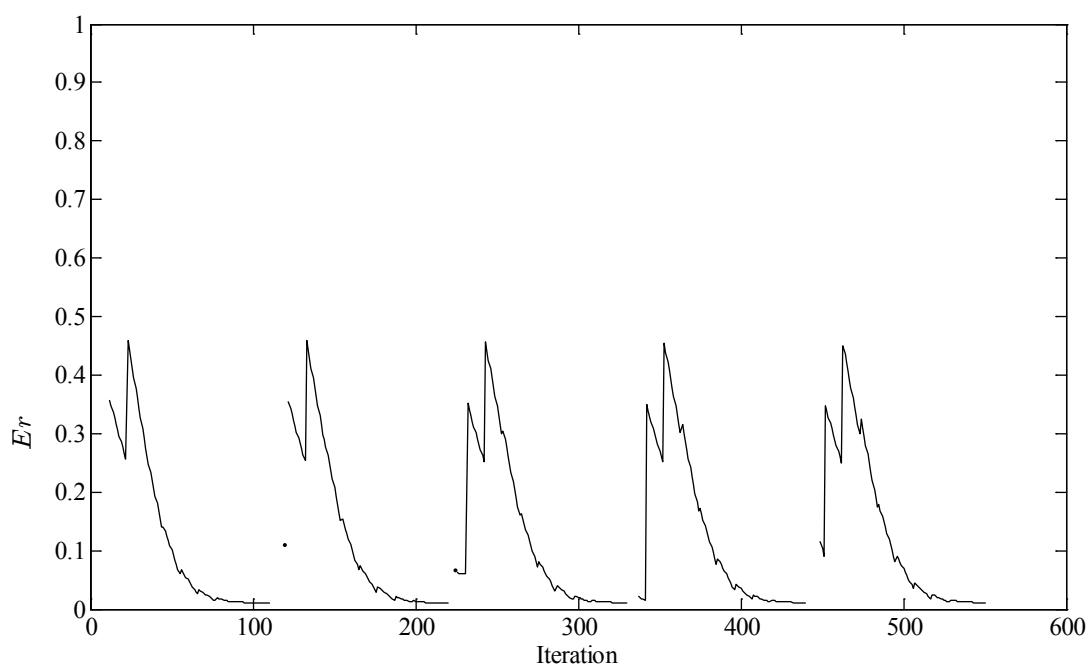


Figure 5.16 Average error for IR measurements function of A , E , Q_p and thermal properties function of decomposition state.

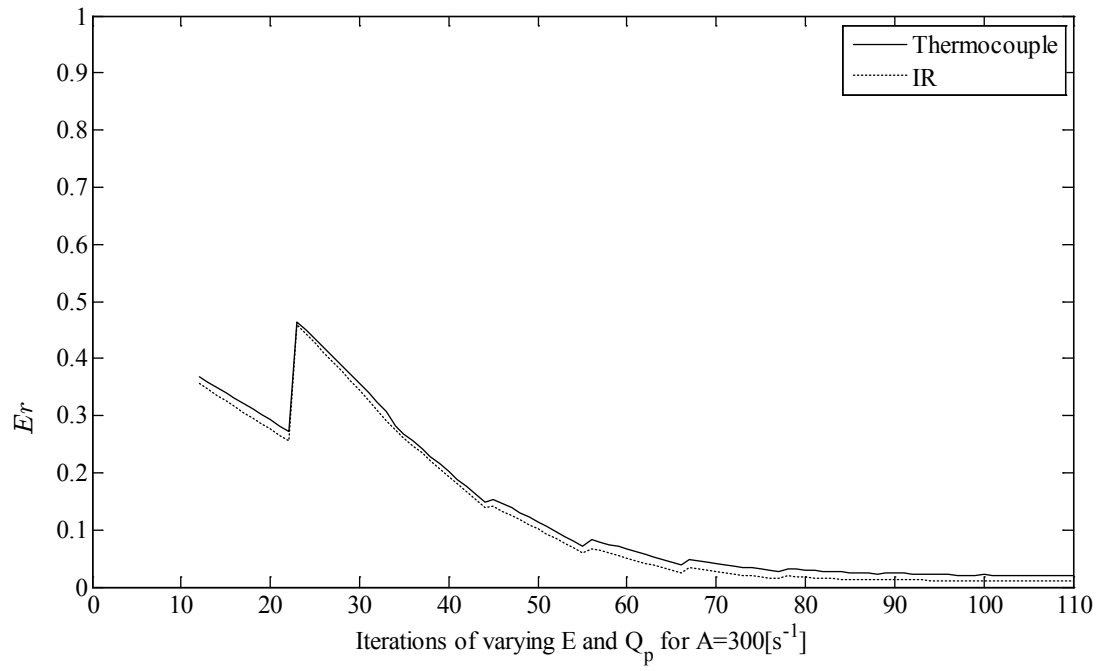


Figure 5.17: Error function for varying E and Q_p , $A=300\text{ s}^{-1}$ and thermal properties function of decomposition state.

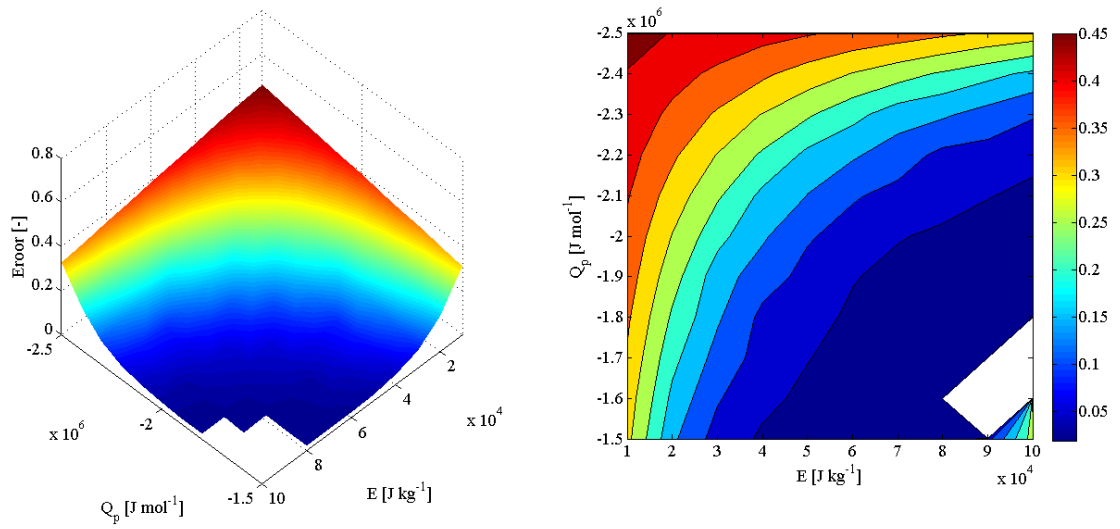


Figure 5.18: 3D surface and contour plots of average error function in respect to thermocouple measurements for $A=300\text{ s}^{-1}$.

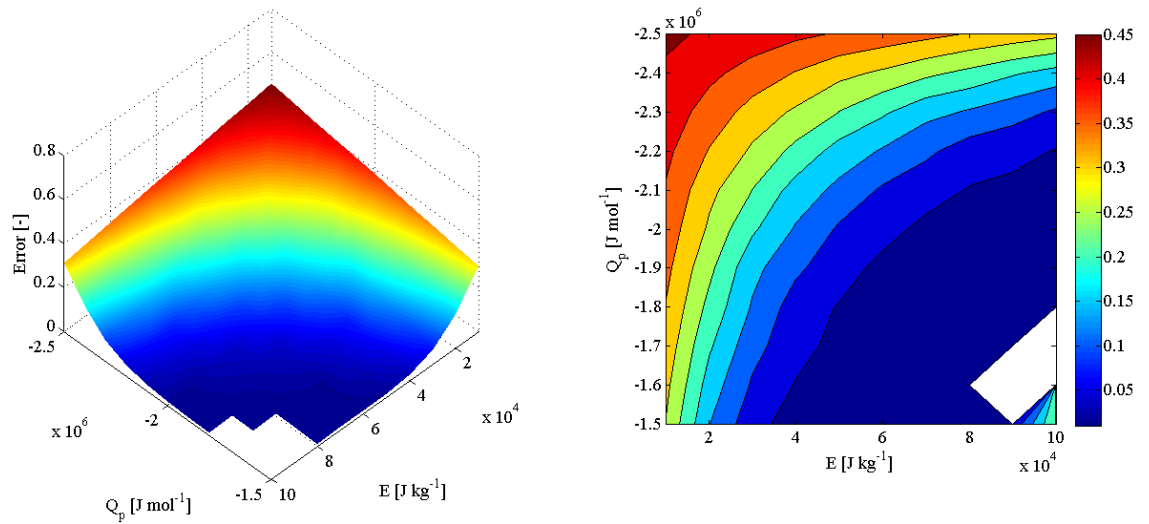


Figure 5.19: 3D surface and contour plots of average error function in respect to IR measurements for $A=300 \text{ s}^{-1}$.

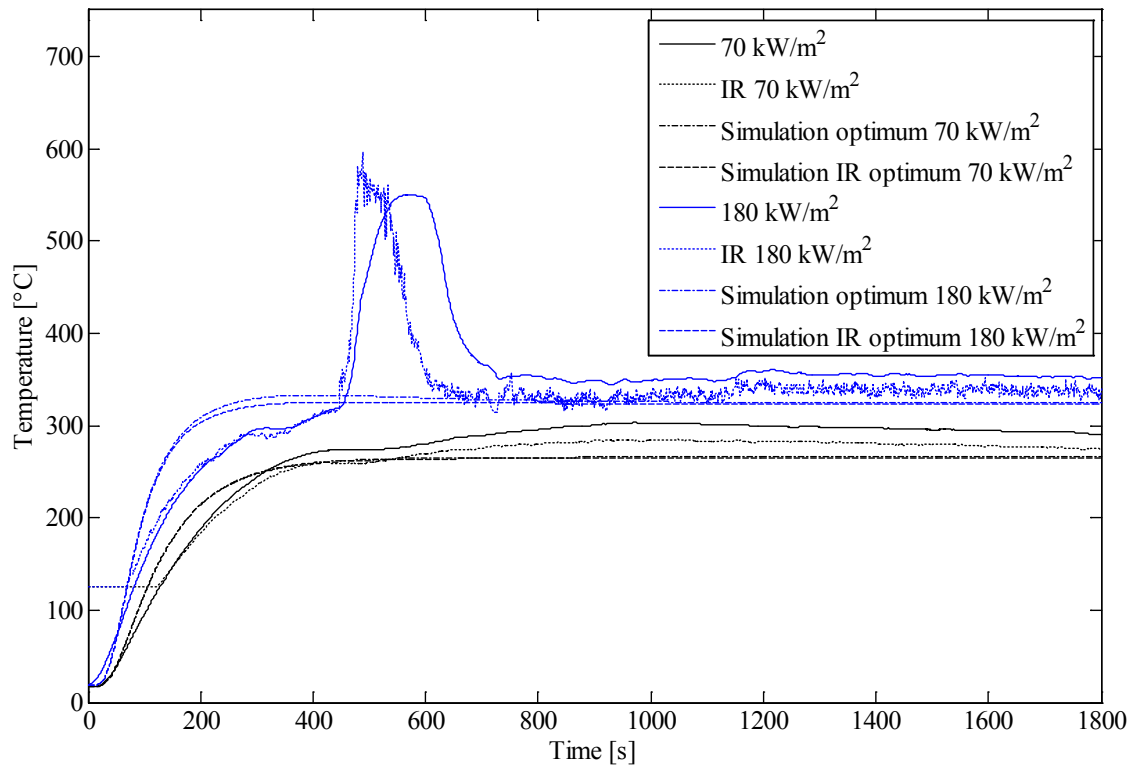


Figure 5.20: Long-fire-exposure temperature profiles for both 70 kW m^{-2} and 180 kW m^{-2} using thermocouple and IR camera results: the black lines are the 70 kW m^{-2} and the blue lines are 180 kW m^{-2} results; the calculated temperatures were produced using the parameter sets reported in Table 5.6.

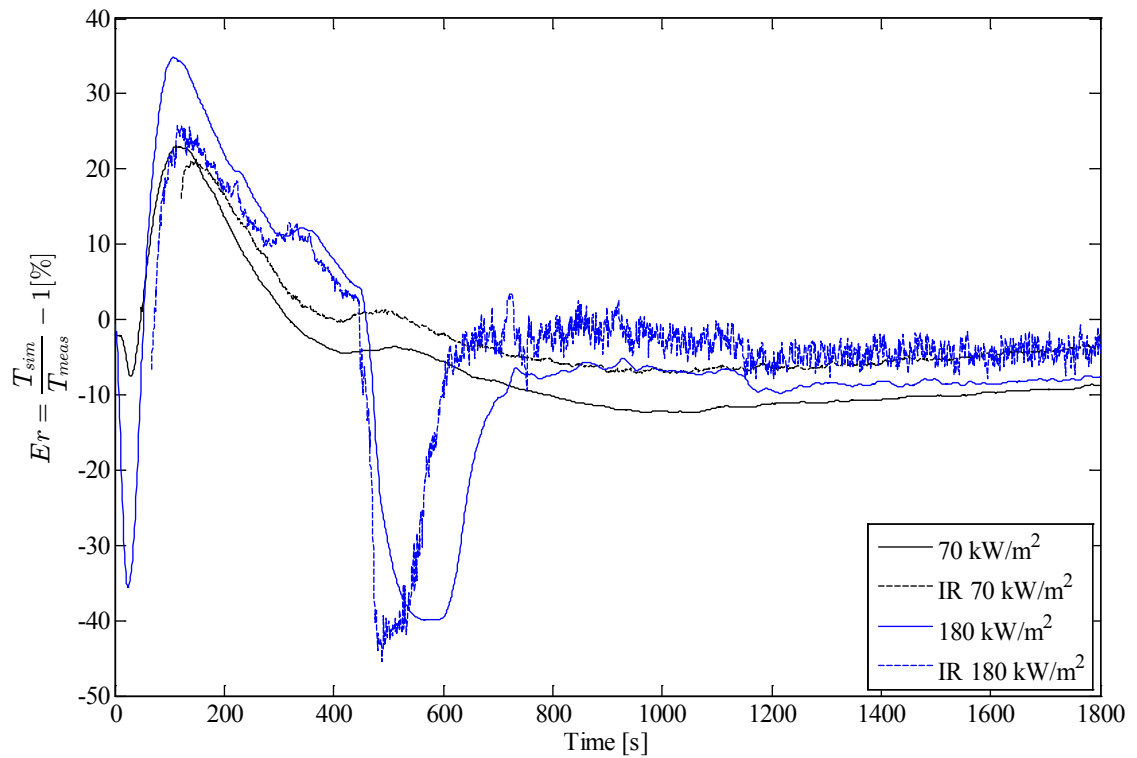


Figure 5.21: Temperature error percentage between the measured and calculated temperature using the best fitting Arrhenius and resin decomposition parameter sets reported in Table 5.6.

The overall minimum error is 0.018 and 0.008 for Thermocouple and IR measurements respectively, lower than the previous minimum errors. The search could be continued for further refinements but since the error between the two last searches is similar to each other, this last set of parameters and thermal properties evolution will be kept to model the fire-under-load tests as well.

Despite the already good fitting, it is believed that if thermal properties vs temperature were measured up to 800 °C, which is the temperature reached by the exposed face according to the calculated results, a better result could be achieved especially for the transient response. Lattimer et al. (2011) and Cain and Lattimer (2010) used a reverse engineering approach to find the best fitting thermal property vs temperature functions that would best fit their experimental results with good agreement. Although it is a very interesting and valuable approach, Nawaz (2011) found inconsistency with results following the same approach of Lattimer et al. (2011) and Cain and Lattimer (2010). In fact, Nawaz (2011) optimisation of the thermal property functions of temperature, fitting

the experimental fire results on carbon fibre epoxy laminates, led to different thermal property functions dependent on the thickness of the samples. This phenomenon was not observed by the previously mentioned authors since they used just one thickness. Having different sets of thermal properties for different thicknesses of the same material is not physically possible so this route will not be followed in this work since it leads to physically unacceptable results.

5.1.2 Thermal modelling of fire-under-load tests

Using the final Arrhenius and heat of decomposition parameters found and reported in Table 5.6, the thermal modelling of the fire-under-load tests was performed and a comparison with experimental data revealed good results. The model inputs are reported in Table 5.7. The modelled mathematical problem corresponds to an infinite composite slab made of carbon fibres (considered not reacting or decomposing) and epoxy resin (decomposing according to Arrhenius parameters optimised in the previous section) exposed to one sided constant heat flux. Resin decomposition is allowed, thermal properties are changing according to remaining resin content and the initial uniform temperature of each simulation depends on the initial temperature of the different samples tested.

Table 5.7: Parameters values used to obtain the results reported in Figure 5.22 and Figure 5.23.

Parameter	Units	Value
Epoxy resin density (ρ_m)	kg m ⁻³	1300
Epoxy resin Specific Heat ($C_{p,m}$)	J kg ⁻¹ K ⁻¹	1850
Epoxy Resin Thermal conductivity ($k_{\perp m}$)	W m ⁻¹ K ⁻¹	0.35
Final epoxy resin residue	%	2
Epoxy Arrhenius pre-exponential factor (A)	s ⁻¹	300
Epoxy resin activation energy (E)	J mol ⁻¹	10000
Epoxy resin heat of decomposition (Q_p)	J kg ⁻¹	-1700000
Gas Specific Heat (C_{pg})	J kg ⁻¹ K ⁻¹	2386.5
Resin Heat of combustion (H_g)	J kg ⁻¹	22.11
Carbon Fibre density (ρ_f)	kg m ⁻³	1750
Carbon fibre specific heat ($C_{p,f}$)	J kg ⁻¹ K ⁻¹	660
Carbon fibre bulk thermal conductivity ($k_{\perp f}$)	W m ⁻¹ K ⁻¹	0.32
Thickness	mm	10
Fibre volume fraction (V_f)	%	58.76
Constant Heat flux	kW m ⁻²	70; 116; 180
Thermal properties option	-	Function of remaining resin content
Simulation duration	min	3
Fourier number	-	0.1
Room starting temperature	°C	According to experimental value
Flames heat flux feedback	-	Included
Heat source emissivity	-	0.8
Hot face absorptivity	-	0.8
Hot face emissivity	-	0.8
Hot face boundary condition	-	Convection + radiation
Cold face boundary condition	-	Free convection + radiation
Number of nodes	-	11

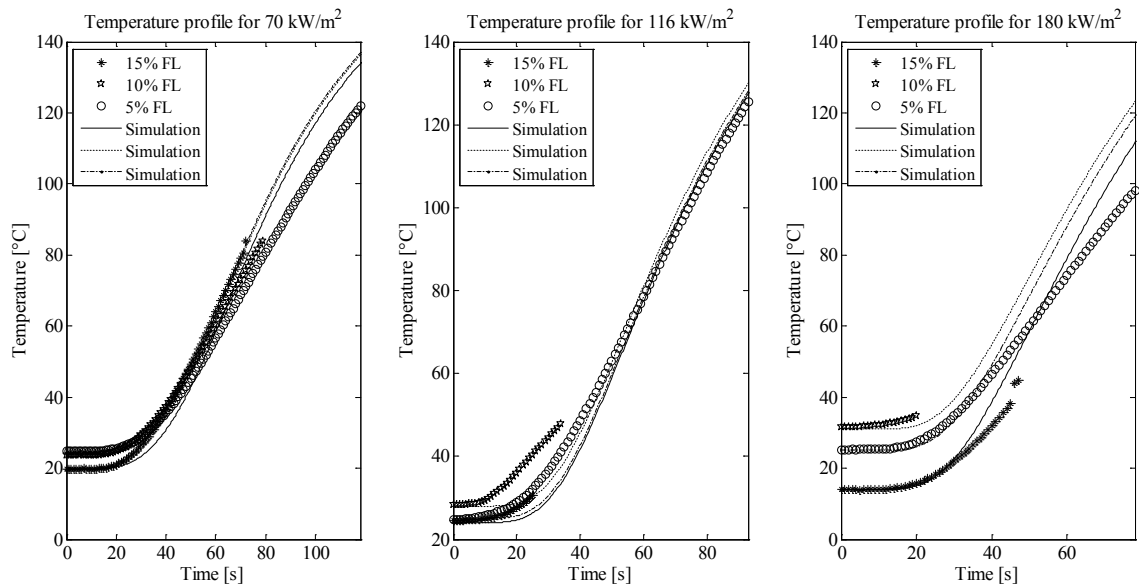


Figure 5.22: Fire-under-load cold face temperature profiles and simulated cold face temperature at different heat fluxes and applied loads for 10mm thick UD CFRP samples.

Cold face experimental temperatures and simulated results are reported in Figure 5.22. It can be noticed how the simulated results for the 70 kW m^{-2} and 116 kW m^{-2} fire tests have particularly good agreement with the experimental results compared to the 180 kW m^{-2} . The errors between the predictions and the experimental measurements, in percentage of the measured temperatures of each experiment, are reported in Figure 5.23, visually confirming the good temperature estimation for the 70 kW m^{-2} and 116 kW m^{-2} , with an average absolute error within 15%, with the exception of 116 kW m^{-2} 10%FL and 180 kW m^{-2} 5%FL tests which have both an error below 25%. The trends in terms of temperature profiles and associated error for the fire-under-load tests are the same observed in the transient response of the long-fire-exposure tests. Although, due to the high compressive load used, the insertion of an insulating material could not be used (because it would have caused imprinting and eventually crushing of the CFRP sample in the insulating material with subsequent possible rotation of the sample edges, causing a premature failure) the results do not seem to have been significantly affected by heat conduction between the samples and the testing rig. The test results might have been affected by either a loss of heat towards the testing rig, resulting in a slightly colder unexposed face temperature, or by a positive heat conduction form the testing rig towards the sample when the testing rig would get hotter than the sample.

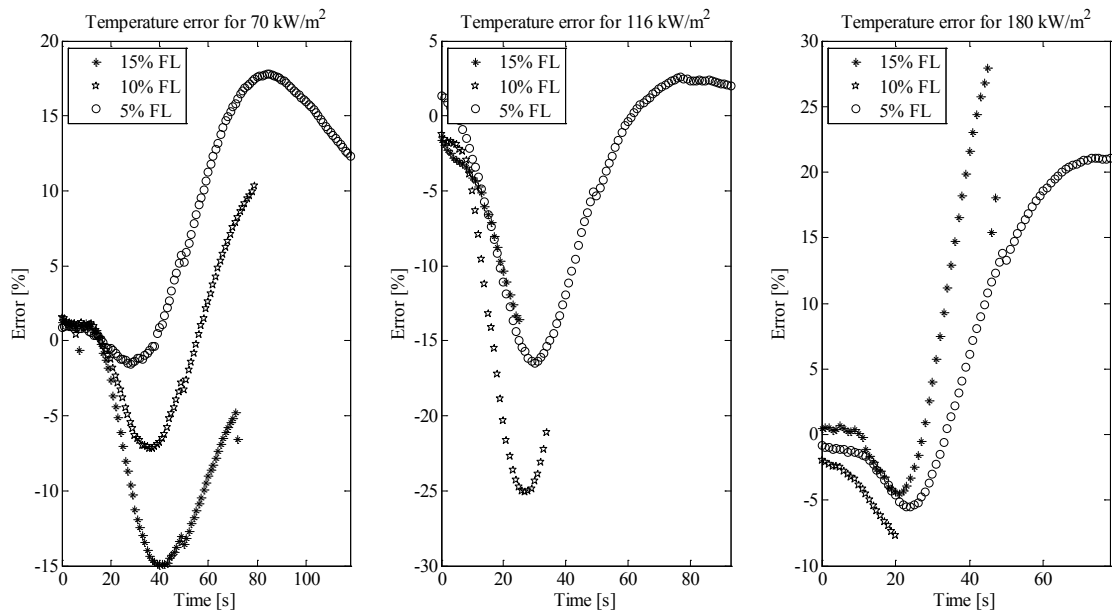


Figure 5.23: Error between simulated and experimental results in % of the measured temperature.

Once again the thermal profiles seem not to have been considerably affected by this effect, with the exception of the test of 180 kW m⁻² and 10%FL, which was tested after a couple of hours of cooling down time of the rig. Evidently this time was not enough and in fact this tests has a markedly higher starting temperature than all the others.

5.2 Mechanical response

This section describes the mechanical prediction results. Once the thermal problem had been solved, the mechanical module of COMFIRE-50 was used to fit the failure time predictions of the fire-under-load tests, previously described in section 4.4.2. The software inputs, parameter values and model options to evaluate the mechanical response are reported in Table 5.8. Time to failure, buckling failure time and compression failure time for every test conditions are reported in Figure 5.24.

Table 5.8: Parameters values used to obtain the results reported in Figure 5.24 and Figure 5.25.

Parameter	Units	Value
Initial thickness	mm	10
Sample width	mm	100
Composite failure load (FL)	kN	1330
Applied stresses	%FL	According to applied test load
Mechanical model type	-	Average Strength Model with 1 transition stage
End boundary condition constant	-	1 (simply supported)
Unsupported sample length	mm	100
Unrelaxed Compressive strength	MPa	Equation 4.5 with data from Table 4.6
Relaxed compressive strength	MPa	140
Strength transition temperature (T')	°C	160
Breath of strength transition constant (k)	-	0.08
Strength RRC sensitivity exponential factor (n)	-	0.5
Unrelaxed compressive modulus	MPa	Equation 4.9 and data from Table 4.8
Relaxed compressive modulus	MPa	0
Modulus transition temperature (T')	°C	160
Breadth of Modulus transition constant (k)	-	0.08
Modulus RRC sensitivity exponential factor (n)	-	3

Failure time predictions have been performed according to the average strength model explained in section 2.2.9.2. The input mechanical properties used for the modelling are the ones reported in section 4.3.2 and 4.3.3. It can be noticed that the time to failure predictions for the 70 kW m^{-2} are well aligned with the time to buckling failure, this being the first cause of failure for any applied load. This phenomenon is constant for all the heat fluxes used, which means that to measure the time to failure as mechanical property (i.e. in terms of compressive failure), buckling failure should be avoided either by using different mechanical edge restraining methods, e.g. a CAI fixture, and/or by performing tests on thicker samples or an appropriate combination of these two options.

As mentioned before, the accumulated thermal energy of the testing rig may have caused a different temperature distribution across the thickness which might result in a different residual compressive strength and compressive modulus distribution in the through-thickness direction. This phenomenon may explain the earlier testing failure compared to the modelled predicted failure of the tests at 116 kW m^{-2} and 180 kW m^{-2} , although intrinsic scatter in fire-under-load tests may be the cause of these discrepancies, as can be found in works by Bausano et al. (2005), Bausano et al. (2006), Feih et al. (2007a) and Nawaz (2011), the buckling prediction predicts surprisingly well the 70 kW m^{-2} and almost all the tests at 180 kW m^{-2} .

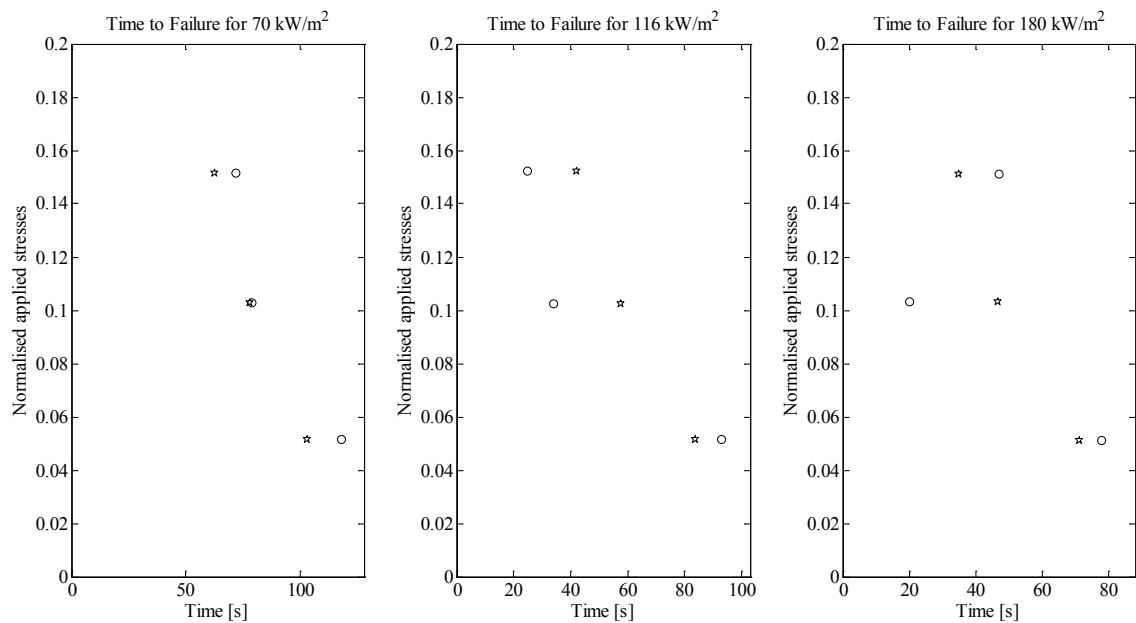


Figure 5.24: Experimental time to failure and COMFIRE-50 failure time prediction according to modelling parameters reported in Table 5.7 and Table 5.8; “o” are experimental measurements, “★ ” are the buckling failure predictions while the compressive failure predictions are not visible because out of x axis range.

Other effects that could justify variations between experimental and modelled results include the non-perfect parallelism between the sample edges and the compression plate surfaces, due to sample manufacturing or plate alignment, and the non-perfect fibre alignment with the load direction for every sample.

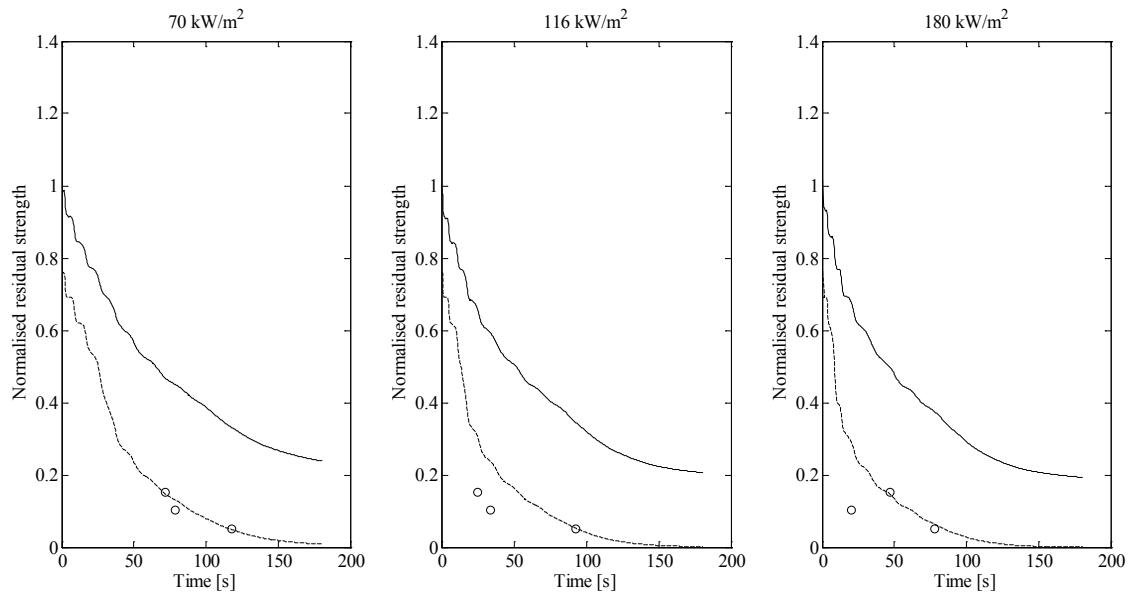


Figure 5.25: Experimental time to failure, normalised residual compression and normalised buckling strength curves for the different heat fluxes and loads used for the fire-under-load tests; o are experimental measurements, continues line is the normalised compressive strength and the dashed line is the normalised buckling strength.

Figure 5.25 shows the residual buckling failure loads and residual compressive strength function of time, along with the time to failure registered during the tests, for all the tests conditions. The apparently different results Figure 5.24 and Figure 5.25 are due to the fact that (as explained in section 2.2.9) to find the correct time to failure, the remaining buckling and/or compressive strength is compared to the increased applied stresses due to the loss of material in the through-thickness direction, assuming width and height are constant.

Chapter 6 **General discussion and conclusions**

This study represents the only work on long-fire-exposure tests and fire tests under load of aerospace grade unidirectional carbon fire epoxy composites at high heat fluxes. Thermal transport properties are very important for modelling purposes, especially when high temperatures are involved. Though there is data available in literature on the value of composite thermal properties at high temperature, little information is available for CFRP. However it has been shown that measurements of different authors on nominally similar materials might lead to different results and according to Ramroth et al. (2006) good accurate values of thermal transport properties are necessary to achieve good thermal modelling results. For this reason, thermal property measurements have been performed in this work with a new technique and validated against measurements with standardised techniques with good results. Although the measurements could only be performed up to 90 °C, because of the School's Health and Safety regulations, the results found are comparable to published results for similar materials, proving that the measuring technique is valid in this range of temperatures; however extension to higher temperatures seems to be straight forward. In the present study, measuring mechanical properties of high performance materials, such as aerospace grade UD CFRP, was challenging for the reasons noted below and special equipment is needed to achieve the correct result, according to standards. The difficulty lays on the fact that aerospace grade UD CFRP from prepregs have a tensile failure of 2000 MPa or higher, which makes it difficult to test 2 mm thick samples since the failure load of a standard BS EN ISO 527-5 (1999) size sample would be of around 65 kN, with a necessary adhesive lap shear strength for the tabs higher than 40 MPa and constant up to temperature above 200 °C. Though a thinner sample would have solved the problem, there was no possibility to obtain more material from Cytec. Nevertheless the techniques and methods developed in this work have proven to be valid despite the technical limitations.

The aims of the PhD thesis have been accomplished, such as the development of innovative techniques to measure thermal diffusivity, the execution of low-cost fire tests with a repeatable heat flux calibration technique and the development of a software to

predict thermal and mechanical behaviour, in spite of some difficulties with mechanical testing and fire-under-load testing, which limited model validation. The Matlab® program capable of performing thermo-mechanical modelling of composites under compressive load developed is available for the scientific community in a user friendly GUI with several inputs options and with the capability of using material data in table or function format. Validation of the thermal model for UD CFRP has been successful, while validation of the mechanical model using fire-under-load tests is not conclusive, in spite of the promising results shown. The following paragraphs will deal in more detail with the findings of this work.

6.1 Thermal characterisation

Thermal diffusivity measurements have been performed using a new technique, the step-change method. Possible causes of error have been identified and minimised or their influence estimated when possible. Measurements showed low error. Comparison with the guarded hot plate, a standardised measuring method, has been performed and the results showed good agreement. Further comparison with available literature data from Fanucci (1987), Kalogiannakis et al. (2004), Pilling et al. (1979), Rolfes and Hammerschmidt (1995) and Zalameda (1999), for similar material has been performed, confirming that the step-change technique is valid at least in the range of temperature used in this work. Since, to the knowledge of the author, there are no detailed literature data regarding thermal conductivity or diffusivity above 125 °C, with the exception of Fanucci (1987) which reported just 2 equal constant points between 510 and 3315 °C, further attempts to extend the measurements using a fluidised sand bath were attempted without encouraging results due to a too low convective heat transfer coefficient of the sand bath and possible sand boundary layer formation. The step-change technique has proven to be a valid and low-cost alternative to measure thermal diffusivity of UD CFRP materials although further experiments using high boiling point liquids should be performed to validate the technique at higher temperatures. Unfortunately this was not possible in this study due to health and safety regulations but, since the technique is based on basic physical principles, the validation at high temperatures should not be an issue in future studies. It has also been found that in general, thermal diffusivity of materials tends

to increase with increasing temperature, with the exception of CFRPs thermal diffusivity in the through-thickness direction, which seems to decrease with temperature according to Kalogiannakis et al. (2004) and in agreement with present results. The only two studies of thermal diffusivity vs temperature are of Zalameda (1999), which used room temperature thermal diffusivity measurements to detect defects in the laminate, and Kalogiannakis et al. (2004) which measured thermal diffusivity just up to 125 °C. Just Kalogiannakis et al. (2004) measured the CFRP through-thickness thermal diffusivity at high temperatures and confirmed that it decreases with temperature. Most of the other studies focused on thermal conductivity but without the corresponding value of specific heat and density at the different temperatures, and for this reason thermal diffusivity comparison is not possible. It has also been shown, and confirmed by literature data, that CFRP thermal diffusivity is strongly anisotropic with the thermal diffusivity along the fibres direction being 10 to 12 times higher compared to the one across the fibres, as it can be noticed comparing Figure 4.7 a) and b). The marked anisotropy of carbon fibres is the reason of this behaviour as stated by Kucner and McManus (1994) and Mouritz and Gibson (2006).

The step-change technique has proven to be a low cost and valid alternative to other techniques to measure thermal diffusivity without measuring any other material thermal property. Sources of errors have been identified and minimised, successfully measuring thermal diffusivity, and estimating thermal conductivity, of aerospace grade UD CFRP by comparing the results with guarded hot plate method and the available literature data.

6.2 Mechanical properties

Tensile strength and tensile modulus of 2 mm aerospace grade UD CFRP have been measured at temperatures from RT to 200 °C. During fire, the sample experiences temperatures far higher than the ones used in this work but due to project restrictions, health and safety issues and limited material availability the tests could not be performed at higher temperatures. Tensile strength was be measured up to 160 °C, while tensile modulus was be measured up to 180 °C. After 160 °C the high lap shear strength adhesive

was not capable of transmitting the load up to sample failure and tabs pull out phenomenon invalidated the results at temperature higher than 180 °C. Results show that both tensile strength and modulus agree with manufacturer and literature values and that CFRP can still bear tensile load at high temperature. In fact, several authors (Cao et al., 2009; Fitzer, 1988; Feih and Mouritz, 2012; Sauder et al., 2002 and Sauder et al., 2004) found that carbon fibres do not soften in inert atmosphere up to 700 °C or eventually higher temperatures. In oxidising environment they start softening at about 500-550 °C because of the loss of the outer layer which is made by a highly oriented carbon structure (Feih and Mouritz, 2012). The authors observed tensile strength loss regardless of the atmosphere used to heat the carbon fibres, the tensile strength, considering the fibre diameter loss, decreased between 400 °C and 600 °C, reaching a steady state value of around 60% of the original strength beyond 600 °C. In a fire, the inner fibres are not exposed to an oxidising atmosphere and so it is expected that CFRP retain most of their tensile modulus up to 700 °C or higher and their tensile strength at least up to 400 °C or higher. The proposed tensile strength and modulus function of temperature are reported in Figure 6.1.

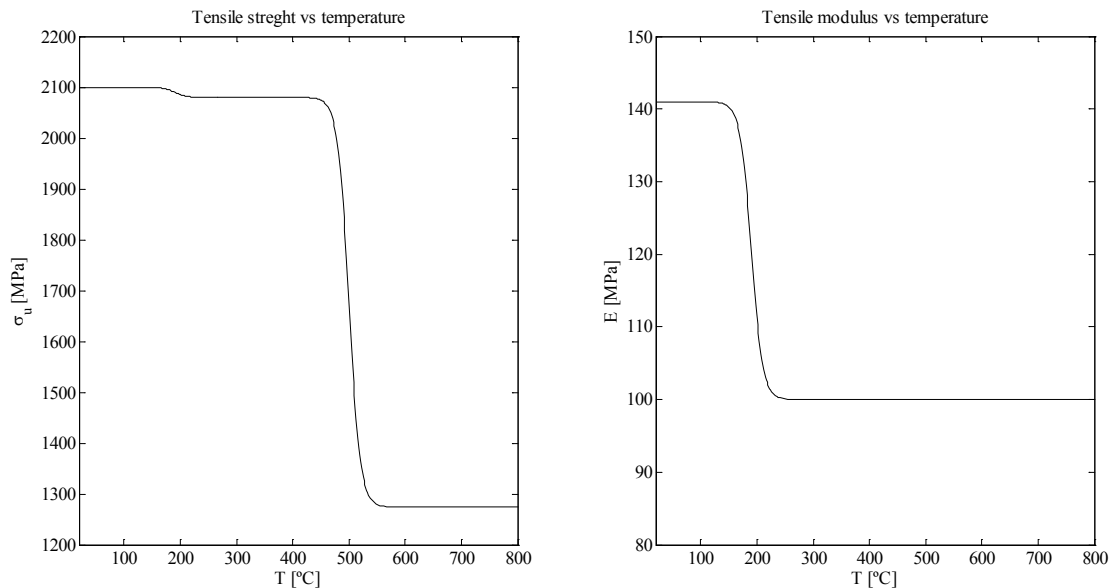


Figure 6.1: Tensile strength and modulus vs temperature for UD CFRP according to Equation 4.3 and Equation 4.4, respectively.

Compressive modulus could not be measured and therefore only the compressive strength was measured, in the same range of temperature used for the tensile properties measurements and for the same reasons. The in-house testing method did not work properly for the whole range of temperature and the only good result was the test at 200 °C. Compressive strength from RT to 200 °C was then evaluated using the RT and 90 °C compressive strength from material manufacturer as well as 200 °C compressive strength from the tests. Yoon and Kim (2000) found similar trends for CFRP longitudinal and transverse moduli vs temperature. This phenomenon is dependent on the fact that composite compressive properties are matrix dominated properties and matrix properties are highly dependent on temperature. This means that composites compressive properties are more temperature dependent compared to tensile properties which, on the other hand, are fibre dominated. According to the same authors, this temperature dependency could be described by a linear equation. A good agreement has been found using Gibson model, assuming the unrelaxed property not as a constant, but as a linear function of temperature, and fitting this linear equation with the points at RT and 90 °C. This approach is validated also by the DMA results on the transverse modulus, which linearly decreases up close to T_g . To rigorously validate the model more data is necessary, covering the full temperature range experienced by composites in fire scenarios. Nevertheless, although there is no study on compressive strength of unidirectional aerospace grade CFRP, the results align with findings on other materials by Burns et al. (2010), Feih et al. (2007a), Feih et al. (2007b) and Nawaz (2011) in the sense that, since compressive properties are matrix dominated properties, a gradual, small decrease in compressive strength occurs from room temperature up to near transition temperature because of resin behaviour with increasing temperature. The steep loss of compressive failure occurs between transition temperature and resin T_g . The transition temperature, the temperature corresponding to 50% compressive strength loss, has been reported to vary between 0.7 to 0.9 of T_g for different type of composites (Burns et al., 2010; Feih et al., 2007b; Nawaz et al., 2011) and the findings of this work (in the tested temperature range) align with literature reported data.

DMA measurements have been performed in the 2 principal directions of the UD CFRP samples using 3 different frequencies. There was no considerable difference between the responses to the different frequencies and therefore only the results at 1 Hz have been reported. These align with literature data from Li et al. (2000) and Zhou et al. (2007) for modulus vs temperature up to 200 °C of epoxy adhesive and neat resin, respectively, as well as Yoon and Kim (2000) for CFRP moduli up to 140 °C. It has been found that longitudinal modulus experiences a sensitive reduction around T_g although this should not happen, as it is a fibre dominated property. The reason being that the shear contribution of the displacement after T_g eclipses the bending one (see section 4.3.3 and Mouritz and Gibson (2006)) and this is not taken into account by the machine program therefore correction or a different fixture, e.g. four point bending or tension/compression, should be applied. Fixture choice is dictated by the accuracy wanted and the expected stiffness of the sample so a trade-off is always necessary. DMA measurements are an effective valid option, which is simple to use and requires minimum material to characterise material behaviour vs temperature even at high temperatures. Apart from measuring T_g , DMA results are useful to model composite behaviour on fire by giving indication on moduli evolution vs temperature. In this work T_g identification has been successful in finding the same value as declared by the manufacturer and the DMA results have been important to highlight the different behaviour of fibre and matrix dominated properties, in agreement with literature data.

6.3 Fire tests

Long-fire-exposure and fire-under-load tests were performed to validate COMFIRE-50. The small scale fire testing technique developed in this work has proven to be inexpensive in the implementation, repeatable and very useful for material screening and development. The fire calibration technique to achieve the required heat flux used in this work is validated by several standards in terms of flame temperature, it is repeatable and the prediction of heat flux can be made based on the gas flow expressed in l min^{-1} with a simple linear dependency. Some fire tests are characterised by flames impinging on the surface of the specimen, such as the jet fire test and the aerospace Park or “NexGen” burner, while on others the flames do not impinge on the sample surface, such as the

ISO2685 burner or radiant gas/electrical panels. The small scale propane burner tests is characterised by hot gases generally impinging on the sample surface at high speed. Although radiation is considered the main mean of heat transfer in the case of fire, because convection effects are usually negligible compared to radiation contributions, when the hot gases have a certain speed and the convection passes from natural to forced, the thermal contribution due to convection becomes not negligible anymore and can lead to underestimation of the actual heat flux sensed by the sample of more than 10%. There are no current techniques that takes into account this phenomenon and this might be one of the reasons why different methods lead to different results and why modelled results may differ from experimental results (Le Neve, 2008).

Long-fire-exposures were performed just at 70 and 180 kW m⁻² because of the lack of material for further testing. However, if the thermal simulation is in good agreement in both extreme heat fluxes, then it should keep being in agreement with all the intermediate heat fluxes. For these tests an IR camera was available and the temperature was measured with both thermocouple and IR camera. This showed that the IR camera measurements which represent the cold face temperatures are constantly between 10-20 °C lower, compared to the thermocouple measurements. Since the accuracy of the type k class 1 thermocouple used, in the range of temperature of this study, is within ± 1.5 °C, this discrepancy is most likely due to the small insulation effect of the resin keeping in place the measuring thermocouple. This effect is clear in the IR camera snapshots, see Figure 4.33 and Figure 4.34. In the case of the unavailability of non-contact measurements techniques capable of avoiding this effect, other temperature measuring devices or other techniques have been suggested, such as embedding thermocouple or fibre Bragg gratings in the manufacturing process or using thin film thermocouples with a very thin and conductive adhesive layer.

The setup of the fire tests under load, the thickness of the samples and the loads used did not allow for anti-buckling guides and thermal insulation between testing rig and sample interface to be used, as explained previously. This allowed buckling failure to occur

before compressive failure could be achieved. To obtain accurate measurements of fire resistance properties the sample has to be insulated from the testing rig, especially in the case of a very conductive material among composites such as CFRP (see Figure 6.2 (Ashby et al., 2013)), and anti-buckling fixtures should be used since, upon fire exposure, buckling is the first failure phenomenon to occur and it is dependent on geometry and thermally induced out of plane displacement (Nawaz, 2011). Due to scarcity of material, just one sample per condition could be tested and since according to Bausano et al. (2005), Bausano et al. (2006), Feih et al. (2007a) and Nawaz (2011) fire-under-load tests are characterised by intrinsic scatter, the results found in this work are not conclusive but they should be further supported by future tests to assess the actual time to failure scatter. Nevertheless the results are interesting and the trends align with literature data on other carbon fibres laminates with different layups.

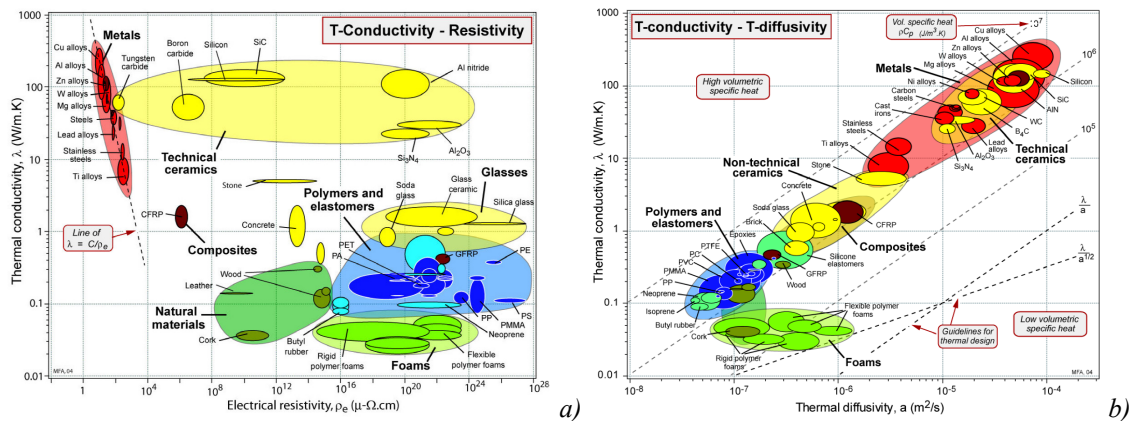


Figure 6.2: Ashby plots for engineering materials: a) thermal conductivity vs electrical resistivity; b) thermal conductivity vs thermal diffusivity, (pictures taken from GRANTA booklet at http://www.mie.uth.gr/ekp_yliko/2_materials-charts-2009.pdf).

6.4 Modelling

Modelling of both long-fire-exposure tests and the fire tests under load has been performed. Arrhenius parameters (A and E) and heat of decomposition (Q_p) values were changed to best fit the long-fire-exposure tests. In a first optimisation, the thermal properties were kept constant and then varied according to remaining resin content. Findings reveal that the model is not very sensitive to the values of A while it is quite

sensitive to the combination of the values of E and Q_p . The transient response was best fit with single point thermal properties, while the steady response was best fit with thermal properties changing according to remaining resin content. This suggests that, although physically thermal properties are function of temperature, the range of variability might be small during the initial transient response. On the other hand, the model that changes the thermal properties as function of the remaining resin content fits better the steady state response, suggesting that the variation of thermal properties influences more the steady state response than the transient response. These findings align with sensitivity analysis performed by Ramroth et al. (2006) using a finite element method to solve the same mathematical problem used in this work.

Fire-under-load tests were modelled using the best optimised Arrhenius parameters and heat of decomposition with thermal properties changing with remaining resin content, although the model with single point thermal properties fits better the thermal transient response and the fire-under-load tests lasts less than the whole transient response time. Although the fire-under-load tests were not done in replicate (for the reason stated in section 6.3) and are usually characterised by having intrinsic large scatter (Bausano et al. 2005, Bausano et al. 2006, Feih et al. 2007a and Nawaz 2011), the calculated buckling survival times are well predicted for the 70 kW m⁻² heat flux tests and for the 180 kW m⁻² heat flux tests (with the exception of the 10% FL); on the other hand the model prediction for the 116 kW m⁻² heat flux are not as good. As stated before, this might just be because of intrinsic scatter of fire tests and since replicate tests were not possible, this results are inconclusive in stating if the model well replicate the physical problem. Nevertheless the results are encouraging and further studies should be done, performing further tests in the same conditions using the same material, using anti buckling devices and insulation on the sample sides.

The model has predicted well the thermal behaviour UD CFRP at high heat fluxes, in particular at 70 and 180 kW m⁻². Fire resistance modelling in terms of hindering fire penetration and heat conduction throughout aerospace grade UD CFRP was performed

with good results for high heat fluxes between 70 and 180 kW m⁻² and for times up to 30 minutes. In regards to modelling fire resistance in terms of structural survivability to a compressive load (time to failure) results are not conclusive, but limited to the data available and to the tests conditions used in this work, i.e. low compressive load (max 15% of RT compressive failure load), high heat flux (between 70 and 180 kW m⁻²), short time to failure and hence low cold face temperature. The model ignores any time dependent material behaviour, though these are not expected to affect material failure at heat fluxes of 50 kW m⁻² and above, as it is the case in this study.

6.5 Future recommendations

Recommendations have been given throughout the thesis and the most significant one are recalled below.

The step-change method used to measure thermal diffusivity is both simple and low-cost, but future developments are recommended in order to use the step-change technique with lower *Bi* or changing the convective heat transfer coefficient by using high boiling point liquids such as oils or liquid metals.

Thermal and mechanical properties should be measured at temperature above 200 °C to improve the modelling of thermal and mechanical response of carbon fibre composites in fire. Although Burns et al. (2010) had good agreement using the strength based model used in this work, this is contrary to Nawaz (2011), who further implementing other models, such as the progressive failure model. Implementation of other models than the strength based one should be further explored to include other factors that may affect failure of composites in fire such as thermally induced bending moments, delamination, thermal gradient, thermal expansion and progressive failure.

For a better fit between modelled and experimental data, further tests are needed and fire under load tests should be performed using an insulating material between sample edges and testing rig to avoid any heat loss or gain due to conduction between sample and testing rig. It is advisable to use a CAI fixture with smaller sample thickness (or a modified CAI fixture allowing testing of 10mm thick samples or thicker) and inserting a thin layer of Rockwool or Fiberfrax® between the sample edges and the CAI fixture. In this way the CAI fixture will at the same time avoid global buckling and thermal contact, so that no heat conduction will occur between sample and CAI fixture. These suggestions have been applied to fire tests under load on quasi isotropic CFRP laminates after this PhD work had finished, and though results are protected by intellectual property agreement and cannot be used, scatter was clearly decreased. Further to this, an IR camera is advisable to accurately measure the cold face surface temperature. In fact, recent IR cold face temperature measurements on burn-through tests have shown that the actual surface temperature is considerably and consistently lower than the one recorded using thermocouples.

The experimental techniques and the modelling tool presented in this work have the potential to become a standard for measuring composites thermal and mechanical properties at high temperature. In particular the small-scale propane burner technique could be the first step to a new cheaper material development fire testing framework before performing the final full-scale certified fire tests. In fact, it has already been modified, analysed and improved by Tranchard et al. (2015). The model, on the other hand, could be used to predict fire resistance performances of carbon fibre composites in terms of thermal insulation and/or fire penetration. It might also be useful to further understand composite in the design stage of composites components that may be exposed to fire, helping to decide on different parameters, such as materials to be used, fibre volume fraction, thickness, among others.

Chapter 7 List of publications

Di Modica, P., Holliday, R., Humphrey, J., Christke, S., Kotsikos, G., and Gibson, A.G., Post-fire structural integrity of phenolic composite gratings for offshore platforms, Proceedings 13th Fire Retardance and Protection of Materials Conference, FRPM13, 2013.

Humphrey, J., Kotsikos, G., Gibson, A. G., Christke, S., Di Modica, P., and Holliday, R. (2013, September). Post-fire Structural Integrity of Composite Gratings for Offshore Platforms. In SPE Offshore Europe Conference Exhibition 2013.

Gibson, A. G., Humphrey, J. K., Di-Modica, P., Christke, S., Kotsikos, G., Holliday, R. (2013). Post-fire integrity of composite gratings for offshore platforms. *Journal of Reinforced Plastics and Composites*, 0731684413495933.

Di Modica, P., Vollaro, P., Gibson, A. G., Thermal diffusivity measurements of fibre reinforced polymer through the step-change technique, Proceedings 16th European Conference on Composites Materials, ECCM16, 2014.

Di Modica, P., Kotsikos, G., Gibson, A. G., Fire behaviour of carbon fibre composites under load, Proceedings 16th European Conference on Composites Materials, ECCM16, 2014.

Di Modica, P., La Rosa, A. D., Cicala, G., Kotsikos, G., Gibson A. G., Fire Resistance and Fire Reaction of Bio-Composite Sandwiches for Building Construction, Proceedings of 2nd International Conference on Natural Fibers, ICNF 2015.

Gibson, A. G., Di Modica, P., Kotsikos, G., Feih, S., Mouritz, A. P., Kandare, E., and Hoydonckx, H., A Rapid Route to the Development of Composite Passive Fire Protection Systems for Steel Structures, Proceedings of Fire Retardance and Protection of Materials Conference, 2015, FRPM15, 2015.

Di Modica, P., Gibson, A. G., Kotsikos, G., Hoydonckx, H., Bio-resin for new bio-composite passive fire protection for off-shore application, Proceedings of 20th International Conference of Composite Materials, ICCM20, 2015.

Di Modica, P., Gibson, A. G., Kotsikos, G., Hoydonckx, H., Monti, M., Sanchez, I. and Bachmann, J., Polyfurfuryl alcohol thermosets resins in fire resistant composite applications, Proceedings of 20th International Conference of Composite Materials, ICCM20, 2015.

Kandare, E., Di Modica, P., Chevali, V. S., and Gibson, A. G. (2015). Evaluating the heat resistance of thermal insulated sandwich composites subjected to a turbulent fire. *Fire and Materials*, 40(4), 586-598.

Chapter 8 **Appendix**

8.1 Appendix 1: Cytec MTM44-1 Datasheet

MTM® 44-1

MTM44-1 is a high performance, 180°C (356°F) curing, toughened epoxy resin formulated for the production of primary and secondary aircraft structures.

MTM44-1 can be processed via low pressure vacuum bag Out-of-Autoclave (OoA) moulding or autoclave moulding.

Advantages of MTM44-1 include excellent Tg retention under wet conditions, low density and a high level of damage tolerance.

MTM44-1 meets NASA outgassing requirements and can be used in space structures.

Features

- 21 days out life at 21°C (70°F)
- 12 months storage at -18°C (0°F)
- Meets NASA outgassing standards when tested to ECSS-Q-ST-70-02C
- Low density offers 2-4% weight saving compared to standard aerospace matrices
- Available in unidirectional prepreg for hand lay-up, ATL and AFP
- Available in fabric formats
- Out-of-Autoclave (OoA) or autoclave cure
- 130°C (266°F) or 180°C (356°F) initial cure options
- 190°C (374°F) dry Tg following 180°C (356°F) cure
- 150°C (302°F) wet Tg following 180°C (356°F) cure
- Excellent damage tolerance
- Fully compatible HTA®240 OoA adhesive film

Related documents

- De-bulking guidelines (TDS1036)
- MTM44-1 and MTM45-1 lay-up and bagging guidelines (TDS1043)
- Autoclave processing lay-up and bagging guidelines (TDS1037)

Related products

- HTA240 adhesive film (PDS1207)
- MTF246 surfacing film (PDS1240)

Cure cycle

Oven vacuum bag cure

Vacuum bag pressure	Minimum of 980 mbar (29"Hg)*
Ramp rate	1 to 2°C (1.8 to 3.6°F)/minute
Recommended cure cycle	2 hours at 130°C (266°F) + 2 hours at 180°C (356°F)
Cool down	Maximum of 3°C (5.4°F)/minute to 60°C (140°F)

*This is the ideal vacuum level, however, it is recognised that it is not always possible to attain. If in doubt, please contact our technical support staff for advice.

Autoclave cure

Vacuum bag pressure	Minimum of 980 mbar (29" Hg)*
Autoclave pressure	6.2 bar (90 psi)**
Ramp rate	1 to 2°C (1.8 to 3.6°F)/minute
Recommended cure cycle	2 hours at 130°C (266°F) + 2 hours at 180°C (356°F)
Cool down	Maximum of 3°C (5.4°F)/minute to 60°C (140°F)

*This is the ideal vacuum level, however, it is recognised that it is not always possible to attain. If in doubt, please contact our technical support staff for advice.

**If producing sandwich panels, apply the maximum pressure allowable for the honeycomb type.

Alternative cure cycle

Temperature	Duration
130°C (266°F)	4 hours

Notes:

- The alternative cure cycle is recommended when using tooling that cannot withstand 180°C.
- Parts cured using the alternative cure cycle must be post-cured for 2 hours at 180°C (356°F)

Post-cure

Following a 130°C (266°F) initial cure, the material will be in a relatively low state of cure. To develop full mechanical performance and maximum T_g, parts must be post-cured to 180°C (356°F) for 2 hours.

Ramp rate	0.3°C (0.5°F)/minute
Post-cure cycle	2 hours at 180°C -0/+5°C (356°F -0/+9°F)*
Cool down	2°C (3.6°F)/minute to 60°C (140°F)

* Temperature must be measured by the lagging thermocouple attached to the part.

Notes:

- Parts may be loaded into a pre-heated oven or heated at 3°C (5.4°F)/minute to the initial cure temperature.
- Large components should be adequately supported to avoid distortion.

Physical properties

Test	Sample/test conditions	Results
Cured resin density		1.18 g/cm ³
DMA E' onset T _g , SACMA	Dry	190°C (374°F)
	Wet*	155°C (311°F)
	Skydrol*	190°C (374°F)
Resin gel time	At 130°C (266°F)	140 minutes
Viscosity	At 80°C (176°F)	200 Pa.s
	At 130°C (266°F)	10 Pa.s
	At 140°C (284°F)	6 Pa.s
	At 160°C (320°F)	1.5 Pa.s
Moisture pick-up (cast resin)	At 25°C (77°F)/60%RH	1.46% ± 0.01%
	At 60°C (140°F)/60%RH	1.45% ± 0.05%
Moisture pick-up (MTM44-1/M55J 32%)	At 25°C (77°F)/60%RH	0.39% ± 0.02%
	At 60°C (140°F)/60%RH	0.39% ± 0.01%
Outgassing (MTM44-1/M55J 32%) Test Method ECSS-Q-5T-70-02C	Total mass loss (TML)	0.307%
	Recovered mass loss (RML)	0.056%
	Water vapour release (WVR)	0.251%
	Collected volatile condensable material (CVC/M)	0.002%

*14 days immersion at 70°C (158°F)

Note:

All data generated on samples cured for 2 hours at 180°C (356°F)

DELIVERING TECHNOLOGY BEYOND OUR CUSTOMERS' IMAGINATION
Aerospace Materials | Industrial Materials | Process Materials

CYTEC

Mechanical properties

Cure cycle: 2 hours at 180°C (356°F), oven vacuum bag cure.
Test conditions: Room temperature, dry

Test	Test method	Units	145 g/m ² 12k HTS5631 UD	268 g/m ² 24k IMS5131 UD	283 g/m ² 3k HTA5131 5- HS Fabric (CF0604)
0° Tensile modulus	ASTM D3039	GPa (msi)	128.9 (18.6)	174.6 (25.3)	62.6 (9)
0° Tensile strength		MPa (ksi)	2159 (313)	2738 (397)	927 (134.4)
0° Compressive modulus	ASTM D695 (MOD)	GPa (msi)	123.2 (17.8)	147.2 (21.3)	59.4 (8.6)
0° Compressive strength		MPa (ksi)	1330 (192.8)	1459 (211.5)	729 (105.7)
In-plane shear modulus (IPSM)	ASTM D3518	GPa (msi)	4.11 (0.6)	3.60 (0.5)	3.98 (0.58)
In-plane shear strength (IPSS)		MPa (ksi)	112.7 (16.3)	76 (11)	133 (19.3)
0° Flexural modulus	Crag 200	GPa (msi)	121.9 (17.7)	154.9 (22.4)	57.1 (8.2)
0° Flexural strength		MPa (ksi)	1958 (283.9)	1874 (271.7)	1181 (171.2)
0° Interlaminar shear strength (ILSS)	ASTM D2344	MPa (ksi)	106.6 (15.4)	109.4 (15.8)	75.4 (10.9)

All data, except for ILSS and IPSS & IPSM normalised to 55% Vf for fabric reinforced samples and 60% Vf for unidirectional reinforced samples.

Hot/wet laminate performance

Test	Test method	Units	Test conditions	Stitched NCF HTS5631 UD	134g/m ² 12k HTS5631 UD	285g/m ² 6k HTA5131 2x2 Twill Fabric
0° Interlaminar shear strength (ILSS)	EN2563	MPa (ksi)	RT/dry	96 (13.9)	94 (13.6)	69 (10)
			120°C (248°F)/dry	68 (9.86)	58 (8.4)	48 (6.9)
			120°C (248°F)/wet*	50 (7.25)	50 (7.25)	39 (5.6)

* Equilibrium at 70°C (158°F)/85% R.H.

Open hole compression strength

Test	Test method	Units	Test conditions	134g/m ² 12k HTS5631 UD	268g/m ² 24k IMS5131 UD	285g/m ² 6k HTA5131 2x2 Twill Fabric
OHC – Quasi-isotropic	LIS/MECH/280	MPa (ksi)	RT/dry	311 (45.1)	304 (44.1)	319 (46.3)

Unidirectional data normalised to 60% Vf, fabric data to 55% Vf.

Compressive strength after impact (CSAI)

Test	Test method	Units	Test conditions	32-ply 145g/m ² 12k HTS5631 UD	16-ply 268g/m ² 24k IMS5131 UD	16-ply 283g/m ² 3k HTA5131 5-HS Fabric (CF0604)
CSAI – Quasi-isotropic	SRM 2R-94 Impact 6.7J/mm	MPa (ksi)	RT/dry	259 (37.6) [32 J]	247 (35.8) [28 J]	329 (47.7) [33.5 J]

Unidirectional data normalised to 60% Vf, and fabric data to 55% Vf.
[J] = Actual impact energy for test laminate.

Availability

MTM44-1 is available as a fabric prepreg, unidirectional prepreg or slit tape.

Storage

Out life* at 21°C (70°F)	21 days
Storage at -18°C (0°F)	12 months from date of manufacture

*Out life refers to accumulated time out of the freezer before the part is cured.

Note:

The actual freezer storage life and out life are dependent on a number of factors, including: fibre type, format and application. For certain formats, it may be possible for the storage life and out life to be longer than stated. Please contact our technical support staff for advice.

Exotherm

MTM44-1 is a reactive formulation, but has a low exotherm risk and can be used for moulding thick sections. If in doubt, contact the Group's Technical support staff for advice when moulding sections greater than 50mm (2in) thick.

Health & safety

MTM44-1 contains epoxy resins which can cause allergic reactions by skin contact. Avoid contact with the skin. Gloves and protective clothing must be worn.

Wash skin thoroughly with soap and water or resin removing cream after handling. Do not use solvents for cleaning the skin.

Use mechanical exhaust ventilation when heat curing the resin system. Exhaust from vacuum pumps should be vented to external atmosphere and not into the work place.

For further information, consult Cytec Safety Data Sheet number:

SDS 413

All statements, technical information and recommendations contained in this data sheet are given in good faith and are based on tests believed to be reliable, but their accuracy and completeness are not guaranteed. They do not constitute an offer to any person and shall not be deemed to form the basis of any subsequent contract. All products are sold subject to the Cytec's Standard Terms and conditions of Sale. Accordingly, the user shall determine the suitability of the products for their intended use prior to purchase and shall assume all risk and liability in connection therewith. It is the responsibility of those wishing to sell items made from or embodying the products to inform the user of the properties of the products and the purposes for which they may be suitable, together with all precautionary measures required in handling those products. The information contained herein is under constant review and liable to be modified from time to time.
© Copyright 2012 – Cytec Industrial Materials (Derby) Ltd. All rights reserved worldwide. All trademarks or registered trademarks are the property of their respective owners.

DELIVERING TECHNOLOGY BEYOND OUR CUSTOMERS' IMAGINATION
Aerospace Materials | Industrial Materials | Process Materials

CYTEC

8.2 Tensile test report summary from Cytec



Header, Delivered, 0875 757 08

Mechanical Test Department. Tensile Strength, Modulus, Poisson's & Strain (ZT03). Zwick Z250

21.06.13

Parameters:

Batch	: NEWCASTLE UNI	Test Condition	: VARIOUS TEMPERATURES
J. No.	: J13455	Temp/Humidity	: RT-200°C
Job No.	: F00241	Curing Method	: OVBC
Product Code	: MTM44-1/1FE UD	Cure Cycle	: 180°C
Specification	: FIRE-RESIST	Tab Adhesive	: EA9394
Test Method	: LIS/MEC/059	Tab Adhesive Cure	: 1HR@100°C

Test Details:

Tester	: EW	End E-Modulus	: 0.3 %
Test speed	: 2 mm/min	Laminate Number	: MT9565
Speed, E-Modulus	: 2 mm/min	Orientation	: 0°
Start E-Modulus	: 0.1 %		

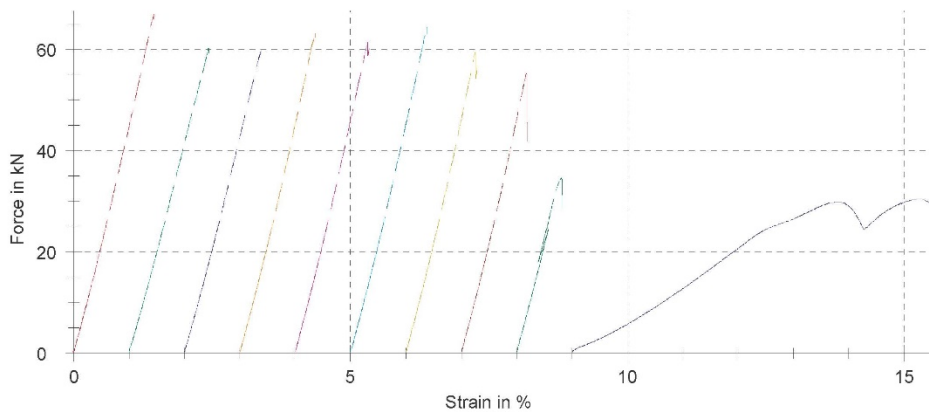
Results:

No.	Width mm	Thickness mm	Fmax. kN	Stress MPa	Modulus GPa	Poisson's	Ult Strain (%)	Failure Mode	Comments
1	15.01	1.98	67.01	2254.80	140.99	0.28	1.60	Explosive	RT
2	15.01	1.96	60.34	2051.01	132.32	0.31	1.55	Explosive	40°C
3	15.00	1.98	59.85	2015.19	134.46	0.30	1.50	Explosive	60°C
4	15.06	2.01	63.28	2090.49	138.21	0.31	1.51	Explosive	80°C
5	15.08	2.01	61.40	2025.72	140.28	0.30	1.44	Explosive	100°C
6	15.07	2.04	64.52	2098.78	136.72	0.31	1.54	Explosive	120°C
7	15.08	2.03	59.57	1945.82	138.25	0.31	1.41	Explosive	140°C
8	15.07	2.01	55.45	1830.57	139.34	0.28	1.31	Explosive	160°C
9	15.08	2.02	34.51	1132.80	136.92	0.26	0.83	At Tab	180°C
10	15.07	2.02	30.33	996.44	14.92	-	34.73	At Tab	200°C

Statistics:

Series n = 10	Width mm	Thickness mm	Fmax. kN	Stress MPa	Modulus GPa	Poisson's	Ult Strain (%)
x	15.05	2.01	55.63	1844.16	125.24	0.29	4.74
s	0.03	0.03	12.66	426.13	38.85	0.02	10.54
v	0.22	1.25	22.76	23.11	31.02	6.37	222.25

Series graphics:



8.3 Hysol EA9394 Lap shear strength extracted from Product data sheet,
LOCTITE HYSOL EA9394, Rev. 9/2013.



Technical Process Bulletin

LOCTITE EA 9394 AERO Epoxy Paste Adhesive (KNOWN AS Hysol EA 9394)

- Do not allow the adhesive to sit in the static mixer unattended for more than 90 minutes.
 - The material is curing within the static mixer and when pressure is re-applied back onto the plungers, back pressure will occur and potentially result in cartridge failure.

Failure to follow the recommended procedures stated in this TDS will void the Warranty of the Adhesive.

Note: Special precautions are recommended to minimize carbonate formation in large assemblies subject to extended open times in humid environments. A special memo is available upon request from Henkel providing users with suggestions for minimizing carbonate formation.

Curing - LOCTITE EA 9394 AERO may be cured for 3 to 5 days @ 77°F/25°C to achieve normal performance. Accelerated cures up to 200°F/93°C (for small masses only) may be used as an alternative. For example, 1 hour @ 150°F/66°C will give complete cure.

Cleanup - It is important to remove excess adhesive from the work area and application equipment before it hardens. Denatured alcohol and many common industrial solvents are suitable for removing uncured adhesive. Consult your supplier's information pertaining to the safe and proper use of solvents.

Bond Strength Performance

Tensile Lap Shear Strength - tested per ASTM D1002 after curing for 5 days @ 77°F/25°C. Adherends are 2024-T3 bare aluminum treated with phosphoric acid anodized per ASTM D3933.

<u>Test Temperature, °F/°C</u>	<u>Typical Results</u>	
	<u>psi</u>	<u>MPa</u>
-67/-55	3,300	22.7
77/ 25	4,200	28.9
180/82	3,000	20.7
200/93	2,900	20.0
250/121	2,300	15.8
300/149	1,600	11.0
350/177	1,200	8.3
400/204	600	4.1



Chapter 9 References

AC20-135 (1990). Powerplant installation and propulsion system component fire protection test methods, standards and criteria. Federal Aviation Administration (FAA).

Anderson, D. A., Freeman, E. S. (1959). The kinetics of the thermal degradation of the synthetic styrenated polyester, laminac 4116. *Journal of Applied Polymer Science*, 1(2), 192-199. doi: 10.1002/app.1959.070010210.

Anjang, A., Chevali, V. S., Lattimer, B. Y., Case, S. W., Feih, S., and Mouritz, A. P. (2015). Post-fire mechanical properties of sandwich composite structures. *Composite Structures*, 132, 1019-1028.

Anjang, A., Chevali, V. S., Kandare, E., Mouritz, A. P., and Feih, S. (2014). Tension modelling and testing of sandwich composites in fire. *Composite Structures*, 113, 437-445.

Asaro, R. J., Lattimer, B., and Ramroth, W. (2009). Structural response of FRP composites during fire. *Composite Structures*, 87(4), 382-393.

Ashby, M. F., Shercliff, H., and Cebon, D. (2013). Materials: engineering, science, processing and design. Butterworth-Heinemann.

ASTM D2863-13, Standard Test Method for Measuring the Minimum Oxygen Concentration to Support Candle-Like Combustion of Plastics (Oxygen Index), ASTM International, West Conshohocken, PA, 2013, www.astm.orgLOI.

ASTM D3675-14, Standard Test Method for Surface Flammability of Flexible Cellular Materials Using a Radiant Heat Energy Source, ASTM International, West Conshohocken, PA, 2014, www.astm.org.

ASTM D7137/D7137M – 12, Standard Test Method for Compressive Residual Strength Properties of Damaged Polymer Matrix Composite Plates, ASTM International, West Conshohocken, PA, 2012, www.astm.org.

ASTM E1269-11, Standard Test Method for Determining Specific Heat Capacity by Differential Scanning Calorimetry, ASTM International, West Conshohocken, PA, 2011, www.astm.org.

ASTM E1321-13, Standard Test Method for Determining Material Ignition and Flame Spread Properties, ASTM International, West Conshohocken, PA, 2013, www.astm.org.

ASTM E162-13, Standard Test Method for Surface Flammability of Materials Using a Radiant Heat Energy Source, ASTM International, West Conshohocken, PA, 2013, www.astm.org

ASTM E1623-11, Standard Test Method for Determination of Fire and Thermal Parameters of Materials, Products, and Systems Using an Intermediate Scale Calorimeter (ICAL), ASTM International, West Conshohocken, PA, 2011, www.astm.org.

ASTM E662-13d, Standard Test Method for Specific Optical Density of Smoke Generated by Solid Materials, ASTM International, West Conshohocken, PA, 2013, www.astm.org.

ASTM E84-13a, Standard Test Method for Surface Burning Characteristics of Building Materials, ASTM International, West Conshohocken, PA, 2013, www.astm.org.

ASTM E906 / E906M -10,: Standard Test Method for Heat and Visible Smoke Release Rates for Materials and Products Using a Thermopile Method, ASTM International, West Conshohocken, PA, 2010, www.astm.org.

ASTM F814-84b, Test Method for Specific Optical Density of Smoke Generated by Solid Materials for Aerospace Applications (Withdrawn 1995), ASTM International, West Conshohocken, PA, 1995, www.astm.org.

Babrauskas, V. (2000). Fire test methods for evaluation of fire-retardant efficacy in polymeric materials. *Fire Retardancy of Polymeric Materials*, 803, 81.

Bai, Y., and Keller, T. (2011). Delamination and kink-band failure of pultruded GFRP laminates under elevated temperatures and compression. *Composite Structures*, 93(2), 843-849.

Bai, Y., Vallée, T., and Keller, T. (2007). Modeling of thermo-physical properties for FRP composites under elevated and high temperature. *Composites Science and Technology*, 67(15), 3098-3109.

Bai, Y., Vallée, T., and Keller, T. (2008). Modeling of thermal responses for FRP composites under elevated and high temperatures. *Composites Science and Technology*, 68(1), 47-56.

Bausano, J. V., Boyd, S. E., Lesko, J. J., and Case, S. W. (2005). Composite Life Under Sustained Compression And One Sided Simulated Fire Exposure: Characterization And Prediction. *Science and Engineering of Composite Materials*, 12(1-2), 131-144.

Bausano, J. V., Lesko, J. J., and Case, S. W. (2006). Composite life under sustained compression and one sided simulated fire exposure: characterization and prediction. *Composites Part A: Applied Science and Manufacturing*, 37(7), 1092-1100.

Berlin, P., Dickman, O., and Larsson, F. (1992). Effects of heat radiation on carbon/PEEK, carbon/epoxy and glass/epoxy composites. *Composites*, 23(4), 235-243.

Bowles, D. E., and Tompkins, S. S. (1989). Prediction of coefficients of thermal expansion for unidirectional composites. *Journal of Composite Materials*, 23(4), 370-388.

Boyd, S. E., Case, S. W., and Lesko, J. J. (2007a). Compression creep rupture behavior of a glass/vinyl ester composite subject to isothermal and one-sided heat flux conditions. *Composites Part A: Applied Science and Manufacturing*, 38(6), 1462-1472.

Boyd, S. E., Lesko, J. J., and Case, S. W. (2007b). Compression creep rupture behavior of a glass/vinyl ester composite laminate subject to fire loading conditions. *Composites Science and Technology*, 67(15), 3187-3195.

British Gas plc, 1996, OTH 95 477, HSE, Assessment of the uniformity of the interim jet fire test procedure *Offshore Technology Report*: HSE.

Browne, T. N. A. (2006). A model for the structural integrity of composite laminates in fire. Doctoral Thesis, Newcastle University.

BS 476-6:1989+A1:2009, Fire tests on building materials and structures. Method of test for fire propagation for products, British Standards Institution, London.

BS 476-7:1997, Fire tests on building materials and structures. Method of test to determine the classification of the surface spread of flame of products, British Standards Institution, London.

BS 6401:1983, Method for measurement, in the laboratory, of the specific optical density of smoke generated by materials British Standards Institution, London.

BS EN 13823:2010+A1:2014, Reaction to fire tests for building products. Building products excluding floorings exposed to the thermal attack by a single burning item, British Standards Institution, London.

BS EN ISO 11357-1:2009, Plastics — Differential scanning calorimetry (DSC), British Standards Institution, London.

BS EN ISO 14126:1999, Fibre-reinforced plastic composites — Determination of compressive properties in the in-plane direction, British Standards Institution, London.

BS EN ISO 527-5:1997, Plastics — Determination of tensile properties *Part 5: Test conditions for unidirectional fibre-reinforced plastic composites*, British Standards Institution, London.

BS EN ISO 9773:1999, Plastics — Determination of burning behaviour of thin flexible vertical specimens in contact with a small-flame ignition source, British Standards Institution, London.

BS ISO 22899-1:2007, Determination of the resistance to jet fires of passive fire protection materials. General requirements, British Standards Institution, London.

BS ISO 2685:1998, Aircraft - Environmental test procedure for airborne equipment - Resistance to fire in designated fire zones, British Standards Institution, London.

BS ISO 4589-2:1999, Plastics -- Determination of burning behaviour by oxygen index -- Part 2: Ambient-temperature test, British Standards Institution, London.

BS ISO 5660-1:2015, Reaction-to-fire tests. Heat release, smoke production and mass loss rate. Heat release rate (cone calorimeter method) and smoke production rate (dynamic measurement), British Standards Institution, London.

BS ISO 9772:2012, Cellular plastics - Determination of horizontal burning characteristics of small specimens subjected to a small flame, British Standards Institution, London.

BS PD ISO/TS 5660-3:2012, Reaction-to-fire tests. Heat release, smoke production and mass loss rate. Guidance on measurement, British Standards Institution, London.

BS ISO 18352:2009, Carbon-fibre-reinforced plastics. Determination of compression-after-impact properties at a specified impact-energy level, British Standards Institution, London.

Burns, L. A., Feih, S., and Mouritz, A. P. (2010). Composite properties of carbon–epoxy laminate in fire. *J Aircraft*, 27, 528-533.

Cain, C., and Lattimer, B. (2010). Measuring properties for material decomposition modeling. In *Advances in the State of the Art of Fire Testing*. ASTM International.

Cao, S., Zhis, W. U., and Wang, X. (2009). Tensile properties of CFRP and hybrid FRP composites at elevated temperatures. *Journal of Composite Materials*, 43(4), 315-330.

Cengel, Y. A. (2003). Heat Transfer: A Practical Approach, Second Edition., McGraw-Hill publication, pp 138- 140.

Chen, J. K., Sun, C. T., and Chang, C. I. (1985). Failure analysis of a graphite/epoxy laminate subjected to combined thermal and mechanical loading. *Journal of Composite Materials*, 19(5), 408-423.

Croft, D. R., Lilley, D. G. (1977). *Heat transfer calculations using finite difference equations*: Applied Science Publishers London.

Dao, D. Q., Luche, J., Richard, F., Rogaume, T., Bourhy-Weber, C., and Ruban, S. (2013). Determination of characteristic parameters for the thermal decomposition of epoxy resin/carbon fibre composites in cone calorimeter. *International journal of hydrogen energy*, 38(19), 8167-8178.

Dimitrienko, Y. I. (1995). Thermal stresses and heat-mass transfer in ablating composite materials. *International journal of heat and mass transfer*, 38(1), 139-146.

Dimitrienko, Y. I. (1997). Thermomechanical behaviour of composite materials and structures under high temperatures: 1. Materials. *Composites Part A: Applied Science and Manufacturing*, 28(5), 453-461.

Dodds, N., Gibson, A. G., Dewhurst, D., and Davies, J. M. (2000). Fire behaviour of composite laminates. *Composites Part A: applied science and manufacturing*, 31(7), 689-702.

Easby, R. C., Feih, S., Konstantis, C., Delfa, G. L., Miano, V. U., Elmughrabi, A., Gibson, A. G. (2007). Failure model for phenolic and polyester pultrusions under load in fire. *Plastics, Rubber and Composites*, 36(9), 379-388. doi: 10.1179/174328907x248212

Eastop, T. D., McConkey, A. (1978). *Applied thermodynamics for engineering technologists : S.I. units* (3d ed.). London ; New York: Longman.

Engelke, W. T., Pyron Jr, C. M., and Pears, C. D. (1967). *Thermal and mechanical properties of a nondegraded and thermally degraded phenolic-carbon composite*. SOUTHERN RESEARCH INST BIRMINGHAM AL.

FAA, A. (1990). AC 20-135—Powerplant Installation and Propulsion System Component Fire Protection Test Methods, Standards and Criteria.

Fanucci, J. P. (1987). Thermal response of radiantly heated kevlar and graphite/epoxy composites. *Journal of composite materials*, 21(2), 129-139.

Feih, S., and Mouritz, A. P. (2012). Tensile properties of carbon fibres and carbon fibre–polymer composites in fire. *Composites Part A: Applied Science and Manufacturing*, 43(5), 765-772.

Feih, S., Mouritz, A. P. Mathys, Z. (2005). Finding kinetic parameters from TGA curves with a multi-branch least squares fit. TR05002, CRC-ACS.

Feih, S., Mathys, Z., Gibson, A. G., and Mouritz, A. P. (2007a). Modelling the tension and compression strengths of polymer laminates in fire. *Composites science and technology*, 67(3), 551-564.

Feih, S., Mathys, Z., Gibson, A. G., and Mouritz, A. P. (2007b). Modelling the compression strength of polymer laminates in fire. *Composites Part A: Applied Science and Manufacturing*, 38(11), 2354-2365.

Feih, S., Mouritz, A. P., Mathys, Z., and Gibson, A. G. (2007c). Tensile Strength Modeling of Glass Fiber—Polymer Composites in Fire. *Journal of composite materials*, 41(19), 2387-2410.

Fisher, K. J. (1993). Is fire a barrier to shipboard composites. *Advanced Composites*, 8(3).

Fitzer, E. (1988). Composites for high temperatures. *Pure and Applied Chemistry*, 60(3), 287-302.

Florio Jr, J., Henderson, J., and Test, F. L. (1989). Measurement of the thermochemical expansion of porous composite materials. *High Temperatures. High Pressures*, 21(2), 157-165.

Fredlund, B. (1993). Modelling of heat and mass transfer in wood structures during fire. *Fire safety journal*, 20(1), 39-69.

Friedman, H. L. (1964). *Kinetics of thermal degradation of char-forming plastics from thermogravimetry. Application to a phenolic plastic*. Paper presented at the Journal of Polymer Science Part C: Polymer Symposia.

FTT Ltd. (2014). newdualcone.jpg. In <http://www.fire-testing.com/cone-calorimeter-dual> (Ed.).

Gabbott, P. (2008). *Principles and Applications of Thermal Analysis* Retrieved from <http://NCL.ebilib.com/patron/FullRecord.aspx?p=470531>.

Gibson, A. G., Browne, T. N. A., Feih, S., and Mouritz, A. P. (2012). Modeling composite high temperature behavior and fire response under load. *Journal of composite materials*, 46(16), 2005-2022.

Gibson, A. G. , Wright, P. N. H., Wu, Y-S. J. T. Evans, (2006). Laminate theory analysis of composites under load in fire. *Journal of Composite Materials*, 40(7), 639-658.

Gibson, A. G., Wright, P. N. H., Wu, Y. S., Mouritz, A. P., Mathys, Z., and Gardiner, C. P. (2004). The integrity of polymer composites during and after fire. *Journal of Composite Materials*, 38(15), 1283-1307.

Gibson, A. G., Di Modica, P., Kotsikos, G., Feih, S., Mouritz, A. P., Kandare, E. and Hoydonckx, H. (2015). A Rapid Route to the Development of Composite Passive Fire Protection Systems for Steel Structures, *Proceedings of Fire retardant Polymer materials 2015*, FRPM15.

Gibson, A. G., and Hume, J. (1995). Fire performance of composite panels for large marine structures. *Plastics rubber and composites processing and applications*, 23(3), 175-183.

Gibson, A. G., Humphrey, J. K., Di Modica, P., Christke, S., Kotsikos, G., Holliday, R. (2013). Post-fire integrity of composite gratings for offshore platforms. *Journal of Reinforced Plastics and Composites*, 33(6), 543-555.

Gibson, A. G., Wu, Y.-S., Chandler, H. W., Wilcox, J.A.D., Bettess, P. (1995). A model for the thermal performance of thick composite laminates in hydrocarbon fires. *Revue de l'Institut Français du Pétrole*, 50(1), 69-74 (special issue).

Grange, N., Chetehouna, K., Gascoin, N., and Senave, S. (2016). Numerical investigation of the heat transfer in an aeronautical composite material under fire stress. *Fire Safety Journal*, 80, 56-63.

Grenier, A. T., Dembsey, N. A., and Barnett, J. R. (1998). Fire characteristics of cored composite materials for marine use. *Fire safety journal*, 30(2), 137-159.

Griffis, C. A., Masumura, R. A., and Chang, C. I. (1981). Thermal response of graphite epoxy composite subjected to rapid heating. *Journal of Composite Materials*, 15(5), 427-442.

Griffis, C. A., Nemes, J. A., Stonesifer, F. R., and Chang, C. I. (1986). Degradation in strength of laminated composites subjected to intense heating and mechanical loading. *Journal of Composite Materials*, 20(3), 216-235.

Gupta, R. N., Lee, K. P., Thompson, R. A., and Yos, J. M. (1991). Calculations and curve fits of thermodynamic and transport properties for equilibrium air to 30000 K, NASA Reference Publication, NASA-RP-1260, 191.

Gu, P., and Asaro, R. J. (2009). Designing sandwich polymer matrix composite panels for structural integrity in fire. *Composite Structures*, 88(3), 461-467.

Gutkin, R., Olsen, H., and Blomqvist, P. (2014). Modelling the structural response of fibre-reinforced composites subjected to fire, Proceedings 16th European Conference on Composites Materials, ECCM16.

Hancox, N. L. (1975). The compression strength of unidirectional carbon fibre reinforced plastic. *Journal of Materials Science*, 10(2), 234-242.

Heisler, M. P. (1947). Temperature Charts for Induction Heating and Constant-Temperature *Trans. ASME* (Vol. 69, pp. 227-236)

Henderson, J. B., and Doherty, M. P. (1987). Measurement of selected properties of a glass-filled polymer composite. *High Temperatures. High Pressures*, 19(1), 95-102.

Henderson, J. B., and Wiecek, T. E. (1987). A mathematical model to predict the thermal response of decomposing, expanding polymer composites. *Journal of Composite Materials*, 21(4), 373-393.

Henderson J.B., Wiebelt, J. A., Tant M.R., Moore G.R. (1982). A method for the determination of the specific heat and heat of decomposition of composite materials. *Thermochimica Acta*(57), 161-171.

Henderson, J. B., Wiebelt, J. A., Tant, M. R. (1985). A model for the thermal response of polymer composite materials with experimental verification. *Journal of Composite Materials*, 19(6), 579-595.

Hshieh, F. Y., and Beeson, H. D. (1997). Flammability testing of flame-retarded epoxy composites and phenolic composites. *Fire and materials*, 21(1), 41-49.

Hudson, C. W., Carruthers, J. J., and Robinson, A. M. (2010). Multiple objective optimisation of composite sandwich structures for rail vehicle floor panels. *Composite Structures*, 92(9), 2077-2082.

ISO 5660-1:2002 Second Edition, Reaction-to-fire tests - Heat release, smoke production and mass loss rate - Part 1: (cone calorimeter method)", International Organisation for Standardisation.

ISO 834-1:1999. Fire-resistance tests -- Elements of building construction -- Part 1: General requirements. International Organization for Standardization.

ISO 834-3, (First edition, 1999). Fire resistance tests - Elements of building construction - Part 3: Commentary on test method and test data application. International Organization for Standardization.

Johnston, A., Cole, R., Jodoin, A., MacLaurin, J., and Hadjisophocleous, G. (1999) Evaluation of fire performance of composite materials for aircraft structural applications. Proceedings of 12th International Conference of Composite Materials, ICCM12, Paris, France.

Kalogiannakis, G., Van Hemelrijck, D., Van Assche, G. (2004). Measurements of thermal properties of carbon/epoxy and glass/epoxy using modulated temperature differential scanning calorimetry. *Journal of composite materials*, 38(2), 163-175.

Kao, Y. H. (2012). Experimental investigation of NexGen and gas burner for FAA fire test. Doctoral dissertation, University of Cincinnati.

Karadeniz, Z. H., and Kumlutas, D. (2007). A numerical study on the coefficients of thermal expansion of fiber reinforced composite materials. *Composite structures*, 78(1), 1-10.

Kucner, L. K., and McManus, H. L. (1994). Experimental studies of composite laminates damaged by fire. In *50 Years of Progress in Materials Science and Technology: 26 th International SAMPE Techniqueal Conference* (pp. 341-353).

Kung, H. C. (1972). A mathematical model of wood pyrolysis. *Combustion and Flame*, 18(2), 185-195.

Lattimer, B. Y., Ouellette, J., and Trelles, J. (2011). Measuring properties for material decomposition modeling. *Fire and Materials*, 35(1), 1-17.

La Delfa, G. (2010). *Aerospace composite materials in fire*. Doctoral Thesis, Newcastle University.

Le Bras, M., Bourbigot, S., Mortaigne, B., and Cordellier, G. (1998). Comparative study of the fire behaviour of glass-fibre reinforced unsaturated polyesters using a cone calorimeter. *Polymers and polymer composites*, 6(8), 535-539.

Le Neve, S. (2008). *Comparison of Park Oil Burner to Gas Burner according to ISO 2685 or AC 20.135*. Paper presented at the Materials Fire Test Working Group, Atlantic City, New Jersey, USA.

Li, G., Lee-Sullivan, P., and Thring, R. W. (2000). Determination of activation energy for glass transition of an epoxy adhesive using dynamic mechanical analysis. *Journal of thermal analysis and calorimetry*, 60(2), 377-390.

Lifshitz, J. (1982). Strain Rate, Temperature, and Humidity Influences on Strength and Moduli of a Graphite/Epoxy Composite. *Journal of Composites, Technology and Research*, Vol. 4, No. 1, pp. 14-19, <http://dx.doi.org/10.1520/CTR10755J>. ISSN 0884-6804

Liu, L., Kardomateas, G. A., Birman, V., Holmes, J. W., and Simites, G. J. (2006). Thermal buckling of a heat-exposed, axially restrained composite column. *Composites Part A: Applied Science and Manufacturing*, 37(7), 972-980.

Liukov, A. V. (1968). Analytical Heat Diffusion Theory. *Academic Press*.

LOCTITE HYSOL EA 9394, Product data sheet Rev. 9/2013, [https://tds.us.henkel.com/NA/UT/HNAUTTDS.nsf/web/B02C099805BD377385257BC60067B0E3/\\$File/LOCTITE%20EA%209394%20AERO-EN.pdf](https://tds.us.henkel.com/NA/UT/HNAUTTDS.nsf/web/B02C099805BD377385257BC60067B0E3/$File/LOCTITE%20EA%209394%20AERO-EN.pdf).

Looyeh, M. R. E., Rados, K., and Bettess, P. (2001). Thermochemical responses of sandwich panels to fire. *Finite Elements in Analysis and Design*, 37(11), 913-927.

Lua, J., O'Brien, J., Key, C. T., Wu, Y., and Lattimer, B. Y. (2006). A temperature and mass dependent thermal model for fire response prediction of marine composites. *Composites Part A: Applied Science and Manufacturing*, 37(7), 1024-1039.

Lyon, R. (1996). Federal aviation administration research in fire safe materials for aircraft interiors. *SAMPE journal*, 32(3), 29-33.

Lyon, R. E., Demario, J., Walters, R. N., and Crowley, S. (2005, September). Flammability of glass fiber-reinforced polymer composites. In *Proceedings of the fourth conference on composites in fire* (pp. 15-16).

Mableson, A. R., Dunn, K. R., Dodds, N., and Gibson, A. G. (2000). Refurbishment of steel tubular pipes using composite materials. *Plastics, rubber and composites*, 29(10), 558-565.

Mahieux, C. A., Reifsnider, K. L., and Case, S. W. (2001). Property modeling across transition temperatures in PMC's: Part I. Tensile properties. *Applied Composite Materials*, 8(4), 217-234.

Mahieux, C. A., and Reifsnider, K. L. (2002). Property modeling across transition temperatures in polymers: application to thermoplastic systems. *Journal of materials science*, 37(5), 911-920.

Majid, M. A., Assaleh, T. A., Gibson, A. G., Hale, J. M., Fahrner, A., Rookus, C. A. P., and Hekman, M. (2011). Ultimate elastic wall stress (UEWS) test of glass fibre reinforced epoxy (GRE) pipe. *Composites Part A: Applied Science and Manufacturing*, 42(10), 1500-1508.

Mangino, E., Carruthers, J., and Pitarresi, G. (2007). The future use of structural composite materials in the automotive industry. *International Journal of vehicle design*, 44(3-4), 211-232.

Marker, T. R., Speitel, L. C. (2008). Development of a Laboratory-Scale Test for Evaluating the Decomposition Generated Inside an Intact Fuselage During a Simulated Post-crash Fuel Fire: Virginia, Federal Aviation Administration, DOT/FAA/AR-TN07/15.

Matala, A. (2013). Methods and applications of pyrolysis modelling for polymeric materials, Doctoral Thesis, Aalto University.

Matala, A., Lautenberger, C., Hostikka, S. (2012). Generalized direct method for pyrolysis kinetic parameter estimation and comparison to existing methods. *Journal of Fire Sciences*, 30(4), 339-356.

MATHER, P. a. S., R D. (1997). OTO 97 079, HSE: Large scale and medium scale jet fire tests, *Offshore Technology Repor*: HSE.

Mathys, Z., Gardiner, C. P., and Mouritz, A. P. (2002). Tensile and compressive properties of GRP composites with localised heat damage. *Appl Compos Mater*, 9, 353-67.

McGrattan, K., Hostikka, S., and Floyd, J. E. (2010). Fire dynamics simulator (version 5), user's guide. *NIST special publication*, 1019(5), 1-186.

McManus, L. N., and Coyne, D. C. (1982). *TRAP4—a digital computer program for calculating the response of mechanically and thermally loaded aircraft structures to the thermal radiation of a nuclear explosion or high energy laser*. TM-141. Kaman Avidyne Techniqueal Memorandum.

McManus, H. L., and Springer, G. S. (1992a). High temperature thermomechanical behaviour of carbon-phenolic and carbon-carbon composites, I. Analysis. *Journal of Composite Materials*, 26(2), 206-229.

McManus, H. L., and Springer, G. S. (1992b). High temperature thermomechanical behaviour of carbon-phenolic and carbon-carbon composites, II. Results. *Journal of Composite Materials*, 26(2), 230-255.

Menard, K. P. (2008). *Dynamic mechanical analysis: a practical introduction*: CRC press.

Mistry, J., Gibson, A. G., and Wu, Y. S. (1992). Failure of composite cylinders under combined external pressure and axial loading. *Composite structures*, 22(4), 193-200.

Mouritz, A. P. (2003). Fire resistance of aircraft composite laminates. *Journal of materials science letters*, 22(21), 1507-1509.

Mouritz, A. P. (2006). Fire Safety of Advanced Composites for Aircraft, ATSB Research and Analysis Report. *Australian Transport Safety Bureau, Australian Government*.

Mouritz, A. P., Gellert, E., Burchill, P., and Challis, K. (2001). Review of advanced composite structures for naval ships and submarines. *Composite structures*, 53(1), 21-42.

Mouritz, A. P., and Mathys, Z. (2001). Post-fire mechanical properties of glass-reinforced polyester composites. *Composites Science and Technology*, 61(4), 475-490.

Mouritz, A. P. and Gibson, A. G. Ebooks Corporation. (2006). *Fire Properties of Polymer Composite Materials*. Dordrecht: Springer.

Mouritz, A. P., Mathys, Z., and Gibson, A. G. (2006). Heat release of polymer composites in fire. *Composites Part A: Applied science and manufacturing*, 37(7), 1040-1054.

Mouritz, A. P., Feih, S., Kandare, E., Mathys, Z., Gibson, A. G., Des Jardin, P. E., Case, S. W., Lattimer, B. Y. (2009). Review of fire structural modelling of polymer composites. *Composites Part A: Applied Science and Manufacturing*, 40(12), 1800-1814.

Murty Kanury, A. (1972). Thermal decomposition kinetics of wood pyrolysis. *Combustion and Flame*, 18(1), 75-83.

Nakada, M., Miyano, Y., Kinoshita, M., Koga, R., Okuya, T., and Muki, R. (2002). Time–temperature dependence of tensile strength of unidirectional CFRP. *Journal of composite materials*, 36(22), 2567-2581.

NASA-STD-6001, N. (1998). Flammability, odor, offgassing, and compatibility requirements and test procedures for materials in environments that support combustion.

Nawaz, N. (2011). *Modelling and experimental analysis of aerospace composites in fire* (Doctoral dissertation, RMIT University).

NFPA 258, N. (2001). NFPA 258: Recommended Practice for Determining Smoke Generation of Solid Materials (Withdrawn).

Ochs, R. I. (2009). Development of a next-generation burner for use in testing thermal acoustic insulation burnthrough resistance. DOT/FAA/AR-TN09/23, U.S. Department of Transportation, Federal Aviation Administration.

Pering, G. A., Farrell, P. V., and Springer, G. S. (1980). Degradation of tensile and shear properties of composites exposed to fire or high temperature. *Journal of Composite Materials*, 14:54–66

Perry, R., and Green, D. (2008). *Perry's chemical engineers' handbook*. (8th ed). New York: McGraw-Hill.

Piggott, M. R., and Harris, B. (1980). Compression strength of carbon, glass and Kevlar-49 fibre reinforced polyester resins. *Journal of Materials Science*, 15(10), 2523-2538.

Pilling, M. W., Yates, B., Black, M. A., and Tattersall, P. (1979). The thermal conductivity of carbon fibre-reinforced composites. *Journal of Materials Science*, 14(6), 1326-1338.

Poropatic, P., Brayden, T., and S H, J. R. (1989). Determination of heat affected zones across a laminate. In *International SAMPE Symposium and Exhibition, 34 th, Reno, NV* (pp. 1379-1384).

Prasad, K., and Baum, H. R. (2005). Coupled fire dynamics and thermal response of complex building structures. *Proceedings of the Combustion Institute*, 30(2), 2255-2262.

Ramroth, W. T., Krysl, P., and Asaro, R. J. (2006). Sensitivity and uncertainty analyses for FE thermal model of FRP panel exposed to fire. *Composites Part A: Applied Science and Manufacturing*, 37(7), 1082-1091.

Rogers, K. F., Phillips, L. N., Kingston-Lee, D. M., Yates, B., Overy, M. J., Sargent, J. P., and McCalla, B. A. (1977). The thermal expansion of carbon fibre-reinforced plastics. *Journal of Materials Science*, 12(4), 718-734.

Rolfes, R., and Hammerschmidt, U. (1995). Transverse thermal conductivity of CFRP laminates: a numerical and experimental validation of approximation formulae. *Composites Science and Technology*, 54(1), 45-54.

Sauder, C., Lamon, J., and Pailler, R. (2004). The tensile behavior of carbon fibers at high temperatures up to 2400 C. *Carbon*, 42(4), 715-725.

Sauder, C., Lamon, J., and Pailler, R. (2002). Thermomechanical properties of carbon fibres at high temperatures (up to 2000 C). *Composites Science and Technology*, 62(4), 499-504.

Sikoutris, D. E., Vlachos, D. E., Kostopoulos, V., Jagger, S., and Ledin, S. (2012). Fire burnthrough response of CFRP aerostructures. Numerical investigation and experimental verification. *Applied Composite Materials*, 19(2), 141-159.

Sjöström, J., (2013) Thermal properties of carbon fibre/epoxy composites: thermal conductivity, diffusivity, capacity and thermogravimetric analysis, internal report of Fire Resist project NMP3-LA-2010-246037

Scudamore, M. J. (1994). Fire performance studies on glass-reinforced plastic laminates. *Fire and Materials*, 18(5), 313-325.

Seggewiss, P. G. B. (2004, May). Methods to evaluate the fire resistance of carbon fiber reinforced plastics. In *Proceedings of the 60th SAMPE symposium and techniqueal exhibition, Long Beach, CA*.

Sorathia, U., Lyon, R., Gann, R. G., and Gritz, L. (1997). Materials and fire threat. *Fire technology*, 33(3), 260-275.

Stewart, R. (2012). Wind turbine blade production—new products keep pace as scale increases. *Reinforced Plastics*, 56(1), 18-25.

Street, K. N., Russell, A. J., and Bonsang, F. (1988). Thermal damage effects on delamination toughness of a graphite/epoxy composite. *Composites science and technology*, 32(1), 1-14.

Sullivan, R. M., and Salamon, N. J. (1992a). A finite element method for the thermochemical decomposition of polymeric materials—I. Theory. *International Journal of Engineering Science*, 30(4), 431-441.

Sullivan, R. M., and Salamon, N. J. (1992b). A finite element method for the thermochemical decomposition of polymeric materials—II. Carbon phenolic composites. *International Journal of Engineering Science*, 30(7), 939-951.

Sullivan RM. (1990) A finite element method for thermochemically decomposing polymers. PhD dissertation, The Pennsylvania State University.

Sullivan, R. M. (1993). A coupled solution method for predicting the thermostructural response of decomposing, expanding polymeric composites. *Journal of Composite Materials*, 27(4), 408-434.

Summers, P. T. (2010). *Predicting compression failure of fiber-reinforced polymer laminates during fire* (Doctoral dissertation, Virginia Polytechnique Institute and State University).

Tant, M. R., Henderson, J. B., and Boyer, C. T. (1985). Measurement and modelling of the thermochemical expansion of polymer composites. *Composites*, 16(2), 121-126.

Tranchard, P., Samyn, F., Duquesne, S., Thomas, M., Estèbe, B., Montès, J. L., and Bourbigot, S. (2015). Fire behaviour of carbon fibre epoxy composite for aircraft: Novel test bench and experimental study. *Journal of Fire Sciences*, 0734904115584093.

UNITHERM. (2006). Thermal conductivity instrument *User's manual* (2.8 ed.): ANTER CORPORATION, 1700 Universal Road, Pittsburgh, PA 15235-3998, (412) 795-6410.

Urso Miano, V. (2011). Modelling composite fire behaviour using apparent thermal diffusivity. Doctoral Thesis, Newcastle University.

Ventriglio, D. R. (1982). Fire safe materials for navy ships. *Naval Engineers Journal*, 94(5), 65-74.

Vizzini, A. J., and Milke, J. A. (1991). Thermal response of fire-exposed composites. *Journal of Composites, Technology and Research*, 13(3), 145-151.

Yamane, T., Katayama, S. I., Todoki, M., and Hatta, I. (1996). Thermal diffusivity measurement of single fibers by an ac calorimetric method. *Journal of applied physics*, 80(8), 4358-4365.

Yates, B., McCalla, B. A., Sargent, J. P., Rogers, K. F., Phillips, L. N., and Kingston-Lee, D. M. (1978a). The thermal expansion of carbon fibre reinforced plastics. *Journal of Materials Science*, 13(10), 2217-2225.

Yates, B., Overy, M. J., Sargent, J. P., McCalla, B. A., Kingston-Lee, D. M., Phillips, L. N., and Rogers, K. F. (1978b). The thermal expansion of carbon fibre reinforced plastics. *Journal of Materials Science*, 13(10), 2217-2225.

Yovanovich, M. M. (1996). Simple Explicit Expressions for Calculation of the Heisler-Grober Charts. *1996 ASME National Heat Transfer Conference, Thermophysics and Thermophysical Properties Session, Houston, Texas, Aug. 3-6*.

Yoon, K. J., and Kim, J. S. (2000). Prediction of thermal expansion properties of carbon/epoxy laminates for temperature variation. *Journal of composite materials*, 34(2), 90-100.

Zalameda, J. N. (1999). Measured through-the-thickness thermal diffusivity of carbon fiber reinforced composite materials. *Journal of Composites, Technology and Research*, 21(2), 98-102.

Zhou, Y., Pervin, F., Lewis, L., and Jeelani, S. (2007). Experimental study on the thermal and mechanical properties of multi-walled carbon nanotube-reinforced epoxy. *Materials Science and Engineering: A*, 452, 657-664.